DEVELOPMENT OF THE ZEBRAFISH MOTOR UNIT

By

Robert R. Buss

Department of Biology

McGill University, Montreal

June, 2002

A thesis submitted to

the Faculty of Graduate Studies and Research

in partial fulfilment of the requirements of the degree

of

Doctor of Philosophy

Your file Votre référence
ISBN: 0-612-85689-5
Our file Notre référence
ISBN: 0-612-85689-5

TABLE OF CONTENTS

Abstract

The development of swimming was investigated in zebrafish aged 1.5 to 5 days postfertilization by examining both the swimming behavior and its generation by the nervous system. Upon hatching (at day 2), swimming is undirected and occurs in sustained bursts of high frequency (mean = 67 Hz) tail undulations. By 4 days, the swimming pattern matures to a more directed, less erratic, beat-and-glide pattern where slower (mean = 35 Hz) tail undulations, lasting ~200 ms, alternate with longer gliding rest periods. Swimming is powered by two classes of embryonic muscles (embryonic red, ER and white, EW) that are electrically coupled within (but not between) classes and have physiological properties similar to vertebrate tonic and twitch muscle, respectively. ER fibers have a lower chloride ion permeability than EW fibers and do not have sodium dependent action potentials. In paralyzed preparations, motoneurons and muscle fibers received coordinated excitatory synaptic activity (with left to right alternation and head to tail propagation) corresponding to either burst or beat-and-glide swimming. ER muscle was de-recruited at the fastest swimming rates and EW fibers dropped out at the slowest swimming rates. Rhythmic motoneuron output was generated by a phasic glutamatergic and a largely tonic glycinergic synaptic drive. Glutamatergic synapses had either or both AMPA/kainate and NMDA receptors and the kinetics of these synaptic currents were fixed thoughout the developmental period examined. When depolarized, motoneurons fired high frequency (up to 800 Hz) bursts of action potentials that rapidly accommodated (within ~20 ms) due to voltage and calcium dependent outwardly rectifying

conductances. These intrinsic motoneuron properties are hypothesized to interact with the rhythmic synaptic drive to pattern motor output (at ~25-75 Hz) to locomotor muscles. The neural generation of swimming in developing zebrafish is thus fundamentally similar to locomotion in adult fishes and vertebrates in general.

Résumé

Le développement de la nage a été étudié chez le poisson zèbre âgé de 1.5 à 5 jours post-fécondation, par des analyses de son comportement et de sa génération par le système nerveux. À l'éclosion (2ème jour), la nage n'est pas dirigée et se manifeste par des bouffées d'ondulations soutenues de la queue, produites à de hautes fréquences (moyenne de 67 Hz). Suite au 4ème jour, la nage devient plus dirigée et moins erratique, avec un patron de battements suivis de planage, dans lequel des ondulations de la queue (moyenne de 35 Hz) durent ~200 ms et alternent avec des périodes de repos ou planage plus prolongées. La nage est engendrée par deux classes de muscles (rouge embryonnaire (RE) et blanc embryonnaire (BE)) qui sont couplés électriquement à l'intérieur d'une même classe, mais non entre-elles, et qui ont des propriétés physiologiques ressemblant respectivement à celles des muscles toniques et de saccades chez les vertébrés. Les fibres RE ont une perméabilité au chlore plus faible que les fibres BE et n'ont pas de potentiels d'actions dépendant du sodium. Dans des préparations paralysées, les motoneurones et les muscles reçoivent une activité synaptique excitatrice (en alternant de gauche à droite et en se propagant de la tête à la queue), qui correspond à la nage par bouffées ou par battements suivie de planage. Les muscles RE ne sont plus recrutés aux taux de nage les plus rapides, tandis que les muscles BE faillissent aux taux les plus lents. L'activité rythmique chez les motoneurones a été générée par une pulsion synaptique consistant en synapses glutamatergiques phasiques et en synapses glycinergiques largement toniques. Les synapses glutamatergiques contenaient

des récepteurs AMPA/kainate et\ou NMDA, seuls ou en combinaison. Les cinétiques de ces récepteurs ont été établies durant la période du développement examinée. Lors d'une dépolarisation, les motoneurones ont déchargés des bouffées de potentiels d'action à une haute fréquence (jusqu'à 800 Hz) et se sont accomodés rapidement (en 20 ms), dû à des conductances rectificatrices externes qui dépendent du voltage et du calcium. Ces propriétés intrinsèques des motoneurones pourraient interagir avec la pulsion synaptique rythmique pour générer le patron moteur (de 25-75 Hz) des muscles locomoteurs. La génération neuronale de la nage chez le poisson zèbre en voie de développement ressemble donc à la locomotion chez les poissons adultes et chez les vertébrés en général.

Acknowledgments

I thank my supervisor, Dr. Pierre Drapeau, for always supporting my research, for the many discussions, for giving me the freedom to develop my own projects, and for providing a relaxed, enjoyable, and productive environment. Dr. Charles Bourque and Dr. Gerry Pollack of my Supervisory Committee, and Dr. Ronald Chase and Dr. Robert Levine of my Qualifying Exam Committee, provided many suggestions for my project, and I thank them. Chapters Six and Seven of this thesis were done in collaboration with Dr. Declan Ali and Dr. Charles Bourque, and I thank them for the their significant contributions and many stimulating discussions. I thank Dr. Joan Buss for proof reading many of the manuscripts in this thesis and for the countless times I needed the advice of a chemist.

Mr. Guy Laliberté was responsible for raising and breeding the zebrafish used in this study. Drs. J. Dawson and M. Robertson of Queens University, Ontario, provided the high-speed camera and helped with the imaging of larval swimming. Dr. Pascal Legendre provided much guidance in the analysis of miniature postsynaptic potentials. Anonymous reviewers at the Journal of Neurophysiology have provided comments and suggestions for the improvement of Chapters two through seven. I thank you all.

I thank all members of the Drapeau Lab (Dr. Declan Ali, Lauren Brent, Dr. Edna Brustein, Dr. Stefano Catarsi, Mabel Chong, Dr. Joe McDearmid, Brian Pinchuk, and Dr. Louis Saint-Amant) and members of the Bourque/Masoud and David Labs for making these years so enjoyable. I thank Dr. Ted Wiens for

introducing me to neuroscience and Dr. Susan Shefchyk for starting my career as a spinal cord physiologist.

This work was supported by the Canadian Institutes of Health Research (CIHR) and the Natural Sciences and Engineering Research Council (NSERC) though operating grants to P. Drapeau, and a MRC studentship (1998 to 2000) and CIHR Doctoral Research Award (2000 to 2002) to R. R. Buss. I thank the McGill Alma Mater Student Travel Grant Fund and Keystone Symposia Scholarship Fund for providing funds to attend meetings in Sudbury Ontario and Keystone Colorado, and the Marine Biological Laboratory for funds to attend the Methods in Computational Neuroscience course at Woods Hole Massachusets.

Statement of Originality

The study of animal locomotion has interested biologists, physiologists, and philosophers for centuries and there is a wealth of information on the neural control of locomotion in both vertebrates and invertebrates. This thesis examines the development and neural control of swimming in zebrafish and compares the findings with locomotor control in other vertebrates. Zebrafish were chosen for examination because they are an increasingly popular vertebrate genetic model organism and hold promise for identifying genes controlling locomotion and development of locomotor systems. The studies presented in this thesis are the first to examine the neural control of swimming, at the resolution of single, identified cells, during early periods of fish development and in any ray-finned fish. The findings of this thesis contribute to the fields of ichthyology, comparative physiology, locomotor control, and provide a strong foundation for future studies aimed at integrating genetic and physiological approaches to understand motor control.

Contributions of Author

This thesis is based on the work of five papers (Chapters 2, 4, 5 and 6) published in the Journal of Neurophysiology and two manuscripts submitted to the Journal of Neurophysiology (Chapter 7) and the Journal of Comparative Physiology A (Chapter 3). These papers have been modified to produce a more cohesive thesis, and additional material has been added to the introductions and discussions to provide more information for the non-specialist. My contributions to these papers are detailed below.

Chapter 2: from BUSS RR and DRAPEAU P. Physiological properties of zebrafish embryonic red and white muscle fibers during early development. Journal of Neurophysiology 84: 1545-1557, 2000. I conceived, designed, performed, and analyzed the experiments for this study and wrote the manuscript. P. Drapeau provided valuable comments and helped with revisions.

Chapter 3: BUSS RR and DRAPEAU P. Developmental changes in muscle chloride ion permeability. Submitted to Journal of Comparative Physiology A. I conceived, designed, performed, and analyzed the experiments for this study and wrote the manuscript.

Chapter 4: from BUSS RR and DRAPEAU P. Activation of embryonic red and white muscle fibers during fictive swimming in the developing zebrafish. Journal of Neurophysiology 87: 1244-1241, 2002. I conceived, designed, performed, and

analyzed the experiments for this study and wrote the manuscript. P. Drapeau provided valuable comments and helped with revisions.

Chapter 5: from BUSS RR and DRAPEAU P. Synaptic drive to motoneurons during fictive swimming in the developing zebrafish. Journal of Neurophysiology 86: 197-210, 2001. I conceived, designed, performed, and analyzed the experiments for this study and wrote the manuscript. P. Drapeau provided valuable comments and helped with revisions.

Chapter 6: from ALI DW, BUSS RR and DRAPEAU P. Properties of miniature glutamatergic EPSCs in neurons of the locomotor regions of the developing zebrafish. Journal of Neurophysiology 83: 181-191, 2000. This study was designed in equal collaboration (as co-first author) with D. Ali. In this study, the properties of glutamatergic mEPSCs where examined in spinal motoneurons (R. Buss) and reticulospinal neurons (D. Ali). The manuscript was written primarily by D. Ali and P. Drapeau; I wrote approximately 10% of the text.

Chapter 7: BUSS RR, BOURQUE CW and DRAPEAU P. Electrophysiological characteristics of zebrafish motoneurons. Submitted to Journal of Neurophysiology. I conceived, designed, performed, and analyzed the experiments for this study and wrote the manuscript. C. Bourque and P. Drapeau provided valuable contributions in the analysis and interpretation of the results and on the final manuscript.

Publications Arising from Thesis Work

REFEREED PAPERS

DRAPEAU P, ALI DW, BUSS RR and SAINT-AMANT L. In vivo recording from identifiable neurons of the locomotor network in the developing zebrafish. *J Neurosci Methods* 88: 1-13, 1999.

ALI DW, BUSS RR and DRAPEAU P. Properties of miniature glutamatergic EPSCs in neurons of the locomotor regions of the developing zebrafish. *J Neurophysiol* 83: 181-191, 2000.

BUSS RR and DRAPEAU P. Physiological properties of zebrafish embryonic red and white muscle fibers during early development. *J Neurophysiol* 84: 1545-1557, 2000.

BUSS RR and DRAPEAU P. Synaptic drive to motoneurons during fictive swimming in the developing zebrafish. *J Neurophysiol* 86: 197-210, 2001.

DRAPEAU P, BUSS RR, ALI DW, LEGENDRE P and ROTUNDO RL. Limits to the development of fast neuromuscular transmission in zebrafish. *J Neurophysiol* 86: 2951-2956, 2001.

BUSS RR and DRAPEAU P. Activation of embryonic red and white muscle fibers during fictive swimming in the developing zebrafish. *J Neurophysiol* 87: 1244-1241, 2002.

BUSS RR, BOURQUE CW and DRAPEAU P. Electrophysiological characteristics of zebrafish motoneurons. Submitted to *J Neurophysiol*.

BUSS RR and DRAPEAU P. Developmental changes in the chloride permeability of zebrafish muscle. Submitted to *J Comp Physiol A*.

DRAPEAU P, SAINT-AMANT L, BUSS RR, CHONG M, MCDEARMID JN and BRUSTEIN E. Development of the locomotor network in zebrafish. *Prog Neurobiol*. In Press.

ABSTRACTS

BUSS RR, LEGENDRE P, CATARSI S and DRAPEAU P. Inhibitory synaptic activity in zebrafish motor neurons and 'crazy fish' locomotor mutants. *Soc Neurosci Abst* 24: 1318, 1998.

BUSS RR, ALI DW and DRAPEAU P. Properties of synaptic currents and fictive motor behaviors in neurons of the locomotor regions of the developing zebrafish. *Soc Neurosci Abstr 25*: 467.463, 1999.

BUSS RR and DRAPEAU P. Synaptic drive to myotomal motoneurons during fictive swimming in the developing zebrafish. *Soc Neurosci Abstr* 26: 830.811, 2000.

DRAPEAU P, SAINT-AMANT L and BUSS RR. How embryos wiggle and larvae swim. *Zebrafish Development and Genetics*, Cold Spring Harbor, NY, 2000.

BUSS RR and DRAPEAU P. The role of zebrafish embryonic red and white muscle in two fictive motor behaviors: coiling and swimming. *Soc Neurosci Abstr* 27: 830.833, 2001.

BUSS RR and DRAPEAU P. Electrophysiological characteristics of larval zebrafish (Danio rerio) motoneurons. *40th Ann Meet Can Soc Zool*, Sudbury, ON, 2001.

BUSS RR, DRAPEAU P and BOURQUE CW. Synaptic drive to myotomal motoneurons during fictive swimming in the developing zebrafish. *Canadian Physiological Society Winter Meeting*, Mont Tremblant, QC, 2001.

DRAPEAU P, SAINT-AMANT L, BUSS RR, BRUSTEIN E and CHONG M. Zebrafish as an experimental model for understanding the development of locomotor networks. *XXIIIrd International Symposium of the CRSN*. Spinal Cord Trauma: Neural Repair and Functional Recovery, Montreal, QC, 2001.

BUSS RR, SAINT-AMANT L, BRUSTEIN E, CHONG M and DRAPEAU P. Zebrafish as a model for the development of locomotor networks. *Development of the spinal cord and neural crest*, Keystone, CO, 2002.

BUSS RR, BOURQUE CW and DRAPEAU P. Electrophysiological characteristics of zebrafish motoneurons. *Soc Neurosci Abstr* 28: 2002.

List of Abbreviations and Symbols

3,4-AP	3,4-diaminopyridine
AP-5	DL-2-amino-5-phosphonovalerate
CC	crossed caudal projecting reticular interneuron
CiB	circumferential bifurcating interneuron
CiD	circumferential descending interneuron
CNQX	6-cyano-7-nitroquinoxaline-2,3-dione
CoB	commissural bifurcating interneuron
CoBL	commissural bifurcating longitudinal interneuron
CoLA	commissural longitudinal ascending interneuron
CoPA	commissural primary ascending interneuron
CoSA	commissural secondary ascending interneuron
C-start	C-bend escape response
day	days post fertilization
dlf	dorsal lateral fascicle
DoLA	dorsal longitudinal ascending interneuron
E_{Cl}	chloride ion equilibrium potential
EHP	extrinsic hyperpolarizing potential
E_K	potassium ion equilibrium potential
EPP	end-plate potential
EPSC	excitatory postsynaptic current
EPSP	excitatory postsynaptic potential
ER	embryonic red
EW	embryonic white
GΩ	gigaohmn (10^9 ohm)
GABA	gamma-aminobutyric acid
G_{Cl}	chloride ion conductance
hpf	hours post fertilization
IC	ipsilateral caudal projecting reticular interneuron
LCI	late collateral inhibition
llf	lateral longitudinal fascicle
MΩ	megaohm (10^6 ohm)
MCoD	multipolar commissural descending interneuron
mEPC	miniature end-plate current
mEPP	miniature end-plate potential
mlf	medial longitudinal fascicle
mOsm	milliosmole
NMDA	*N*-methyl-D-aspartate
nMLF	nucleus of the medial longitudinal fascicle
P_{Cl}	chloride ion permeability
PHP	passive hyperpolarizing potential
P_K	potassium ion permeability
PSC	post-synaptic current
R_I	input resistance
SD	standard deviation

SE	standard error
T	T-shaped commissural reticular interneuron
TEA	tetraethylammonium
TTX	tetrodotoxin
UCoD	unipolar commissural descending interneuron
VeLD	ventral lateral descending interneuron
VeMe	ventral medial interneuron
VI	voltage-current relation
vlf	ventral lateral fascicle
V_m	membrane potential

Chapter One : Introduction to the Zebrafish Motor System

Studies into the workings of the spinal cord and the control of movements have a rich history dating back more than a century. Prior to the advent of intracellular recording techniques, Sherrington and co-workers (Sherrington 1947) dominated the field with their studies of spinal reflexes in decerebrate cats and dogs. Intracellular recording techniques (Brock et al. 1952) revolutionized the field and permitted the identification of interneuron pathways that mediated these reflexes (Jankowska 1992), a formidable task that continues to this day (Edgley 2001; Hultborn 2001; Jankowska 2001). During locomotion, these reflexes provide sensory feedback to the nervous system for maintaining posture and adapting to changes in terrain. Some interneurons in these reflex pathways are a part of the rhythm generating neuronal network for locomotion and examination of these reflexes has given insight into how locomotion is generated by the nervous system (Burke 1999; McCrea 2001). The study of the neural control of locomotion and spinal reflexes are complementary and often one in the same.

In a comprehensive review of vertebrate locomotor control, Grillner (1975) concluded that there were fundamental similarities in the neural control of locomotion throughout the vertebrate phylogeny. This led to the development of many vertebrate model locomotor systems, including the lamprey (Grillner et al. 1991; Grillner et al. 1998b; Rovainen 1979) and frog embryo (Dale and Kuenzi 1997; Roberts et al. 1986; Roberts et al. 1998), which have provided valuable contributions to our understanding of the neural control of locomotion. These model systems have the experimental advantages of a simpler motor and

sensory system, which is accessible to intracellular recording techniques and pharmacological manipulation. Unfortunately, these locomotor model organisms have not been chosen as genetic model organisms and the use of modern molecular and genetic techniques is not feasible. Embryonic and larval zebrafish share with the established locomotor model organisms the advantages of a simpler nervous system as well as the advantage of being an increasingly utilized model for the study of vertebrate development, where modern genetic and molecular techniques are routinely used and are increasingly being developed. The goal of this Thesis is to show that it is feasible to study locomotor control in larval zebrafish and to develop zebrafish as a vertebrate model organism for studying the neural control of locomotion. As a first step, I examined the development of the zebrafish locomotor unit and its activation during fictive swimming. The findings are compared with what is known about locomotor control in other vertebrates and many fundamental similarities are found with other vertebrates. To begin, I review the zebrafish nervous and muscular systems involved in locomotion and then present my findings on the development of the zebrafish motor unit.

Development of Zebrafish Motor Behaviors

During embryonic and larval development, zebrafish show several stereotypic motor behaviors that have been described in varying detail by a number of investigators (Budick and O'Malley 2000a; Eaton and Farley 1973; Fuiman and Webb 1988; Grunwald et al. 1988; Kimmel et al. 1974; Myers et al. 1997; Saint-Amant and Drapeau 1998). The first motor behavior, slow and

spontaneous side-to-side coiling contractions of the trunk and tail, is observed at approximately 17 hours post fertilization (hpf; fish raised at 28.5 °C). The spontaneous coiling contractions reach a rate of 1 Hz by 19 hpf and then slow to 0.1 Hz or less by 26 hpf. The first response to touch, a more vigorous coiling contraction, where the tail wraps around the head, is observed at 21 hpf and swimming is later observed at 26 hpf. At 26 hpf, tail touch evokes a partial coiling contraction while head touch evokes a full coil of the tail around the head. At 26 hpf, swimming undulations are slow (approximately 7 Hz) and increase to 30 Hz at day 1.5 and up to 100 Hz at day 2.5. At hatching (after day 2), larvae swim only infrequently and in sustained bursts of high-frequency undulations. By day 4, the swimming style changes to an intermittent beat-and-glide pattern where there is a brief (approximately 200 ms) period of active tail undulation followed by a longer and more variable period of rest and gliding. When startled, larvae make a fast C-bend (or C-start) that is often followed by robust and rapid swimming (30-75 Hz) with a large degree of yaw (14-27°). Routine swimming is characterized by a slower undulation rate (25-40 Hz) where most of the undulation is in the tail and there is very little yaw (<3°). Slow turns may precede a bout of swimming. In addition to the intensively studied C-start, which may or may not be followed by swimming, startle can also initiate pectoral fin movements, evoke a slight tail flexure, or vigorous tight coiling and twisting tail movements.

Adult zebrafish are strong swimmers (undulations from 16-56 Hz) that are not easily fatigued and, for their size, are among the fastest swimming teleost fishes (Liu and Westerfield 1988; Plaut 2000; Plaut and Gordon 1994).

Intermittent swimming, startle evoked C-bends and struggling behaviors are observed in adult zebrafish (Fuiman and Webb 1988; Liu and Westerfield 1988; Muller et al. 2000).

The zebrafish motor behaviors are generated by the axial locomotor muscles, which are innervated by spinal motoneurons that are synaptically driven by spinal interneurons and neurons descending from the brain. This introduction examines the development, anatomy, neurophysiology and function of zebrafish locomotor muscle and neurons (motor and sensory) located within, or with projections to, the spinal cord. The motor systems of related (*i. e.*, ray-finned fishes) fish species where neurophysiological investigations have been more comprehensive are then compared to those of the zebrafish and inferences are made. For brevity, jawless fishes and chondrichthyes are not discussed in the general introduction but are, where relevant, in later Chapters.

Body Segmentation

Body segmentation is clearly visible in the trunk and tail where the axial musculature is divided into approximately 30 myotomes (Kimmel et al. 1995; Myers 1985). The spinal cord is also segemented (Myers 1985) and each spinal segment corresponds to a myotomal segment, except for the most caudal segments that contain ciliated epithelial cells and are devoid of neurons (Myers 1985). Segments 5 to 20 are very similar in gross morphology and contain serially homologous sets of spinal neurons (Bernhardt et al. 1990; Myers 1985). Rostral segments have neurons common to both the spinal cord and hindbrain, which is divided into 9 neuromeres (Hanneman et al. 1988; Metcalfe et al. 1986;

Trevarrow et al. 1990) and segments caudal to 20 have not been investigated. In cross section, the spinal grey mater takes the shape of an inverted Y after two weeks of development and grey and white mater is distinguishable at the 30 somite stage (Hisaoka and Firlit 1960; Weis 1968).

Development of Locomotor Muscle

At approximately 11 hpf (in rostral somites), midline Hedgehog signals induce medial paraxial mesoderm to differentiate into adaxial muscle precursor cells (Barresi et al. 2000; Blagden et al. 1997; Coutelle et al. 2001; Currie and Ingham 1996; Devoto et al. 1996; Du and Dienhart 2000; Du et al. 1997; Lewis et al. 1999; Norris et al. 2000). The *ubo* gene acts downstream of Hedgehog signaling pathways, through activation of the slow muscle-specific homeobox gene *prox1*, to direct the specification and differentiation of slow fiber types (Roy et al. 2001). One population of adaxial cells maintains its medial location and develops into the first contractile myotomal fibers, the muscle pioneers, and a second population migrates laterally where they elongate and form the mononucleate superficial embryonic red muscle (ER) (Devoto et al. 1996; Stickney et al. 2000). ER fibers are thought to develop into adult red muscle rim. Ectopic expression of *Dorsalin-1*, a TGF-β gene family member, prevents differentiation of muscle pioneers, which indicates that spatially restricted TGF-β signals may be involved in differentiation of adaxial cell precursors into muscle pioneers and ER fibers *via* inhibition of Hedgehog signaling pathways (Du et al. 1997). The myogenic regulatory factors *myf5* and *myoD* are early markers

expressed in adaxial cells (Coutelle et al. 2001; Weinberg et al. 1996).

Lateral paraxial mesoderm later differentiates into lateral presomitic muscle precursor cells independently of Hedgehog signaling, ultimately forming the multinucleate embryonic white (EW) fibers that constitute the bulk of the myotomal muscle. EW fibers develop into adult white muscle. *MyoD* and *Myf5* expression also occurs in lateral presomitic cells but at a later stage of development (Coutelle et al. 2001). Additional slow fiber types are added during late larval development and arise from dorsal and ventral myogenic precursors independent of Hedgehog induction (Barresi et al. 2001). There are at least 5 types of muscle in the adult zebrafish. These include the superficial adult red layer, intermediate pink layer, deep white layer, scattered dorsal and ventral fiber layer, and the red muscle rim layer (van Raamsdonk et al. 1978; van Raamsdonk et al. 1980; van Raamsdonk et al. 1982a; van Raamsdonk et al. 1987; Waterman 1969).

When embryonic myotomal segments first form they are block shaped with ER and EW fibres running parallel to the notochord. Within a few hours, the deeper EW fibers take on their characteristic oblique chevron-shaped (V) orientations and ER fibers retain their parallel orientation forming a blanketing layer of approximately 30 fibers per segment (van Raamsdonk et al. 1974). Primitive myofibrils are first observed in the caudal segments (van Raamsdonk et al. 1974), primary motoneurons form the first synapses onto muscle pioneers (Melancon et al. 1997), and the first spontaneous coiling contractions (reviewed above) are observed at approximately 17 hpf. At this time EW and ER (including muscle pioneers) are the only muscle fiber types present (Stickney et al. 2000;

van Raamsdonk et al. 1982b; Waterman 1969). EW fibers are innervated soon afterwards and a second stage of motoneuronal innervation begins at approximately 26 hpf (Myers et al. 1986) when innervation by secondary motoneurons begins and undulatory swimming is first observed. Myotomal morphology changes dramatically from the simple chevron (V) shape of the embryo to the more complicated (W) shape of the adult myotome, which is optimized for power production during undulatory swimming (Mos and van der Stelt 1982; van Raamsdonk et al. 1974).

Locomotion and Muscle Recruitment

Liu and Westerfield (1988) examined the activation of zebrafish axial muscle during swimming. Electomyographic recordings showed that adult white muscle was active at a range of swimming speeds, but unfortunately red or pink muscles were not examined. In fishes with muscular systems organized similarly to zebrafish (*e. g.*, goldfish and sunfish), red muscle is active during slow steady undulatory swimming, pink muscle is recruited at intermediate speeds, and both are maximally active at the fastest steady swimming speeds. Swimming becomes unsteady at even greater speeds when white muscle is recruited and red muscle de-recruited during short bursts of high-speed swimming. All muscle is maximally activated in the escape response (Bone 1978; Coughlin and Rome 1996; Jayne and Lauder 1996). This pattern of recruitment has been observed in a wide range of fishes and is likely to be true for the zebrafish as well.

Similar to other vertebrates (Jordan 1998), locomotion can be evoked in ray-finned fishes (goldfish and carp) by electrical or chemical stimulation of a

region of the midbrain, the mesencephalic locomotor region (Fetcho and Svoboda 1993; Kashin et al. 1974; Uematsu and Ikeda 1993; Uematsu and Todo 1997). Furthermore, the swimming rhythm can be reset by activation of the hindbrain Mauthner neuron (Svoboda and Fetcho 1996), a phenomenon similar to the reseting of the tetrapod step cycle by sensory afferent activation (Burke 1999).

Development of Spinal Motoneurons

Spinal motoneurons undergo two waves of neurogenesis during embryonic development. In each hemi-segment, a population of 3-4 large primary motoneurons exit the cell cycle between 9 and 16 hpf and a larger population (approximately 20) of smaller secondary motoneurons exit the cell cycle from 15-25 hpf (the last age examined) (Bernhardt et al. 1990; Eisen et al. 1990; Myers 1985; Myers et al. 1986). Primary motoneurons migrate from the ventral neural rod to their final, more dorsal location, between 18 hpf and day 2 (Myers et al. 1986). Some primary motoneurons are transiently dye coupled prior to exiting the spinal cord (Eisen et al. 1989). Axons form as early as 18 hpf in primary motoneurons and secondary motoneurons follow on average 6 hours later (Myers et al. 1986). The innervation of muscle by primary motoneurons (Liu and Westerfield 1990; Liu and Westerfield 1992) is closely correlated with observations of the first embryonic movements (Myers et al. 1986; Saint-Amant and Drapeau 1998) and rhythmic activity in primary motoneurons (Saint-Amant and Drapeau 2000). By day 5, primary motoneurons have developed elaborate dorsal and rostal-caudal dendritic trees and processes from their ventrally

projecting axons (Myers 1985). Secondary motoneurons develop similar dorsal, but smaller rostral-caudal, dendritic trees and their fine axons lack processes (Myers 1985).

Two anatomically distinct classes of muscle fibers (ER and EW) are present at day 5 (see Development of Locomotor Muscle), but it is not known if these are selectively innervated by primary and secondary motoneurons. However, primary motoneurons, and at least some secondary motoneurons, innervate larval EW muscle (Liu and Westerfield 1990; Myers et al. 1986). The number of motoneurons increases from less than two dozen at day 5 (Myers 1985) to 60-80, the adult complement, which is reached by 3 weeks (van Raamsdonk et al. 1983; Westerfield et al. 1986). A number of these new motoneurons likely innervate the growing population of adult red muscle, which is innervated by approximately half of the motoneurons (van Raamsdonk et al. 1983). Contralateral primary and secondary motoneurons are active during escape responses activated by head touches whereas only secondary motoneurons are activated in the ipsilateral spinal cord (Fetcho and O'Malley 1995).

There is a greater number of motoneurons in adult zebrafish and this is associated with the greater diversity of muscle fiber types, which include the anatomically distinct white, pink and red muscle populations (see Development of Locomotor Muscle). The ability to inject axonal tracers into distinct muscle populations has allowed the retrograde labeling and identification of innervating motoneurons (de Graaf et al. 1990; van Raamsdonk et al. 1996; van Raamsdonk et al. 1983). The motoneurons to white muscle (white motoneurons) have the

most dorsal location and motoneurons to red muscle (red motoneurons) have the most ventral location in the longitudinal column in the ventral spinal cord. Motoneurons located between the red and white motoneuron pools (intermediate motoneurons) innervate pink (intermediate) muscle, although there is a partial overlap of the intermediate motoneuron pool with the red and white motoneuron pools (de Graaf et al. 1990; van Raamsdonk et al. 1996; van Raamsdonk et al. 1983). Red motoneurons have the smallest somata and white motoneurons the largest (de Graaf et al. 1990; van Asselt et al. 1993; van Raamsdonk et al. 1983). Examination of the histochemical profiles of five enzymes involved in glucose metabolism led De Graaf et al. (1991) to suggest that red and pink motoneurons are fueled by oxidative metabolism (like the muscle they innervate) while glycolysis plays a greater role in white motoneurons.

Westerfield et al. (1986) has identified 3 large motoneurons in adult zebrafish, with arborizations corresponding to those of the first developing embryonic primary motoneurons (Liu and Westerfield 1990; Myers 1985), as well as numerous small motoneurons, with more restricted arborizations, that are classified as secondary. However, the development of secondary motoneurons from embryonic to adult stages has not been examined and it is probable that the embryonic secondary motoneurons develop into what Westerfield et al. (1986) calls secondary motoneurons as well as into the motoneurons that innervate the later forming muscle types (*e. g.*, pink or red). It is well established that the red, pink and white muscle populations are recruited at different swimming speeds (see Locomotor and Muscle Recruitment) and it is important, both functionally and physiologically, to characterize motoneurons based on the muscle they

innervate and not simply by their size. However, using their definition of adult primary and secondary motoneurons, Liu and Westerfield (1988) concluded (based on electromyograph waveforms) that secondary motoneurons are active during slow swimming, while primary motoneurons are active during fast swimming (swimming undulations ranged from 16-56 Hz), the startle response and struggling.

In addition to axial motoneurons, a population of less than 30 motoneurons (located in segments 3-6) innervates the pectoral fin muscle (Myers 1985). In adult fishes, pectoral fins are used for a variety of functions including slow swimming, steering and braking (Breder 1926; Lindsey 1978). Pectoral fins rhythmically flex and extend in larval zebrafish, but the function of this movement (Schneider et al. 2001) and the development of these motoneurons has not been investigated.

Spinal Interneurons

Zebrafish spinal interneurons have been divided into ten classes (Table 1.1), based on anatomical (but not physiological) characteristics and time of neurogenesis (Bernhardt et al. 1990; Hale et al. 2001). The neurotransmitter phenotype is also known for some interneurons (Bernhardt et al. 1992; Higashijima et al. 2001; Martin et al. 1998). All described interneurons are propriospinal, having either ipsilateral or commissural axons that extend rostrally, caudally or bifurcate through the dorsal lateral fascicle (dlf) or ventral lateral fascicle (vlf). As the retrograde labeling technique used to identify spinal interneurons would only label neurons with long axonal projections, it is not

known if additional local spinal interneurons (restricted to 1-3 segments) exist. In addition to interneurons, there are also approximately 20 ventral floor plate cells and approximately 5-8 Kolmer-Agduhr cells that contact the central canal and express GAD65, GAD67 (enzymes in the pathway for GABA synthesis) and show GABA immunoreactivity (Bernhardt et al. 1992; Kuwada et al. 1990b; Martin et al. 1998).

By 18-20 hpf, up to 7 neurons have undergone axogenesis in each segment. These neurons include the VeLD, DoLA, CoPA and CoSA interneurons, which are joined by CiD, CiA and CoB interneurons by 22-23 hpf (Bernhardt et al. 1990; Kuwada et al. 1990a; Kuwada et al. 1990b). Saint-Amant and Drapeau (2001) recorded from these embryonic interneurons, when the embryonic coiling behavior was occurring, and found that varying proportions of individual interneurons in these classes (except for the DoLA) were active. VeLD and CoPA interneurons were nearly always active, whereas many of the later forming secondary interneurons were not. Gap junctional coupling synchronized the activity of the active interneurons and chemical synaptic transmission played no role in the generation of this rhythmic behavior (Saint-Amant and Drapeau 2001). Presumably, intrinsic pacemaker properties of individual or connected populations of interneurons pattern the rhythmic activity underlying embryonic coiling contractions. It was hypothesized that with maturity, the then inactive secondary interneurons would be added to the active network (Saint-Amant and Drapeau 2001). However, it is also possible that the anatomically defined interneurons are not functionally homogenous populations. For example, interneurons classified as CoSA are not all GABAergic (Bernhardt et al. 1992;

Martin et al. 1998).

Two ipsilateral interneurons, the DoLA (dorsal longitudinal ascending) and VeLD (ventral lateral descending) interneurons have only been described in embryos. DoLA interneurons are located in the dorsal spinal cord and have an axon that ascends in the dlf and terminates in the hindbrain (Bernhardt et al. 1990; Kuwada et al. 1990a). There are very few DoLA interneurons in the spinal cord. VeLD interneurons are located in the ventral spinal cord and descend less than 10 segments in the vlf (Bernhardt et al. 1990; Kuwada et al. 1990a). Both DoLA and VeLD interneurons react with GABA antibodies and express GAD65 and GAD67 (Bernhardt et al. 1992; Martin et al. 1998). Whether these neurons die or dramatically change morphology in the adult is unknown. Hale et al. (2001) suggested that VeLD interneurons transform into commissural MCoD (multipolar commissural descending) interneurons. However, since interneurons originally classified as VeLD have a GABAergic phenotype, and the MCoD interneurons have a glutamatergic phenotype (based on the expression of glutamate transporter genes; Martin et al. 1998), the transformation of VeLD into MCoD interneurons would also have to include a change in neurotransmitter phenotype.

Less is known about the function of inteneurons at larval stages. There are many more interneuron classes at larval stages and there is evidence supporting functional divisions within classes. Interneuronal synaptic connectivity is unknown, neurotransmitter phenotypes are just beginning to be investigated and motor and sensory functions are largely unknown. In the adult, premotor interneurons to white and red/pink motoneurons have been labeled transynaptically (although with low definition) by injecting wheat-germ agglutinin

into white or red/pink muscle (van Asselt et al. 1991).

The activation of CiD and MCoD interneurons during escape and swimming has been examined using calcium imaging by Ritter et al. (2001). CiD interneurons were only active during escape behaviors and not swimming whereas MCoD were only active during swimming but not escape. Thus, Ritter et al. (2001) concluded that the interneurons have unique roles in escape or swimming. However, this study only examined very slow swimming rates (13-29 Hz) and an alternative explanation (which is dismissed in their discussion) is that CiD interneurons are not recruited at slow swimming speeds. In light of the complex patterns of muscle recruitment observed in larval zebrafish (Chapter 4), the functional roles of CiD interneurons should be re-evaluated.

Hindbrain, Midbrain and Forebrain Projections to the Spinal Cord

Nineteen distinct brain nuclei, located in the diencephalon, mesencephalon and hindbrain, project to the spinal cord of the adult zebrafish (Table 1.2) (Becker et al. 1997; Lee and Eaton 1991; Wullimann et al. 1996). The development of descending projections has been investigated from their first appearance to approximately day 6, a time prior to the formation of all descending tracts. In the larval zebrafish, the majority of descending projections arise from the reticular formation (approximately 50 neurons on each side of the midline) and caudal hindbrain (number unknown, likely >30 neurons) with minor projections from the vestibular nucleus (approximately 8 neurons) and midbrain (<10 neurons) (Kimmel 1982; Kimmel et al. 1982; Kimmel et al. 1985; Mendelson 1986a; Mendelson 1986b; Metcalfe et al. 1986). These larval neurons, as well as

neurons that have not yet developed, persist into adult life (Lee and Eaton 1991).

Most larval, and many adult, reticulospinal neurons can be uniquely identified based on morphology and have been divided into three groups (rostral, Ro; middle, Mi; caudal, Ca) based on their rostral-caudal location in the hindbrain (Kimmel 1982; Kimmel et al. 1982; Lee and Eaton 1991; Mendelson 1986a). Reticulospinal neurons have either ipsilateral or contralateral projections that descend though the spinal cord in either the medial longitudinal fascicle (mlf) or the lateral longitudinal fascicle (llf). Nearly all reticulospinal neurons project caudally as far as segment 15, but only 2 descend to segment 25 (Metcalfe et al. 1986). The majority of reticulospinal neurons send an ipsilateral projection into the spinal cord that descends in either the mlf (approximately 28 neurons) or the llf (approximately 13 neurons). There are fewer reticulospinal neurons with contralateral projections (approximately 3 project in the mlf and 9 in the llf). The intensively studied Mauthner neuron is included in this group (Eaton et al. 1977b). Some reticulospinal neurons express GAD65 or GAD67 indicating an inhibitory phenotype, but the majority are likely excitatory glutamatergic neurons (Martin et al. 1998). Reticulospinal neurons exit the cell cycle at times ranging from 6 to 30 hpf and the birth dates of identified reticulospinal neuron has been determined; *e. g.*, the Mauthner neuron is the first born reticulospinal neuron exiting the cell cycle at an average age of 7.5 hpf (Mendelson 1985; Mendelson 1986b) and axogenesis begins approximately 10 hours later (range 10-19 hours) at a rate of approximately 100 μm per hour (Mendelson 1986a). There are two waves of axogenesis among the population of reticulospinal neurons, one

beginning at 20-24 hpf and the second at 30-34 hpf (Mendelson 1986a).

Classically the Mauthner neuron has been considered as a command neuron for activating the C-start (DiDomenico and Eaton 1988; Nissanov and Eaton 1989). A key finding supporting this view came from studies in larval zebrafish where γ-irradiation of whole embryos just prior to Mauthner neuron birth ablated the Mauthner neuron and abolished the C-start response (Eaton and Kimmel 1980; Kimmel et al. 1980). However, as it is now known that over 80% of reticulospinal neurons are activated during the head tap evoked startle response (Gahtan et al. 2002; O'Malley et al. 1996), γ-irradiation undoubtedly affected more than Mauthner neurogenesis.

The Mauthner neuron is the most intensively studied neuron in the zebrafish. The Mauthner axon emerges at 17-18 hpf (Kimmel et al. 1990) and projects to the spinal cord by 20 hpf, when vesicle filled axonal swellings, presumed synaptic contacts, are observed (Jontes et al. 2000). The lateral dendrite is distinguishable by 22-23 hpf (Kimmel et al. 1990) and an adult morphology is present by day 6 at which time many distinct synaptic structures, both chemical and electrical, have formed (Kimmel et al. 1981). Trigeminal and cranial nerve VIII afferents reach the Mauthner neuron at approximately 18 hpf and 23 hpf respectively (Kimmel et al. 1990). A large extracellular spike, associated with the C-start, can be recorded when the Mauthner neuron spikes (Eaton and Farley 1975) and one study has reported that this spike is large enough to be recorded outside the body (Prugh et al. 1982). However, it is more likely that the externally recorded activity is a compound spike composed of the

population of neurons and muscle fibers active during the startle response (Featherstone et al. 1991). Intracellular recording has shown that the Mauthner neuron of the adult zebrafish fires a single action potential when activated (Hatta and Korn 1998) whereas a short burst of spikes is observed in larvae (Drapeau et al. 1999). This difference could be due to incomplete development of recurrent and reciprocal inhibitory circuits in the hindbrain (Takahashi et al. 2000) but this remains to be determined (see The Mauthner Neuron). The C-bend remains after laser ablation of the Mauthner neuron but the latency to and speed of the C-bend is decreased (Liu and Fetcho 1999). The Mauthner neuron itself is preferentially activated by tail touch whereas its segmental homologues (MiD2cm and MiD3cm) respond to head touch (Eaton et al. 1984; O'Malley et al. 1996). Examination of mutant zebrafish (Granato et al. 1996), such as *space cadet* (Lorent et al. 2001), that have abnormal startle responses, may lead to a greater understanding of this behavior. The kinetics of glycine-gated chloride channels and development of glycinergic synapses has been examined in the zebrafish Mauthner neuron (Ali et al. 2000b; Imboden et al. 2001a; Imboden et al. 2001b; Legendre 1997; Legendre 1998; Legendre 1999; Legendre and Korn 1994; Legendre and Korn 1995; Suwa et al. 2001; Triller et al. 1997). The hindbrain and spinal circuitry of the Mauthner neuron has been more fully examined in the adult goldfish (see The Mauthner Neuron) and a comparative study has shown it to be indistinguishable from the zebrafish (Hatta and Korn 1998).

Three classes of descending neurons (T interneurons, CC interneurons and IC interneurons) are located in the caudal hindbrain (between the caudal reticular formation and rostral spinal cord) (Kimmel et al. 1985). T interneurons

(approximately 10) have a bifurcating commissural axon that ascends as far as the midbrain tegmentum (to innervate the occulomotor and numerous cranial nerve nuclei) and descends to the pectoral (fin motoneuron) motor nucleus. Many collaterals arise from both the ascending and descending axons and project to the cell bodies of reticulospinal neurons including the Mauthner. The cell bodies of T interneurons are in close proximity to ascending spinal tracts (likely sensory), the descending tract of the trigeminal nerve, and descending reticulospinal tracts. T interneurons are homologous to goldfish cranial relay neurons and hatchetfish giant fibers (Barry and Bennett 1990; Kimmel et al. 1985). Hatchetfish giant fibers project to the trigeminal, facial and pectoral fin motor nuclei and their activation is believed to lead to closure of the operculum and mouth, and adduction of the pectoral fins, during the escape response. The C-start and associated adduction of the large pectoral fins propels the more streamlined (due to mouth and operculum closure) hatchetfish forwards and upwards (often out of the water) during the startle response (Wiest 1995). Morphological and electrophysiological studies have shown chemical monosynaptic connections from the Mauthner neuron to giant fibers (bilateral) and direct electrical activation of an electrically coupled pool of pectoral fin adductor motoneurons (Auerbach and Bennett 1969a; Auerbach and Bennett 1969b; Barry and Bennett 1990; Day et al. 1985; Gilat et al. 1986; Hall et al. 1985; Huse et al. 1985; Model et al. 1972). The homologous T interneurons in larval zebrafish are activated by head-taps (Gahtan et al. 2002) and likely function in streamlining, balancing or propelling the larva during the startle response.

CC interneurons are interspersed among T interneurons and differ in

having only a descending commissural projection and a more extensive dendritic tree (Kimmel et al. 1985). The number of CC interneurons, their sites of spinal termination, and behavioral roles have not been reported. T and CC interneurons have not been observed in labeling experiments performed at 24 hpf and when they exit the cell cycle is unknown.

The third class of neurons in the caudal hindbrain, which also project into the rostral spinal cord are the ipsilateral descending IC interneurons (Kimmel et al. 1985). IC interneurons are the first hindbrain neurons to project into the spinal cord (in the mlf) at 19-20 hpf. The first ascending spinal projections, originating from Rohon-Beard neurons (Bernhardt et al. 1990), enter the caudal hindbrain (*via* the llf) at this time in close proximity (as observed using light microscopy) with IC dendrites. If synaptic contacts are made, this would be the first spino-reticulospinal reflex pathway. This pathway might play a role in coordinating spontaneous coiling contractions and the embryonic touch response that appears at 21 hpf. IC interneurons are active during spontaneous embryonic coiling contractions (Saint-Amant and Drapeau 2001) but not during head-tap evoked C-starts in day 5-7 larvae (Gahtan et al. 2002).

The octavolateralis area of the adult zebrafish contains 6 nuclei that have spinal projections. There are only 8-10 descending vestibulospinal neurons in larval zebrafish (Kimmel 1982; Kimmel et al. 1982; Metcalfe et al. 1986), which are thought to correspond to the adult magnocellular octaval nucleus. The first vestibulospinal neurons project to the rostral spinal cord (in the mlf) by 30-34 hpf (Mendelson 1986a). Vestibulospinal neurons have not been examined electrophysiologically or by using calcium imaging. They are expected to respond

to changes in body orientation and acceleration.

The midbrain population is made of 4-10 neurons located in the nucleus of the medial longitudinal fascicle (nMLF) and project descending ipsilateral axons to the spinal cord in the mlf (Kimmel 1982; Kimmel et al. 1982). These neurons are born at approximately 12 hpf, axons are first observed in the rostral spinal cord at approximately 24 hpf, and by 36 hpf all neurons in the population have projected to the rostral spinal cord (Mendelson 1986a; Mendelson 1986b). At least some neurons in the nMLF respond to head-taps (Gahtan et al. 2002). Laser ablation of these neurons does not affect measured kinematic variables in the escape response or swimming although it leads to occasional, multiple, spontaneous C-bends in larvae (Budick and O'Malley 2000b). Neurons in the nMLF are immunoreactive to GABA (Doldan et al. 1999), which suggests an inhibitory role consistent with the multiple C-starts observed after their ablation.

In the adult zebrafish, there is a dense horizontal band of catecholaminergic varicosities just dorsal to the central canal as well as diffuse varicosities at more dorsal and ventral locations (Ma 1997). The spinal catecholaminergic fibers likely originate from the three medullary catecholaminergic groups described by Ma (1997) and from the locus coeruleus (Ma 1994a; Ma 1994b), as there are no catecholaminergic cell bodies in the spinal cord (Ma 1997). Catecholaminergic cell bodies and fibers have been reported in the locus coeruleus and rostral spinal cord, respectively, at approximately 28 hpf and the adult complement of locus coeruleus neurons (<10) is present by day 4 (Guo et al. 1999). The medullary catecholaminergic groups were not observed at the early larval stages examined by Guo et al. (1999).

Serotonergic fibers are distributed through large areas of the adult zebrafish spinal cord but are in highest density in the dorsal and lateral neuropil, the motoneuron pool, and the ventro-medial spinal cord (van Raamsdonk et al. 1996). The dorsal and lateral fibers arise from descending brainstem neurons (van Raamsdonk et al. 1996), likely the inferior raphe nuclei described by Becker et al. (1997), whereas the ventral fibers arise from serotonergic neurons intrinsic to the spinal cord (van Raamsdonk et al. 1996). Serotonergic cell bodies are present in the hindbrain and spinal cord by 2 days of development (Brustein et al. 2000). At this time the serotonergic innervation of the spinal cord arises from intrinsic interneurons as hindbrain neurons have not begun their descent into the spinal cord at day 5. Larva do not show a behavioral response to serotonergic agonists or antagonists until after day 4 when a beat-and-glide style of swimming has developed (Brustein et al. 2001). At this time, serotonin increases the occurrence and number of cycles of beat-and-glide swimming, while serotonergic antagonists reduce the occurrence of swimming as well as the number of consecutive beat-and-glide swimming cycles.

Cutaneous Free Nerve Endings

Rohon-Beard neurons are a transient population of cutaneous primary sensory neurons located in the dorso-lateral spinal cord. They undergo programmed cell death by day 3.5-5 and are replaced by dorsal root ganglion neurons (Bernhardt et al. 1990; Svoboda et al. 2001; Williams et al. 2000). Rohon-Beard neurons are first observed at 15 hpf, most have axons by 24 hpf, and by day 3-5 they number 1-4 per segment (Bernhardt et al. 1990; Kuwada et

al. 1990a). Their axon bifurcates and projects in the dlf caudally (up to 10 segments) and rostrally to the level of the otolith, where they pass over the lateral dendrite of the Mauthner neuron (Bernhardt et al. 1990). By day 3-4, when many Rohon-Beard neurons are undergoing programmed cell death (Williams et al. 2000), there is approximately 1 dorsal root ganglion neuron per segment (Bernhardt et al. 1990). Similar to Rohon-Beard neurons, dorsal root ganglion neuron axons have both ascending and descending projections (up to 10 segments) in the dlf (Bernhardt et al. 1990). Rohon-Beard neurons were the first electrophysiologically characterized spinal neurons in zebrafish (Ribera and Nusslein-Volhard 1998). Whole-cell patch clamp recordings made from the soma revealed a resting membrane potential of approximately -70 mV, a TTX sensitive action potential and voltage activated potassium currents, but no spontaneous synaptic inputs (Ribera and Nusslein-Volhard 1998). Electrical stimulation of the body surface induces a calcium transient in larval Rohon-Beard neurons (Fetcho and O'Malley 1995). The sensory physiology of the Rohon-Beard and dorsal root ganglion neurons has not been investigated; for example, it is unknown if or when in development any of these sensory neurons respond to pain or thermal stimuli. Furthermore, synaptic targets of these neurons in the spinal cord and hindbrain have not been investigated.

Cutaneous sensation in the head is mediated by trigeminal ganglia afferents that enter the hindbrain *via* the trigeminal nerve and project (in the dlf) as far as the rostral spinal cord by 22-24 hpf (Kimmel et al. 1990; Mendelson 1986a). Trigeminal afferents pass by many hindbrain neurons, chemical synapses onto the Mauthner neuron have been reported, and it is likely that

synapses are made on other hindbrain neurons (Kimmel et al. 1990). Olfactory receptors are also present on the dermis of many fish and the trigeminal nerve may also contain these gustatory afferents (Kotrschal et al. 1991).

Lateral Line - Neuromast System

In addition to the sensory free nerve endings, arising from Rohon-Beard or dorsal root ganglia neurons, sensory neuromasts, free or within lateral line structures, are also distributed on the skin surface (Metcalfe 1989). Neuromasts contain a cluster of sensory hair cells that respond to local water currents (Dijkgraaf 1962). They are innervated by afferent fibers originating in the anterior and posterior lateral nerve ganglia (located at the level of the otolith) and efferent fibers originating in the rostral and caudal rhombencephalic nuclei (cholinergic neurons) and diencephalic nuclei (catecholaminergic neurons) (Bricaud et al. 2001; Metcalfe et al. 1985; Raible and Kruse 2000). Afferent fibers are ipsilateral with arborizations in the hindbrain that are in close proximity to the octavolateral nuclei and reticulospinal neurons, including the Mauthner neuron (Metcalfe et al. 1985). Lateral line afferents first make contact with the Mauthner neuron at approximately 25 hpf (Kimmel et al. 1990). The posterior lateral line ganglia is first present at 18 hpf while the anterior ganglia forms between 24 and 40 hpf (Raible and Kruse 2000). Neuromasts form soon after and by day 4 the adult complement of lateral lines and associated neuromasts are present (Raible and Kruse 2000). In addition to their efferent projection to neuromasts, which is largely complete by day 3, diencephalic catecholaminergic neurons also project into the spinal cord, reaching the 12th somite by 56 hpf (Bricaud et al. 2001).

Sensory Evoked Reflexes

In larvae and adult zebrafish, tactile stimulation of the head or trunk leads to either a C-start, rapid swimming away from the stimulus, or a combination of both. During development, responses to tactile stimulation are first observed at 21 hpf when head or tail touch evokes a coiling of the trunk and tail around the head (Saint-Amant and Drapeau 1998). The embryonic response to touch is likely relayed *via* Rohon-Beard neurons as it appears prior to the differentiation of dorsal root ganglion neurons and sensory neuromasts. Larval and adult responses likely involve neuromast afferents and dorsal root ganglia neurons (as well as Rohon-Beard neurons during the first week of larval development).

All three sensory systems send projections to the hindbrain where they activate a hindbrain initiated startle response. Acoustic, vibration, or visual stimuli can also initiate this hindbrain initiated startle response, and an understanding of this behavior and how it is generated by the nervous system has been subject to much investigation. It is not known if the startle response is entirely due to the activation of descending reticulospinal commands, or if local spinal reflexes also contribute to the response.

The Mauthner Neuron

The C-start is the most extensively investigated motor behavior in zebrafish. The Mauthner neurons and their postsynaptic targets are involved in the generation of the C-start and have been examined at a detailed cellular level in many fishes (*e. g.* goldfish) closely related to the zebrafish. The neurobiology of the Mauthner neuron in ray-finned fishes is reviewed and shown to be similar

to zebrafish.

The Mauthner neurons, named for their discoverer Ludwig Mauthner (Seyfarth and Zottoli 1991), are a bilateral pair of neurons located in the medulla oblongata that have contralateral descending axons in the spinal cord. These prominent neurons, found in many fishes and amphibians, captured the interest of early neurologists because of their large size and ease of identification (Stefanelli 1951; Zottoli 1978). The first extracellular recordings of Mauthner axon activity were reported by Graham and O'Leary (1941) and Berkowitz (1956) in catfish and carp, and the first intracellular recordings (soma) were by Tasaki et al. (1954) in catfish. Retzlaff (1957) and Berkowitz (1956) noted that electrical stimulation of fiber pathways containing the Mauthner axon evoked rapid tail flips. These findings were further substantiated by Wilson (1959) who showed that electrical stimulation evoked rapid tail flips only when sharp, short latency, all-or-none spike activity (corresponding to Mauthner neuron activation) was observed in extracellular recordings, thus implicating a critical role for the Mauther neuron in startle responses. Retzlaff (1957) also observed (in bullhead) that both Mauthner neurons could not be evoked to fire simultaneously upon bilateral stimulation of cranial nerve VIII and suggested an ipsilateral excitation and contralateral inhibition by cranial nerve VIII fibers. Together, these studies laid the foundation for our present understanding of the role of the Mauthner neuron in the startle response and the neural circuitry underlying this response (Diamond 1971; Eaton and Hackett 1984; Eaton et al. 2001; Faber et al. 1989; Furukawa 1966; Korn et al. 1990; Nissanov and Eaton 1989; Roberts 1992; Zottoli and Faber 2000).

A series of papers published in the early 1960s (Fukami et al. 1965; Furshpan and Furukawa 1962; Furukawa and Furshpan 1963; Furukawa et al. 1963; Furukawa et al. 1964) established the goldfish as the premier model organism for the neurophysiological examination of the Mauthner neuron. However, many of the properties described in the goldfish have been confirmed in adult winter flounder (Zottoli 1981), gymnotid electric fish (Borde et al. 1991) and zebrafish (Faure and Korn 1997; Faure et al. 2000; Hatta and Korn 1998; Hatta and Korn 1999; Hatta et al. 2001). Antidromic activation (by stimulation of the spinal axon) or orthodromic activation (by stimulation of cranial nerve VIII) have been used to examine the electrical properties of the Mauthner soma and the nature of excitatory and inhibitory synaptic inputs.

Action potentials are initiated at the axon hillock of the Mauthner neuron and passively propagate, attenuating as they do so, into the soma and dendrites (Furshpan and Furukawa 1962). A spike produces a large negative (up to 50 mV) extracellular spike within the axon cap (Furshpan and Furukawa 1962), a dense conglomeration of fine unmyelinated fibers ensheathed by a layer of glia that envelopes the axon hillock and initial segment of the Mauthner neuron (Kohno 1970; Nakajima 1974). Passive dendritic spikes are observed as positive potentials in extracellular recordings made at the soma (current sink) (Furshpan and Furukawa 1962). Within the axon cap, the negative spike is followed (<1 ms) by a positive potential (<15 mV, approximately 1 ms) that does not produce an apparent change in membrane conductance (Furshpan and Furukawa 1962; Furukawa and Furshpan 1963). The positive potential or "extrinsic hyperpolarizing potential - EHP" is inhibitory as it blocks antidromic spikes and

raises EPSP spike threshold (Fukami et al. 1965; Furukawa and Furshpan 1963). The inhibition appears to be the result of an extracellular positivity within the axon cap produced by the passive spread of action potentials into densely packed unmyelinated fibers located within the cap. The large extracellular positivity results in a hyperpolarization, and inhibition, of the Mauthner neuron at the axon hillock. A longer lasting (>10 ms) strychnine-sensitive chloride conductance, capable of attenuating EPSPs and passively propagating spikes, immediately follows the EHP (Diamond et al. 1973; Fukami et al. 1965; Furukawa and Furshpan 1963; Furukawa et al. 1964). This inhibition is referred to as "late collateral inhibition - LCI". The chloride equilibrium potential is close to the resting membrane potential (-70 to -80 mV) in the Mauthner neuron and the shunting chloride conductance is only visualized when neurons are filled with chloride by using KCl electrodes. In addition to the cranial nerve VIII evoked EPSP attenuation, due to a postsynaptic conductance change, a presynaptic inhibition (referred to as "the third type of inhibition"), or possibly a remote inhibition (Diamond and Huxley 1968), mechanism also appears to be present (Furukawa et al. 1963).

Initiation of a spike (antidromic, orthodromic or by intracellular current injection) in one Mauther neuron generates an EHP and LCI in that Mauthner neuron as well as the contralateral Mauthner neuron. Thus, both chemical and electrical inhibition acts to prevent bilateral Mauthner neuron activation. In the event that both Mauthner neurons are activated at exactly the same time, both neurons spike before the inhibitory mechanisms are activated. When this occurs, both Mauthner neurons will propagate spikes into the spinal cord (Yasargil and

Diamond 1968) but a startle response will not occur because of a short latency strychnine-sensitive spinal inhibition of motoneurons (Yasargil and Diamond 1968).

Furukawa and Furshpan (1963) suggested that the EHP was produced by passive spike propagation in small unmyelinated fibers within the axon cap but it was not until Faber and Korn (1973) and Korn and Faber (1975a) that the presence and identity of these neurons was confirmed. Neurons in the vicinity of the axon cap were recorded from that displayed a small hyperpolarization synchronous with the large negative Mauthner neuron extracellular spike, which was termed a "Passive hyperpolarizing potential - PHP' (Faber and Korn 1973; Korn and Faber 1975a). The PHP was inhibitory as it blocked the propagation of spikes. These neurons sent a projection into the axon cap that approached the Mauthner neuron and when stimulated produced a small extracellular depolarization in the axon cap (*i.e.*, an intracellular hyperpolarization and electrical inhibition) and unitary IPSPs in the soma (Korn and Faber 1976; Korn et al. 1978; Triller and Korn 1981; Zottoli and Faber 1980). PHP interneurons with both ipsilateral and contralateral projections were observed, which could subserve the collateral and contralateral inhibition observed upon VIII nerve stimulation. PHP interneurons are not spiral fiber neurons (Scott et al. 1994) as originally suggested. Besides their projections to the Mauthner neurons, projections to reticular and vestibular nuclei were also observed (Korn et al. 1978; Triller and Korn 1981; Zottoli and Faber 1980).

In the spinal cord, the Mauthner axon forms monosynaptic chemical synapses onto contralateral primary motoneurons and descending interneurons,

which are presynaptic and electrically coupled to secondary motoneurons (Fetcho 1992a; Fetcho and Faber 1988). The Mauthner axon also has an electrical connection to glycinergic commissural interneurons that inhibit contralateral motoneurons as well as the excitatory descending interneurons (Fetcho 1990; Fetcho and Faber 1988). Together, these neurons form a spinal circuit that would activate contralateral axial muscle and inhibit the activation of ipsilateral muscle during a C-start.

Sources of Excitation to the Mauthner Neuron

The startle response can be evoked by sound, vibration, visual or tactile stimuli. Most species of fish (including goldfish and zebrafish) respond to startle with a C-bend where there is a short latency unilateral contraction of the trunk and tail into the shape of a C (stage 1) which is followed by a rapid straightening of the tail (stage 2) which propels the fish away (Eaton and Emberley 1991; Eaton et al. 1977a). Fishes such as eels and larval lampreys respond to startle by retracting the head and forming a S shape and in some species the response is a rapid forward burst of swimming (Eaton et al. 1977a). Only the neural control of the C-bend startle has been examined. In addition to its role in the escape response, the Mauthner neuron is also activated during feeding (Canfield and Rose 1993) and its activation increases the frequency of electric organ discharge in gymnotid electric fish (Curti et al. 1999; Falconi et al. 1995).

Saccular afferents located in the posterior branch of cranial nerve VIII are a strong source of excitation to the Mauthner neuron (Casagrand et al. 1999). These afferents form predominantly electric (with a small chemical component)

synapses onto the lateral dendrite (Furshpan 1964; Lin and Faber 1988a; Lin and Faber 1988b; Pereda et al. 1995). The afferents in the vestibular branch of cranial nerve VIII also synapse (predominantly chemical) on the Mauthner neuron (Zottoli and Faber 1979). Spiral fibers, arising from the contralateral trigeminal nucleus, form electrical synapses on the axon hillock and provide another strong source of excitation to the Mauthner neuron (Scott et al. 1994).

Stimulation of the lateral line nerves evokes monosynaptic EPSPs followed by a strychnine sensitive disynaptic IPSP in the soma and proximal lateral dendrite of the Mauthner neuron (Korn and Faber 1975b). Lateral line stimulation also evokes EPSPs in PHP neurons which are facilitated to spike threshold when the collateral inhibitory pathway is activated suggesting that these interneurons are shared and are the source of the lateral line evoked disynaptic inhibition (Faber and Korn 1975). Conversely, Mauthner neuron activation inhibits a disynaptic pathway from the lateral line and excites lateral line efferent fibers which "might" inhibit lateral line receptors (hair cells) (Russell 1974).

Chronic electrode implantation has been used to record the distinct extracellular negative spike of the Mauthner neuron (and likely other co-activated neurons) in the behaving fish. When the ipsilateral Mauthner neuron fires, robust contralateral electromyograph activity or a C-bend away from the ipsilateral side is observed. Startle responses were not observed in the absence of Mauthner neuron firing (Eaton et al. 1981; Zottoli 1977).

Activation of a singe Mauthner neuron activates both ipsilateral and contralateral muscle fibers (Yasargil and Diamond 1968). However, contralateral fibers are activated at a slightly shorter latency and with a greater intensity (Eaton

et al. 1988; Yasargil and Diamond 1968). Co-activation of ipslateral and contralateral muscle during the C-start is prominent in the bowfin and bichir, where it has been proposed to play a role in muscle stiffening for maintaining body form (Westneat et al. 1998). This finding indicates that the spinal organization of the escape response is more complicated than originally proposed.

Summary

Zebrafish display two main locomotor behaviors, C-starts and swimming. The C-start has been intensively investigated behaviorally and the neurophysiology and neuroanatomy of the neurons involved in this response is largely known. In contrast, an understanding of the neural control of swimming is minimal.

In this thesis, I examine the development of swimming in zebrafish larvae through an investigation of the motor unit. Its component motoneurons and muscles can be unequivocally identified anatomically. I begin by examining the physiological properties of axial locomotor muscle (Chapters 2 and 3) and how it is activated during swimming (Chapter 4). Motoneuron activity and how motoneurons are activated to produce a rhythmic output during swimming is examined last (Chapters 5, 6, and 7). These are the first neurophysiological studies of the development of the motor unit and swimming in any fish.

TABLES

Table 1.1. Spinal interneurons in larval (day 3-5) zebrafish (Bernhardt et al. 1990 and Hale et al. 2001).

Abbreviated Name	Number per segment	Spinal Tract	Projection	Projection Distance	Neuro-transmitter
CiD	≤3	DLF	ipsilateral descending	≤13	glutamate
CiB	≤1	DLF	ipsilateral bifurcating	≤13 caudal 1-2 rostral	unknown
CoPA	1	DLF	commissural ascending	telencephalon	glutamate
CoSA	≤5	DLF	commissural ascending	≤20	~2 GABA ~3 unknown
CoLA	≤1	DLF	commissural ascending	≤5	unknown
CoBL	≤4	DLF	commissural bifurcating	≤14 caudal ≤1 rostral	unknown
VeMe	≥1	VLF	ipsilateral descending	≤9	serotonin ?
UCoD	≥1	VLF	commissural descending	≤14	unknown
MCoD	≥1	VLF	commissural descending	≤13	glutamate
CoB	unknown	VLF	commissural bifurcating	unknown unknown	glycine

CiD: circumferential descending interneuron, CiB: circumferential bifurcating interneuron, CoPA: commissural primary ascending interneuron, CoSA: commissural secondary ascending interneuron, CoLA: commissural longitudinal ascending interneuron, CoBL: commissural bifurcating longitudinal interneuron, VeMe: ventral medial interneuron, UCoD: unipolar commissural descending interneuron, MCoD: multipolar commissural descending interneuron, CoB: commissural bifurcating interneuron. Transmitter phenotypes have been determined by using antibodies to GABA and serotonin, by expression of GAD65 and GAD67, and expression of the vesicular glutamate transporters and glycine transporters (Bernhardt et al. 1992; Brustein et al. 2000; Higashijima et al. 2001; Martin et al. 1998).

Table 1.2. Hindbrain, midbrain and forebrain nuclei that project to the spinal cord of adult zebrafish (Becker et al. 1997 and Wullimann et al. 1996).

Nuclei and Brain Regions	**Sources of Input or Function**
Diencephalon	
magnocellular preoptic nucleus	visual system
posterior part of parvocellular preoptic nucleus	visual system
gigantocellular part of magnocellular preoptic nucleus	visual system
periventricular nucleus of posterior tuberculum	unknown
Mesencephalon	
*nucleus of the medial longitudinal fasicle	cerebellum
nucleus ruber	cerebellum
nucleus of the lateral lemniscus	cerebellum
Reticular Formation	
*superior reticular formation	premotor integration and motor activation
*intermediate reticular formation	premotor integration and motor activation
*inferior reticular formation	premotor integration and motor activation
inferior raphe	premotor integration and motor activation
Octavolateralis Area	
anterior octaval nucleus	vestibular system
*magnocellular octaval nucleus	vestibular system
descending octaval nucleus	vestibular system
tangential nucleus	vestibular system
medial octavolateralis nucleus	lateral line neuromasts system
caudal octavolateralis nucleus	lateral line neuromasts system
Somato-sensory System	
*nucleus of the descending trigeminal tract	trigeminal nerve
medial funicular nucleus	trigeminal and vagal nerve

* described in day 5 larva.

Chapter Two: Physiological Properties of Embryonic Red and White Muscle Fibres During Early Development

LINKING STATEMENT

The physiological properties and development of the two axial locomotor muscle fiber classes (embryonic red and white) are examined first. Both fiber types are found to be mechanically functional and synaptically innervated and this study forms the groundwork for future studies aimed at understanding their roles during swimming.

ABSTRACT

The zebrafish is a model organism for studies of vertebrate muscle differentiation and development. However, an understanding of fish muscle physiology during this period is limited. The membrane, contractile and synaptic properties of embryonic red (ER) and white (EW) muscle fibers were examined in developing zebrafish from 1-5 days post-fertilization. Resting membrane potentials were -78 mV in ER and -83 mV EW muscle and depolarised 17 and 7 mV, respectively, by 5 days. Action potentials were occassionally observed in EW but never in ER fibers. Voltage-current relationships were linear in EW fibers and day 1 ER fibers but were outwardly rectifying in some ER fibers at 3-5 days. Both ER and EW fibers were contractile at all ages examined (1 to 5 days) and could follow trains of electrical stimulation of up to 30 Hz without fatiguing for up to 5 minutes. Synaptic activity consisting of miniature end-plate potentials (mEPPS) was observed at the earliest ages examined (1.2-1.4 days) in both ER and EW fibers. Synaptic activity increased in frequency, and mEPP amplitudes were larger by 5 days. Miniature EPP rise times and half-widths decreased in ER fibers by 5 days, while EW fiber mEPPs showed fast kinetics as early as 1.2-1.4 days. Embryonic red and EW muscle fibers showed extensive dye coupling but not heterologous (red-white) coupling. Dye coupling decreased by 3 days yet remained at 5 days. Somites were electrically coupled and this allowed filtered synaptic potentials to spread from myotome to myotome. It is concluded that at early developmental stages the physiological properties of ER and EW muscle are similar but not identical and are optimized to the patterns of swimming observed at these stages.

INTRODUCTION

Two types of muscle fibers are easily recognized in most fishes (Greer-Walker and Pull 1975) by their characteristic red and white coloration in fresh specimens (Bone 1978; Johnston 1981). A typical teleost myomere, zebrafish included, has a superficial band of red muscle fibers that runs parallel to the rostral-caudal axis of the body and deeper layers of white muscle that run at an oblique angle to this axis (Alexander 1969; van Raamsdonk et al. 1979). Microscopic, immunological, and histochemical examination reveals a greater diversity of fish muscle fiber types. The myotome of the adult zebrafish is composed of 5 distinguishable layers of muscle cells: the superficial adult red layer, intermediate pink layer, deep white layer, scattered dorsal and ventral fiber layer, and the red muscle rim layer (van Raamsdonk et al. 1978; van Raamsdonk et al. 1980; van Raamsdonk et al. 1982a; van Raamsdonk et al. 1987; Waterman 1969). At one extreme, superficial red fibers have small diameters, contain many mitochondria, have high succinate dehydrogenase activity, low lactate dehydrogenase activity, are richly innervated with blood capillaries, and show a low level of myofibrillar ATPase activity. Such metabolic specialization make red muscle suitable for sustained activity but not rapid contractions. At the other extreme, the deep white muscle fibers have larger diameters, contain fewer mitochondria, have low succinate dehydrogenase activity, high lactate dehydrogenate activity, are sparsely innervated with blood capillaries and show high levels of myofibrillar ATPase activity. These characteristics suggest a rapidly fatiguing muscle capable of fast and powerful contractions. How these different muscle fibers develop and their precise functional roles in the embryo are less

well understood.

Morphological development of muscle fibers has been studied in considerable detail in the zebrafish, although the physiological roles of different muscle fibers have not been directly examined. A functional characterization of muscle development is important to understand motor control during normal development and to assess dysfunction in the numerous interesting locomotor mutants that have been isolated in the first large genetic screens of vertebrate development (Granato et al. 1996). At a morphological level, a simpler pattern of muscle fibers is observed in embryonic and young larval zebrafish. When embryonic myotomal segments first form they are block shaped and composed entirely of fibers running parallel to the notochord. Within a few hours the deep embryonic white (EW) muscle fibers take on their characteristic oblique chevron-shaped orientations (van Raamsdonk et al. 1974). A thin band of muscle consisting of approximately 30 fibers per segment (embryonic red fibers, ER) blankets these deep fibers and retains their parallel orientation. An anatomical and histochemical division into these 2 fiber types at early developmental stages is present in a diversity of fish species examined including guppy (Veggetti et al. 1993), whitefish (Forstner et al. 1983), herring (Batty 1984), northern anchovy (O'Connell 1981), red sea bream (Matsuoka and Iwai 1984), trout (Proctor et al. 1980; Rescan et al. 2001; Stoiber and Sanger 1996), and a number of cyprinid species related to zebrafish (El-Fiky et al. 1987; Stoiber and Sanger 1996; Stoiber et al. 1998; Vieira and Johnston 1992). During the first week of development, the ER and EW fibers are the only muscle types present. El-Fiky and Weiser (1988) suggest the ER fibers are the main organs of gas exchange

prior to gill development and that the deeper muscle layers are involved in locomotion. In later larval development the ER fibers divide to ultimately form the red muscle rim fibers (van Raamsdonk et al. 1979; van Raamsdonk et al. 1982b; Waterman 1969).

Aspects of the genetic and cellular regulation of muscle development have been studied in considerable detail in zebrafish. The differentiation of ER fibers is regulated by the Hedgehog and TGF-β gene families (Blagden et al. 1997; Currie and Ingham 1996; Du et al. 1997). Embryonic red fibers (adaxial cells) form at the midline next to the notochord and then migrate to the surface of the muscle whereas EW fibers (lateral presomitic cells) form mediolateraly and do not migrate (Du et al. 1997). Primitive myofibrils are first observed in the caudal segments around 16 hpf (van Raamsdonk et al. 1974); ages according to Kimmel et al. (1995) for animals raised at 28.5 °C. Primary motoneurons extend axons into myotomal muscle at 16-17 hpf and trigger transient acetylcholine receptor clustering first on muscle pioneers and then stable clustering on other muscle fibers (Liu and Westerfield 1992). The first movements (17 hpf; Liu and Westerfield 1992; Saint-Amant and Drapeau 1998) are observed shortly after neuromuscular innervation commences which is when muscle contractile properties emerge (van Raamsdonk et al. 1977). Muscle pioneers are the first fibers contacted by primary motoneurons, are the first to form functional synapses, and the first to contract in response to motoneuronal output (Melancon et al. 1997). Secondary motoneurons begin to innervate muscle at approximately 26 hpf (Myers et al. 1986) and swimming is first observed soon after at 27 hpf

(Saint-Amant and Drapeau 1998). At this period, all fibers have metabolic properties similar to adult white muscle *i.e.*, they are fatigable, and it is not until near the fifth day that the superficial fibers begin to acquire the metabolic characteristics of adult red muscle (van Raamsdonk et al. 1978). However, even at this early age, both fibers have distinct red and white myofibrillar properties (Blagden et al. 1997). A rapidly fatigable muscle may be one reason why brief periods of burst swimming, followed by extended periods of rest (van Raamsdonk et al. 1974), are only observed at early larval stages. Rapidly fatiguing swimming in early larval life appears to be a consequence of muscle metabolic properties in a variety of cyprinids (El-Fiky et al. 1987) and whitefish (Forstner et al. 1983).

The goal of this study was to compare the physiological properties of, and synaptic inputs to, developing ER and EW muscle fibers of the zebrafish. Developmental changes in the properties of these muscles are examined from when swimming behaviour is first manifested (day 1) to when zebrafish actively swim to capture prey (day 5).

METHODS

Preparation

Experiments were performed on zebrafish (Tubingen and Longfin lines) embryos and larvae raised at 28.5 °C and obtained from a breeding colony maintained according to Westerfield (1995). Results are taken from recordings made on 84 muscle fibers. All procedures were carried out in compliance with the guidelines stipulated by the Canadian Council for Animal Care and McGill University. Zebrafish were anaesthetised in 0.02% tricaine (MS-222) dissolved in

physiological extracellular Evans (1979) solution consisting of (in mM; Drapeau et al. 1999) 134 NaCl, 2.9 KCl, 2.1 $CaCl_2$, 1.2 $MgCl_2$, 10 HEPES and 10 glucose, osmolarity adjusted to approximately 290 mOsm, pH 7.8. The fish was then pinned through the notochord to a silicon elastomer Sylgard-lined dish and the skin overlying the axial musculature removed with a glass pipette and fine forceps. The preparation was moved to the recording set-up and then continuously perfused with a tricaine-free Evans solution containing 15 μM D-tubocurarine or 1 μM tetrodotoxin (TTX) to paralyze the animals. In dye coupling measurements (n = 25) a high magnesium and low calcium extracellular Evans solution (in mM: 123 NaCl, 2.9 KCl, 0.7 $CaCl_2$, 10 $MgCl_2$, 10 HEPES, 10 glucose, osmolarity adjusted to approximately 290 mOsm, pH 7.8) was used instead of a paralyzing agent. Although these fibers were not used for electrophysiological measurements, robust spontaneous synaptic activity was observed in all 25 cells. Recordings made in this solution were very stable due to an absence of muscle contractions and for this reason this solution was used during paired recordings (n = 5).

Whole-cell recordings

Standard whole-cell recordings (Hamill et al. 1981) were performed on the superficial ER muscle fibers and the first 2 layers of EW muscle fibers (van Raamsdonk et al. 1982b). Embryonic red and EW fibers correspond to the adaxial and lateral presomitic cells of Devoto et al. (1996) and Du et al. (1997). All physiological measurements were performed on dorsal and ventral fibers located 1-2 segments rostral or caudal to the anus. A patch pipette controlled by a micromanipulator was used to tease off 1-2 overlying ER fibers to expose the

underlying EW fibers. Muscle fibers were visualized with Hoffman modulation optics (X40 water immersion objective). Experiments were performed at room temperature (approximately 22 °C). Patch-clamp electrodes were pulled from thin-walled Kimax-51 borosilicate glass and were filled with either a K-gluconate (for physiological measurements), Cs-gluconate (for paired recordings), or CsCl (for dye coupling measurements) solution to yield electrodes with resistances of 1.5-3 MΩ as described previously (Drapeau et al. 1999). The K-gluconate solution was composed of (in mM) 116 D-gluconic acid-potassium salt, 16 KCl, 2 $MgCl_2$, 10 HEPES, 10 EGTA, 4 Na_2ATP, osmolarity adjusted to 290 mOsm, pH 7.2. K-gluconate and KCl were replaced with Cs-gluconate and CsCl in the Cs-gluconate solution or with CsCl in the Cs-chloride ion solution. The liquid junction potential was -10 mV for K-gluconate and Cs-gluconate electrodes and -3 mV for CsCl electrodes and records were corrected for this potential. Recordings were made with an Axoclamp-2A amplifier (Axon Instruments) in bridge mode and were low-pass filtered at 10 kHz and digitized at 20-30 kHz. In paired recordings an Axopatch 1D (Axon Instruments) was used as a second amplifier. Cells were discarded if their resting membrane potential was more depolarised than –50 mV. Measurements were made 3-5 min after obtaining whole-cell configuration to ensure complete cell dialysis.

Dye coupling between muscle fibers

All fibers reported in this study were filled with fluorescent sulforhodamine B to examine the extent of dye coupling between muscle fibers, and electrophysiological measurements were taken from these same fibers. Images were captured with a Panasonic BP510 CCD camera and a Scion Corporation

LG3 frame grabber using Scion/NIH Image software. Whole-cell configuration was maintained for 10-15 min in each fiber. Dye coupling was quantified by counting the number of fluorescent fibers and the number of segments that contained fluorescent fibers.

Voltage-current relationships and membrane time constants

Recordings were made in D-tubocurarine to eliminate central nervous system evoked muscle contractions. Current steps were manually incremented through an A-M Systems isolated pulse stimulator, captured using Axotape software (Axon Instruments), and measurements were made in Axoscope 7 software (Axon Instruments). Current injections of 300 ms duration were made once every 2-4 s. A small hyperpolarizing or depolarizing current was injected and constantly adjusted to maintain a membrane potential of –70 mV in 3 and 5 day larvae. Some embryonic muscle fibers were unstable at –70 mV so all recordings were performed at –80 mV which is closer to the resting membrane potential at this age. During recordings, the electrode response was constantly monitored at high gain and high sweep speed on an analogue oscilloscope and the electrode balanced using the bridge circuitry. Electrode resistance was generally low (3-5 MΩ) but was as high as 10 MΩ in some recordings, and the electrode capacitance was <3 pF. Both the electrode resistance and capacitance were an order of magnitude smaller than those for the muscle membrane, resulting in small and fast transients that were easily compensated and unlikely to contribute to measurement errors.

Membrane time constants were determined by fitting the voltage response to a hyperpolarizing current injection (15 to 25 mV deflection) with a sum of

exponential curves. The presence of 1 or 2 exponential components was tested by comparing the sum of squared errors of the fits.

Muscle contraction rates

In many muscle fibers it was possible to inject sufficient current in the centre of the fiber to evoke a muscle contraction and still maintain the whole-cell configuration. Following voltage recordings, the current pulse duration was reduced to 15-20 ms and the intensity increased to 2-7 nA, which was sufficient to evoke a muscle contraction. A duration of 15-20 ms was chosen to mimic the cycle duration of motoneuron output that must be occurring for the larvae to swim at the observed tail beat frequencies of approximately 30 to 60 Hz (Budick and O'Malley 2000a; Eaton et al. 1977b; Saint-Amant and Drapeau 1998). Briefer durations of current were usually ineffective regardless of the intensity of stimulation up to 10 nA. The contraction of the muscle was observed on a video monitor and recorded on a VCR (Panasonic S-VHS) along with stimulus parameters, which were recorded on Axotape for later analysis. Inter-pulse interval was gradually decreased until the individual contractions fused together, which is referred to as the tetanus fusion rate. Long (300 ms) depolarizing current injections were used to determine the rheobasic contraction threshold, which was recorded as the membrane potential at which the first twitch contraction was observed.

Analysis of miniature endplate potentials (mEPPs)

Miniature endplate potentials (mEPPs) were recorded in Evans solution containing TTX to block central nervous system-evoked muscle contractions but not spontaneously occurring synaptic vesicle release. A small hyperpolarizing or depolarizing current was injected into the fiber to hold the membrane potential at

–70 mV (larvae) or –80 mV (embryos). Five minute recordings were made in Fetchex (Axon Instruments) and analysis was performed off-line using Axograph 4.0 (Axon Instruments). Events were detected using the template function set at 4-5 SD above baseline noise. It was not possible to discriminate events less than 0.5 mV in amplitude due to the background noise even with Cs-gluconate pipettes. Small events were excluded followed by visual examination and deletion of erroneous events. The remaining events were used to calculate peak amplitudes, 20-80% rise times, half-widths, and mEPP frequencies.

Paired Recordings

Paired recordings were performed in a high magnesium (10 mM) and low calcium (0.7 mM) solution which abolished muscle contractions and allowed stable recordings with 2 electrodes. A Cs-gluconate intracellular solution was used to potentiate mEPPs and facilitate their detection. These fibers were not used for calculating any parameters listed in Tables 2.1 or 2.2. All paired recordings were made from longitudinally adjoining ER fibers of day 3 larvae. Positive or negative current was ejected through the recording electrodes to equalize the membrane potential of each cell.

The goal of this experiment was to determine if the small and slow mEPPs occurred simultaneously with large and fast mEPPs in adjacent fibers, the small and slow events being due to filtering through intercellular junctions. Digitized data were examined by scrolling through 50 ms windows in Axoscope 7. Whenever an event was detected (>0.5 mV) in 1 fiber, a simultaneous corresponding event was searched for in the other fiber. This preliminary analysis revealed that events large enough to be detectable, *i.e.*, >0.5 mV, always

occurred simultaneously in both fibers with 1 mEPP appearing as a filtered and attenuated version of the other mEPP. Time-to-peak and peak amplitude measurements were then made by eye for fifty consecutive paired mEPPs. The peak amplitude and time-to-peak values of the larger mEPP was divided by the peak amplitude and time-to-peak value of the smaller mEPP and was normalized to 100% to express the extent of filtering between each pair of mEPPs.

Results are presented as mean ± SE and significant relationships ($P<0.05$) determined using the Student's *t-test*, Mann-Whitney rank sum test, ANOVA, or Kruskal-Wallis ANOVA. Correlations were tested using the Pearson Product Moment Correlation and a significant relation was noted when $P<0.05$. Sulforhodamine B was purchased from Molecular Probes (Eugene, OR) and all other chemicals from Sigma Chemical Co. (St. Louis, MO).

RESULTS

To avoid the errors inherent in voltage-clamp recording from electrically coupled muscle cells, *e.g.* Broadie (1999) and Nguyen et al. (1999), experiments were performed in current-clamp mode. Muscle fibers were examined at 3 time periods of development: in embryos (day 1.2-1.5; referred to as day 1) near the time swimming-like behaviour is first observed (Saint-Amant and Drapeau 1998), in quiescent post-hatching larvae (day 3.4-3.6; referred to as day 3 larvae) and in active free-swimming larvae (day 4.9-5.8; referred to as day 5 larvae). As the appearance of the 2 types of muscle fibers did not change over the brief (4 day) interval examined, they are refered to as ER or EW muscle fibers. Resting membrane potentials recorded with K-gluconate intracellular solutions (Table 2.1)

were large in day 1 ER, (-78 ± 1.7 mV) and EW fibers, (-83 ± 1.0 mV) and depolarised by 7 mV (EW) and 17 mV (ER) during development to the free swimming larvae stage (day 5). At all stages examined, the resting membrane potentials of the EW fibers were more negative than that of the ER fibers. By day 5 the difference in resting membrane potential between EW and ER fibers was 15 mV.

Dye coupling

Dye coupling was observed in 69 of 74 muscle fibers examined in this study, the exceptions being 5 EW fibers in 3-5 day larvae. No obvious differences in dye coupling were observed in rostral or caudal segments (± 10 segments from the anus) or in dorsally or ventrally located fibers. Dye coupling in ER fibers spanned up to 5 segments (only 3 segments are shown in Figure 2.1) at all stages, which included up to 38 labelled fibers at day 1 and 12 at day 3. The average number of dye coupled segments decreased by 38% and the number of fibers filled decreased by 73% (Table 2.1) during the transition from day 1 to day 3 and there was no further change by day 5. Fibres were dye-coupled in both dorso-ventral and rostro-caudal directions (2. 1, A2 and B2).

Dye coupling was less extensive in the EW than in the ER fibers at all corresponding stages examined (Figure 2.1; Table 2.1) but showed a similar decrease in segmental coupling (by 39%) and decrease (by 70%) in the number of fibers coupled from day 1 to day 3, and similar to the ER fibers, no further change in coupling was observed by day 5. Unlike ER fibers, coupling in the EW fibers was generally restricted (21 of 26 fibers) to the rostro-caudal axis in larvae where 1-4 segments could contain dye filled fibers. Dorso-ventral coupling in

addition to rostro-caudal coupling was observed in day 1 EW fibers where 3 to 13 fibers were found coupled over 3 to 5 segments at later stages. Coupling between EW fibers running in different oblique orientations (Figure 2.1, A3) was observed occasionally. Coupling was never observed between ER and EW fibers.

Voltage-current (VI) relationships

The VI relationship of each type of muscle fiber was examined to reveal any differences or changes in the membrane properties during development of the ER and EW fibers. At day 1, ER fibers had mean input resistances of 31 ± 2 MΩ (Table 2.1), showed no rectification near the resting membrane potential, and the time course of the voltage response was similar in both depolarizing and hyperpolarizing directions (Figure 2.2A1). The mean input resistance of day 3 ER fibers increased to 74 ± 10 MΩ (Table 2.1) when hyperpolarizing currents were injected. In some cells outward rectification was observed with depolarizing currents and initial voltage response was steeper in the depolarizing direction (Table 2.1 and Figure 2.2A2). The more extensive coupling in these cells may have contributed to the rectification. Interestingly, the input resistance of day 5 larvae decreased to 30 ± 5 MΩ, a value similar to that observed in embryos. It is likely that the initial increase in input resistance from day 1 to day 3 was principally due to muscle fiber uncoupling whereas the later decrease was due to insertion of ion channels into the membrane. Similar to day 3, some day 5 fibers rectified and showed a steeper initial voltage response in the depolarizing direction (Figure 2.2A3; Table 2.1). Action potentials were not observed in any ER fibers.

Day 1 EW fibers had a mean input resistances of 33 ± 6 MΩ (Table 2.1)

and showed a similar voltage response in both depolarizing and hyperpolarizing directions (Figure 2.2B1). Similar to ER fibers, input resistance in day 3 fibers were slightly higher (46 ± 8 MΩ) and then decreased to 27 ± 5 MΩ by day 5 (Table 2.1). Rectification was not observed in any EW fibers. The initial voltage response was steeper in the depolarizing direction than the hyperpolarizing direction in day 3 EW fibers (Figure 2.2B2) but this was not apparent in day 5 EW fibers (Figure 2.2B3). Action potentials were rare and only observed in 2 EW fibers.

Membrane time constants

Membrane voltage responses to 300 ms hyperpolarizing current injections were fit with the sum of 2 exponential curves with membrane time constants τ_{fast} and τ_{slow}. At all ages and in both ER and EW fibers τ_{fast} mean values ranged from 0.5 to 4.4 ms, and τ_{slow} means ranged from 16 to 76 ms (Table 2.1). At day 1, although EW fibers had a much faster τ_{fast} (0.5 ± 0.2 ms) than that of ER fibers (3.2 ± 0.8 ms). The τ_{fast} exceeded the membrane time constant and may reflect an active conductance, or the presence of unfused myoblasts as observed previously (Nguyen et al. 1999). The τ_{slow} was very similar in both types of muscle fibers (ER = 71 ± 3 ms *vs* EW = 76 ± 4 ms; Table 2.1). However, τ_{slow} contributed to 75% of the response amplitude in ER fibers, whereas in EW fibers only 21% of the response amplitude was due to τ_{slow}. This difference might be explained by the more extensive dye coupling observed in ER fibers. At day 3, τ_{slow} decreased similarly in EW and ER fibers to 40 ± 9 and 39 ± 11 ms. The contribution of τ_{slow} to the peak amplitude changed little (21 to 19%) in EW fibers while it decreased from 75 to 36% in ER fibers. These changes in membrane time constants closely

parallel the changes in dye coupling observed at these same ages. Accordingly, τ_{fast} likely corresponded to the membrane response of the fiber recorded from and perhaps immediately adjacent fibers (immediate compartment), whereas τ_{slow} was the response of more distant coupled muscle fibers (remote compartment). However, changes in fiber size and ion channel composition, which were not examined in this study, are also likely to influence the changes in time constants observed. By day 5, τ_{slow} changed little (36 ± 7 *vs* 40 ± 9 ms) and only contributed to 12 ± 1% of the amplitude of the voltage response. At this age τ_{slow} contributed to 49% of the amplitude of the voltage response in ER fibers, which by this time had developed a significantly faster τ_{slow} (16 ± 3 ms *vs* 36 ± 7 ms) than day 5 EW fibers.

Contraction thresholds and maximal contraction rates

During the VI recordings (300 ms current pulses) the membrane depolarization required for muscle to twitch was noted. The voltage threshold for muscle contraction changed little in day 1-5 ER fibers (means varied from –47 ± 4 mV to –53 ± 7 mV; Table 2.1). In contrast, EW fibers did not contract in response to long depolarizing current which depolarised the membrane to –40 mV. Larger current injections that depolarised the membrane well above 0 mV resulted in robust muscle twitches and the loss of whole-cell configuration. It was apparent that EW muscle did not respond well to focal stimulation, which was not unexpected in these multiply innervated muscle fibers.

Following VI recordings, stimulus parameters were adjusted to resemble more closely the currents the muscle fibers would presumably receive during swimming. The electrode seal was lost in several fibers once muscle contractions

started but recordings were relatively stable in others. The local (point) current necessary to evoke a muscle contraction depolarized the membrane well above 0 mV, providing further evidence for the requirement for distributed, multi-terminal innervation to evoke muscle contraction. Of the successful recordings, ER and EW fibers at all stages were capable of following trains of 15-20 ms stimulation delivered at frequencies up to 30 Hz (observed in a day 5 ER fiber), which predicts a sustainable upper limit of 30 Hz for alternating tail beat. 30 Hz is below the maximum tail beat frequencies (approximately 40-80 Hz; Budick and O'Malley 2000a; Buss and Drapeau 2001a) reported in larvae zebrafish. This discrepancy is likely because this study measured sustained muscle contraction rates and cannot rule out the possibility that more rapid muscle contraction rates, which fatigue within a few muscle contractions, are possible. In addition, the fusion frequencies were measured on unloaded muscle and not during the cyclical tension changes that are a result of the alternating ipsilateral and contralateral muscle contractions occurring during undulatory swimming. The average muscle tetanus fusion rates (Table 2.1) were fastest at day 5 and appear slower at day 1, which correlates well with the gradual increase in swimming tail beat frequency observed in developing zebrafish embryos and larvae (Budick and O'Malley 2000a; Buss and Drapeau 2001a; Eaton et al. 1977b; Saint-Amant and Drapeau 1998). Stimulation was generally delivered for 2-5 minutes, during which time muscle fatigue was not observed.

Miniature endplate potentials

Figure 2.3A-D shows representative examples of mEPPs recorded in day 1 and day 5 ER and EW muscle fibers. Readily apparent are the higher

frequency of events at day 5 *vs* day 1 and the prominence of large amplitude events at day 5 compared with smaller event amplitudes at day 1. Representative mEPPs are shown at an expanded time scale in Figure 2.3, A1-D1. At day 1, mean mEPP amplitudes were similar in ER (0.8 ± 0.1 mV) and EW (0.87 ± 0.04 mV) fibers and then increased approximately 3 and approximately 5 times, respectively, by day 5 (Table 2.2). The mEPP time courses were highly similar in day 5 ER and EW fibers and in day 1 EW fibers, but the time courses were distinctly slower in day 1 ER fibers. Mean rise times and half-widths were 4 and 6 times faster, respectively, in day 1 EW fibers than they were in ER fibers (0.58 ± 0.06 ms *vs* 2.3 ± 0.2 ms rise times and 3.8 ± 0.1 ms *vs* 24 ± 2 ms half-widths; Table 2.2). In contrast, by day 5 these values were comparable (0.33 ± 0.05 ms *vs* 0.39 ± 0.04 ms rise times and 3.5 ± 0.2 ms *vs* 3.6 ± 0.2 ms half-widths; Table 2.2). The frequency of detectable mEPPs increased in both ER and EW fibers from day 1 to day 5, but this increase was greatest in EW fibers where it increased 10 times compared with ER fibers where the frequency increased only 1.5 times. Specifically, day 1 ER fibers received a higher frequency of mEPPs (0.38 ± 0.04 Hz) than EW fibers (0.10 ± 0.02 Hz), but this difference was reversed by day 5 when ER fibers received mEPPs at 0.57 ± 0.11 Hz compared with frequencies of 1.00 ± 0.24 Hz observed in EW fibers. Differences in passive membrane properties did not account for slow events in day ER 1 fibers. Even though day 1 ER fibers had slower time constants than in day 1 EW fibers, these values (as well as the resistances) were more similar to those of both types of fibers at day 5 (Table 2.2). Therefore, the kinetics of mEPPs recorded in day 1

ER fibers were fundamentally slower than in day 1 EW fibers and in both fiber types at later stages.

The properties of mEPPs were further examined by comparing the distributions of event amplitudes, rise times, and half-widths. Representative mEPP distributions from a day 1 ER and EW fiber are shown in Figure 2.4. The amplitude distributions were very similar in the day 1 ER and EW fibers and appeared to be normally distributed, but the rise time and half-width distributions are clearly wider and displaced to the right in the ER fibers. Scatter plots of event rise times *vs* amplitude and half-widths (Figure 2.5) do not reveal more than 1 population of events and further illustrate the difference between mEPPs in day 1 ER and EW fibers.

Miniature EPP distributions appeared normally distributed and were similar in day 5 ER and EW fibers. Thus amplitude, rise time, and half-width distributions are only shown for EW fibers (Figure 2.6). Unlike day 1, some day 5 fibers displayed 1 population of mEPP amplitude, rise time, and half-width distributions (Figure 2.6A) while others displayed 2 distributions (Figure 2.6B). This was also apparent in scatter plots of rise times *vs* amplitudes (Figure 2.7, A1 and B1) or half-widths (Figure 2.7, A2 and B2). The distribution common to all fibers was composed of events with large amplitudes (>1-2 mV), fast rise times (<0.2-0.4 ms), and short half-widths (<4-5 ms) (Figure 2.7A). In the majority of cells (3 of 5 ER; 3 of 4 EW) a second population of events with smaller amplitudes (<1-2 mV), slower rise times (>0.2-0.4 ms), and longer half-widths (>4-5 ms) were observed (Figure 2.7B). Closer examination of the fibers where this second population of small and slow events was observed revealed a lower baseline noise in these

fibers. Thus, 2 populations of events may be present in all larval fibers but baseline noise prevents the detection of these smaller and slower events. No clear differences could be detected in the amplitude distributions of day 5 ER and EW fibers, and mean mEPP amplitudes were not significantly different in EW (3.7 ± 0.84 mV) and ER (2.3 ± 0.43 mV) fibers.

Evidence for the filtered propagation of mEPPs between dye coupled muscle fibers

A simple explanation for the 2 types of events is that the population of large and fast mEPPs originated from synapses located on the cell recorded from, whereas the population of smaller and slower mEPPs would represent mEPPs originating in electrically coupled neighbouring fibers that were recorded as filtered mEPPs. To test this possibility, simultaneous recordings were made from adjacent fibers, and the presence of a large, fast event in 1 fiber occurring simultaneously with a small, slow event in the other fiber was investigated. A total of 5 paired recordings were performed on adjacent ER fibers in day 3 larvae. A pair of dye-coupled fibers is shown in Figure 2.8, A and B and the corresponding paired recording is shown in Figure 2.8C. Apparent is the presence of a large and fast event recorded from 1 electrode paired with a smaller and slower event recorded with the second electrode (Figure 2.8, C and D). The larger and faster event was observed with equal occurrence in either of the electrodes. Fifty consecutive mEPPs were observed in each of the 5 paired recordings and time-to-peak and peak amplitude measured. In every instance, a larger and faster event occurred simultaneously with a smaller and slower event. On average the amplitude of filtered events was one-half (45 ± 7%) as small and the time-to-peak

twice (2.0 ± 0.1) as slow. In addition, a trend observed (R = 0.64) was that the events with the least attenuated amplitudes also showed the smallest increase in time-to-peak. These were events where the lowest amplitude was small to begin with (*e.g.*, Figure 2.8, C and D). Conversely, events with the greatest amplitude attenuation showed the greatest increase in time-to-peak. These events resembled 2 of Figure 2.8, C and D, where the large amplitude event was big to begin with. Thus, the electrical coupling acted as a low-pass filter strongly attenuating the synaptic events from immediately adjacent fibers while only weakly attenuating synaptic events from more distant cells.

DISCUSSION

This is the first study examining the physiological development of red and white fish muscle. At all stages examined, the resting membrane potential of the ER fibers was more depolarized than that of the EW fibers. A more depolarized resting potential in fish red muscle has been reported in jawless fishes (hagfish, Andersen et al. 1963; lamprey, Teravainen 1971), cartilaginous fishes (dogfish, Stanfield 1972) and ray-finned fishes (snake fish, Takeuchi 1959; silver carp, Hidaka and Toida 1969a). The absolute membrane potential of the EW muscle at the latest stage examined (day 5) was –76 mV, which contrasts with a mean resting potential of –82 mV in zebrafish adult white muscle (Westerfield et al. 1986). Chapter 3 reveals that this small difference is due to experimental error introduced by using an electrode solution containing 20 mM Cl^- in muscle fibers developing a permeability to Cl^-.

The input resistance of adult red muscle is generally lower than that of white muscle with the values for both fibers ranging from less than 1 MΩ to over 10 MΩ (hagfish, Nicolaysen 1976a; Nicolaysen 1976b; lamprey, Teravainen 1971; dogfish, Stanfield 1972; silver carp, Hidaka and Toida 1969a; green sunfish, Klein and Prosser 1985). In contrast, the input resistances of zebrafish ER and EW muscle were higher (means of 31 to 74 MΩ) than in these other preparations, presumably due to the smaller size of the muscle fibers, although ER and EW fiber input resistances were similar at the same age. The red and white muscle of adult fish shows rectification (near the resting membrane potential) in some species of ray-finned fishes (5 species of marine teleosts) but not in the silver carp (Hagiwara and Takahashi 1967; Hidaka and Toida 1969a) and not in the cartilaginous fishes (3 species of rays, Hagiwara and Takahashi 1967). The VI curves of day 5 EW muscle were linear while the day 3 and 5 ER muscle showed outward rectification.

Action potentials were not observed in ER, and only rarely in EW, muscle fibers. However, when an electode solution containing 10 mM Cl^- is used and more negative resting membrane potentials are observed, action potentials are routinely present in EW fibers (Chapter 3). The absence of action potentials in some EW fibers is presumably due to inactivation of voltage gated sodium channels. The absence of action potentials does not rule out the existence of voltage-gated channels which is suggested by the presence of a faster rising membrane response to positive, compared to negative, current injections in both ER and EW fibers (Figure 2.2). The white fibers of adult fish generate action

potentials which may or may not be overshooting, whereas adult red fibers in a wide variety of fishes are incapable of generating action potentials (hagfish, Andersen et al. 1963; lamprey, Teravainen 1971; ray-finned fishes including snake fish, Takeuchi 1959; banjo catfish, Gainer 1967; sculpin, Hudson 1969; silver carp, Hidaka and Toida 1969a; zebrafish, Westerfield et al. 1986). Although both fiber types have distinct characteristics at day 1 and day 5, their resting potentials, input resistances and excitatory properties are not comparable to those reported in other adult fish, suggesting that the complement of ion channels and pumps is not fully expressed at these stages.

Intercellular coupling between developing muscle cells has been reported in mammals, birds, amphibia and fish and is lost with developmental maturation (Dennis 1981). Intercellular junctions have been observed in ultrastructure studies of embryonic zebrafish (Waterman 1969) and rainbow trout (Nag and Nursall 1972). There was a clear trend toward fiber uncoupling with age in this study (Figure 2.1), although fibers were not fully uncoupled at the latest stages examined. It cannot be assumed that all fibers are fully uncoupled in adult zebrafish because in other fish, muscle fibers remain coupled into adulthood (*e. g.*, the lamprey; Teravainen 1971).

If it is assumed that the extent of detectable fiber coupling was limited by diffusional barriers then it appears that the cytoplasm of all myotomal muscle (ER and EW) is connected at these developmental stages. The absence of coupling between ER and EW fibers could restrict diffusion of intracellular factors involved in muscle differentiation and growth to these distinct fiber types. No evidence was found to suggest electrical coupling between motor axons and muscle (Dennis

1981) as dye did not pass from muscle into motoneuron axons and the bursting patterns of action potentials observed in motoneuron recordings (Drapeau et al. 1999) were not observed as patterns of depolarization in curarized muscle.

With the exception of the lamprey (Teravainen 1971), the white muscle fibers of the typical teleost will contract in response to sub-threshold synaptic stimuli (Bone 1964; Hagiwara and Takahashi 1967; Hidaka and Toida 1969a). The maximal contraction rates (mean rates of 23-27 Hz, Table 2.1) of both the ER and EW fibers changed little during day 3 to day 5, although contraction rates may have been slower in embryonic (day 1) fibers. These contraction rates are within the range of contraction rates observed in other fish myotomal muscle which range from 13-20 Hz (eel), 40-60 Hz (sculpin), 5-10 Hz (cuckoo ray), and 35-45 Hz (cod) (Altringham and Johnston 1988; Johnston 1980). The similar contraction rates observed in the ER and EW muscle show that ER muscle could be co-active with EW muscle at undulation rates less than ~30 Hz. However, this would contrast with the situation in adult zebrafish muscle where red muscle is believed to be active at slower swimming speeds and white muscle is recruited during short bursts of rapid swimming (Liu and Westerfield 1988).

In rays (Hagiwara and Takahashi 1967) and lamprey (Teravainen 1971) membrane time constants were longer in red muscle than in white whereas the opposite was true in the silver carp (Hidaka and Toida 1969a). In day 1-3 zebrafish the membrane time constants were similar in both ER and EW muscle although the contribution of τ_{slow} was always greater in ER fibers. By day 5, the ER fibers had faster time constants than that of the EW fibers, which is the same pattern observed in the silver carp, which like zebrafish, is a member of the

Cyprinid family.

There have been a limited number of studies examining synaptic properties in fish muscle. Comparable mEPP amplitudes were observed in ER and EW fibres at the same stages (approximately 1 mV at day 1 and 2-4 mV at day 5, Table 2.2). Miniature EPP amplitudes are generally less than 2.5 mV in silver carp, lamprey and hagfish (Alnaes et al. 1964; Balezina and Gulyaev 1985; Hidaka and Toida 1969b) while events of 7 mV were found in the fast contracting sonic muscle of the toadfish (Gainer and Klancher 1965; Skoglund 1959). Synaptic events recorded in fish muscle have rapid decay kinetics. Excitatory junction currents have half-widths of 1.5 ms in silver carp fin muscle (Hidaka and Toida 1969b), approximately 2 ms in lamprey white muscle (Balezina and Gulyaev 1985), and time constants of 1 ms (*Trachurus novaezelandiae*; Macdonald 1983) and 2-3 ms (*Pagothenia borchgrevinki*; MacDonald and Montgomery 1986) in extraocular muscles. Mean mEPP half-widths of approximately 5 ms were found in toadfish sonic muscle (Gainer and Klancher 1965). The decay kinetics of day 5 zebrafish mEPPs were at least as fast having mean half-widths of <4 ms (Table 2.2) due to mEPCs with decay time constants of <2 ms (Nguyen et al. 1999) and were comparable to the mEPPs recorded in 2 day old zebrafish myotomal muscle shown in Figure 2.3 of Felsenfeld et al. (1990). Rapid mEPC kinetics are consistent with the fast contraction rates during swimming as the zebrafish is one of the fastest swimming teleosts of its size (Plaut 2000).

All non-teleost and most basal teleost groups have terminally innervated white muscle fibers (Bone and Ono 1982), which are innervated by a single motor

axon in most groups with the exception of the Hagfish, Lampreys, Elasmobranchs (*e.g.*, sharks and rays), Dipnoe (*e.g.*, lungfishes) and Clupeomorpha (*e.g.*, anchovies and herrings) where 2 motor axons are observed at the terminal endings (Best and Bone 1973; Ono 1983). However, in the vast majority of teleosts, including the zebrafish, red and white muscle receive numerous distributed endings from a plexus of nerves spread over the surface of the muscle fibers (Altringham and Johnston 1981; Barets 1961; Bone 1964; Gainer 1969; Gainer and Klancher 1965; Hudson 1969; Ogata 1988; Shenk and Davidson 1966; Takeuchi 1959; Westerfield et al. 1986). The function of this multiterminal innervation may be to allow the presynaptic motoneuron action potential to reach several points of the muscle fiber faster and with greater efficiency than would be possible by active or passive conduction along the muscle fiber if activated by a single terminal junction (Shenk and Davidson 1966). Short duration (<10 ms) current injected though the patch electrode was ineffective at eliciting muscle contraction and in EW fibers long duration (300 ms) current injections did not evoke a muscle twitch until the membrane potential approached or overshot 0 mV.

Multiterminal innervation would distribute the action of the rapid mEPCs over many sites of the muscle fiber to enable excitation contraction coupling. In the zebrafish, the biophysical properties of individual acetylcholine receptor molecules at the neuromuscular junctions are also optimized to maximize current spread. At these junctions, the endplate current is generated upon reversal from open channel block following removal of acetylcholine (Drapeau et al. 2001; Legendre et al. 2000). This results in a delayed closing of the acetylcholine

receptors and consequently a transient, rebound synaptic current. The net consequence is a larger charge distributed over a broader time course, presumably enhancing the distributed depolarization leading to muscle contraction.

Distinct changes were observed in the properties of mEPPs over the stages examined. Miniature EPP amplitudes increased in ER and EW fibers suggesting an increase in acetylcholine receptor density postsynaptically or an increase in the acetylcholine content of a transmitter quantum or both. The increase in mEPP frequencies could be due to an increase in the number of synaptic sites and/or probability of vesicle release. Liu and Westerfield (1992) reported an increase in the number and size of acetylcholine receptor clusters during synaptogenesis and a histological study on the development of toadfish sonic muscle (Skoglund 1959) revealed an increased coverage of neuromuscular junctions during development (Hirsch et al. 1998). Miniature EPP kinetics were similar in day 1 and day 5 EW fibers but were distinctly slower in day 1 ER fibers. Nguyen et al. (1999) reported a similar developmental increase in mEPC kinetics as observed in ER fibers in this study, thus making it likely that the superficial ER fibers were the fibers examined at the embryonic stages by Nguyen et al. (1999). The large difference in synaptic kinetics and frequency of occurrence in ER and EW fibers at the embryonic stages could be due to immaturity of the ER fibers or differential innervation of ER and EW muscle by different populations of motoneurons or both.

In adult zebrafish, populations of motoneurons with dorsal and ventral positions in the spinal cord have been found to innervate white and red muscle,

respectively, with high specificity (Myers 1985; van Asselt et al. 1993; van Raamsdonk et al. 1983). The dorsal population of motoneurons undoubtedly include the primary motoneurons described by Myers et al. (1986), which are the first motoneurons to exit the spinal cord and form synapses on muscle fibers. In the adult zebrafish there is a greater diversity of fibers types and most secondary motoneurons innervate more than one class of muscle *e. g.*, white and intermediate (de Graaf et al. 1990). It is possible that the outgrowing secondary motoneurons are forming synapses on ER fibers as well as EW fibers in this period. I suggest that the primary motoneurons of Myers et al. (1986) only innervate EW muscle fibers, and having started synaptogenesis at 17 hpf (Liu and Westerfield 1992), have undergone upward of 10 hours of synaptic development by the time of recording. I therefore hypothesize that both the ER and EW fibers are innervated by the population of ventral secondary motoneurons (Myers et al. 1986), which do not exit the spinal cord until approximately 26 hpf. Recordings made on ER fibers could potentially be at the initial period of synaptogenesis when synaptic currents are expected to have slow kinetics (Kullberg and Owens 1986; Kullberg et al. 1977; Nguyen et al. 1999; Schuetze and Role 1987).

Paired recordings performed on day 3 ER fibers clearly demonstrate that small amplitude mEPPs with slow kinetics do not all arise as events with distinct kinetics but are due to low pass filtering through an electrically coupled syncytium of muscle fibers. All small and slow mEPPs are not necessarily filtered mEPPs and I would expect that an unknown fraction of these events (including undetected events <0.5 mV in amplitude) would arise from newly formed

synapses. Electrical coupling between adjacent muscle fibers undoubtedly places a limit on the possible movements of the zebrafish embryo and larvae. During swimming, propulsion is generated by alternating, neural-mediated waves of contractions progressing down the body of the fish (Lindsey 1978). Electrical coupling would spread (limited by low pass filtering) the neurally evoked mEPPs to adjacent myotomes, depolarizing the membrane closer to contraction threshold. However, the electrical coupling would limit the degree of curvature in the body of the fish only allowing shallow body bends like those observed in the swimming movements of the eel. Larval zebrafish swim with eel-like movements (Budick and O'Malley 2000a; Buss and Drapeau 2001a), which is an energetically efficient means of movement for small larval fish (Batty 1984). Thus, the physiological properties of larval zebrafish muscle complement the most energetically favourable form of swimming in this developing fish.

TABLES AND FIGURES

Table 2.1. Developmental changes in the properties of ER and EW muscle fibers

Day 1	Embryonic Red	Embryonic White
V_m (mV)	-78 ± 2 (n = 10)[3,4,5]	-83 ± 1 (n = 10)[1,2,3]
R_I (MΩ)		
hyperpolarizing	31 ± 2 (n = 5)[9,10]	33 ± 6 (n = 5)
depolarizing	no rectification	no rectification
Tau (ms)		
τ_{fast}	3.2 ± 0.8 (n = 5)[15]	0.50 ± 0.16 (n = 5)[13,14,15]
τ_{slow}	71 ± 3[19,20]	76 ±4[17,18]
(% amplitude)	(75 ± 4)[22,23,24]	(21 ± 5)[22]
Dye Coupling		
number of cells	23 ± 2 (n = 13)[30,31,32]	7.7 ± 1.3 (n = 10)[28,29,30]
number of segments	5.0 ± 0.2[37,38,39]	3.6 ± 0.3[35,36,37]
Tetanus Fusion (Hz)	24-25 (n = 2)	14-18 (n = 2)
Contraction Threshold (mV)	-49 ± 3 (n = 5)	no response

Day 3	Embryonic Red	Embryonic White
V_m (mV)	-68 ± 1 (n = 5)[4,6,7]	-74 ± 2 (n = 5)[1,6]
R_I (MΩ)		
hyperpolarizing	74 ± 10 (n = 5)[9,12]	46 ± 8 (n = 5)[11]
depolarizing	36 ± 8	no rectification
Tau (ms)		
τ_{fast}	2.7 ± 0.3 (n = 5)[16]	4.4 ± 0.7 (n = 5)[13]
τ_{slow}	39 ± 11[19]	40 ± 9[17]
(% amplitude)	(36 ± 7)[23,26]	(19 ± 0.4)[25,26]
Dye Coupling		
number of cells	6.2 ± 0.8 (n = 14)[31,33]	2.3 ± 0.2 (n = 22)[28,33]
number of segments	3.1 ± 0.3[38,40]	2.2 ± 0.2[35,40]
Tetanus Fusion (Hz)	25 ± 1 (n = 5)	23 ± 2 (n = 5)
Contraction Threshold (mV)	-53 ± 7 (n = 3)	no response

Day 5	Embryonic Red	Embryonic White
V_m (mV)	-61 ± 1 (n = 10)[5,7,8]	-76 ± 3 (n = 9)[2,8]
R_I (MΩ)		
hyperpolarizing	30 ± 5 (n = 5)[12]	27 ± 5 (n = 5)[11]
depolarizing	19 ± 3[10]	no rectification
Tau (ms)		
τ_{fast}	1.2 ± 0.1 (n = 5)[16,42]	2.4 ± 0.5 (n = 5)[14,42]
τ_{slow}	16 ± 3[20,21]	36 ± 7[18,21]
(% amplitude)	(49 ± 2)[24,27]	(12 ± 1)[25,27]
Dye Coupling		
number of cells	6.4 ± 0.5 (n = 16)[32,34]	2.4 ± 0.3 (n = 9)[29,34]
number of segments	3.1 ± 0.1[39,41]	2.0 ± 0.3[36,41]
Tetanus Fusion (Hz)	27 ± 1 (n = 5)	26 ± 1 (n = 2)
Contraction Threshold (mV)	-47 ± 4 (n = 4)	no response

Values are means ± SE; number in parenthesis is the number of fibers examined. *, no twitch contractions observed with depolarizations up to –40 mV. Paired superscript numbers indicate a significant difference of means (Student's *t-test*, Mann-Whitney rank sum test, ANOVA, or Kruskal-Wallis ANOVA) and comparisons were made both horizontally and vertically in the Table.

Table 2.2. Developmental changes in the properties of mEPPs

Muscle Fibre	Amplitude (mV)	Rise time (ms)	Half-width (ms)	Frequency (Hz)
Day 1 ER (*n* = 5)	0.87 ± 0.04^{2}	$2.3 \pm 0.2^{3,5}$	$24 \pm 2^{6,7}$	0.38 ± 0.04^{3}
Day 1 EW (*n* = 5)	0.80 ± 0.10^{1}	$0.58 \pm 0.06^{3,4}$	3.8 ± 0.1^{6}	$0.10 \pm 0.02^{3,9}$
Day 5 ER (*n* = 5)	2.3 ± 0.4^{2}	0.39 ± 0.04^{5}	3.6 ± 0.2^{7}	0.57 ± 0.11
Day 5 EW (*n* = 4)	3.7 ± 0.8^{1}	0.33 ± 0.05^{4}	3.5 ± 0.2	1.0 ± 0.2^{9}

Values are mean ± SE, *n* is the number of fibers. Day 1 embryos were 29-33 hpf. Paired superscript numbers indicate a significant difference of means (Student's *t-test*, Mann-Whitney rank sum test, ANOVA, or Kruskal-Wallis ANOVA) and comparisons were made both horizontally and vertically in the Table.

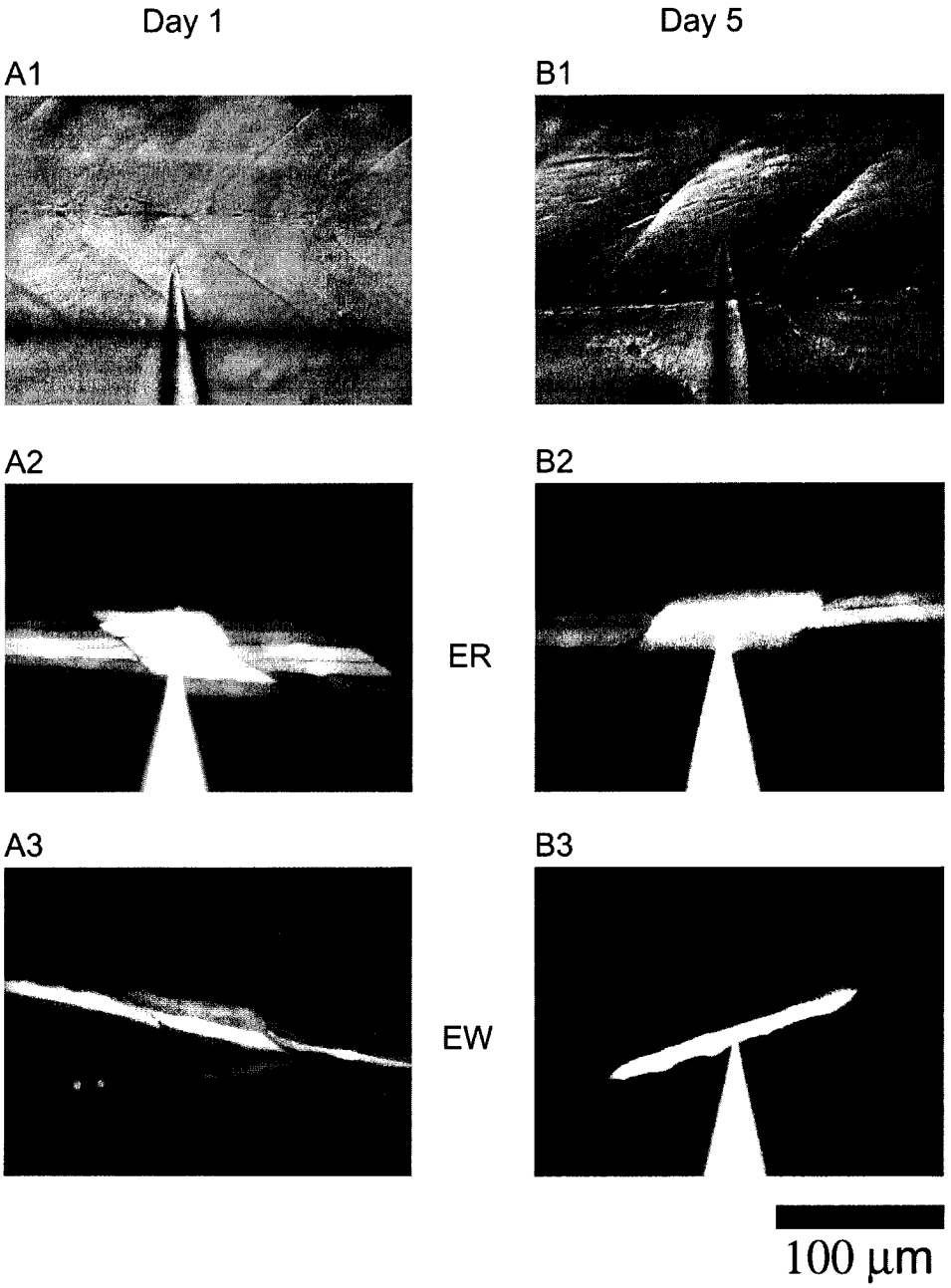

Figure 2.1. Coupling between ER and EW muscle fibers. A1 and B1: bright field illumination images corresponding to the fluorescent images shown in A2 and B2. Dye coupling in sulforhodamine B filled day 1 ER (A2) and EW (A3) muscle fibers and in day 5 ER (B2) and EW (B3) muscle fibers. The middle brightest cell in A3 was filled.

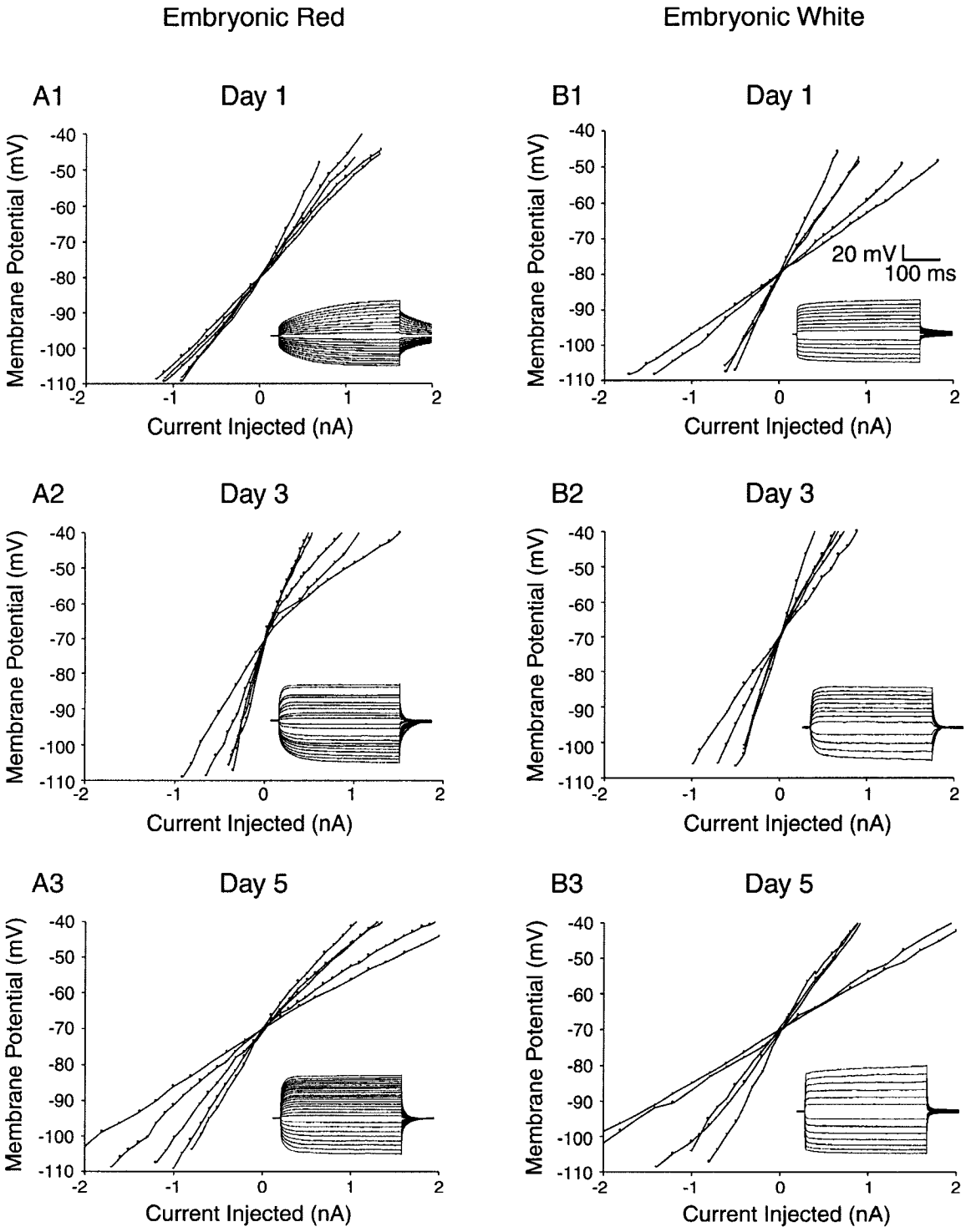

Figure 2.2. Voltage-current relationships of 5 ER muscle fibers at day 1 (A1), day 3 (A2), and day 5 (A3) and 5 EW muscle fibers at day 1 (B1), day 3 (B2), and day 5 (B3). Insets show voltage responses to step depolarizing and hyperpolarizing current injections. Day 1 fibers were held at -80 mV and day 3 and 5 fibers at -70 mV.

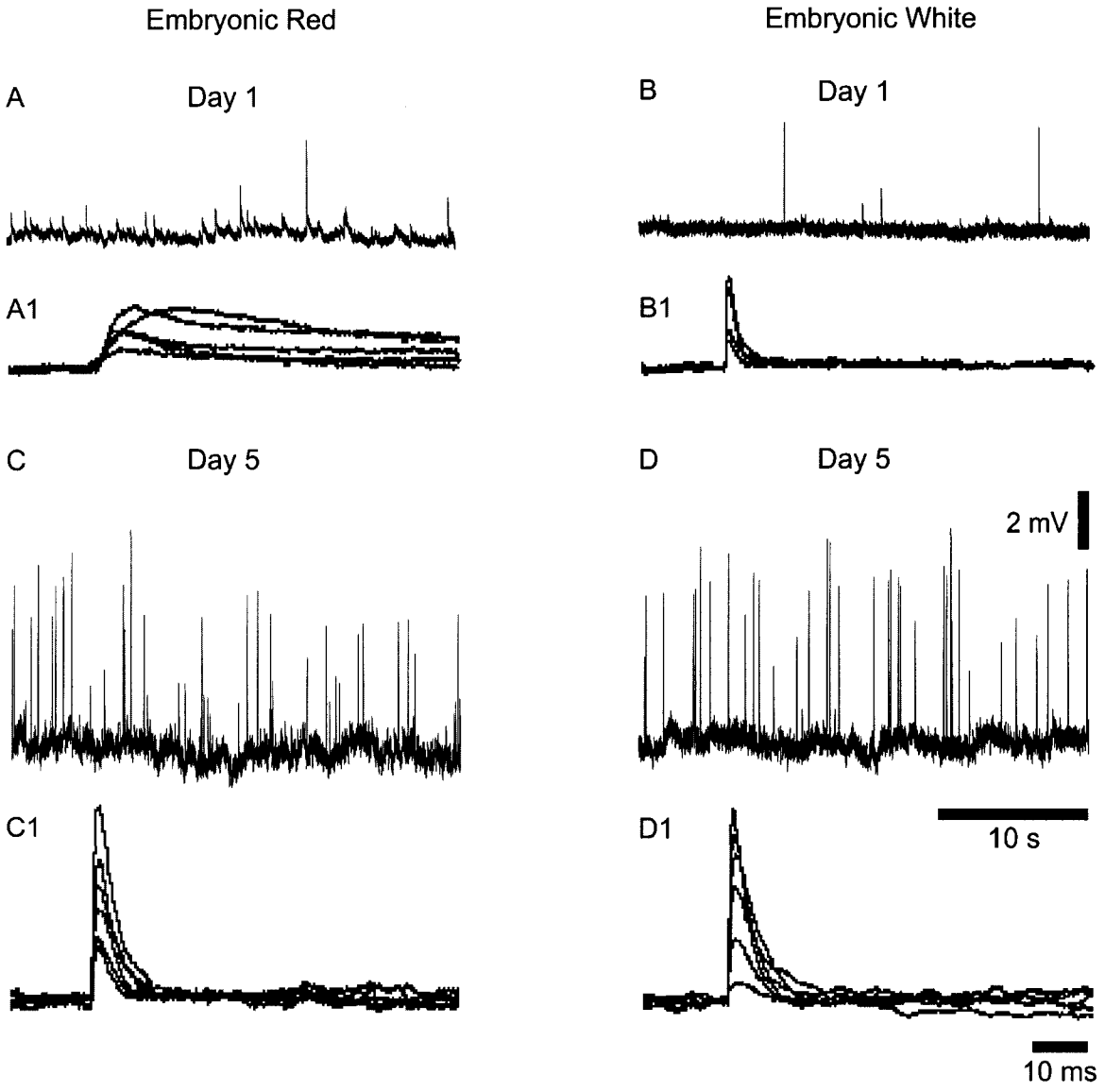

Figure 2.3. Representative examples of spontaneous mEPP activity recorded in day 1 ER (A) and EW (B) muscle fibers held at -80 mV. Day 5 ER (C) and EW (D) fibers were held at –70 mV. A1 to D1 show representative examples of mEPPs on an expanded time scale.

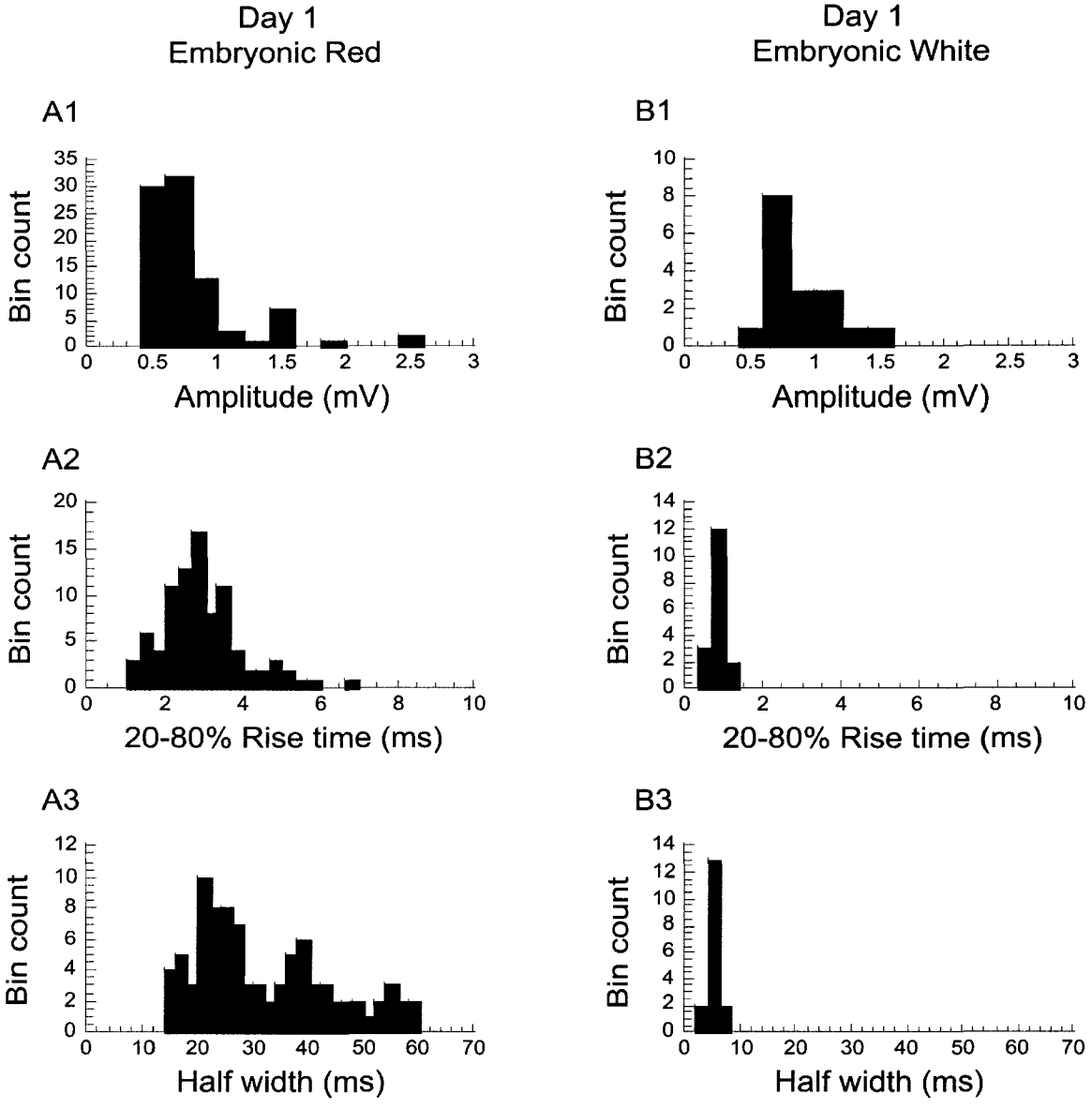

Figure 2.4. Parameters of day 1 ER and EW fiber mEPPs. Histograms of mEPP amplitude (A1 and B1), 20-80% rise time (A2 and B2), and half-width (A3 and B3) distributions from recordings in Day 1 ER (A1-A3) and EW (B1-B3) muscle fibers. A: 89 events. B (17 events). A1 and B1: bin width = 0.20 mV. A2 and B2: bin width = 0.33 ms. A3 and B3: bin width = 2 ms.

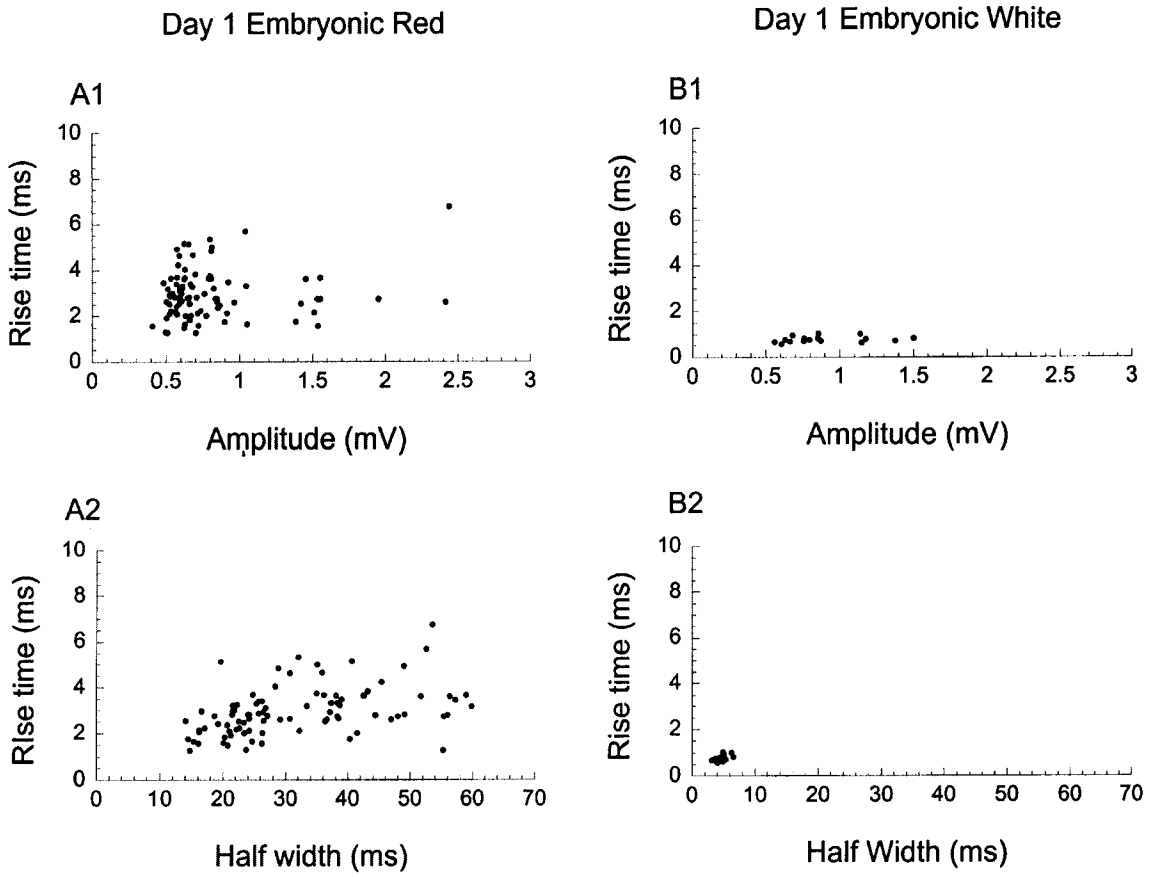

Figure 2.5. Scatter plots of rise time *vs* amplitude for mEPPs recorded in day 1 ER (A1) and EW (B1) muscle fibers. A2 and B2 show scatter plots of rise time *vs* half-width for mEPPs recorded in the same day 1 ER and EW fibers. The same mEPPs used to construct Figure 2.4 are used here.

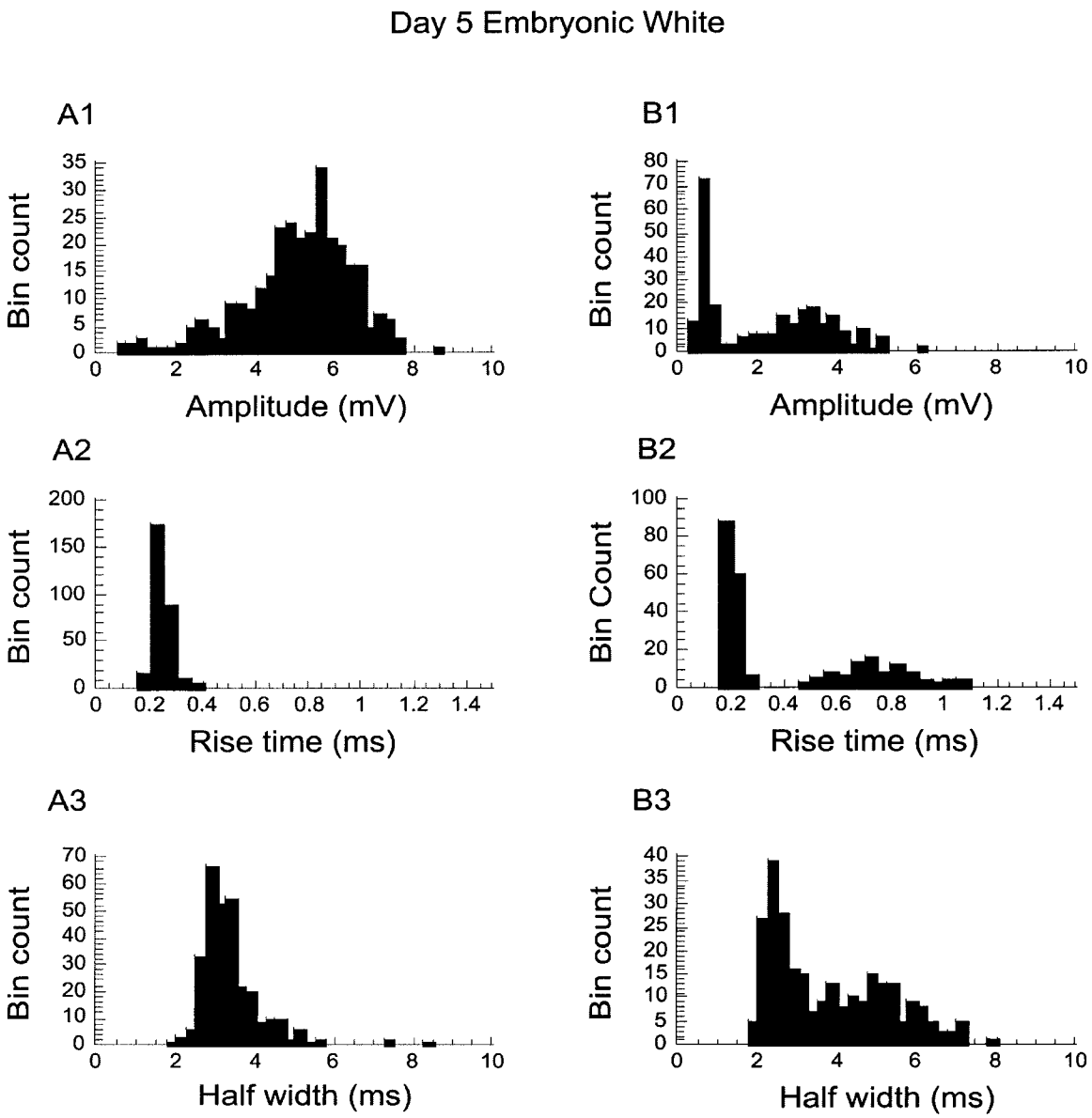

Figure 2.6. Parameters of day 5 EW fiber mEPPs. Histograms of mEPP amplitude (A1 and B1), 20-80% rise time (A2 and B2), and half-width (A3 and B3) distributions from recordings in Day 5 EW muscle fibers displaying 1 population of events (A1-A3) or 2 populations of events (B1-B3). A: 302 events. B: 266 events. A1 and B1: bin width = 0.25 mV. A2 and B2: bin width = 0.05 ms. A3 and B3: bin width = 0.25 ms.

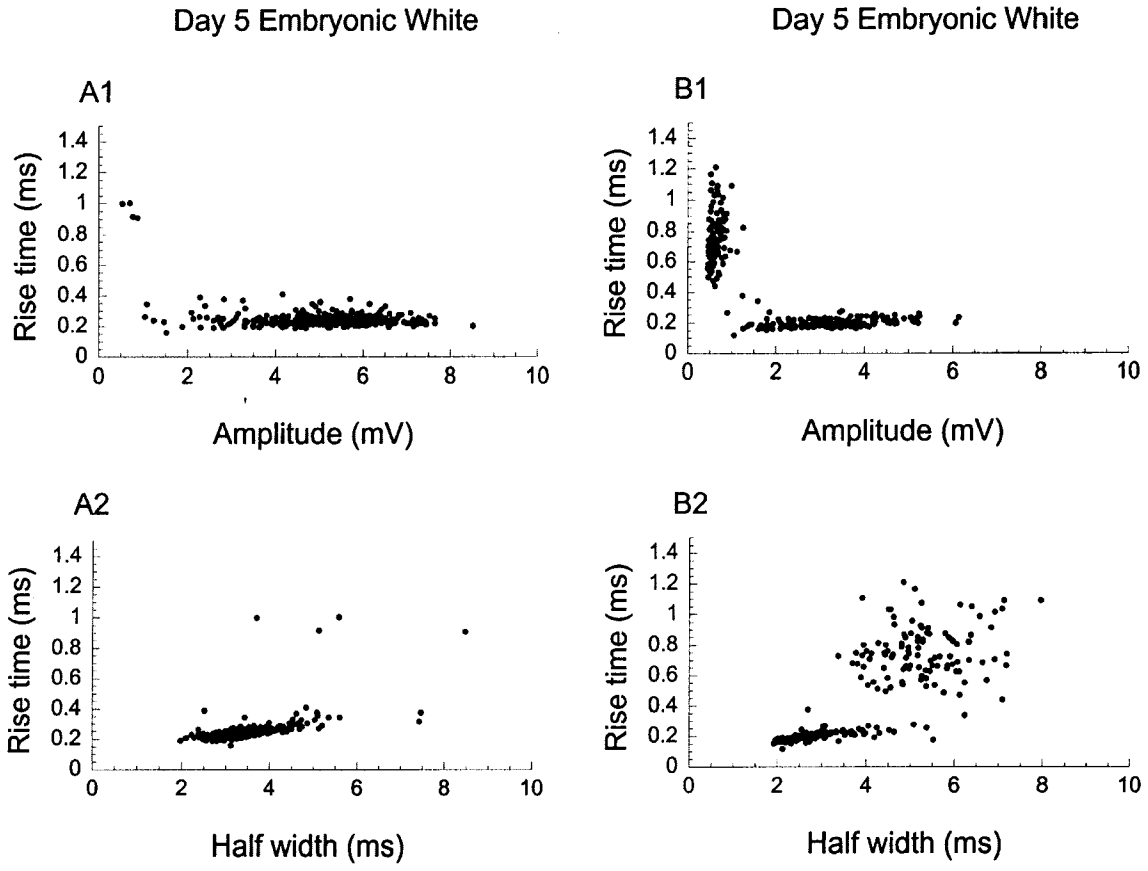

Figure 2.7. Scatter plots of rise time *vs* amplitude for mEPPs recorded in day 5 EW fibers displaying a single population (A1) or 2 populations (B1) of mEPPs. A2 and B2 show scatter plots of rise time *vs* half-width for mEPPs recorded in the same day 5 EW fibers. The same mEPPs used to construct Figure 2.6 are used.

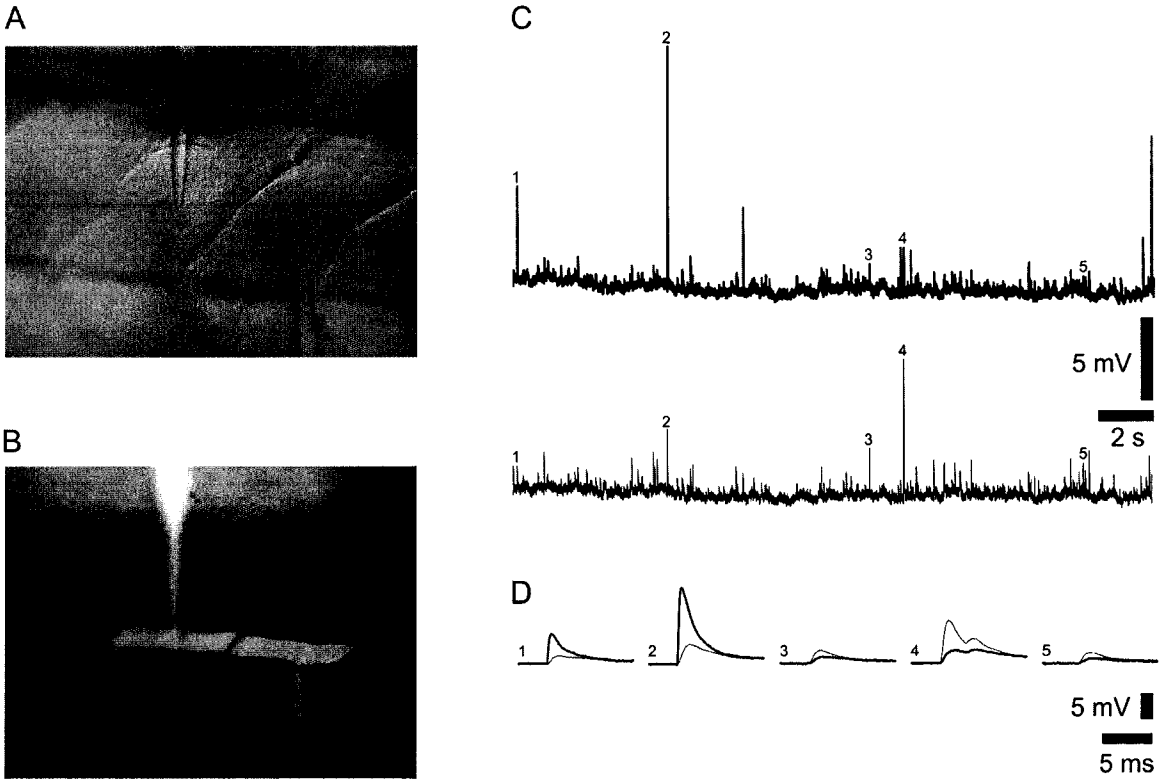

Figure 2.8. Paired recordings from adjacent day 3 ER muscle fibers. Bright field (A) and fluorescent image (B) of the pair of fibers recorded from in C and D. The recordings contain the 50 events used for analysis of the mEPPs. Representative mEPPs are numbered 1 to 5 in C and are shown in an enlarged scale in D. The bold top trace in C corresponds to the bold mEPPs shown in D.

Chapter Three: Developmental Changes in Muscle Chloride Ion Permeability

LINKING STATEMENT

During the developmental stages examined, there were changes in the input resistance and resting membrane potential of ER and EW muscle fibers that were not explained by fiber uncoupling, but were consistent with the development of a membrane leak conductance. I hypothesized and verified that this leak conductance was due to developmental changes in the chloride ion permeability of zebrafish muscle.

ABSTRACT

Developmental changes in the chloride ion permeability (P_{Cl}) of embryonic red (ER) and white (EW) muscle fibers was examined by dialyzing fibers with 10-140 mM [Cl^-], using the whole-cell patch-clamp technique, in 1-5 day old zebrafish. Changes in membrane potential (V_m) were examined as the V_m of muscle fibers with large P_{Cl} will equilibrate near the Cl^- equilibrium potential (E_{Cl}). Alternately, the V_m of fibers lacking P_{Cl} will be largely determined by the permeability of other ion species (*i.e.*, K^+) and will be unaffected by patch pipette [Cl^-]. Resting V_m determined using sharp electrode recordings confirmed whole-cell patch-clamp values. From day 1 to 5, the P_{Cl} of EW fibers increased substantially while only small changes were observed in ER fibers. In addition, the resting membrane potential of ER fibers depolarized 15-20 mV between day 1 and day 3-5 and this was not due to a change in P_{Cl}.

INTRODUCTION

The membranes of many vertebrate and invertebrate muscles are permeable to Cl^- (Bretag 1987; Foskett 1998; Jentsch et al. 1999; Pusch and Jentsch 1994) but the developmental changes in Cl^- permeability (P_{Cl}) have been studied in only a few species. In zebrafish, previous studies have focussed on morphological and molecular aspects of muscle development, while little is known of the physiological changes occurring during muscle development (Buss and Drapeau 2000a). During the first week of development, zebrafish have 2 distinct forms of striated skeletal muscle; embryonic white (EW) and embryonic red (ER) (Buss and Drapeau 2000a). The goals of this study were to determine the P_{Cl} of

ER and EW muscle, the time-course of its development, and how these relate to the development of locomotor behaviors.

Among the vertebrates, the skeletal muscle chloride ion conductance (G_{Cl}) has been most fully characterized in amphibians in which its characteristics include voltage dependency, pH sensitivity and slow kinetics (Bertran and Kotsias 1996; Hui and Chen 1994; Hutter and Warner 1967a; Hutter and Warner 1967b; Hutter and Warner 1967c; Loo et al. 1981; Spalding et al. 1990; Vaughan and Nok 1978; Vaughan and Trotter 1982; Warner 1972). Vertebrate fast-twitch muscle has a higher G_{Cl} than slow-twitch muscle and G_{Cl} is negligible in slow-tonic muscle fibers (Farnbach et al. 1978; Huerta and Stefani 1981; Hutter and Warner 1967c; Lorkovic and Tomanek 1977; Poznansky and Steele 1984; Stanfield 1972; Stefani and Steinbach 1969). The characteristics of the skeletal muscle G_{Cl} of fish (Eugene and Barets 1982; Hagiwara and Takahashi 1967; Hagiwara and Takahashi 1974; Klein 1985; Klein and Prosser 1985; Nicolaysen 1976a; Stanfield 1972) and mammals (Dulhunty 1978; Fahlke and Rudel 1995; Palade and Barchi 1977) is similar to amphibians; less is known in birds (Huerta and Stefani 1981; Lebeda and Albuquerque 1975; Poznansky and Steele 1984). The ClC-1 voltage-gated Cl^- channel underlies the macroscopic G_{Cl} observed in mammalian skeletal muscle (Foskett 1998; Jentsch et al. 1999; Pusch and Jentsch 1994) and mutation of this channel is the cause of myotonia congenita (Lehmann-Horn and Jurkat-Rott 1999; Rudel and Lehmann-Horn 1985). Thus, understanding how muscle P_{Cl} develops is important for addressing the physiology and pathology of muscle Cl^- homeostasis.

Rat and mouse skeletal muscle G_{Cl} increases during the first post-natal

month (Conte Camerino et al. 1989; Farnbach et al. 1978), in parallel with expression of ClC-1 mRNA (Klocke et al. 1994; Steinmeyer et al. 1991), from undetectable levels at birth. The G_{Cl} of chick fast-twitch muscle develops during the last week of embryonic development reaching adult values at hatching (Poznansky and Steele 1984). Therefore, in the rat and chick, a significant G_{Cl} is present when weight support and locomotion develops (Bekoff 1992; Clarac et al. 1998). The skeletal muscle G_{Cl} decreases during aging in rats (De Luca et al. 1990; De Luca et al. 1997; Pierno et al. 1999). The membranes of rat and *Xenopus* myogenic cells grown in culture are largely impermeable to Cl^- (Kidokoro 1975; Ritchie and Fambrough 1975; Spruce and Moody 1992) whereas the G_{Cl} is sufficient to initiate a slow rising and long lasting regenerative action potential in cultured chick skeletal muscle (Fukuda 1974; Fukuda 1975; Fukuda et al. 1976a; Fukuda et al. 1976b). This aberrant development of muscle G_{Cl} in tissue culture reinforces the need to study developmental changes *in vivo*.

To determine zebrafish muscle P_{Cl}, fibers were dialyzed with $[Cl^-]$ in the range of 10 mM to 140 mM using the whole-cell patch-clamp technique at days 1-5 of development. This is the period when embryonic muscle is innervated (day 1), larvae hatch (day 2) and motor behaviors mature (day 5) (Buss and Drapeau 2001a). Changes in membrane potential (V_m) were examined as the V_m of muscle fibers with large P_{Cl} will equilibrate near the Cl^- equilibrium potential (E_{Cl}). Alternately, the V_m of fibers lacking P_{Cl} will be largely determined by the permeability of other ion species (*i.e.*, K^+) and will be unaffected by patch pipette $[Cl^-]$. Resting V_m determined using sharp electrode recordings confirmed whole-cell patch-clamp values.

METHODS

Experiments were performed on zebrafish (Tubingen and Longfin lines) larvae raised at 28.5 °C and obtained from a breeding colony maintained according to Westerfield (1995). All procedures were carried out in compliance with the guidelines stipulated by the Canadian Council for Animal Care and McGill University. The experimental methodology has been described (Buss and Drapeau 2000a; Chapter 2). A small positive pressure was applied to the patch pipette, which was moved towards a muscle fiber until a slight dimple formed in the membrane. Positive pressure was released, a gigaohm seal formed (with or without suction), patches were ruptured by suction, and recording commenced. Results are taken from recordings made in 126 whole-cell patch-clamp and 7 sharp electrode recordings from ER and EW muscle fibers of zebrafish aged 1.3-1.6 (day 1), 3.2-3.4 (day 3) or 5.1-5.4 (day 5) days post fertilization. Experiments were performed at room temperature (approximately 22 °C). The fish saline recording solution (Buss and Drapeau 2001a; Drapeau et al. 1999) contained (in mM) 134 NaCl, 2.9 KCl, 2.1 $CaCl_2$, 1.2 $MgCl_2$, 10 HEPES, 10 glucose, 15 μM D-tubocurarine, osmolarity adjusted (with glucose) to 290 mOsm and pH 7.8. Patch-clamp electrodes (1.5-4 MΩ) contained a K-gluconate solution consisting of (in mM) 2 $MgCl_2$, 10 HEPES, 10 EGTA, and 6, 36, 76 or 136 KCl added to sufficient D-gluconic acid potassium salt to reach a final osmolarity of 290 mOsm, pH 7.2. The liquid junction potentials of the electrode solutions containing 10, 40, 80 or 140 mM Cl^- were measured as –12, -8, -6 and –3 mV respectively and records were corrected for this potential.

Recordings were performed with an Axoclamp-2A patch-clamp amplifier (0.01 headstage; 1 kHz low-pass filter) and data were digitized at 1 KHz except for when action potentials were evoked. A 10 mM Cl^- patch-clamp electrode solution was used during action potential recordings and data were filtered at 10 KHz (low-pass), digitized at 10 KHz, and a 0.1 headstage used to pass the large currents required to bring the EW fibers to threshold. Theoretical Cl^- reversal potentials were calculated, taking into consideration the activity coefficient of Cl^- (Parsons 1959), using the Nernst equation. The P_{Cl}/P_K permeability ratio was determined using the Goldman-Hodgkin-Katz equation. Sharp electrodes were filled with 3 M KCl and had resistances of 25-30 MΩ. All chemicals were purchased from Sigma Chemical Co. (St. Louis, MO). Analyses were performed using pClamp 8 software (Axon Instruments) and results are presented as mean ± SE throughout the text.

RESULTS

Membrane potentials varied positively with patch pipette $[Cl^-]$ in both ER and EW fibers at all ages examined (Figure 3.1). In ER fibers (Figure 3.1, A and A1) this difference was relatively small, ranging on average from 10 mV at day 1 to 18 mV at day 5 in fibers dialyzed with 10 *vs* 140 mM Cl^-. The V_m of ER fibers dialyzed with 10 mM Cl^- was on average 19-34 mV positive to E_K. In addition, there was a clear 15-20 mV depolarizing shift in membrane potential between day 1 and day 3-5 that was independent of patch pipette $[Cl^-]$.

In contrast to ER fibers, large differences in V_m (54-68 mV) were observed

in day 3-5 EW fibers (Figure 3.1, B and B1) dialyzed with 10 mM *vs* 140 mM Cl^-, which is attributed to the development of a larger P_{Cl} at these ages. The V_m of EW fibers dialyzed with 10 mM Cl^- approached E_K (-96 ± 2 mV). At most ages V_m was considerably hyperpolarized to E_{Cl}. P_{Cl}/P_K was determined in day 5 EW fibers which had developed a substantial P_{Cl}. P_{Cl}/P_K varied from 0.15 (in fibers dialyzed with 10 mM P_{Cl} where V_m remained close to the resting V_m) to values of 0.65 to 1.3 (in fibers dialyzed with 40-140 mM Cl^- that had more depolarized V_m). Cl^- permeability was negligible in day 1 EW fibers (P_{Cl}/P_K = 0.04-0.30) and day 3 appeared to be a transition period where P_{Cl} was only observed in fibers dialyzed with 140 mM Cl^-. Action potentials were not evoked during the slow membrane depolarization occurring during Cl^- dialysis. At day 1, EW fibers had a slightly more hyperpolarized (4-10 mV) membrane potential than ER fibers that was also independent of patch pipette [Cl^-].

Sharp electrode impalement led to a rapid deterioration of V_m and the structure of the small and fragile EW and ER muscle fibers. To minimize impalement damage, experiments were performed on day 5 zebrafish when fibers had grown to a size more amenable for sharp electrode recording. An impalement was considered successful if there was an immediate sharp and rapid drop in V_m. The resting V_m of EW fibers was -84±1 mV (n = 3) and that of ER fibers -49±1 mV (n = 5).

The resting membrane potential of day 3-5 EW fibers, examined using 10 mM Cl^- electrode solutions or sharp electrodes, was at least 15 mV more hyperpolarized (due to the large Cl^- permeability of the membrane) than reported by Buss and Drapeau (2000a). Therefore, Buss and Drapeau (2000a) may not

have observed action potentials in EW fibers because of sodium channel inactivation. Action potentials, that were blocked by 1 μM TTX, were observed in 5 EW fibers dialized with 10 mM Cl^- that a had resting V_m <-85 mV (Figure 3.2). However, action potential were never observed in ER fibers, even when negative current was used to hyperpolarize the membrane well below normal values.

DISCUSSION

Developmental Changes in Muscle Chloride Ion Permeability

All zebrafish muscle fibers have some permeability to Cl^-, as V_m was on average more depolarized in fibers dialyzed with 140 *vs* 10 mM Cl^-. During development from day 1 to 5, P_{Cl} of EW fibers increased substantially while smaller changes were observed in ER fibers. In day 5 EW fibers that had developed a large P_{Cl}, P_{Cl}/P_K varied (0.15-1.3) with intracellular [Cl^-] and V_m (P_{Cl}/P_K was larger at depolarized V_m). These values are considerably less than those reported in elasmobranch fish (4-10), frog (approximately 2), chick (4-5) and mammals (generally 2-6 but as high as 20) but are consistent with values found in other teleost fish (Bretag 1987). The dominance of P_{Cl} at depolarized potentials may be due to a combination of a larger P_{Cl} due to the voltage sensitivity of ClC channels as well as a lower P_K due to inactivation of inward rectifier K^+ channels. The development of P_{Cl} between days 3 and 5 likely contributes to the decrease in input resistance observed in EW fibers at this time (Buss and Drapeau 2000a).

The acquisition of a large P_{Cl} in EW muscle occurs when mature goal directed swimming develops in zebrafish larva (Buss and Drapeau 2001a). A

parallel maturation of locomotion and skeletal muscle P_{Cl} also occurs in rat and chick (Bekoff 1992; Clarac et al. 1998; Conte Camerino et al. 1989; Poznansky and Steele 1984). P_{Cl} is thought to provide an electrical shunt allowing rapid membrane repolarization during muscle contractions (Bretag 1987). Interestingly, zebrafish are capable of swimming (although erratically) prior to the development of EW P_{Cl}. At this time, electrical coupling between muscle fibers may provide an electrical shunt equivalent to P_{Cl}.

When EW fibers were dialyzed with 10 mM Cl^-, V_m approached E_K whereas the V_m of ER fibers was considerably depolarized to E_K. From day 1 to days 3-5, ER fibers depolarized 15-20 mV, as shown previously by Buss and Drapeau (2000a). The present study revealed that this change is not due to developmental changes in E_{Cl}, nor is it likely due to a decrease in G_K because R_i approximately doubles (Buss and Drapeau 2000a) during this period. It is hypothesized that the depolarization of ER fibers is due to the addition of a non-selective cation conductance, possibly mediated by the channels described by Chua and Betz (1991). Buss and Drapeau (2000a) also reported a slight depolarization of EW fibers from day 1 to day 5. This is likely an experimental artifact due to the use of 20 mM Cl^- in their patch recording solution, as the resting V_m of day 1 EW fibers was at a level found in adult zebrafish white muscle (Westerfield et al. 1986) and the day 5 EW muscle examined with sharp electrodes in this study.

It is generally believed that Cl^- is distributed close to equilibrium in skeletal muscle largely because of the difficulty in maintaining an electrochemical Cl^- gradient in tissue highly permeable to Cl^- (Alvarez-Leefmans and Russell 1990;

Bolton and Vaughan-Jones 1977). However, when the muscle G_{Cl} is blocked, an intracellular accumulation of Cl^- has been observed (Harris and Betz 1987). In zebrafish, it is conceivable that Cl^- levels are regulated to values out of equilibrium in ER and day 1 EW muscle fibers that have a low P_{Cl}. If a passive distribution of Cl^- is assumed, ER fiber [Cl^-] will be higher than EW fiber [Cl^-] due to differences in resting V_m.

Comparison of ER and EW Muscle Properties

In the first study of the physiological properties of zebrafish ER and EW muscle, Buss and Drapeau (2000a) concluded that ER and EW fibers have similar but not identical physiological properties. The different P_{Cl} of ER and EW fibers found in this study reveals that their membrane properties are more distinct than originally thought. Buss and Drapeau (2000a) found that age matched ER and EW fibers had similar input resistances. It is now evident that this similarity was due to different amounts of electrical coupling in ER and EW fibers. The low membrane permeability of ER being compensated by an increased amount of electrical coupling to neighboring cells. Physiologically, this would act to equalize the synaptic drive to ER and EW muscles, which are similarly, but not identically activated during larva swimming (Buss and Drapeau 2001b; Buss and Drapeau 2002), but that also have more complex patterns of recruitment during larval and adult swimming (Bone 1978; Buss and Drapeau 2002; Coughlin and Rome 1996; Jayne and Lauder 1996).

The physiological differences in ER and EW fibers are similar to the differences in vertebrate slow-tonic and twitch muscle. Slow-tonic and ER muscle both display low P_{Cl}, outward rectification, depolarized resting V_m, a low

contraction threshold, and an absence of action potentials. EW fibers are similar to twitch muscle, both having large P_{Cl}, minimal rectification (-100 to -40 mV), hyperpolarized resting V_m, high contraction threshold, and the presence of action potentials. Action potentials (in EW fibers) were rarely observed by Buss and Drapeau (2000a). However, their presence was consistently detected in this study when low (10 mM) intracellular chloride ion concentrations were used and fibers had resting potentials were <-85 mV (Figure 3.2).

It is interesting that separate populations of embryonic slow-tonic and twitch muscle fibers (*i.e.*, ER and EW) have not been described in amphibian embryos. However, it may be that the thin dermatome layer of cells examined by Blackshaw and Warner (1976) is homologous to fish ER muscle fibers. Similar to zebrafish ER fibers, the dermatome layer is 1-2 cells thick, is located superficial to the myotomal muscle, is electrically coupled to other fibers in the dermatome layer but not to myotomal muscle, and has a more positive resting membrane than the myotomal muscle fibers (Blackshaw and Warner 1976; Buss and Drapeau 2000a). Furthermore, studies in zebrafish, using molecular and histochemical techniques, have classified muscle fibers as fast and slow, and have not physiologically distinguished fibers as slow-tonic and twitch muscle (Hughes and Salinas 1999). Whether the development of zebrafish tonic and twitch muscle will provide insight into the development of mammalian slow and fast twitch muscle remains to be determined.

FIGURES

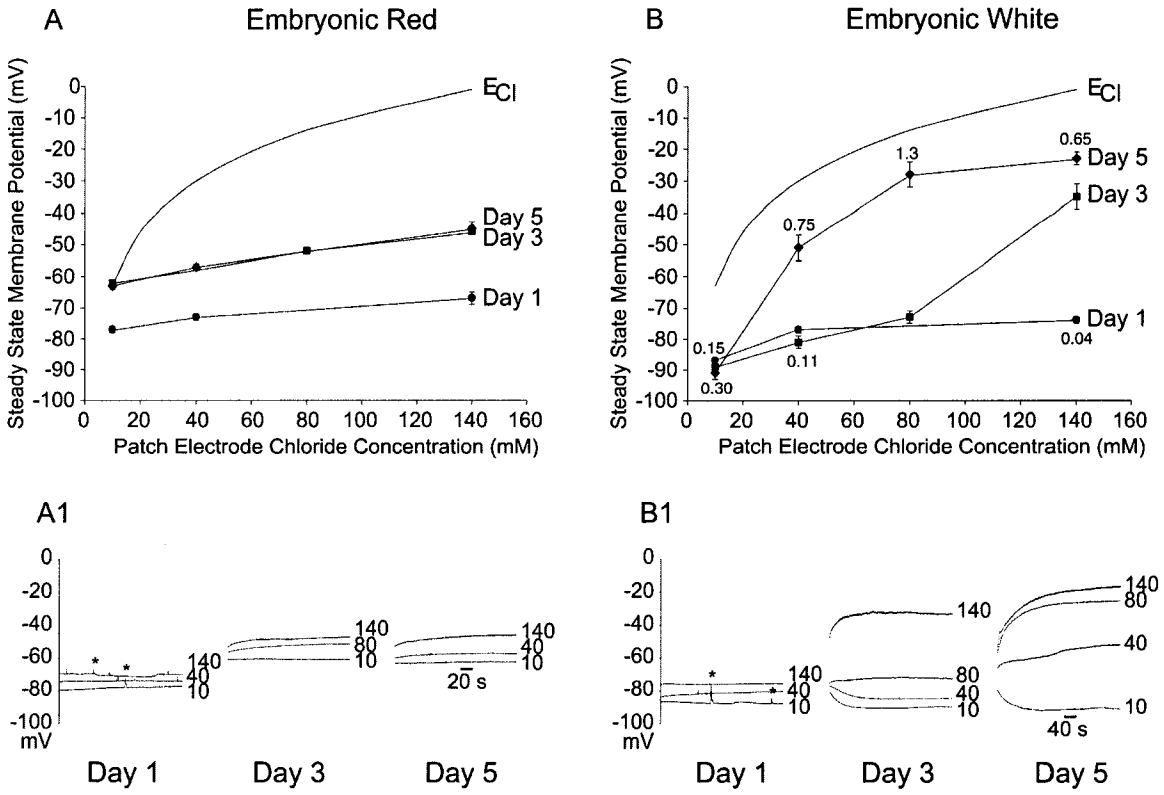

Figure 3.1. (A) and (B): Average membrane potential values of zebrafish muscle fibers dialyzed with patch pipette solutions containing 10-140 mM Cl^-. Each data point represents the mean ± SE steady state membrane potential of 5-8 muscle fibers dialyzed with 10, 40, 80, or 140 mM Cl^- contained in the patch pipette solution. Day 1 (●), day 3 (■) and day 5 (◆). Values below and above Day 1 and Day 5 EW fiber data points are P_{Cl}/P_K values determined for that data point. Data points are joined by straight lines for clarity. E_{Cl} values were calculated for 10, 40, 80 and 140 mM Cl^- and fit with spline curves. A1 and B1: Changes in zebrafish muscle fiber membrane potentials due to dialysis of patch pipette solutions containing 10-140 mM Cl^-. Patch pipette [Cl^-] is shown at the right of each trace. The * in day 1 traces show episodes of motoneuron evoked synaptic activity.

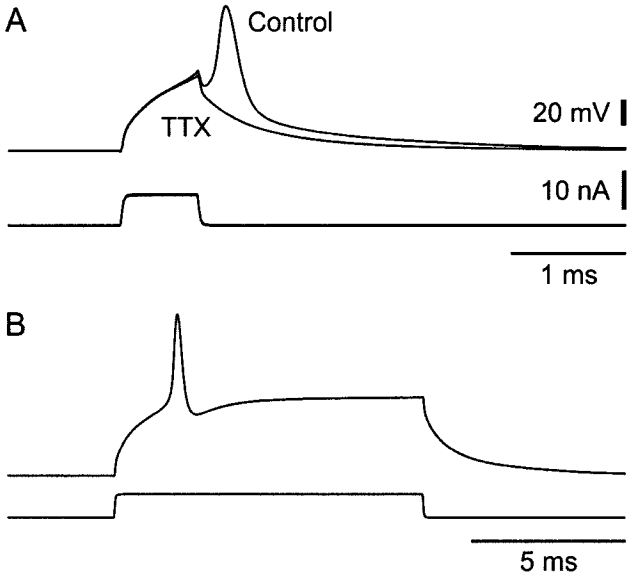

Figure 3.2. Action potentials in a day 3 EW muscle fiber. (A) The action potential is eliminated in TTX (1μm). An afterhyperpolarization is revealed during a longer (10 ms) depolarization (B). The EW fiber was held a –90 mV.

Chapter Four: Activation of Embryonic Red and White Muscle Fibers During Fictive Swimming

LINKING STATEMENT

Chapters 2 and 3 established that ER and EW fibers have unique physiological properties but did not address how these muscle fibers are used by the motor system. This Chapter examines the synaptic activation of ER and EW muscle fibers during two motor behaviors, fictive swimming and coiling, and shows that they are uniquely activated during swimming.

ABSTRACT

Sub-threshold, motoneuron-evoked synaptic activity was observed in zebrafish embryonic red (ER) and white (EW) muscle fibers paralyzed with a dose of D-tubocurarine insufficient to abolish synaptic activity, in order to determine whether muscle activation was coordinated to produce the undulating body movements required for locomotion. Paired whole-cell recordings revealed a synaptic drive that alternated between ipsilateral and contralateral myotomes and exhibited a rostral-caudal delay in timing appropriate for swimming. Both ER and EW muscle were activated during fictive swimming. However, at the fastest fictive swimming rates, ER fibers were de-recruited, whereas they could be active in isolation of EW fibers at the slowest fictive swimming rates. Prior to hatching, fictive swimming was preceded by a lower frequency, more robust and rhythmic synaptic drive resembling the "coiling" behavior of fish embryos. The motor activity observed in paralyzed zebrafish closely resembled the swimming and coiling behaviors observed in these developing fishes. At the early developmental stages examined in this study, myotomal muscle recruitment and coordination were similar to that observed in adult fishes during swimming. The results indicate that the patterned activation of myotomal muscle is set from the onset of development.

INTRODUCTION

Studies on the locomotor behaviors of larval zebrafish have largely focussed on the startle response (Eaton and DiDomenico 1986; Eaton et al.

2001; Kimmel et al. 1974; Liu and Fetcho 1999, and references therein) while swimming behaviors have received less attention (Budick and O'Malley 2000a; Buss and Drapeau 2001a; Fuiman 1986; Fuiman and Webb 1988; Muller et al. 2000; Saint-Amant and Drapeau 1998). Knowledge of the neural control of larval zebrafish swimming is restricted to motoneuron activity patterns and the synaptic drive to motoneurons in paralyzed zebrafish during fictive swimming (Buss and Drapeau 2001a). Whether the activity of myotomal motoneurons is coordinated to produce the undulating body movements required for locomotion, and whether both forms of myotomal muscle, embryonic red (ER) and embryonic white (EW), are activated during fictive swimming is unknown.

The activity of zebrafish motoneurons is fundamentally similar to the motoneuron activity observed in lampreys and amphibian tadpoles during fictive swimming. This is not unexpected considering similarities in locomotion and spinal cord neuroanatomy (Grillner et al. 1998a; Roberts 2000; Roberts et al. 1998). Furthermore, similarities in synaptic drive to motoneurons during fictive locomotion extend to mammalian (feline) preparations (see discussion in Buss and Drapeau, 2001a). Accordingly, studies of zebrafish spinal cord physiology and locomotor control provide a framework for genetic and molecular investigations (Granato et al. 1996) into locomotor control in this vertebrate model which has the advantages of a simpler nervous system with identifiable components.

In the present study, paired whole-cell recordings of the rhythmic activation of larval zebrafish (day 3) muscle fibers, paralyzed with a dose of D-tubocurarine insufficient to abolish synaptic activity, were used to test whether or

not the circuitry of embryos is sufficient to generate swimming with the attributes of the adult motor pattern. The recordings revealed a synaptic drive that alternated between ipsilateral and contralateral sides and exhibited a rostral-caudal delay in timing. Both ER and EW muscle fibers were active during fictive swimming and at this early developmental period their recruitment was similar to that of adult fish. Prior to hatching (day 1), fictive swimming was preceded by a lower frequency (1-13 Hz), more robust rhythmic synaptic drive resembling the "coiling" behavior of fish embryos (Herrick 1949; Hooker 1952; Whiting 1955). The characteristics of fictive swimming are compared with the swimming patterns observed in fishes and amphibian tadpoles.

METHODS

Experiments were performed on zebrafish (Tubingen and Longfin lines) larvae and embryos raised at 28.5 °C and obtained from a breeding colony maintained according to Westerfield (1995). All procedures were carried out in compliance with the guidelines stipulated by the Canadian Council for Animal Care and McGill University. The experimental methodology has been described (Buss and Drapeau 2000a). Results are taken from 25 paired and 28 single whole-cell patch-clamp recordings from ER and EW muscle fibers of zebrafish embryos aged 1.3-1.6 (day 1, length approximately 2.5 mm) and larvae aged 3.0-3.3 (day 3, length approximately 3.5 mm) days postfertilization. Fictive swimming and coiling occurred spontaneously or was evoked (day 3) by changes in illumination. The swimming style of larval zebrafish changes from a sustained burst swimming pattern to a beat-and-glide pattern between day 2 (hatching) and

day 4. Day 3 is a transition period where a beat-and-glide like swimming pattern emerges yet burst swimming is still observed (Buss and Drapeau 2001a). Beat-and-glide like fictive swimming was observed in all day 3 larvae examined (*n* = 32) and burst swimming was additionally observed in 10 preparations.

Experiments were performed at room temperature (approximately 22 °C). The Evan's fish saline recording solution (Buss and Drapeau 2001a; Drapeau et al. 1999) contained (in mM) 134 NaCl, 2.9 KCl, 2.1 $CaCl_2$, 1.2 $MgCl_2$, 10 HEPES, 5-10 glucose, 3 (day 3) or 15 (day 1) μM D-tubocurarine, osmolarity adjusted (with glucose) to 290 mOsm and pH 7.8. Patch-clamp electrodes (1.5-4 MΩ) contained a K-gluconate solution consisting of (in mM) 2 $MgCl_2$, 10 HEPES, 10 EGTA, 10 D-gluconic acid sodium salt, and 6 KCl added to sufficient D-gluconic acid potassium salt to reach a final osmolarity of 290 mOsm, pH 7.2. All chemicals were purchased from Sigma Chemical Co. (St. Louis, MO). A liquid junction potential of –12 mV was experimentally determined according to Barry and Lynch (1991) and Neher (1992) and records were corrected for this potential.

Recordings were performed with an Axoclamp-2A (0.1 headstage) and an Axopatch-1D (CV-4 headstage) amplifier. Data were low-pass filtered at 10 KHz and digitized at 1KHz (day 1) or 10 KHz (day 3). Analyses were performed using pClamp 8 software (Axon Instruments). ER fibers were distinguished by their superficial distribution and longitudinal orientation, whereas EW fibers were deeper and had an oblique orientation (Buss and Drapeau 2000a). Measurements of fictive swimming and coiling duration, rhythmic end plate potential (EPP) frequency, and rostral-caudal delay were made by eye (cursor

measurement). Measurements on 50 consecutive EPPs were used to calculate mean fictive swimming and coiling EPP frequencies and rostral-caudal delay. Rostral-caudal delay was determined by measuring the fictive swimming rhythmic EPP delay (from EPP onset) between 9-12 segments centered on the anal segment. Rostral-caudal delay *per* segment was calculated by dividing the mean time delay by the number of separating segments. Percent phase lag was calculated by dividing the rostral-caudal delay *per* segment by the mean cycle period (Wallen and Williams 1984). Paired recordings between ER and EW fibers located within a segment revealed differences in recruitment at day 3. When fictive swimming rhythmic EPPs were observed in EW fibers, synchronous activity was observed in ER fibers. However, ER fibers were often active in the absence of EW fiber activity. Instantaneous fictive swimming rhythmic EPP frequencies were measured during ER-EW fiber co-activity and ER fiber activity. Results are presented as mean ± SD throughout the text. The term significant denotes a relationship with $P<0.05$ determined using the Student's *t-test*.

RESULTS

Rostral-Caudal Delay and Ipsilateral-Contralateral Alternation of Synaptic Drive to Myotomal Muscle During Fictive Swimming

The propulsive forces used in undulatory swimming are generated by an alternating rostral-caudal wave of myotomal muscle contraction, initiated by a synaptic drive originating from myotomal motoneurons, which interacts with the mechanical properties of body tissues (Blight 1977; Grillner and Kashin 1975; Grillner et al. 1998a; Hoff and Wassersug 2000; Lindsey 1978; Roberts et al.

1998; Roberts 1981; Wardle et al. 1995; Wassersug 1989). Therefore, during a cycle of undulatory swimming, rostral myotomal muscle fibers receive synaptic drive prior to caudal fibers and within a segment the synaptic drive alternates between ipsilateral and contralateral sides of the musculature. To examine the synaptic drive to myotomal muscle fibers, embryos and larvae were paralyzed with a low concentration of the neuromuscular antagonist D-tubocurarine, which reduced, but did not abolish neuromuscular synaptic drive. Thus, the rhythmic synaptic drive (*i. e.*, fictive swimming) underlying swimming, was examined in immobilized larvae using the whole-cell patch-clamp technique.

Paired recordings revealed a synchronous synaptic drive to muscle fibers within an ipsilateral myotomal segment (Figure 4.1; n = 11) and an alternating synaptic drive to contralateral muscle fibers (Figure 4.2; n = 6). A rostral-caudal delay was observed in paired recordings from ipsilateral muscle fibers separated by 9-12 myotomal segments (Figure 4.3; n = 7). On average, this delay was 0.55 ± 0.20 ms *per* myotomal segment and there was strong negative relationship (Figure 4.5C) between the time delay *per* segment and the rhythmic EPP frequency (*i. e.*, fictive tail beat frequency). Intersegmental phase lag *per* segment ranged from 0.8% to 2.7% and averaged 1.8 ± 0.6%. Synchronous activity within ipsilateral myotomal segments, alternation between ipsilateral and contralateral segments, and rostral-caudal delays were similarly observed in paired recordings between ER and ER (Figures 4.1 and 4.3), ER and EW (Figures 4.2 and 4.4), and EW and EW fibers (data not shown).

Differences in the Recruitment of ER and EW Muscle Fibers During Fictive Swimming

Fishes that swim by undulatory propulsion generally use red muscle for slow swimming, recruit white muscle for faster swimming, and de-recruit red muscle at the fastest speeds of burst swimming (Bone 1978; Coughlin and Rome 1996; Jayne and Lauder 1996; Johnston 1981; Johnston 1983). Whether the embryonic forms of red and white muscle (ER and EW) found in larval fish are recruited as their adult forms has not been examined. Comparison of mean fictive swimming rhythmic EPP frequencies measured in ER (24 fibers, 1200 EPPs) and EW fibers (13 fibers, 650 EPPs) revealed a small but significantly different (P = 0.03) frequency of rhythmic EPPs in EW *vs* ER fibers (44 ± 7 Hz *vs* 39 ± 7 Hz). Both ER and EW fibers were recruited during fictive swimming (Figures 4.2 and 4.4). However, within a swimming episode, there were periods, especially during the end of a fictive beat period, when ER fibers were active in the absence of EW fiber activation (Figure 4.4). Fictive swimming rhythmic EPP frequencies were lower when ER fibers were active in isolation (Figure 4.4D) of EW fibers. This is graphically illustrated in Figure 4.5 (A and B) where intrasegmental paired ER-EW recordings (n = 6) were used to measure rhythmic EPP frequencies during periods when only ER fibers were active (mean = 32±3 Hz) and when both ER and EW fibers were active (mean = 44±7 Hz). Furthermore, an attenuation of synaptic drive to ER fibers was observed during periods of robust high frequency synaptic drive to EW fibers (Figure 4.4D). The duration of fictive swimming, measured as long periods of repetitive brief swim episodes, was variable and ranged from <1 s to 2-3 minutes (Figure 4.5D).

Fictive Coiling and Swimming Behaviors Prior to Hatching

The rhythmic EPPs observed during fictive swimming strongly summated in ER fibers, whereas EPPs quickly decayed to baseline in EW fibers (Figures 4.1-4.4). However, the time course of larval ER and EW muscle miniature EPPs are similar (Buss and Drapeau 2000a; Nguyen et al. 1999) indicating that the rhythmic EPP summation was likely due to other factors. EPP summation could be due to EPPs originating from adjacent electrically coupled ER muscle fibers as EW fiber coupling is minimal at day 3 whereas ER fibers are extensively coupled (Buss and Drapeau 2000a). To test whether the summation of rhythmic EPPs in ER but not EW fibers was due to electrical coupling, recordings were made from day 1 ER and EW muscle fibers which are both extensively electrically coupled at this age (Buss and Drapeau 2000a).

Rhythmic EPPs summated during fictive swimming similarly in both day 1 ER and EW fibers, providing evidence that the summation was due to electrical coupling and not differences in EPP time course (Figure 4.6, A and B). However, in addition to a rhythmic motor output expected for swimming, a slower and more robust rhythmic motor pattern, resembling the coiling behavior of embryonic fishes (Armstrong and Higgins 1971; Gideiri 1966; Gideiri 1968a; Gideiri 1968b; Harris 1962; Myers et al. 1997; Richards and Pollack 1987; Saint-Amant and Drapeau 1998; Whiting et al. 1992; Yoshida et al. 1996) was observed either alone or following fictive swimming (Figure 4.6, A and B). A fictive coiling episode contained 1-13 rhythmic EPPs, occurring at a mean frequency of 5.1±3 Hz (n = 21) (Figure 4.6D), and was often (11/21) followed by rhythmic EPPs occurring at a faster frequency (Figure 4.6C; mean = 24±12 Hz) that resembled fictive

swimming. A faster frequency of rhythmic EPPs (mean = 60±3 Hz), characteristic of day 2 burst swimming (Buss and Drapeau 2001a), was observed in 1 EW fiber (Figure 4.6C). When this value was excluded from the average, no significant difference in fictive swimming rhythmic EPP frequency was observed in ER (mean = 20±2 Hz) and EW (mean = 22±2 Hz) fibers. Fictive coiling/swimming episodes lasted from 0.3 to 10s (mean = 2.2±2 s) and occurred every 10 to 420 s (mean = 140 ± 80 s). At this age, changes in illumination were not effective at initiating fictive coiling or swimming behaviors.

DISCUSSION

Coordinated Synaptic Drive to Myotomal Muscle During Fictive Swimming

Requirements for fictive undulatory swimming are appropriate cycle periods, alternating ipsilateral-contralateral motoneuron activity, a rostral-caudal delay in motoneuron activity, and a relationship between rostral-caudal delay and cycle period. By recording sub-threshold motoneuron evoked EPP activity in myotomal muscle fibers, a coordinated motor output appropriate for swimming was revealed in paralyzed larval zebrafish (Figures 4.1-4.5). An appropriate motor coordination for swimming has previously been reported in paralyzed or isolated spinal cord preparations of lamprey (Cohen and Wallen 1980; Poon 1980; Wallen and Williams 1984), dogfish (Grillner et al. 1976), goldfish (Fetcho and Svoboda 1993), and amphibian tadpoles (Kahn and Roberts 1982; Kahn et al. 1982; Soffe and Perrins 1997; Soffe et al. 1983); however, see (Blight 1977; Stehouwer and Farel 1980).

Phase lag *per* segment averaged 1.8±0.6%, a value similar to the 2.1%

reported in a related cyprinid (goldfish; Fetcho and Svoboda 1993) but considerably larger than the value (1%) reported in the lamprey (Wallen and Williams 1984). Therefore, a larval zebrafish with 30-34 myotomal segments will have approximately 58% of a full wave of undulatory activity along its body at any point in time. This compares with 63% in goldfish (29-30 segments) and a full wave (100%) in lamprey (approximately 100 segments). A full wave of activity is a characteristic of anguilliform swimming while the briefer wave of activity observed in zebrafish and goldfish is a characteristic of subcarangiform swimming (Lindsey 1978). Thus, although visual inspection of swimming larval zebrafish revealed an eel-like (anguilliform) style of swimming (Buss and Drapeau 2001a), due to a large amount of head yaw, examination of phase lag values reveal the subcarangiform style used by the adult. During carangiform swimming, anterior myotomes are active for a longer duration than caudal myotomes; *i.e.*, some ipsilateral and contralateral muscle is synchronously active (Altringham and Ellerby 1999; Wardle et al. 1995). Whether a rostral-caudal variation in the duration of muscle activation exists in larval zebrafish was not determined. One prediction of this pattern of muscle recruitment would be different motoneuron outputs in the rostral and caudal spinal cord during fictive swimming.

Larval Locomotor Muscle Recruitment

ER and EW muscle fibers were recruited for both burst and beat-and-glide swimming. At the highest rates of fictive undulatory swimming, ER fiber activity was reduced but not abolished whereas at the slowest fictive swimming rates ER fibers could be active in isolation. These swimming rates were comparable to those observed in free swimming zebrafish (Budick and O'Malley 2000a; Buss

and Drapeau 2001a) as well as those previously observed during fictive swimming (Buss and Drapeau 2001a). Thus, the pattern of muscle recruitment in larval zebrafish was organized as in adult fishes, where red muscle is recruited during slow undulatory swimming (Bone, 1978; Coughlin & Rome, 1996) and de-recruited at the fastest unsteady burst speeds when white muscle is recruited (Jayne & Lauder, 1996). The neural basis for this pattern of muscle recruitment is unknown. However, the present findings and those of Bone (1966), Jayne and Lauder (1994) and Mos et al. (1990a) indicate that 2 unique populations of motoneurons, that can be activated or inactivated independently of each other, innervate ER and EW muscle fibers.

A de-recruitment of slow (*i.e.,* red muscle) muscle fibers during locomotion is not unique to fishes. In crabs, tonic firing of the common inhibitor neuron abolishes residual tension in slow tonic (but not fast phasic) muscle fibers during rapid walking and swimming (Bevengut and Clarac 1990; Rathmayer 1990; Wiens 1989).

The facilitation of fictive swimming EPPs in larval ER muscle fibers was likely due to summation of filtered and attenuated EPPs from adjacent electrically coupled ER fibers (Buss and Drapeau 2000a). ER fibers have a low contraction threshold (approximately -40 mV) and many similarities to vertebrate slow tonic muscle (*i.e.,* outward rectification, a depolarized resting potential, and a low chloride ion permeability - (Buss and Drapeau 2000a; Chapter 3). During swimming, EPPs from neighboring ER fibers may summate to contraction threshold and provide a tonic level of muscle contraction, on which is superimposed the rhythmic swimming contractions. The locomotor function of

tonic ER activation might include body stiffening, maintenance of posture or steering, but its true function or existence during free swimming remain to be determined. EW fibers have a high contraction threshold, which is likely reached in an all or none fashion *via* a regenerative voltage activated current. Thus tonic muscle activation would not be expected in EW fibers which have characteristics more similar to vertebrate twitch muscle (*i.e.,* a nearly linear VI near the resting potential, a hyperpolarized resting potential, and a high chloride ion permeability - (Buss and Drapeau 2000a; Chapter 3). Recently Ono et al. (2001) observed action potentials in dissociated larval zebrafish muscle, a property not frequently observed by Buss and Drapeau (2000a). This was attributed to a combination of weak, undeveloped voltage gated conductances and the inability to charge the membrane fast enough from a point source of current due to fiber cable properties. However, reexamination *in vivo* has revealed the presence of a TTX sensitive action potential in some EW fibers (but not ER fibers) dialyzed with a low chloride ion patch pipette solution and with resting potentials <-85 mV (Chapter 4), thus revealing further similarities between EW fibers and vertebrate twitch muscle. Thus, although ER and EW fibers have many similar electrophysiological properties (*i.e.,* input resistance, mEPP timecourse and amplitude) they are functionally unique and are recruited differently during swimming, and due to differences in electrical coupling, show different degrees of synaptic facilitation.

Embryonic Fictive Swimming and Coiling

Embryonic (day 1) ER and EW fibers both have extensive electrical coupling and were examined to provide evidence that the summated fictive

swimming EPPs were due to electrical coupling and not EPP kinetics. As predicted, EPPs summated in both day 1 ER and EW fibers during fictive swimming. In contrast to larval fictive swimming (day 3), ER and EW fibers were recruited similarly in embryos (day 1). Rhythmic EPPs assumed to underlie fictive swimming occurred at a lower frequency in embryos than in larvae as observed by Buss and Drapeau (2001a) and Saint-Amant and Drapeau (1998) in behaving zebrafish. A second, slower and more robust fictive motor pattern that had the characteristics of the coiling behavior of embryonic fishes was also observed in embryos. However, the coiling observed in this study is not identical to the coiling and fictive coiling behavior described in younger embryos (Myers et al. 1997; Saint-Amant and Drapeau 1998; Saint-Amant and Drapeau 2000) where single coils are observed. Rather they are more similar to the bursts of coils observed in zebrafish embryos >24 hpf (Saint-Amant and Drapeau 1998) and in the angelfish (Yoshida et al. 1996).

In conclusion, the motor output observed in paralyzed larval zebrafish is coordinated appropriately for generating undulatory swimming. Furthermore, at the early developmental stages examined in this study, muscle recruitment and swimming style (subcarangiform) were similar to that of adult fishes. Thus, there is a considerable degree of sophistication in the organization of the locomotor circuitry at the onset of development of locomotion in the zebrafish.

FIGURES

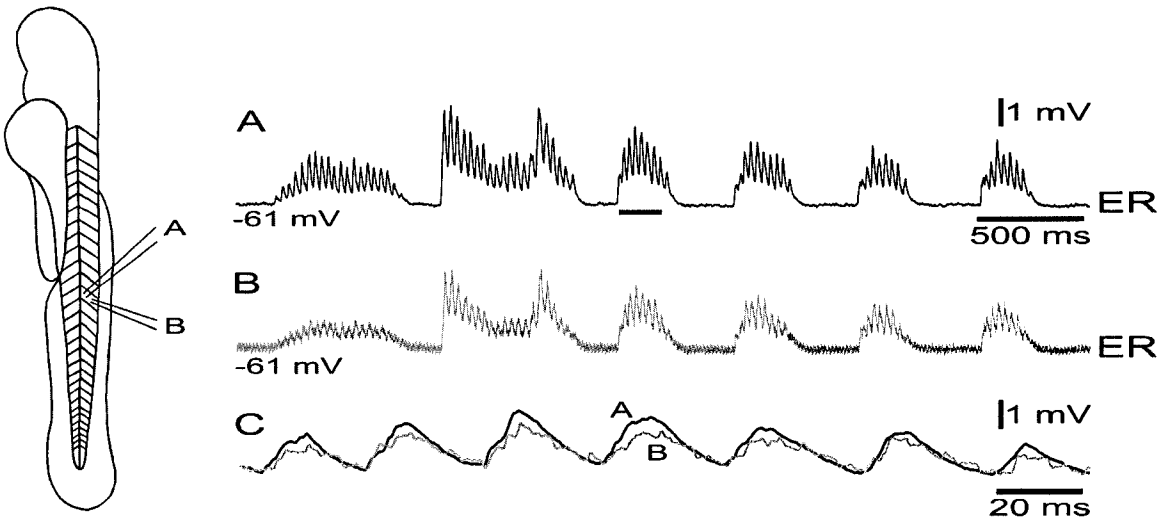

Figure 4.1. Synchronous co-activation of ER fibers within an ipsilateral myotomal segment during larval (day 3) fictive swimming (A and B). The region encompassing the black bar in A is shown on an expanded time scale in C.

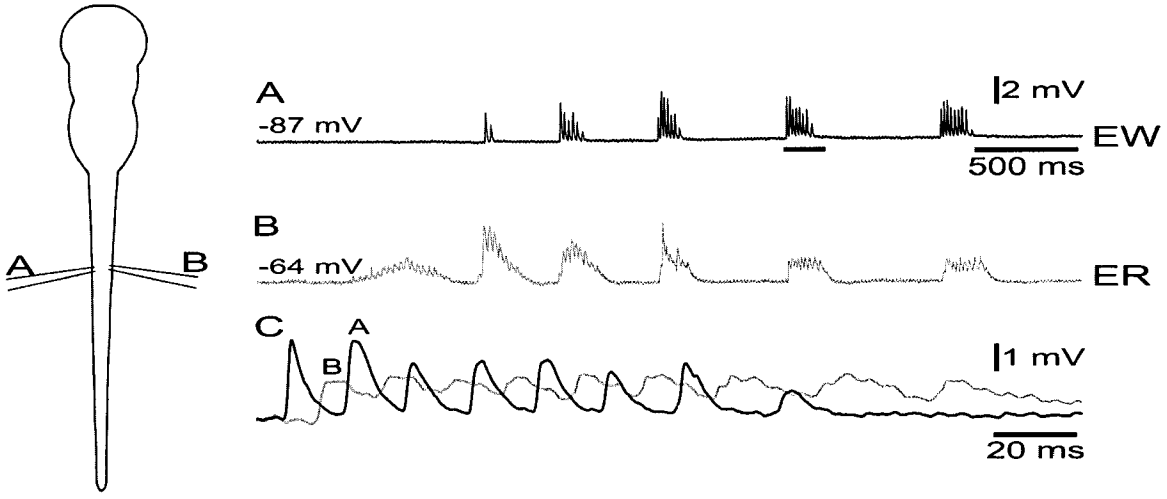

Figure 4.2. Alternating activation of ipsilateral (A) and contralateral (B) muscle fibers during larval (day 3) fictive swimming. The region encompassing the black bar in A is shown on an expanded time scale in C. Note the lack of EPP summation in the EW fiber A and its presence in the ER fiber B.

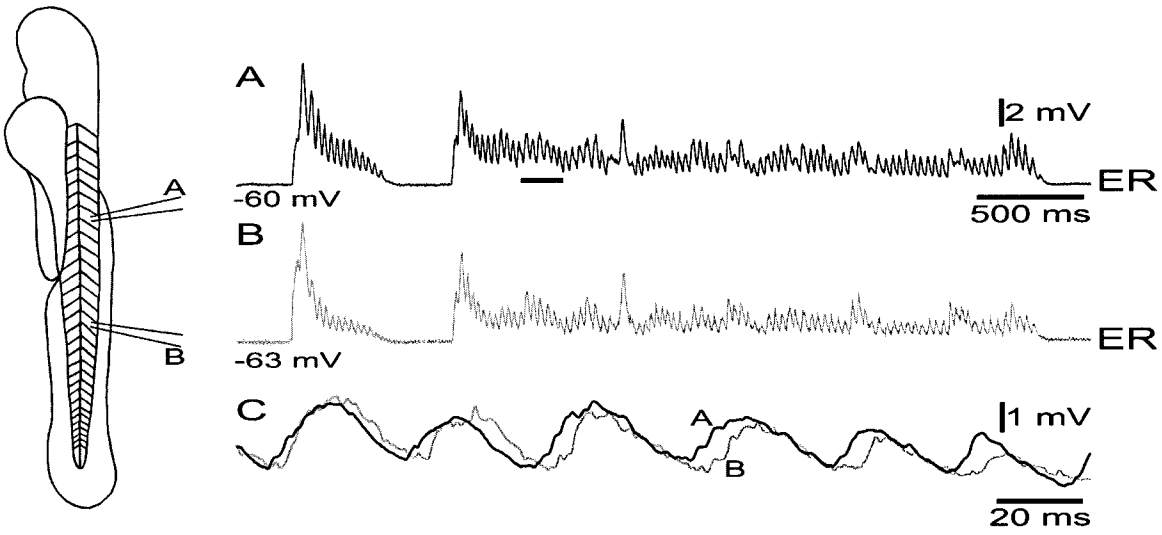

Figure 4.3. Rostal-caudal delay of larval (day 3) fictive swimming EPPs (A and B). The region encompassing the black bar in A is shown on an expanded time scale in C.

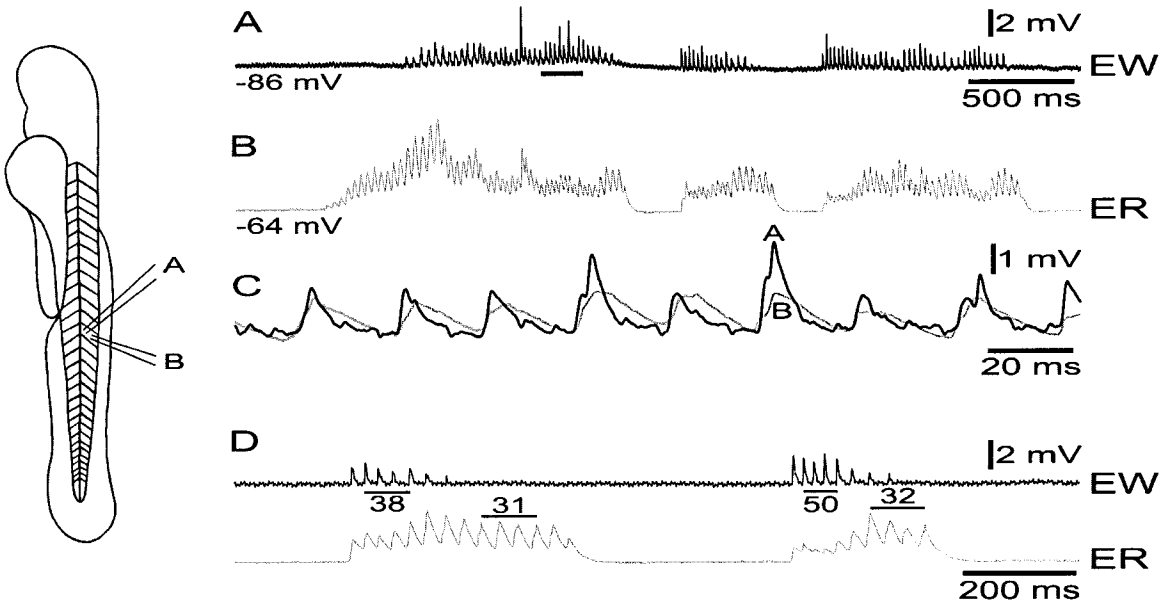

Figure 4.4. Intrasegmental ER and EW fibers are synchronously active (A-C) but are recruited differently during larval (day 3) fictive swimming (A, B and D). The region encompassing the black bar in A is shown on an expanded time scale in C. During high frequency rhythmic EPPs, synaptic drive to ER fibers decreases D. ER fibers are activated in isolation at low fictive swimming rhythmic EPP frequencies D. Bars in D and associated values state the mean rhythmic EPP frequency during that time period.

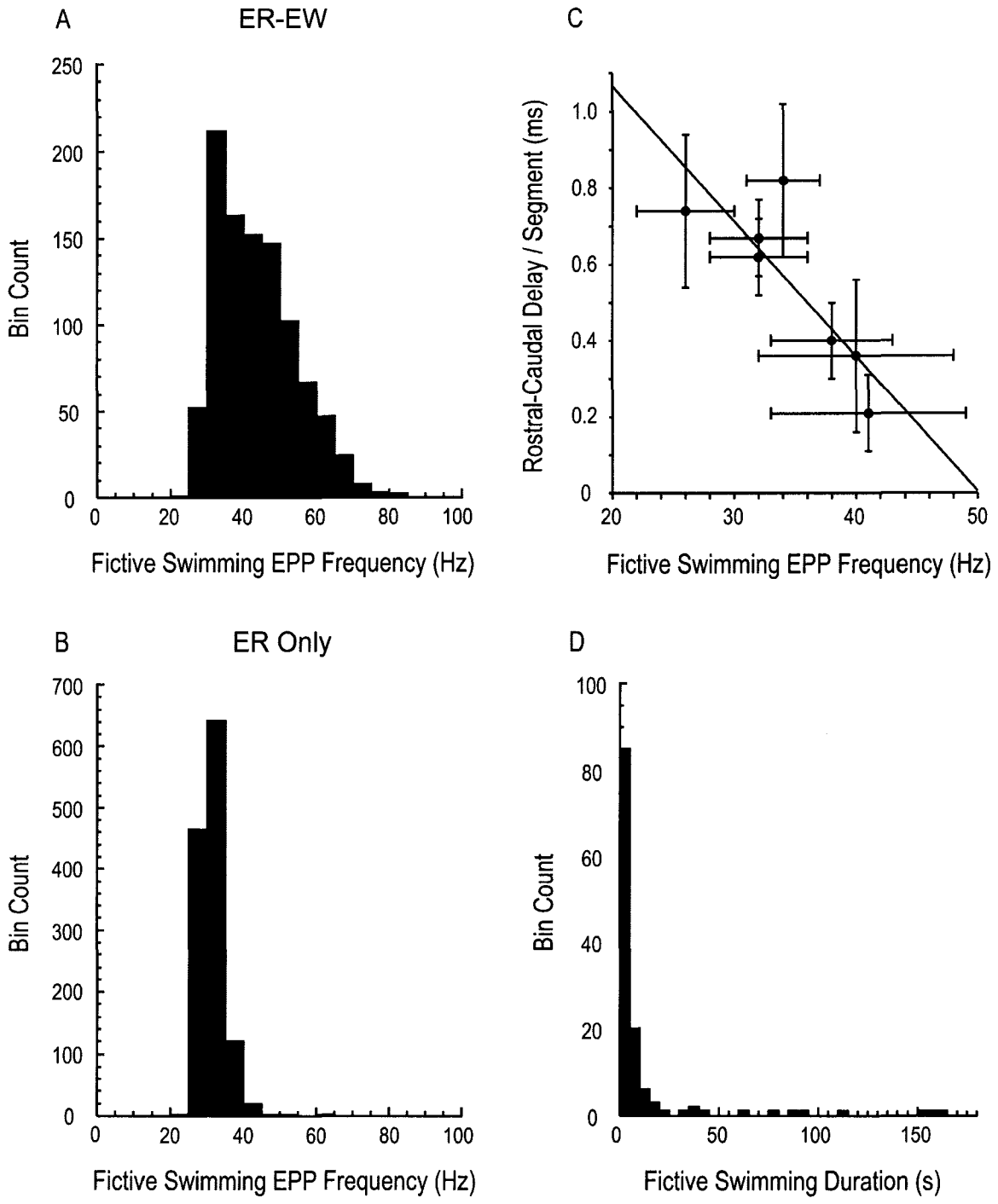

Figure 4.5. Range of fictive swimming rhythmic EPP frequencies during ER-EW fiber co-activation (A) and during independent ER fiber activation (B) in day 3 larvae. Instantaneous frequencies of 186-500 consecutive rhythmic EPPs observed in 6 larvae (n = 2273) are graphed (bin width = 5 Hz). Rostral-caudal delay of fictive swimming rhythmic EPPs decreases with increased fictive swimming rhythmic EPP frequency (C). Each data point represents the mean ± SD rostral-caudal delay and EPP frequency during fictive swimming recorded in a single day 3 larva. Regression fit to mean values; Y = -0.035X + 1.78; R = 0.84. D: Range of durations of fictive swimming observed in 32 day 3 larvae during 127 swimming episodes (bin width = 5 s).

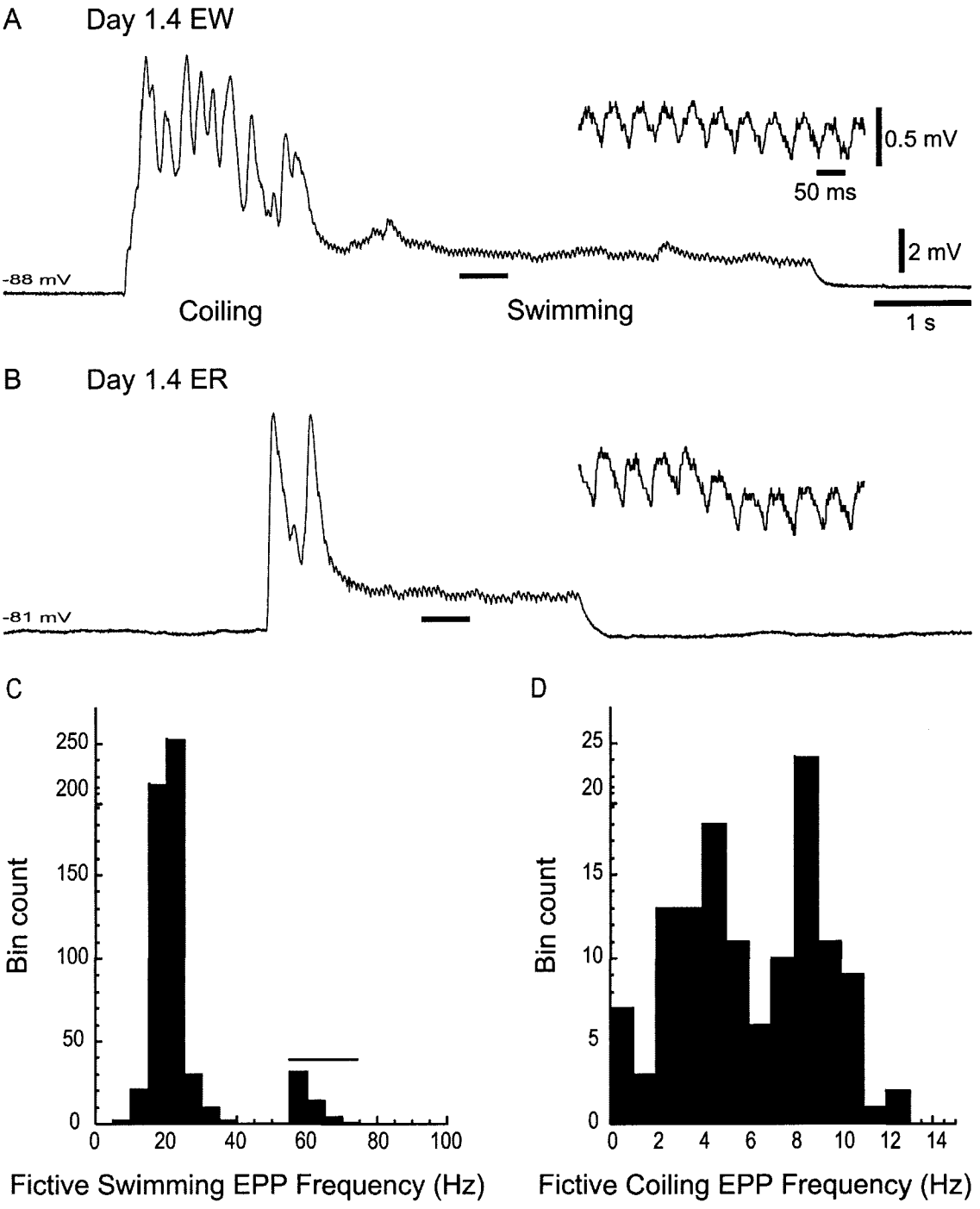

Figure 4.6. Fictive coiling and swimming behaviors observed in EW (A) and ER (B) fibers of 2 different day 1 embryos. Insets show rhythmic fictive swimming EPPs of the regions encompassed by the black bar in A and B. Range of embryonic fictive swimming (C) and coiling (D) rhythmic EPP frequencies. Values below — in C are from a single day 1 embryo that displayed fictive swimming rhythmic EPPs at a frequency characteristic of day 2 burst swimming. C: bin width = 5 Hz; *n* = 550. D: bin width = 1 Hz; *n* = 126. Graphed values are taken from fictive swimming episodes observed in 11 day 1 embryos and fictive coiling episodes observed in 21 day 1 embryos.

Chapter Five: Synaptic Drive to Motoneurons During Fictive Swimming

LINKING STATEMENT

Rhythmic motor output from myotomal motoneurons patterns the synaptic drive observed in ER and EW muscle fibers during fictive swimming. What remained unknown was how the rhythmic motor output was generated in motoneurons. This Chapter shows that motoneurons receive a rhythmic synaptic drive that patterns motor output during swimming.

ABSTRACT

The development of swimming behavior and the correlated activity patterns recorded in motoneurons during fictive swimming in paralyzed zebrafish larvae were examined and compared. Larvae were studied from when they hatch (after 2 days) and are first capable of locomotion to when they are active swimmers capable of capturing prey (after 4 days). High-speed (500 Hz) video imaging was used to make a basic behavioral characterization of swimming. At hatching and up to day 3 the larvae swam infrequently and in an undirected fashion. They displayed sustained bursts of contractions ('burst swimming') at an average frequency of 60-70 Hz, which lasted from several seconds to a minute in duration. By day 4 the swimming had matured to a more frequent and less erratic 'beat-and-glide' mode, with slower (approximately 35 Hz) beats of contractions for approximately 200 ms alternating with glides that were twice as long, lasting from just a few cycles to several minutes overall. In whole-cell current-clamp recordings, motoneurons displayed similar excitatory synaptic activity and firing patterns, that had similar timing to either fictive burst swimming (day 2-3) or beat-and-glide swimming (day 4). The resting potentials were similar at all stages (approximately -75 mV) and the motoneurons were depolarized (to approximately -45 mV) with generally non-overshooting action potentials during fictive swimming. The frequency of sustained inputs during fictive burst swimming and of repetitive inputs during fictive beat-and glide swimming corresponded to the behavioral contraction patterns. Fictive swimming activity patterns were eliminated by application of glutamate antagonists (kynurenic acid or CNQX and AP-5) and were modified but maintained in the presence of the glycinergic

antagonist strychnine. The corresponding synaptic currents underlying the synaptic drive to motoneurons during fictive swimming could be isolated under voltage-clamp and consisted of cationic (glutamatergic PSCs) and anionic inputs (glycinergic PSCs). Either sustained or interrupted patterns of PSCs were observed during fictive burst or beat-and-glide swimming, respectively. During beat-and-glide swimming a tonic inward current and rhythmic glutamatergic PSCs (approximately 35 Hz) were observed. In contrast, bursts of glycinergic PSCs occurred at a higher frequency, resulting in a more tonic pattern with little evidence for synchronized activity. I conclude that a rhythmic glutamatergic synaptic drive underlies swimming and that a tonic, shunting glycinergic input acts to more closely match the membrane time constant to the fast synaptic drive.

INTRODUCTION

The use of simple model systems, such as the lamprey (Grillner et al. 1991; Grillner et al. 1998b; Rovainen 1979) and frog embryo (Dale and Kuenzi 1997; Roberts et al. 1986; Roberts et al. 1998), has greatly increased the understanding of cellular aspects of the neural control of vertebrate locomotion. Zebrafish embryos and larvae share with lampreys and frog embryos the experimental advantages of a simple motor and sensory system (Drapeau et al. 1999) and are a popular vertebrate model system for a wide range of scientific disciplines (Eisen 1996; Laale 1977; Vascotto et al. 1997). An advantage of zebrafish is that they hold promise for identifying the genes controlling locomotion during development of the nervous system (Granato et al. 1996). An

understanding of the physiology of the zebrafish locomotor system is necessary for eventually assessing genetic mutations and manipulations in zebrafish, which will ultimately increase our understanding of the mammalian nervous system.

Movement depends on the activation of locomotor muscles, which are under the control of spinal motoneurons. The myotomal locomotor muscle of adult zebrafish is made up of 5 types of muscle fibers (see references in Buss and Drapeau, 2000a) which include red, pink and white muscle. Red muscle is innervated by small motoneurones located ventro-lateral to the central canal and in proximity to the descending Mauthner axons (de Graaf et al. 1990; van Raamsdonk et al. 1983). Pink muscle motoneurones are larger and are located dorsal to red motoneurones, although there is overlap of size and position (de Graaf et al. 1990; van Raamsdonk et al. 1983). Motoneurones innervating the white muscle are divided into 2 classes, primary and secondary motoneurones (Myers 1985). Primary motoneurones form first in development, are the largest motoneurones, are located dorsal to the central canal, and branch extensively making contact with nearly all fibers within their arborization (de Graaf et al. 1990; Myers et al. 1986; van Raamsdonk et al. 1983; Westerfield et al. 1986). Secondary motoneurones form later in development, are smaller than primary motoneurones, overlap in size and location with pink motoneurones, branch less extensively in the muscle, and contact fewer fibers (de Graaf et al. 1990; Myers et al. 1986; van Raamsdonk et al. 1983; Westerfield et al. 1986). Primary motoneurones are generally recruited during fast swimming and the startle response (Fetcho and O'Malley 1995; Liu and Westerfield 1988).

In fishes with muscular systems organized similarly to zebrafish, red

muscle is active during slow steady undulatory swimming, pink muscle is recruited at intermediate speeds, and both are maximally active at the fastest steady swimming speeds. Swimming becomes unsteady at faster speeds when white muscle is recruited for short bursts of high-speed swimming. At the fastest swimming speeds red muscle activity decreases, whereas in the escape response all muscle is maximally activated (Bone 1978; Coughlin and Rome 1996; Jayne and Lauder 1996).

In contrast to the sophisticated muscular organization found in adult zebrafish, the organization is much less complex in embryos and larvae where only 2 embryonic forms of muscle (ER and EW; Buss and Drapeau 2000a) and 2 classes of motoneurons (primary and secondary; Myers 1985)) are present. This simplified motor system, when combined with the transparency of the zebrafish, allows visualization of individual neurones for patch-clamping, making the zebrafish an excellent model organism for studying the neural control of locomotion.

The purpose of this study was to examine the development of swimming in zebrafish larvae, from when they hatch (after 2 days) and are first capable of locomotion, to when they are active swimmers capable of capturing prey (after 4 days). High-speed video imaging was used to make a basic behavioral characterization of swimming, which was then compared with electrophysiological recordings made from identified motoneurons during fictive swimming in paralyzed larvae. The synaptic pharmacology of the network of neurons producing the swimming pattern was investigated by bath-applying antagonists of the major spinal cord synaptic neurotransmitters and examining their effects on

the membrane potential changes occurring during fictive swimming. Voltage-clamping was then used to isolate the cationic and anionic synaptic currents underlying the synaptic drive to motoneurons during fictive swimming. The findings are discussed in relation to the motoneuronal activity patterns observed during fictive locomotion in fishes and mammals.

METHODS

Swimming Behavior

High-speed video (Motionscope 500, Redlake Camera Opticon) was used to analyze the swimming pattern of larval zebrafish aged 2.4-2.8 (n = 11) and 4.9-5.2 (n = 12) days post-fertilization, referred to as day 2 and day 4. Eighteen larvae were placed in a 6 cm plastic Petri dish illuminated by overhead halogen lighting. Spontaneously occurring swimming was filmed at 500 frames s^{-1} and frames were stored on VCRT120 tape with a Panasonic AG7300 VCR. Images were captured to computer using NIH/Scion Image software for further viewing and analysis. Average camera jitter was approximately 3% and was not corrected.

Two distinct forms of swimming were observed in larval zebrafish: continuous bursts of swimming at day 2 (burst swimming) and an intermittent style of swimming characterized by tail beating followed by gliding (beat-and-glide swimming) at day 4. The terminology is taken from Hunter (1972) who used it to describe the swimming patterns of the larval anchovy. The swimming parameters were related to those that were measurable in patch-clamped motoneurons during fictive swimming. The parameters included swim duration, number of tail

beats, tail beat frequency, distance covered, and duration of either phase of beat-and-glide swimming. Figures were created by hand-tracing sequential computer printouts of the high-speed video recordings. Tracings were scanned and enhanced for display purposes using Adobe Photoshop.

Preparation for recording

Experiments were performed on zebrafish (Tubingen and Longfin lines) larvae raised at 28.5 °C and obtained from a breeding colony maintained according to Westerfield (1995). Physiological results are taken from recordings made in 66 morphologically identified (dye-filled) motoneurons. Zebrafish were examined at 3 ages: after hatching (2.0-2.8 dpf; referred to as day 2), a day later in development (3.1-3.4 dpf; referred to as day 3) and after the onset of active swimming and feeding (4.1-4.5 dpf; referred to as day 4). All procedures were carried out in compliance with the guidelines stipulated by the Canadian Council for Animal Care and McGill University, as described previously (Drapeau et al. 1999). Larvae were anesthetized in 0.02% tricaine (MS-222, Sigma) dissolved in fish saline, pinned through the notochord to a Sylgard-lined dish, and the skin overlying the axial musculature removed with a glass pipette and fine forceps. Muscle fibers were removed from 1-2 myotomal segments in the anal region by aspiration with a broken patch pipette to expose the spinal cord. Experiments were performed at room temperature (approximately 22 °C). The fish saline resembled the plasma of freshwater fish (Evans 1998; Heisler 1984; Holmes and Donaldson 1969; McDonald and Milligan 1992) and contained (in mM) 134 NaCl, 2.9 KCl, 2.1 $CaCl_2$, 1.2 $MgCl_2$, 10 HEPES, 10 glucose, osmolarity 280 to 290 mOsm and pH 7.8. In most experiments (n = 42) the neuromuscular blocker α-

bungarotoxin (10 μM, Sigma) was added to the dish for 10-20 minutes and then replaced with a 0.1% collagenase (type XII, Sigma) fish saline solution for 8 to 10 minutes to facilitate the removal of muscle fibers. The collagenase was removed and the preparation was perfused with fish saline for the remainder of the experiment. When D-tubocurarine (15 μM, Sigma) was used as a neuromuscular blocker (n = 24) it was added directly to the fish saline. There was no noticeable difference in the fictive swimming activity of zebrafish paralyzed with α-bungarotoxin or D-tubocurarine.

Whole-cell recordings

Standard whole-cell recordings (Hamill et al. 1981) were performed on motoneuron cell bodies visualized with Hoffman modulation optics (X40 water immersion objective). Patch-clamp electrodes (4-7 MΩ) were pulled from thin-walled Kimax-51 borosilicate glass and were filled with either a potassium gluconate (for current-clamp recordings) or cesium gluconate solution (for voltage-clamp recordings). All voltage-clamp recordings were performed on α-bungarotoxin paralyzed larvae. The potassium gluconate solution was composed of (in mM) 116 D-gluconic acid potassium salt, 16 KCl, 2 $MgCl_2$, 10 HEPES, 10 EGTA, 4 Na_2ATP, 0.2% sulforhodamine B, osmolarity 280 to 290 mOsm, pH adjusted to 7.2. In the cesium gluconate solution, potassium gluconate and KCl were replaced with cesium gluconate and CsCl and 0.5 to 1.0 mM QX314 was added to antagonize voltage activated sodium and calcium currents. The liquid junction potential was –10 mV and records were corrected for this potential. Current-clamp recordings were performed with an Axoclamp-2A patch-clamp amplifier (0.01 headstage; 10 kHz low-pass filter) and voltage-clamp recordings

with an Axopatch 1D (CV-4 headstage; 5 kHz low-pass filter; series resistance ≤10 MΩ compensated 60 to 80%). The digitization rate was at 20-40 kHz. Each neuron was positively identified as a motoneuron by its location just dorsal to the central canal and the presence of an axon exiting the spinal cord and branching throughout the myotomal muscle, as viewed under fluorescence optics. Images were captured with a Panasonic BP510 CCD camera and a Scion Corporation LG3 frame grabber using Scion/NIH Image software. Voltage steps of 20-40 mV elicited fast, transient inward currents (tested immediately after whole-cell configuration was achieved) in all motoneurons. The QX-314 present in the pipette abolished these transient currents within 1-2 minutes.

The motoneurons examined were fully dialyzed with the patch electrode recording solution since sulforhodamine B fluorescence was detected throughout the motoneurons including the extensive axonal arborization in the myotomal muscle. The patch recording solution contained 20 mM chloride ion which, upon consideration of the activity coefficient (Parsons 1959), places the chloride ion reversal potential at -46 mV (calculated using the Nernst equation corrected for Debye-Hückel activities). Thus, at the resting potential glycinergic post-synaptic potentials (*e.g.* irregular IPSPs) were easily identified as small depolarizing PSPs. Buss et al. (1999) and Saint-Amant and Drapeau (2000) have demonstrated that the chloride ion is depolarizing *in vivo* in developing zebrafish such that all post-synaptic potentials are depolarizing at the resting membrane potential.

Pharmacological antagonists were dissolved in fish saline and applied by bath perfusion. Strychnine hydrochloride (2 μM), kynurenic acid (1 mM), and

tetrodotoxin (1 μM) were purchased from Sigma and AP-5 (50 μM) and CNQX (10 μM) from RBI (Natick, MA). Sulforhodamine B was purchased from Molecular Probes (Eugene, OR) and all other chemicals from Sigma Chemical Co. (St. Louis, MO).

Analyses

Analyses were performed using pClamp 6 or Axograph 4.4 (Axon Instruments). Measurements of fictive swimming rhythmic EPSP and EPSC frequency or amplitude, tonic depolarization or current, action potential amplitude or threshold were made by eye (cursor measurement). Rhythmic EPSCs were detected using the template function of Axograph 4.4. Detected events were divided into 2 size groups, averaged and the decay phase (τ) of the averaged EPSC fit to a single exponential function.

Mean rhythmic EPSC amplitudes and frequencies were determined from consecutive measurements made on the first 30-50 EPSCs occurring in an episode of fictive swimming. EPSP measurements were made on approximately 10 consecutive EPSPs, which occurred during periods of fictive swimming, where the synaptic drive was sufficient to drive occasionally the membrane to action potential threshold. The action potential threshold values presented are the membrane potential at which rhythmic EPSPs initiated action potential firing. Results are presented as mean ± SE throughout the text. The term significant denotes a relationship with $P<0.05$ determined using the Student's *t-test*, Mann-Whitney rank sum test, paired *t*-test, ANOVA, or Kruskal-Wallis ANOVA where appropriate.

RESULTS

Behavioral Characterization of Larval Swimming

From hatching (after day 2) through day 3, zebrafish are largely inactive, lying on their sides upon the substrate. Spontaneous swimming is infrequent and occurs in sustained bouts lasting from a few seconds to less than a minute. Changes in light intensity often evoked episodes of swimming. Figure 5.1 shows images taken every 10 ms while recording images at 500 Hz. The swimming effectively propels the larvae but is erratic, with many turns and displacements of the head, and lacks a definite direction (Figure 5.1A). Tail beat frequencies are very rapid, approaching 100 Hz in some instances and averaging 67 ± 6 Hz (n = 11). This form of swimming will be referred to as "burst swimming". The kinematics of swimming is similar in day 2 and day 4 larvae in that swimming movements are eel-like (anguilliform) and are characterized by a wave travelling in a rostral to caudal direction (Figure 5.1, insets). However, at day 4 the larvae maintained a more constant (forward) orientation. Furthermore the structure of the swimming changed from sustained burst swimming to an intermittent style of swimming (Figure 5.1B) where there is a period of active tail-beating and propulsion (beat period) followed by a period of inactivity where the larvae rapidly glide to a stop (glide period). Episodes of beating and gliding could repeat for longer than a minute or could persist for only a few cycles. This form of swimming will be referred to as "beat-and-glide swimming". Beat-and-glide swimming was much less erratic than the earlier burst swimming; larvae made frequent turns but their movements were more directed and they could maintain a suspended position in the water column even though their swim bladders were usually not

yet functional at this stage of development. The average duration of the tail beat periods were 180 ± 20 ms (*n* = 12) and were followed by a period of gliding lasting on average 390 ± 30 ms (Table 5.1). The mean distance traveled during the tail beat period was 4.7 ± 0.5 mm while on average 37 ± 7% of this distance was covered during the glide period. Two to 8 tail beats occurred during the beat period (mean = 4.7 ± 0.5) and tail beat frequencies averaged 35 ± 2 Hz (range = 25-63 Hz).

Properties of Fictive Swimming

The preceding behavioral observations revealed that larval zebrafish spontaneously initiate swimming and that changes in light intensity could induce swimming. As ventral roots are too small and inaccessible for recording in the zebrafish larva, we resorted to whole-cell patch-clamp recordings from motoneurons in order to characterize the cellular and synaptic activity patterns during swimming. Motoneuron activity patterns were examined in paralyzed larval zebrafish with the expectation that the nervous system would continue to produce rhythmic activity destined to activate the myotomal locomotor muscle in a way appropriate for swimming. Current-clamp recordings revealed stable resting membrane potentials ranging from -65 to -81 mV at all stages examined (Table 5.2; mean = -74 ± 1 mV) and small, intermittently occurring (possibly spontaneous) postsynaptic potentials which were never large enough to elicit action potentials (Figure 5.2). Periodically, or in response to changes in illumination, motoneurons depolarized and fired rhythmic action potentials with a temporal pattern consistent with the motoneuron output expected for swimming. This activity, believed to be fictive swimming, was further examined and

compared with the free-swimming behavior.

The fictive swimming consisted of a tonic depolarization and rhythmic postsynaptic potentials. At day 2 (Figure 5.2A) the tonic depolarization driving the fictive swimming was sustained for tens of seconds (mean = 11 ± 2 s). In day 4 motoneurons (Figure 5.2C) the tonic depolarization lasted only a few hundred ms and was followed by a repolarization of the membrane toward the resting potential. At day 4, these periods of depolarization and repolarization could occur repeatedly, often for several minutes or as long as the recordings (in this case making it impossible to quantify the duration of beat-and-glide swimming) but sometimes for only a few cycles. Each of these fictive swimming patterns corresponded closely to the burst swimming observed in day 2 larvae and the beat-and-glide swimming observed in day 4 larvae. Day 3 (Figure 5.2B) motoneurons behaved similarly to day 2 motoneurons. However, in some recordings, an episode of fictive burst swimming was followed by activity resembling beat-and-glide fictive swimming although there was an incomplete membrane repolarization during the glide period. The addition of the beat-and-glide like activity could prolong the day 3 swimming episodes for up to 2-3 min (mean = 33 ± 11 s). As day 3 animals developed further, the swimming style became increasingly more like beat-and-glide swimming. However, even at day 4, short lasting periods of burst like swimming could occur preceding a much longer period of beat-and-glide fictive swimming.

The swimming parameters examined were related to those that were measurable in patch-clamped motoneurons during fictive swimming. The

parameters included swim duration, number of tail beats, tail beat frequency and duration of either phase of beat-and-glide swimming. Tables 5.1 and 5.2 present the values for these and other parameters during free and fictive swimming. The average membrane potential (Table 5.2) reached during the tonic depolarization phase of fictive swimming was -59 ± 1 mV during both fictive burst swimming (day 2-3) and fictive beat-and-glide swimming (day 4). The rhythmic post-synaptic potentials (*i. e.* the network output) could reach action potential threshold (-46 ± 0.8 mV) at all stages. The action potential threshold values were measured as the membrane potential at which rhythmic EPSPs initiated action potential firing. Rhythmic EPSPs during fictive burst swimming (day 2-3) occurred with a mean frequency of 52 ± 2 Hz while the frequency during beat-and-glide fictive swimming was significantly lower (35 ± 3 Hz). All rhythmic EPSPs did not evoke action potentials, nor did all motoneurons fire action potentials during fictive swimming, even though a tonic depolarization and rhythmic EPSPs were clearly visible. Some rhythmic EPSPs could evoke 1-4 action potentials on their rising phase in all larval age groups. Action potentials elicited during fictive swimming reached an average peak membrane potential of –19 ± 2 mV that was similar at all stages but could on occasion be overshooting in an individual motoneuron. Action potentials did not have a noticable afterhyperpolarization at these membrane potentials.

A smaller PSP, occurring between the rhythmic EPSPs, was observed occasionally, in 20 of the 38 motoneurons examined. When present (Figure 5.2, A and B, * in insets), these other PSPs did not occur regularly throughout the

fictive swimming episodes. The irregular PSPs were more clearly resolved under voltage-clamp (described below). The largest and most clearly defined irregular PSPs usually occurred when the excitatory synaptic drive was greatest during a fictive swimming episode. During periods of weak rhythmic synaptic drive, especially during day 4 beat-and-glide fictive swimming, the irregular PSP was not observed (Figure 5.2C, inset).

In day 2 and day 3 larvae, bursts of fictive swimming were sometimes followed by a small 0.5 to 3 mV hyperpolarization which was sustained for 10 to 40 s (Figure 5.2). At day 2, fictive swimming was followed by a 2.1 ± 0.2 mV hyperpolarization lasting 14 ± 3 s, in 12 of 15 motoneurons. Five of 16 day 3 motoneurons displayed a hyperpolarization (mean amplitude = 1.3 ± 0.3 mV; mean duration = 17 ± 3 s) following a burst of fictive swimming. Membrane hyperpolarization was not observed following beat-and-glide swimming in day 4 motoneurons (Figure 5.2C).

From these recordings it was not possible to determine the nature of the depolarizing drive to the motoneurons during fictive swimming. The depolarizing drive appeared synaptic in origin and current pulses sufficient to depolarize or hyperpolarize the membrane potential 20 to 40 mV (for tens to hundreds of milliseconds) during episodes of fictive swimming did not disrupt the following motoneuron output (not shown). Bath application of TTX (n = 4) abolished fictive swimming. However, some motoneurons may have intrinsic oscillatory properties as small (<2 mV), long-lasting (approximately 1 s) membrane depolarizations were observed (3 of 4 motoneurons) in the presence of TTX (see also Ali *et al.*

2000a).

Pharmacology of Fictive Swimming

To gain insight into the pharmacology of the fictive swimming synaptic drive, receptor antagonists of the major zebrafish spinal cord synaptic neurotransmitters, glutamate (Ali et al. 2000a) and glycine (Ali et al. 2000b), were bath applied to the preparation. Addition of the glutamate receptor antagonist kynurenic acid or a combination of the specific AMPA/kainate and NMDA receptor antagonists (CNQX and AP-5) to the fish saline abolished spontaneous or light induced fictive swimming (n = 4). The resting membrane potential was unaffected by the glutamatergic antagonists and the remaining spontaneous synaptic activity was blocked by the glycine receptor antagonist strychnine. Cholinergic synaptic drive was not critical for the production of fictive swimming as motoneuron activity was observed if α-bungarotoxin or D-tubocurarine were used to paralyze the preparations.

In contrast, blocking glycinergic transmission (n = 6) by bath application of strychnine did not abolish rhythmic activity (Figure 5.3) even though it causes spasms of bilateral contractions in intact larvae (Granato et al. 1996). Strychnine did not significantly affect the frequency of rhythmic EPSPs (strychnine = 54 ± 2 Hz, control = 51 ± 2 Hz) or the tonic synaptic drive (-58 ± 2 *vs* -58 ± 2 mV) during a fictive swimming episode observed in single motoneurons. There was an abolition of the irregular PSP and a distinct increase in motoneuron spiking during fictive swimming. Significantly more action potentials occurred per second of fictive swimming (6.5 ± 2 *vs* 2.4 ± 1) which was attributable to the initiation of an extra 1-2 action potentials by many of the rhythmic EPSPs. Action potential

threshold significantly decreased by 5 mV (-45 ± 2 *vs* –50 ± 1 mV, $P = 0.019$) and action potential height significantly decreased by 13 mV (-30 ± 4 *vs* –17 ± 2 mV) in the presence of strychnine. Fictive swimming duration and resting membrane potential were not noticeably affected by strychnine while a hyperpolarization following fictive swimming was revealed in 2 cells that did not display it prior to strychnine application.

Properties of Fictive Swimming Synaptic Drive

The preceding current-clamp recordings revealed that motoneurons depolarized in both a phasic and tonic pattern during fictive swimming although the nature of this depolarization was not positively identified. Bath application of glutamatergic and glycinergic antagonists either abolished or changed, respectively, the fictive swimming motor pattern, a result consistent with a glutamatergic and glycinergic synaptic drive underlying the fictive swimming depolarization. However, bath applied antagonists do not act solely upon motoneurons and the changes observed could be due to indirect actions on other neurons active during fictive swimming. To overcome this shortfall in the current-clamp analysis of motoneuron activity patterns, motoneurons were voltage-clamped at the reversal potential for chloride ion to reveal isolated cation currents (presumably glutamatergic) or at the cation reversal potential to reveal isolated chloride ion currents (presumably glycinergic), without pharmacological perturbation of network activity. Furthermore, due to the small size of larval zebrafish neurons, an effective space-clamp is achieved for synaptic currents (Ali et al. 2000a; Ali et al. 2000b; Drapeau et al. 1999), allowing for a more quantitative index of synaptic activity.

Motoneurons that were voltage-clamped at the chloride ion reversal potential displayed spontaneous or light evoked bursts of inward synaptic currents composed of a tonic inward current and rhythmic EPSCs (Figure 5.4). The chloride ion reversal potential was set in each motoneuron by determining the reversal potential of the spontaneously occurring glycinergic synaptic currents *i.e.*, the reversal potential was not calculated but determined experimentally (approximately -47 mV). In general, the same frequency of activity was observed in voltage-clamped motoneurons as was observed in the current-clamped motoneurons (Table 5.2). Day 2 and 3 motoneurons (Figure 5.4, A and B) displayed activities consistent with the motor output required to produce burst swimming and day 4 motoneurons (Figure 5.4C) that required to produce beat-and-glide swimming. These findings indicated that the depolarizing drive underlying fictive swimming was synaptic in nature and that the rhythmicity producing the motor output was due to a cationic conductance (presumably glutamatergic). The tonic inward current averaged -41 $\pm$ 6 pA and tended to vary from cell to cell but did not change significantly with development (Table 5.2). Rhythmic EPSC amplitudes sometimes exceeded -200 pA (mean = -49 $\pm$ 6 pA) and increased significantly with development (Table 5.2). The frequency of the rhythmic EPSCs (Table 5.2) were higher during day 2 and 3 fictive burst swimming (mean = 45 $\pm$ 2 Hz) than during the fictive beat-and-glide swimming (mean = 37 $\pm$ 3 Hz).

If the rhythmic EPSCs were glutamatergic, they should have kinetic characteristics resembling those of the spontaneous, quantal glutamatergic

synaptic currents previously characterized in zebrafish motoneurons (Ali et al. 2000a). That study revealed biexponential decay time constants for both AMPA/kainate (faster τ = 0.5-0.8 ms, slower τ = 3-6 ms) and NMDA (faster τ = 5-8 ms, slower τ = 30-45 ms) components of spontaneous synaptic currents. To examine the possible contributions of these 2 types of glutamate receptors, decays were fit to a single exponential function to approximate roughly the time-course of decay of the rhythmic EPSCs. Fits to more complex time courses were not possible due to interruption of the summated evoked events. Rhythmic EPSCs varied in amplitude and the largest EPSCs appeared to have a faster rate of decay. To verify this apparent difference, the rhythmic EPSCs were divided into 2 size groups containing small (10-25 pA) or large (>50 pA) EPSCs. The decay time course of the rhythmic EPSCs varied from 2.8 ms (day 2 large EPSCs) to 5.9 ms (day 4 small EPSCs). The time course of the large EPSCs was faster than that of the small EPSCs at all stages examined and this difference was statistically significant in day 2 and day 3 motoneurons (Table 5.3). Furthermore, in low-noise, high-resolution recordings (Figure 5.6C), the rhythmic EPSCs were found to be composed of many small currents that closely resembled the miniature AMPA/kainate synaptic currents described by Ali et al. (2000a).

The preceding current-clamp recordings revealed the presence of an occasional small, irregular PSP at days 2 and 3, which was presumably a glycinergic chloride ion conductance as it was not observed in the presence of strychnine. To gain a greater understanding of this PSP, motoneurons were

voltage-clamped at a potential (approximately -33 mV) intermediate to the chloride ion reversal potential and the cation reversal potential to reveal a mixture of inward cation currents and outward chloride ion currents.

At the intermediate holding potential, rhythmic inward currents were superimposed upon a sustained tonic chloride ion current. This was observed in day 2-3 motoneurons (Figure 5.5B) displaying fictive burst swimming as well as in day 4 motoneurons (Figure 5.6B) displaying fictive beat-and-glide swimming. To study the chloride ion current in isolation, the holding potential was depolarized further to approximately 0 mV, the cation reversal potential (Ali et al. 2000a). At this potential, it was readily apparent that there was mostly a sustained, tonic chloride ion current occurring during fictive swimming (Figures 5.5A and 5.6A). Closer examination revealed that the chloride ion current appeared to be composed of many individual synaptic currents that closely resembled the glycinergic synaptic currents described in larval zebrafish motoneurons (Buss et al. 1999) and reticulospinal neurons (Ali et al. 2000b). The peaks of these synaptic currents showed rhythmicity, which was likely to account for the occasional glycinergic PSPs observed in the current-clamp recordings. Because it was difficult to voltage-clamp motoneurons at such a depolarized level, the rhythmicity of the chloride ion synaptic current peaks was only examined in 11 cells (day 2 = 4; day 3 = 3; day 4 = 4).

Closer examination of the chloride ion PSCs revealed that they did not always display (Figure 5.5A inset *vs* 5.6A) the same high degree of rhythmicity as the rhythmic cationic EPSCs described above. The timing of the chloride ion PSC peaks varied greatly and during a single episode of fictive swimming inter-peak

frequencies could range from 20 to 500 Hz. Although the rhythmic cationic EPSCs were invisible at this potential, it was reasonable to conclude that some of the chloride ion current peaks would be occurring midway between the rhythmic cationic EPSCs. However, many of these chloride ion current peaks could also be occurring synchronously with rhythmic cationic EPSCs. The frequency of the chloride ion current peaks was measured and normalized, on a cell by cell basis, to the frequency of the rhythmic cationic EPSCs believed to underlie the timing of tail beats in the free swimming larvae. On average, the chloride ion current peaks occurred at a frequency 2-3 times higher than the rhythmic cationic EPSCs (2.6 ± 0.2 times, day 2; 2.0 ± 0.5 times, day 3; 2.7 ± 0.6 times, day 4). This finding supports the occurrence of rhythmic synaptic chloride ion current peaks (irregular PSPs) occurring with rhythmic cationic EPSCs. However, the additional conductance added by the peak of the chloride ion current was small compared with the magnitude of the tonic chloride ion conductance occurring during fictive swimming, and the physiological significance of the chloride ion current most likely lies in its tonic component. Noteworthy is the fact that the system-wide antagonism of glycinergic currents did not disrupt rhythmic synaptic activity, while it had clear affects on the firing properties of the motoneuron during this activity.

Comparison of Fictive Swimming and Free Swimming

Motoneurons displayed the same fictive swimming activity whether they were examined using current or voltage-clamp recording techniques (Figures 5.2 *vs* 4-6). The measured parameters were not significantly different so all fictive swimming data were pooled and compared with the parameters measured in free swimming larvae. In both fictive and free swimming, tail beat/rhythmic EPSP

frequency was higher during burst swimming than during beat-and-glide swimming (Table 5.2). The mean tail beat/rhythmic EPSP frequency during beat-and-glide swimming was identical (35 Hz) during fictive and free swimming, although during burst swimming it was significantly higher during the behavior than during fictive swimming (Table 5.1). During day 4 beat-and-glide swimming (Tables 5.1 and 5.2) the mean beat periods were very similar while the mean glide periods were significantly longer during fictive swimming. Although there were differences in the preceding mean values, all values recorded during fictive swimming were within the range of values observed in the free swimming behavior. The higher observed free swimming values could be due to the presence of active sensory feedback during free swimming, or could simply be because the most active (and fastest swimming) larvae swam through the field of view during the high speed video recording. Another difference between free and fictive beat-and-glide swimming was the occurrence of approximately 2 fewer tail beats per beat period (when compared with the mean number of rhythmic EPSPs/EPSCs) occurring during fictive swimming (Table 5.1). This difference is likely because of the inclusion of small sub-threshold EPSPs/EPSCs when calculating the number of rhythmic EPSPs (*i.e.*, fictive tail beats) in the fictive beat period. The addition of these sub-threshold EPSPs would also explain the longer mean burst periods observed during fictive beat-and-glide swimming (Table 5.1).

Dye Coupling Between Motoneurons and Other Neurons

Dye coupling between the patched motoneuron and the axon of another neuron was clearly observed in 3 of the 66 dye-filled motoneurons examined in

this study. In 2 instances, the dye coupled axon could be traced to a dye filled cell body which was always an ipsilateral descending interneuron. Whether the other dye filled axon was a descending interneuron, propriospinal neuron, or descending axon from the brainstem could not be determined. Dye coupling between motoneurons and other motoneurons was never observed.

DISCUSSION

Free Swimming

Beat-and-glide swimming has been previously examined in larval zebrafish (Budick and O'Malley 2000a; Fuiman and Webb 1988) while the transition from burst swimming to beat-and-glide swimming has not. In addition, Saint-Amant and Drapeau (1998) have described the earliest embryonic swimming. From the onset of swimming at 28 to 36 hpf, a period when the embryo remains encapsulated in the egg, the tail beat frequency increases from 7 to 27 Hz. The present study shows a continued two-fold increase in tail beat frequency during the next day of development.

The mean tail beat period (180 ms) and glide period (390 ms) described in this study matched closely with the 130 ms tail beat period and the range of glide periods (400-2000 ms; which average toward the lower range values) described by Fuiman and Webb (1988). As described in this other study, episodes of beat-and-glide swimming regularly began with a turn and swimming in a new direction. The mean tail beat frequency observed in this study (35 Hz) corresponds to the spontaneously initiated swimming described by Budick and O'Malley (2000a). A similar transition from burst swimming to beat-and-glide swimming has been

observed in anchovies by Hunter (1972). Similar to zebrafish, at hatching, anchovies remain motionless except for brief (1-2 s) spontaneous bursts of swimming characterized by continuous tail beating at rates up to 50 Hz. Within a few days, a new dominant mode of intermittent swimming emerges consisting of alternating periods of swimming and gliding using lower tail beat frequencies. For hydrodynamic reasons it is advantageous for small larval fish to swim continuously and rapidly as gliding is not physically possible. Larger larval and adult fish swim and glide, which is then possible due to their larger, more streamlined shape (Webb and Weihs 1986; Weihs 1980). Much later in development, the anguilliform swimming of larval zebrafish (the common mode of swimming in larval fish) is replaced by the subcarangiform mode of the adults, which is characterized by a reduced side-to-side eel-like motion in the anterior end of the fish (Lindsey 1978).

Fictive Swimming

The spontaneous or light evoked episodes of depolarization and rhythmic action potential firing in motoneurons are consistent with a fictive motor pattern which would activate myotomal muscle in a pattern appropriate for swimming in a non-paralyzed preparation. The frequency of rhythmic EPSPs, EPSCs, and action potential firing recorded in paralyzed preparations closely matched the free swimming tail beat frequencies (Tables 5.1 and 5.2). A developmental change from burst to beat-and-glide swimming was similarly observed in the free swimming and paralyzed preparations, and the underlying structure of the beat-and-glide swimming was similar.

A tonic depolarization and rhythmic EPSPs capable of initiating action

potentials characterize fictive swimming in day 2-4 zebrafish. The tonic depolarization arises from cationic synaptic currents, which likely sum with tonic chloride ion synaptic currents, due to the depolarizing nature of chloride ions in these developing motoneurons (Buss et al. 1999; Saint-Amant and Drapeau 2000). Synaptic cation currents are hypothesized to be glutamatergic based on 4 observations: glutamatergic antagonists abolished fictive swimming, glutamatergic antagonists abolished all cationic miniature EPSCs in zebrafish motoneurons (Ali et al. 2000a), summing synaptic currents with the properties of AMPA/kainate mEPSCs were observed in the rhythmic EPSCs, and cholinergic synaptic currents were never observed in larval zebrafish motoneurons (Buss and Drapeau 2000b).

I hypothesize that the rhythmic EPSPs are formed by fast (τ = 0.5-0.8 ms and 3-6 ms) AMPA/kainate synaptic currents, combined with the faster component (with τ = 5-8 ms) of the NMDA synaptic currents (Ali et al. 2000a). Table 5.3 shows that the decay time constant of the largest rhythmic EPSCs (approximately 3 ms) is faster than the faster decay time constant of NMDA synaptic currents. This indicates that the faster AMPA/kainate channels could carry much of this current. The smaller rhythmic EPSC currents (approximately 6 ms) are close to the value of the slow time constant of AMPA/kainate synaptic currents as well as the fast time constant of NMDA synaptic currents and may thus be due to a combination of inputs from these receptors. The prolonged decay time course of NMDA synaptic currents (slower τ = 30-45 ms; Ali et al. 2000a) arising from either mixed NMDA/AMPA synapses or pure NMDA

synapses, could provide much of the sustained tonic depolarization. However, an additional tonic drive mediated by slow acting metabotropic glutamate receptor or muscarinic cholinergic receptor activated channels cannot be ruled out. The glutamatergic synaptic transmission is mediated by action potential evoked synaptic release as fictive swimming was abolished by TTX application.

Chloride ion mediated, glycinergic synaptic currents occurred concurrently with the glutamatergic currents. These chloride ion mediated synaptic currents were concluded to be glycinergic based upon 3 observations: strychnine abolished the irregular PSP, glycinergic antagonists abolished all chloride ion mediated mPSCs (except for rare, infrequently occurring bicuculline sensitive GABAergic mPSCs observed in a small percentage of motoneurons) in larval zebrafish motoneurons (Buss et al. 1999) and resticulospinal neurons (Ali et al. 2000b), and the decay time course and appearance of the chloride ion mediated synaptic currents observed during fictive swimming resembled glycinergic synaptic currents described by Buss et al. (1999) and Ali et al. (2000b).

I hypothesize that the peaks of these synaptic chloride ion currents formed the irregular PSPs, which were present in approximately one-half of the motoneurons examined but represented only a third of all the peaks observed. Moreover the chloride ion currents were largely tonic in nature and were not essential to the patterning of the locomotor rhythm since eliminating glycinergic synaptic currents with strychnine had no significant effect on the frequency of the rhythmic EPSPs. However, strychnine did affect motor output, causing a significant increase in the frequency of action potentials during fictive swimming, as well as a decrease in action potential amplitude and threshold.

The tonic chloride ion conductance occurring during fictive swimming could act to decrease the input resistance and consequently the membrane length and time constants of the motoneurons. Strychnine caused a decrease in action potential threshold and amplitude and these effects may reflect an increased motoneuron input resistance, length, and time constants. As the action potentials of larval zebrafish motoneurons occur during the decay of the membrane depolarization evoked by short (2 ms) current injections (Chapter 7), the spikes are likely initiated in the axon and not the soma. A longer membrane length constant, after application of strychnine, would lessen the attenuation of the membrane depolarization from the spike initiation zone to the soma, resulting in a perceived lowering of the action potential initiation threshold measured at the soma.

Blocking the chloride ion conductance with strychnine would increase the membrane time constant and reduce the recording bandwidth, resulting in filtered action potentials of smaller amplitude. Alternatively, shifting the spike initiation zone to a more distal axonal location could also result in a decrease in action potential amplitude. Shortening of the membrane time constant due to a sustained, glycinergic chloride ion conductance will serve to shorten the time-course of synaptic potentials. Larval zebrafish motoneurons have input resistances an order of magnitude larger than reported in adult fish but have to swim with much faster undulations in order to propel themselves through the water. Glutamatergic synaptic currents (AMPA/kainate) have very fast kinetics (0.5-0.8 ms; Ali et al. 2000a) and motoneurons produce a coordinated rhythmic synaptic output sometimes reaching 100 Hz during swimming.

Electrical Transmission

Although the sources of synaptic drive to motoneurons during fictive swimming are attributed to chemical synapses (glutamatergic and glycinergic), it is probable given the results of dye coupling experiments that electrical synapses provide an additional source of synaptic drive. In the zebrafish embryo, electrical transmission appears to play a critical role in the production of the spontaneous motor activity occurring during the first day of development prior to the appearance of chemical synaptic transmission in embryonic motoneurons (Saint-Amant and Drapeau 2000). Electrical synapses have been extensively examined in adult fishes as well (Batueva 1987; Bennett 1966; Bennett 1997; Pappas and Bennett 1966; Rovainen 1979; Shapovalov 1980). A number of the descending axons that were dye coupled to motoneurons originated from segmental descending interneurons that are likely homologous to a class of descending interneurons described in the goldfish (Fetcho 1992a). These interneurones are active during the escape response receiving excitatory chemical monosynaptic inputs from the Mauthner cell and forming electrical monosynaptic outputs onto motoneurones (Fetcho 1992a). It is not known if these cells are active during fictive swimming in the larval zebrafish but this is likely given the similarity of these cells to descending interneurones, which are active during fictive locomotion in the frog embryo and lamprey (Fetcho 1992b).

Developmental Changes

The most obvious developmental change to occur, the switch from burst swimming to beat-and-glide swimming, was associated with a lowering of tail beat frequency. However, at a cellular level, there were few changes. The hyperpolarization following fictive swimming common at day 2 was not observed

in day 4 beat-and-glide fictive swimming. This could be due to the loss of this conductance, to it being obscured by synaptic activity following the fictive swimming, or because of a lower input resistance of day 4 motoneurons. Rhythmic EPSC amplitudes increased from day 2 to day 4, which could compensate for the reduction in input resistance and is likely due to the increase in size of the unitary AMPA/kainate synaptic events described by Ali et al. (2000a). There were no significant changes in most cellular properties including resting membrane potential, fictive swimming tonic depolarization, action potential amplitude or threshold, or rhythmic EPSC decay time course.

Comparison With Fictive Swimming Described in Other Fish

The neural control of swimming has been extensively examined at the cellular level in the lamprey (reviewed in Grillner et al. 1991; Grillner et al. 1998b; Rovainen 1979) through the use of the isolated or paralyzed spinal cord preparations. The activity of motoneurons and unidentified interneurons has been examined during fictive swimming in dogfish (Mos et al. 1990a; Mos et al. 1990b) and stingray (Williams et al. 1984) with intracellular techniques. However, most studies, in fishes other than the lamprey, have been limited to extracellular recording techniques (goldfish, Fetcho and Svoboda 1993; carp, Uematsu et al. 1994; angelfish, Yoshida et al. 1996; stingray, Leonard 1986; dogfish, Roberts 1981).

During glutamate-induced fictive locomotion in lamprey, phasic excitation alternates with a phasic inhibition which is mediated by a glycinergic chloride ion conductance (Alford and Williams 1989; Dale 1986; Kahn 1982; Russell and Wallen 1983). These alternating excitatory and inhibitory oscillations are

superimposed upon a tonic depolarization when locomotion is evoked by sensory stimuli (Alford and Williams 1989). Fictive swimming is antagonized by glutamatergic antagonists (Brodin and Grillner 1985) and the phasic excitation is mediated by glutamatergic synaptic inputs having both AMPA and NMDA components (Alford and Sigvardt 1989; Alford and Williams 1989; Dale 1986; Dale and Grillner 1986; Hagevik and McClellan 1994; Moore et al. 1987). Spontaneously occurring fictive swimming recording in stingray motoneurons (Williams et al. 1984) is characterized by a tonic depolarization with superimposed rhythmic PSPs, with little sign of alternating inhibition. Similarly, fictive swimming recorded from dogfish motoneurons does not reveal alternating inhibition (Mos et al. 1990a).

Blocking glycinergic inhibition, by bath application of strychnine, increases the rate of fictive swimming in the lamprey (Cohen and Harris-Warrick 1984; Grillner and Wallen 1980), but not in the zebrafish, and synchronizes normal alternating ipsilateral/contralateral fictive motor output in the lamprey (Alford and Williams 1989; Cohen 1987; Cohen and Harris-Warrick 1984). Thus, Cohen and Harris-Warrick (1984) concluded that the neuronal network generating the rhythmic excitatory oscillations, observed during fictive swimming, operates independently of glycinergic inhibitory connections. The lack of effect of strychnine on the rhythmicity of zebrafish fictive swimming supports this conclusion. Furthermore, strychnine does not disrupt the rostral to caudal phase lag of motor output that underlies the propulsion for undulatory swimming in the lamprey (Alford and Williams 1989; Cohen 1987). The present study examined the activities of individual motoneurons and could not determine whether the

rostral-to-caudal phase lag of motoneuron activity was affected. The ipsilateral/contralateral alternation during swimming is perturbed by strychnine, resulting in bilateral contractions resembling the phenotype of *accordion* mutants (Granato et al. 1996).

The synaptic drive to zebrafish myotomal motoneurons is very similar to that observed in other fishes. The principal difference is the presence of a tonic glycinergic drive, which I hypothesize to be an adaptation to the high frequencies of motor output required for undulatory locomotion in these small larval fish. The patterning of rapid undulatory movements by the nervous system may underlie fundamental features in the vertebrate nervous system because this form of locomotion is observed in phylogenetically distant organisms having a pre-vertebrate chordate ancestry (*e. g.*, Lancets; Stokes 1997). Phasic glycinergic inhibition during fictive swimming is not prominent in the motoneurons of the 2 elasmobranch fish examined (Mos et al. 1990a; Williams et al. 1984), suggesting that phasic glycinergic inhibition of *motoneurons* is not critical for locomotor activity. The apparent necessity for the involvement of glycinergic inhibition in ipsilateral/contralateral alternation likely lies at a pre-motoneuronal level.

Similarities with Mammalian Locomotion

The properties of the synaptic drive to zebrafish motoneurons during fictive swimming have many similarities with the synaptic drive to feline motoneurons during fictive locomotion. In both preparations, motoneuron output is determined largely by a rhythmic excitatory synaptic drive (Jordan 1983; Pratt and Jordan 1987). In the cat, reciprocal relationships underlying extensor and flexor motoneuron output during locomotion are believed to be determined at a

premotoneuronal level by interactions among interneurons forming the flexor reflex afferent pathways (Jankowska 1992; Jankowska et al. 1967a; Jankowska et al. 1967b; Schomburg et al. 1998; Shefchyk and Jordan 1985a). Similarly, motoneuron rhythmic activity remains after glycinergic inhibition is antagonized by strychnine (Pratt and Jordan 1987), or nicotinic cholinergic transmission in antagonized with mecamylamine (Noga et al. 1987), but not when glutamatergic antagonists are administered (Douglas et al. 1993). The synaptic drive to motoneurons is due to a sequential excitatory and inhibitory synaptic drive that overlap during the step cycle (Orsal et al. 1986; Perret and Cabelguen 1980; Shefchyk and Jordan 1985a; Shefchyk and Jordan 1985b). Two classes of identified interneurons have been shown to provide this inhibitory synaptic drive to motoneurons during fictive locomotion. Renshaw cell activity provides an inhibitory drive concurrent with the excitatory phase of the locomotor drive potential and Ia inhibitory interneurons provide an inhibitory drive alternating with the excitatory phase (*i.e.,* midcycle inhibition) of the locomotor drive potential (Feldman and Orlovsky 1975; McCrea et al. 1980; Noga et al. 1987; Pratt and Jordan 1987). Although both interneurons provide inhibitory drive to motoneurons during fictive locomotion, neither are believed to be components of the spinal rhythm generating network (Pratt and Jordan 1987). It is possible that analogous (or homologous) inhibitory interneurons, which are not elements of the spinal rhythm generator, provide the glycinergic drive to zebrafish motoneurons during fictive swimming. I conclude that there are many similarities between zebrafish and mammals, in the properties of the synaptic drive to motoneurons during fictive locomotion, and that the larval zebrafish is a useful preparation for gaining

new insights into the neural control of vertebrate locomotion.

TABLES AND FIGURES

Table 5.1. Comparison of free and fictive beat-and-glide swimming.

Parameter	Free Swimming	Fictive Swimming
Mean Beat Period (ms)	180 ± 20	220 ± 30
Mean Glide Period (ms)	390 ± 30 *	910 ± 100 *
Mean Tail Beats / Beat Period	4.7 ± 0.5 *	6.9 ± 0.8 *
Mean Tail Beat Frequency (Hz)	35 ± 2	35 ± 2

Values shown are means ± SE. Mean beat periods were significantly different from mean glide periods during both free and fictive swimming (not indicated in the Table). The numbers of larvae or motoneurons examined to calculate the presented mean values in free swimming was 12 and in fictive swimming was 11. * Significant difference of means (Student's *t*-test or Mann-Whitney rank sum test); comparisons were made horizontally in the Table.

Table 5.2. Developmental changes in swimming parameters.

Parameter	Day 2	Day 3	Day 4
Free Swimming Tail Beat Frequency (Hz)	67 ± 6 (11) *	not measured	35 ± 2 (12) *
Fictive Swimming EPSP Frequency (Hz)	52 ± 4 (15) *	51 ± 2 (16) **	35 ± 3 (7) * **
Fictive Swimming EPSC Frequency (Hz)	44 ± 2 (6)	48 ± 4 (5)	37 ± 3 (4)
Pooled Fictive Swimming Frequency (Hz)	49 ± 3 (21) *	51 ± 2 (21) **	35 ± 2 (11) * **
Fictive Swimming EPSC Amplitude (pA)	37 ± 5 (6) * **	52 ± 10 (5) *	63 ± 20 (4) **
Fictive Swimming Tonic Potential (mV)	-59 ± 2 (15)	-59 ± 2 (16)	-60 ± 2 (7)
Fictive Swimming Tonic Inward Current (pA)	35 ± 10 (6)	35 ± 7 (5)	56 ± 20 (4)
Resting Membrane Potential	-74 ± 1 (15)	-75 ± 1 (16)	-74 ± 1 (7)
Action Potential Threshold Potential (mV)	-46 ± 1 (15)	-46 ± 1 (16)	-48 ± 2 (7)
Action Potential Peak Potential (mV)	-20 ± 3 (15)	-18 ± 3 (16)	-18 ± 7 (7)

Values shown are means ± SE. Values in brackets are the number of motoneurons examined to calculate the presented mean values. EPSP and EPSC, excitatory postsynaptic potential and current. * or ** indicates a significant difference of means (ANOVA, or Kruskal-Wallis ANOVA) ; comparisons were made horizontally in the Table.

Table 5.3. Developmental changes in the time course (τ) of decay of large and small amplitude rhythmic EPSCs occurring during fictive swimming.

Parameter	Day 2	Day 3	Day 4
Small EPSC τ (ms)	5.8 ± 0.2 *	4.5 ± 0.4 *	5.9 ± 0.7
Large EPSC τ (ms)	2.8 ± 0.2 *	3.0 ± 0.3 *	5.1 ± 0.7

Values shown are means ± SE. The numbers of motoneurons examined to calculate the presented mean values were 5, 3, and 4, respectively, for days 2, 3, 4. * Significant difference of means (Paired *t*-test); comparisons were made vertically in the Table.

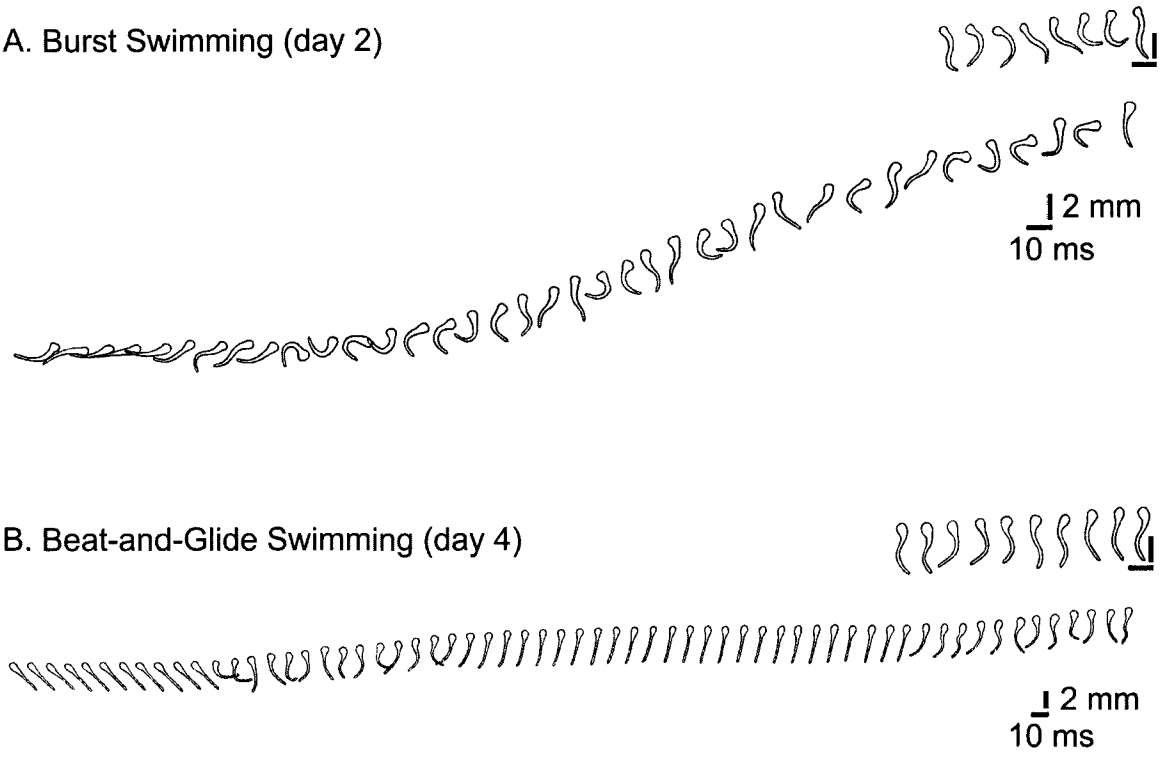

Figure 5.1. Swimming is sustained and continuous (burst swimming) in 2 day-old larvae and intermittent (beat-and-glide swimming) in 4 day-old larvae. A segment of burst swimming (A) and beat-and-glide swimming (B) is shown. The larva in A is gradually turning throughout the period shown. In B, a gliding larva initiates the following tail-beat period with a small turn to the right and then glides until the next tail beat period, which begins without a change in direction. High-speed video imaging was performed at 500 Hz (every fifth image is shown). Inserts: propulsion is generated in both cases by a wave of body movement propagating in a rostral to caudal direction; individual images are shown every 2 ms (*i.e.*, at maximal camera rate). Inset scale bars are 2 mm and 2 ms.

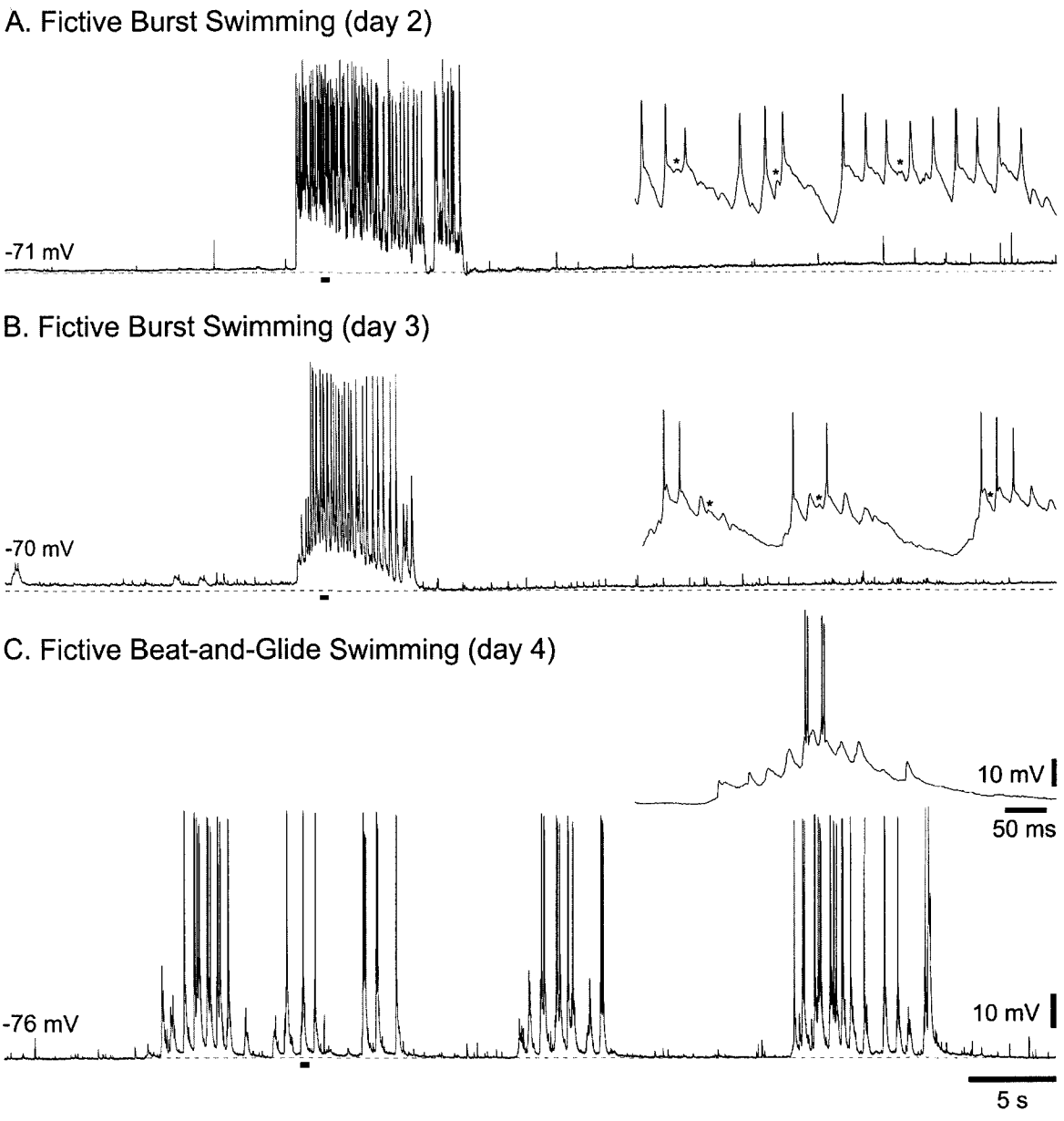

Figure 5.2. Membrane potential changes occurring during fictive burst swimming (A and B) and fictive beat-and-glide swimming (C) in 2 (A), 3 (B), and 4 (C) day-old larvae. Whole-cell current-clamp recordings were made with a potassium gluconate based intracellular solution. Membrane potentials are indicated to the left of each trace. ---- is centered on the peak hyperpolarization following the burst of fictive swimming (A and B) and is not present after the beat-and-glide fictive swimming (C). Insets: enlargements of the portions of the fictive swimming episodes marked with a ■. * in A and B indicate irregular PSPs. Calibrations shown in C are the same for the traces and insets shown in A and B.

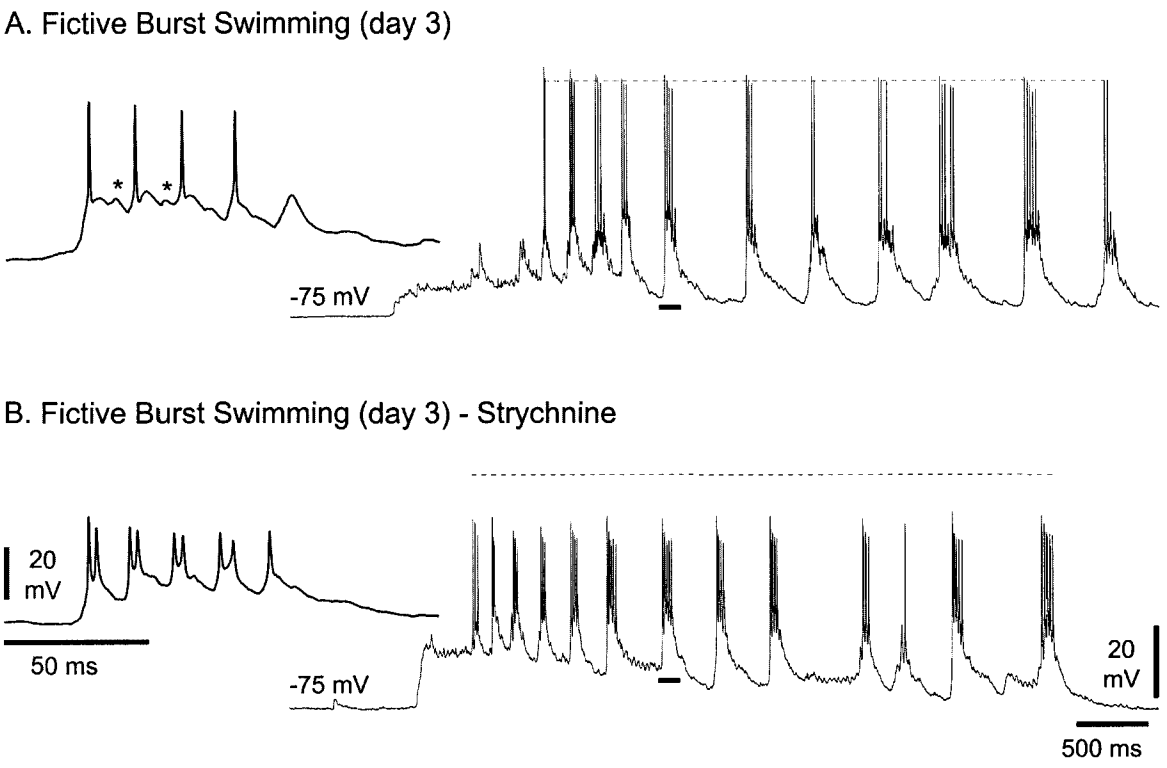

Figure 5.3. Effects of Strychnine on fictive swimming activity patterns. Fictive burst swimming observed before (A) and after bath application of 2 μM strychnine (B). Whole-cell current-clamp recordings were made with a potassium gluconate based intracellular solution. Membrane potentials are indicated to the left of each trace. ---- -10 mV. Insets: enlargements of the portions of the fictive swimming episodes marked with a ■; * in A indicate irregular PSPs which are absent in B. Calibrations shown in B are the same for the traces and insets shown in A.

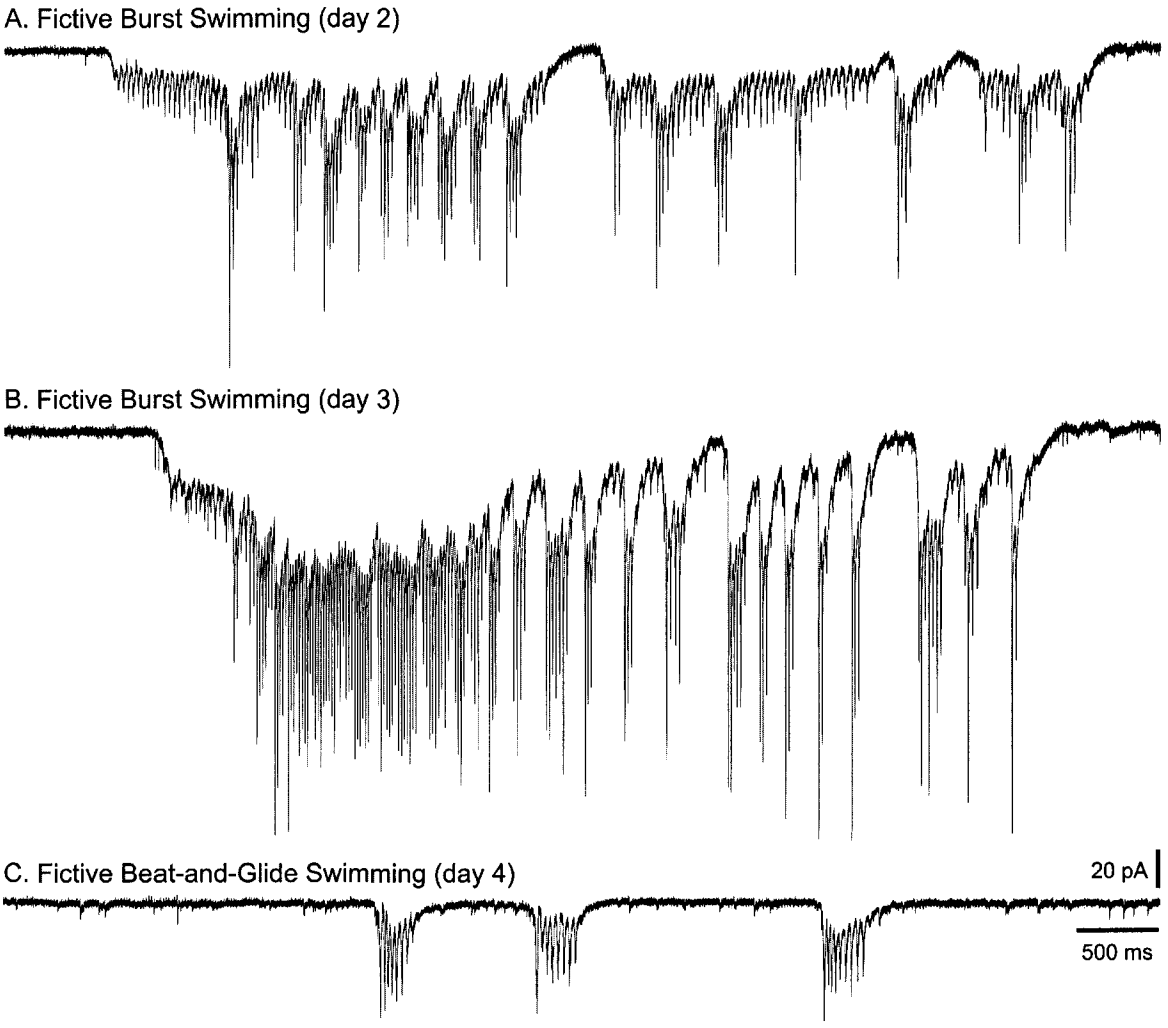

Figure 5.4. Rhythmic and tonic inward cation currents occurring during fictive burst swimming (A and B) and fictive beat-and-glide swimming (C) in 2 (A), 3 (B), and 4 (C) day-old larvae. Whole-cell voltage-clamp recordings were made with a cesium-gluconate-based intracellular solution. The membrane was clamped at the reversal potential for chloride ions (-47 mV) to reveal isolated cation currents. The fictive burst swimming shown in B is followed by a period of beat-and-glide like swimming. Calibrations shown in C are the same for the traces shown in A and B.

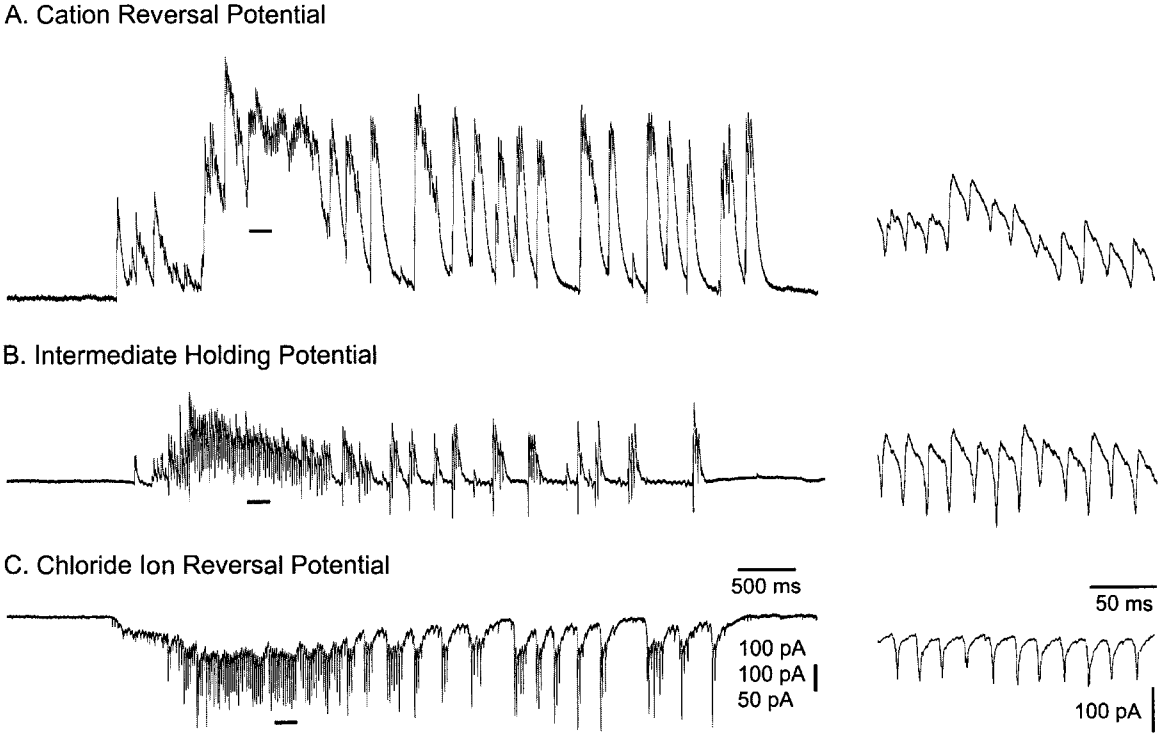

Figure 5.5. The synaptic drive underlying fictive burst swimming is composed of a tonic and slightly rhythmic chloride ion current (A) which occurs concurrently (B) with a tonic and highly rhythmic cation current (C). Whole-cell voltage-clamp recordings were made with a cesium-gluconate-based intracellular solution. Membrane voltage is clamped near the cation reversal potential (0 mV) to reveal isolated chloride ion currents (A) and at the chloride ion reversal potential (-47 mV) to reveal isolated cation currents (C). A mixture of inward cation and outward chloride ion currents is revealed at an intermediate holding potential (-33 mV; B). The day 3 fictive burst swimming is followed by a period of beat-and-glide like swimming. Insets: enlargements of the portions of the fictive swimming episodes marked with ■. The vertical scale bar in C represents 50 pA in C and 100 pA in A and B. Calibrations shown for the inset in C are the same for the insets shown in A and B.

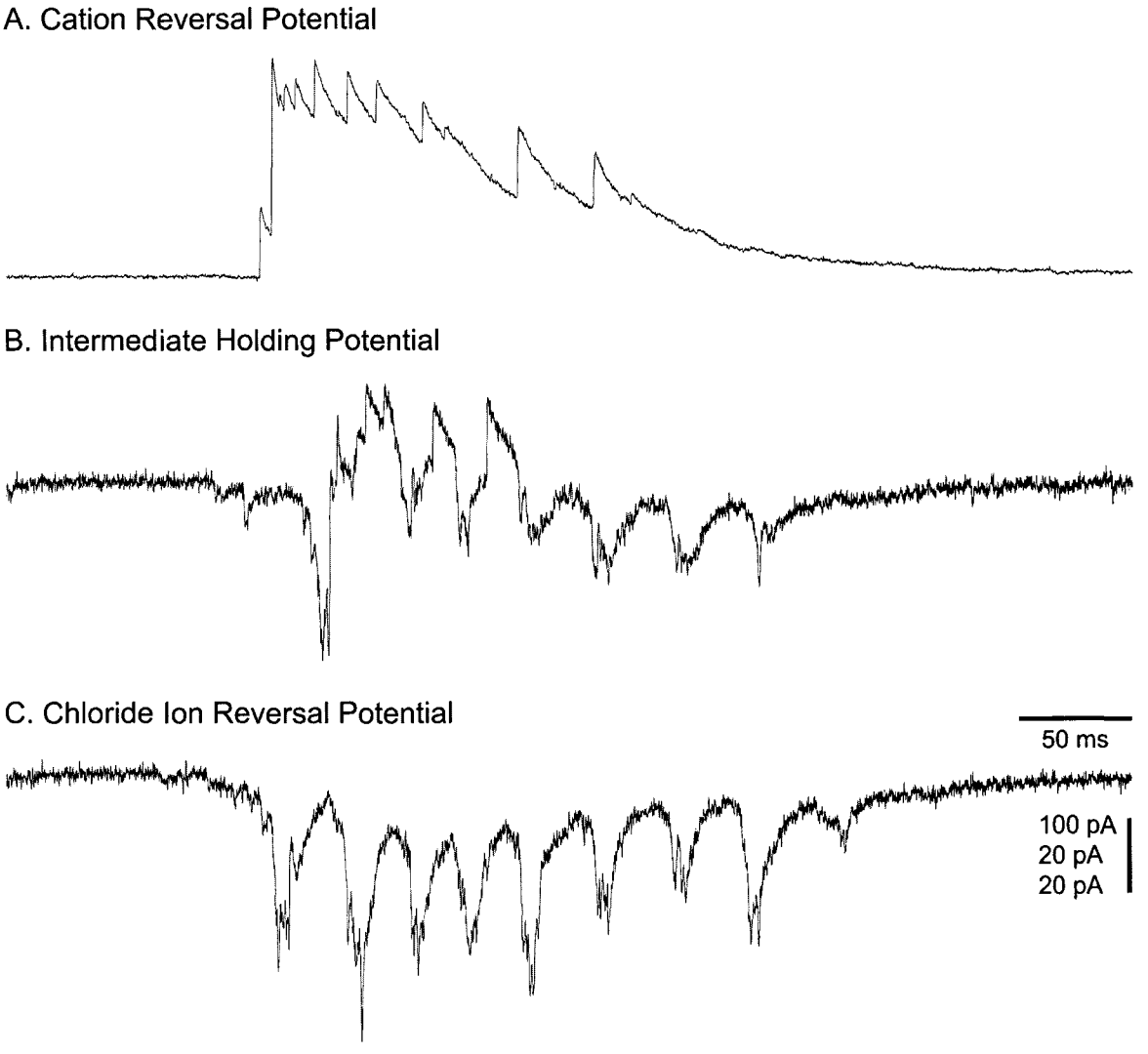

Figure 5.6. The synaptic drive underlying fictive beat-and-glide swimming is composed of a tonic and slightly rhythmic chloride ion current (A), which occurs concurrently (B) with a tonic and highly rhythmic cation current (C). Whole-cell voltage-clamp recordings were made with a cesium-gluconate-based intracellular solution. Format as in Figure 5.5 except that single episodes of synaptic activity are shown. Voltage-clamp near the cation (A; 0 mV) and chloride ion reversal potential (C, -47 mV) and at an intermediate potential (B, -33 mV). Clearly defined synaptic currents closely resembling fast AMPA/kainate synaptic currents are visible in the rhythmic cation currents shown in C. Time calibrations shown in C are the same for the traces shown in A and B, while the vertical scale bar in C represents 20 pA in B and C and 100 pA in A.

Chapter Six: Properties of Miniature Glutamatergic EPSCs in Neurons of the Locomotor Regions

LINKING STATEMENT

A rhythmic glutamatergic synaptic drive underlies the rhythmic activation of motoneurons during fictive swimming. This Chapter examines the synaptic physiology of these glutamatergic synapses at the level of spontaneous activity of individual synapses in neurons of the locomotor regions.

ABSTRACT

To further our understanding of the development of synaptic activation in the locomotor network of the zebrafish, we examined the properties of spontaneous, glutamatergic miniature excitatory postsynaptic currents (mEPSCs). Whole-cell patch-clamp recordings were obtained from visually identified hindbrain reticulospinal neurons and spinal motoneurons of curarized zebrafish 1-5 days post-fertilization (larvae hatch after the 2nd day of embryogenesis). In the presence of tetrodotoxin (TTX) and blockers of inhibitory receptors (strychnine and picrotoxin), we detected fast glutamatergic mEPSCs that were blocked by the AMPA/kainate receptor-selective antagonist 6-cyano-7-nitroquinoxaline-2,3-dione (CNQX). At positive voltages or in the absence of Mg^{2+}, a second, slower component of the mEPSCs was revealed that the *N*-methyl-D-aspartate (NMDA) receptor-selective antagonist DL-2-amino-5-phosphonovalerate (AP-5) abolished. In the presence of both CNQX and AP-5, all mEPSCs were eliminated. The NMDA component of reticulospinal mEPSCs had a large single channel conductance estimated to be 45 pS. Larval AMPA/kainate and NMDA components of the mEPSCs decayed with biexponential time courses that changed little during development. At all stages examined, approximately one-half of synapses had only NMDA responses (lacking AMPA/kainate receptors) while the remainder of the synapses were composed of a mixture of AMPA/kainate and NMDA receptors. There was an overall increase in the frequency and amplitude of mEPSCs with an NMDA component in reticulospinal (but not motoneurons) during development. These results indicate that glutamate is a prominent excitatory transmitter in the

locomotor regions of the developing zebrafish and that it activates either NMDA receptors alone at functionally silent synapses or together with AMPA/kainate receptors.

INTRODUCTION

Glutamate is the major excitatory neurotransmitter of the vertebrate central nervous system, where it mediates fast synaptic transmission through activation of *N*-methyl-D-aspartate (NMDA) and non-NMDA (AMPA/kainate and kainate) receptors. Glutamatergic ionotropic receptors have been suggested to play important roles in synaptic transmission (Edmonds et al. 1995; Madden 2002), plasticity (Nicoll and Malenka 1995) and development (Scheetz and Constantine-Paton 1994), although *in vivo* studies of development have been limited. One of the first central neural networks to develop is that for locomotion, where glutamatergic inputs are essential components of the motor circuits in adult animals (Grillner et al. 1997). Application of glutamate or NMDA can induce fictive activity patterns in the embryonic spinal cord of *Xenopus* (Dale and Roberts 1984), chick (Barry and O'Donovan 1987), and rat (Ozaki et al. 1996). However, little is known of the properties of synaptic glutamate receptors on neurons in the developing locomotor network. Pure AMPA/kainate and NMDA-mediated excitatory postsynaptic potentials (EPSPs) as well as mixed responses have been observed in spinal neurons of the *Xenopus* embryo (in vivo and in culture) in the absence of Mg^{2+} (Dale and Roberts 1985; Gleason and Spitzer 1998; Rohrbough and Spitzer 1999; Sillar and Roberts 1991). Recent studies of spontaneous mEPSCs (Gao et al. 1998) and evoked responses (Bardoni et al.

1998; Hori and Kanda 1996) recorded in neonatal rat spinal cord slices have indicated an early role for AMPA/kainate receptors. This contrasts with observations in the developing rat hippocampus (Durand et al. 1996; Isaac et al. 1995; Kullmann 1994) or frog tectum (Wu et al. 1996) where functionally silent synapses with an NMDA component but lacking an AMPA/kainate component have been described. Whether changes in the proportion of AMPA/kainate and NMDA components occur in the intact spinal cord in other preparations and in locomotor regions in general remains unanswered.

We have examined the *in vivo* development of glutamatergic synapses by recording from neurons in the locomotor regions of the embryonic and larval zebrafish. An advantage of the zebrafish for studies of locomotor network development is that there are relatively few types of neurons within these regions. The two regions that are essential for motor behaviors in the developing zebrafish (in the absence of added neuromodulators) are the hindbrain and spinal cord (Saint-Amant and Drapeau 1998), which are common regions for the locomotor networks of all vertebrates (Grillner et al. 1997). In the developing zebrafish, many neurons have been identified morphologically both in the hindbrain (Kimmel et al. 1981; Mendelson 1985; Mendelson 1986a; Metcalfe et al. 1990) and spinal cord (Bernhardt et al. 1990; Kuwada et al. 1990a; Myers et al. 1986). In this study, we have characterized the properties of spontaneously occurring mEPSCs, including their AMPA/kainate and NMDA components, in hindbrain reticulospinal neurons and spinal motoneurons as an index of the features of excitatory synapses in the locomotor network. We found that glutamate is a prominent excitatory transmitter in the locomotor regions of the developing

zebrafish and that it activates either NMDA receptors alone at functionally silent synapses or together with AMPA/kainate receptors

METHODS

Preparations

Embryos and larvae were raised at 28.5 °C and were obtained from a zebrafish (Tubingen and Longfin lines) colony maintained according to established procedures Westerfield (1995). All procedures were carried out in compliance with the guidelines stipulated by the Canadian Council for Animal Care and McGill University. Embryos and newly hatched larvae were anaesthetized in 0.02% tricaine (MS-222) (Sigma Chemical Co., St. Louis, MO) and dissected as described by Drapeau et al. (1999). Briefly, the entire hindbrain was exposed after removing rostral structures, but leaving the spinal cord intact, and recordings were obtained from reticulospinal neurons located in the central rhombomeres. For spinal neuron recordings, muscle overlaying the spinal cord was removed from 1-3 somites in the mid-trunk region in otherwise intact larvae. The preparations were moved to the recording set-up and the chamber was continuously perfused with an aerated recording solution that contained 15 μM d-tubocurarine (Sigma Chemical Co., St. Louis, MO) to paralyze the preparations but lacked tricaine. The recording solution contained (in mM; Evans 1979: 134 NaCl, 2.9 KCl, 2.1 $CaCl_2$, 1.2 $MgCl_2$, 10 HEPES and 10 glucose, osmolarity adjusted to 280-290 mOsm, pH 7.8. For Mg^{2+}-free solution, $MgCl_2$ was omitted from the recording solution without any further change. Preparations remained healthy for several hours under these recording conditions. We did not need to

add glycine to the solutions during the recording of NMDA-mediated mEPSCs as these were always apparent in its absence and their frequency was unchanged throughout the recordings, presumably due to a maintained endogenous level of spontaneously released glycine.

Cell bodies were easily identified under Hoffman modulation optics. In preliminary experiments, cells were filled with Lucifer Yellow or sulforhodamine B to confirm their identity (Drapeau et al. 1999), and in this study, 6 spinal neurons located dorsal to the central canal were filled with sulforhodamine B and their identity confirmed as motoneurons. However, as not all spinal neurons were filled it is possible that a small percentage could be interneurons. As no differences were found in the properties of the glutamatergic mEPSCs between the Mauthner cells and other reticulospinal neurons, these cells are referred to collectively as reticulospinal neurons.

Whole-cell recordings

Standard whole-cell recordings (Hamill et al. 1981) were performed 20-40 minutes after dissection (Drapeau et al. 1999). Patch-clamp electrodes were pulled from thin-walled, Kimax-51 borosilicate glass and filled with a Cs-gluconate solution and had resistances of 4-7 MΩ. Cs-gluconate intracellular solution was composed of (in mM) 115 Cs-gluconate, 15 CsCl, 2 $MgCl_2$, 10 HEPES, 10 EGTA, 4 Na_2ATP, osmolarity adjusted to 290 mOsm, pH 7.2. Whole-cell currents were recorded using Axopatch 1A and 1D amplifiers (Axon Instruments) and were low-pass filtered at 5-10 kHz (-3 dB) and digitized at 20-25 kHz. The series resistance was monitored during whole-cell recordings by applying 2 mV hyperpolarizing pulses. Series resistances (<10 MΩ) were uncompensated, and neurons that had

input resistances <100 MΩ or resting membrane potentials less than -50 mV were discarded. In all cells examined, voltage steps of 20-30 mV elicited fast, transient inward currents that were blocked by TTX. The liquid junction potential for Cs-gluconate recording solution was -10 mV and was corrected. Measurements were performed ≥5 min after obtaining the whole-cell configuration to ensure cell dialysis. All drugs were dissolved in the aerated recording solution and applied by bath perfusion. Tetrodotoxin (1 μM), strychnine (5 μM) and picrotoxin (100 μM) were obtained from Sigma Chemical Co. (St. Louis, MO) while CNQX (10 μM), AP-5 (50 μM) and L-glutamic acid were obtained from RBI (Natick, MA).

Analysis of mEPSCs

Synaptic activity was monitored using pClamp 6 software (Axon Instruments). The data was refiltered at 2 kHz using a second order Chebychev digital filter and the synaptic events were detected (using the template function for events >2.5 SD above the basal noise) and analyzed with Axograph 3.56 software (Axon Instruments). The software detected all events that could be visually recognized. All events were inspected visually, and those with uneven baselines or overlaying events (<5%) were discarded. The decay time course was analyzed over the first 40 ms for pure AMPA/kainate events and 400 ms for pure NMDA or mixed AMPA/kainate-NMDA events, and was fitted with a sum of exponential curves. The presence of 1, 2, or 3 exponential components during the decay of the mEPSCs was tested by comparing the sum of squared errors of the fits over the same decay ranges (Clements and Westbrook 1991). The rise times were defined as the time from 20% to 80% of the mEPSC amplitude, and

the half-widths were defined as the time between the rising and decay phases of each mEPSC at 50% of the peak amplitude. The amplitude and decay of the NMDA component was determined by analyzing events with both AMPA/kainate and NMDA components. Averages of these events were best fit with 3 exponential curves; 2 exponential curves were sufficient in some motoneurons where the AMPA/kainate component was too small to contribute to the peak amplitude of the mEPSC. The fastest exponential had a time course nearly identical to that of pharmacologically isolated AMPA/kainate events. The amplitude of this exponential was subtracted from the total average amplitude, yielding an estimate of the amplitude of the NMDA component. The 2 slower exponential curves were attributed mainly to the slower AMPA/kainate component and the NMDA component. As there was essentially no developmental change in the kinetics of pharmacologically isolated AMPA/kainate events, any changes observed in the decay of the mixed events could be attributed to the NMDA component. The frequency of synaptic events was determined manually because the Axograph detection software could not always detect the variably shaped pure NMDA or mixed events. Results are presented as means ± SE throughout the text unless otherwise noted. Correlations were tested using the Pearson product moment correlation and a significant relationship was noted when $P<0.05$. The term significant denotes a relationship with $P<0.05$ determined using the paired *t-test*, Student's *t-test*, Mann-Whitney test, ANOVA, Kruskal-Wallis ANOVA, or Kruskal-Wallis test, as appropriate.

RESULTS

In this study, we examined mEPSCs in 1-5 day-old (post-fertilization)

animals, from when embryos (which hatch on day 2) first show motor behaviors (day 1) to when larvae actively swim to feed (day 4 or 5).

Properties of reticulospinal neurons

The embryonic zebrafish hindbrain is segmented into 9 neuromeres, 7 of which possess a few bilateral pairs of descending reticulospinal neurons that innervate the spinal cord (Kimmel et al. 1981; Mendelson 1985; Mendelson 1986a; Metcalfe et al. 1990). These include the largest pair, the Mauthner neurons, whose morphological development has been well characterized in the zebrafish (Kimmel et al. 1981). In addition, their physiological properties have been studied in the adult zebrafish (Hatta and Korn 1998), whereas glycinergic miniature inhibitory postsynaptic currents (mIPSCs) have been characterized in the isolated hindbrain of the zebrafish larva (Legendre and Korn 1994). The Mauthner neurons together with other reticulospinal neurons in the caudal rhombomeres are active during the escape response (O'Malley et al. 1996).

Reticulospinal neurons were recorded from 1.2 day-old embryos to 3.1 day-old larvae. The low input resistance of the larger cells in older larvae precluded high-resolution recordings at later times. The values of the electrophysiological parameters are summarized in Table 6.1. The resting potential was on average -61 ± 1.6 mV (n = 28) and ranged from –50 mV to –74 mV. The input resistance (R_i) of reticulospinal neurons decreased significantly (approximately 5-fold) during development, from 1.0 ± 0.18 GΩ in embryos to 0.19 ± 0.02 GΩ in 3.1 day old larva.

Properties of spinal motoneurons

The spinal cord of the early zebrafish is segmented into some 30 somites,

each half of which contains 2 anatomical classes of sensory neurons, 10 morphologically defined classes of interneurons (Bernhardt et al. 1990; Hale et al. 2001; Kuwada et al. 1990a) and 2 classes of motoneurons (Myers et al. 1986). In the adult zebrafish, the 2 classes of motoneurons underlie activation of the trunk musculature during swimming (Liu and Westerfield 1988). Motoneurons (29 cells; see Table 6.2) from 2.3 to 5.4 day old larvae had a mean resting potential of -68 ± 1.1 mV (range, -55 to -79 mV) and input resistances of 0.35 ± 0.04 GΩ. Resting potentials in motoneurons were significantly more negative in older animals and in comparison with reticulospinal neurons. There was also a trend to decreasing input resistance in motoneurons of older animals. In preliminary current-clamp experiments (n = 4), application of L-glutamic acid (0.7 to 2.0 mM) in the presence of 1 μM TTX was observed to depolarize spinal neurons close to 0 mV (data not shown). This indicated the presence of glutamate receptors and we sought to characterize their synaptic properties at different stages of development by voltage-clamp recording of pharmacologically isolated miniature synaptic currents.

Basal synaptic activity and the AMPA/kainate component of mEPSCs

In Mg^{2+} and Mg^{2+}-free saline with a Cs-gluconate intracellular solution, all reticulospinal neurons in newly hatched (day 2) larvae exhibited a high level of synaptic activity, including regular bursting episodes as shown in Figure 6.1A1. Motoneurons generally received a lower level of basal synaptic activity and bursting episodes that occurred spontaneously or could be evoked by dimming the lights (Figure 6.1B1). These bursts of synaptic activity are likely related to 'fictive' swimming or escape behaviors. In one-half (10/20) of the motoneurons,

small (approximately 10 pA) long-lasting (approximately 1 s) inward currents were observed in the presence of TTX and did not resemble the synaptic currents described here.

The chloride ion reversal potential was –50 mV such that inhibitory currents would be inward at a holding potential of -70 mV. Therefore, to distinguish inward, excitatory currents from inhibitory currents we recorded in the presence of 5 μM strychnine and 100 μM picrotoxin to block glycine- and GABA-mediated currents (Triller et al. 1997). Spontaneous miniature events were recorded in the presence of 1 μM TTX to block Na^+-dependent action potentials. The preparation was continuously perfused with 15 μM D-tubocurarine to prevent muscle contractions during the recordings. The high level of spontaneous synaptic activity was greatly reduced in the presence of TTX, strychnine, and picrotoxin (Figure 6.1, A2 and B2). The remaining spontaneous miniature synaptic events (mEPSCs) recorded in the presence of Mg^{2+} ion were completely abolished by 10 μM 6-cyano-7-nitroquinoxaline-2,3-dione (CNQX; Figure 6.1, A3 and B3), a potent AMPA/kainate receptor antagonist, suggesting that they were due to the activation of glutamatergic AMPA/kainate receptors.

Application of AP-5 had no effect on the decay of the mEPSCs (Figure 6.1, A4 and 1B4) or on their amplitude or frequency (data not shown). Thus, near the normal resting potential (–70 mV holding potential) NMDA receptors were unlikely to contribute to the synaptic response. AMPA/kainate-dependent mEPSCs (recorded in the presence of AP-5 or Mg^{2+} ion) had fast rise times (20-80%) of approximately 0.2 ms and averaged traces were well fit with 2 exponential decays

in both reticulospinal and motoneurons ($P<0.05$). The kinetic parameters of AMPA/kainate events were similar in reticulospinal neurons and spinal motoneurons and were largely unchanged throughout the developmental stages examined (Tables 6.1 and 6.2). The mean event amplitudes and frequencies (the latter of which were highly variable) did not differ significantly but tended to increase in older animals.

An amplitude histogram from a representative cell (reticulospinal, Figure 6.2A) showed that the large majority of AMPA/kainate events were clustered between 10-30 pA, although the distribution was skewed towards larger amplitudes. The 20-80% rise times in both types of neurons were tightly clustered between 0.1 and 0.3 ms (Figure 6.2B), although there were some rare events (<1%) with larger rise times. A concern when recording in the whole-cell configuration is the effectiveness of the space-clamp. Miniature synaptic events that are not space-clamped will be filtered and will appear to have longer rise times, smaller amplitudes and longer decays (Rall 1969). We therefore examined the correlation between the rise time and half-width (Figure 6.2C) or amplitude (Figure 6.2D) of events. The lack of correlation ($R<0.4$ for the reticulospinal neuron of Figure 6.2C and D) in the recordings in both reticulospinal neurons and motoneurons suggests that cells at various developmental stages were adequately space-clamped. This is consistent with our ability to resolve such fast events; except for a minute fraction of the events that were either less well clamped or perhaps were less mature synapses.

NMDA component of the mEPSCs

In order to overcome the voltage-dependent Mg^{2+} ion block of NMDA

receptors (Mayer and Westbrook 1987) and detect their possible contribution to mEPSCs, we voltage-clamped cells at +40 mV (Figure 6.3A). Under these conditions, we were able to detect mEPSCs that were blocked only by adding both CNQX and AP-5, and which reversed near 0 mV. A recording performed on a day 3 motoneuron (Figure 6.3) shows that at +40 mV, averaged mEPSCs had rapid rise times and decayed with a fast component and a much slower, second component. The slow component disappeared in the presence of 50 μM AP-5, and 10 μM CNQX abolished the remaining fast component (not shown), confirming that they were due to the activation of NMDA and AMPA/kainate receptors, respectively. The NMDA component was larger as the holding potential was made more positive. This is shown in Figure 6.3B, where averaged traces of mEPSCs at various holding potentials (-80, -60, -40, -20, and +40 mV) are normalized, inverted where appropriate, and overlaid. The inset shows similarly normalized AMPA/kainate mEPSCs at 3 different potentials (-80, -40, and +40 mV) isolated in the presence of 50 μM AP-5. The later events decayed with similar time courses indicating that the AMPA/kainate component of the mEPSCs was voltage-independent. The above observations were confirmed in 4 other spinal motoneurons and 5 larval reticulospinal neurons.

Recordings made at positive potentials, where the NMDA component was fully revealed, were noisy due to the opening and closing of background voltage-dependent channels. Therefore, in order to resolve better the NMDA events we recorded mEPSCs in Mg^{2+}ion-free extracellular solution as shown in Figure 6.4. Averages of events in the presence of either 10 μM CNQX or 50 μM AP-5 are

shown, respectively, in Figure 6.4A while the inset reveals on an expanded time scale the slower rise time of the CNQX-insensitive events. A rise time-amplitude scatter plot (Figure 6.4B) suggests that there are 2 separate classes of events: slower events (>0.5 ms rise times) with smaller amplitudes (<30 pA), and larger events (>30 pA) with faster rise times (<0.5 ms). Application of CNQX (Figure 6.4C) followed by washout and then application AP-5 (Figure 6.4D) to the same cell revealed separate populations of slow and fast events. The AP-5-resistant events (Figure 6.4, A and D) resembled the AMPA/kainate component of the mEPSCs described above in the presence of Mg^{2+}(Figures 6.1A4, 6.1B4, and 6.2D). A clear separation of events based upon amplitude and rise time as shown in Figure 6.4C was not always observed, thus it was not possible to distinguish AMPA/kainate events from NMDA events based on rise time alone.

To estimate the proportion of the NMDA events without a distinguishable AMPA/kainate component, the frequency of events that were detected after application of AP-5 (AMPA/kainate only) was compared with the frequency of all events (a mixture of AMPA/kainate and NMDA) detected prior to addition of AP-5. In AP-5, the frequency of events in reticulospinal neurons and motoneurons was significantly reduced by 52 ± 4.4% ($P<0.05$, paired *t-test* for all ages pooled: reticulospinal $n = 17$, motoneuron, $n = 16$). This indicated that approximately one-half of the mEPSCs were due to activation of NMDA receptors at synapses with an undetectable AMPA/kainate component, and thus these synapses would be functionally silent at resting membrane potentials. The proportion of these functionally silent synapses did not change significantly during development in

motoneurons where the reduction of mEPSC in AP-5 was 43 ± 9.2%, 43 ± 10% and 57 ± 15 % in 2-3, 3-4, and 4-5 day larvae respectively. In the reticulospinal neurons, the event frequency was reduced by 64 ± 5.6%, 59 ± 10%, and 38 ± 16% in 1.2-1.5, 2.2-2.3 and 3.0-3.1 day old animals respectively.

Isolated NMDA events

The CNQX-insensitive, isolated NMDA events were usually small in amplitude and had highly variable rise times, and prolonged decays (Figure 6.4A inset). Thus, it was difficult to detect the NMDA events in most cells by the automated procedure, which was reliable in only 5 preparations: 4 embryonic reticulospinal neurons and 1 motoneuron (Figure 6.4) at 2-3 days. Figure 6.5 shows pooled data for the NMDA events from the 4 reticulospinal neurons. The majority of the detected events had amplitudes clustered around 10-15 pA (Figure 6.5A). The 20-80% rise times (Figure 6.5B) were 12-fold slower (0.4-18 ms: 2.4 ± 0.13 ms; n = 4 cells) than those of the AMPA/kainate component. Such ranges of rise times were comparable to the rise times of the slower population of mixed glutamatergic mEPSCs observed in both reticulospinal neurons and motoneurons. Figures 6.5 (C and D) reveal the lack of negative correlation (R<0.4) between the rise times and amplitudes or half-widths suggesting that the space-clamp was effective. The NMDA events in reticulospinal neurons was best fit with 2 decay time constants of 14.1 ± 2.1 ms and 132 ± 25 ms (14 ± 4%). The 2 decay time constants for the motoneuron were 7.3 ms and 51 ms (21%). The difficulty in detecting these pure NMDA synaptic events prevented a more detailed analysis of developmental changes. However, developmental changes of NMDA synapses were examined indirectly by subtracting the AMPA/kainate

component from synaptic events, recorded in the absence of Mg^{2+} ion (see below).

Single NMDA channel conductances

Some mixed synaptic events in young reticulospinal embryos (day 1.2 to 1.5) with high input resistances showed single channel openings (Figure 6.6), indicating either a low probability of channel opening or a low density of post-synaptic receptors at these early synapses. The events often started (Figure 6.6A) with a large and brief AMPA/kainate current transient and ended with repeated single, presumably NMDA channel openings. The AMPA/kainate current was presumably generated by the opening of several channels as we could not distinguish single channel events; this is not suprising as the AMPA/kainate channel conductances are reported to be small (Edmonds et al. 1995). In other cases (Figure 6.6B), the fast AMPA/kainate component could not be distinguished because of the opening of few or possibly no channels. These events had highly variable time courses that represent NMDA channel openings rather than spurious openings of background channels as the activity was largely abolished by perfusion with AP-5 (not shown). An amplitude histogram of the late currents of a single mixed event recorded at -70 mV (Figure 6.6C) indicated a primary peak of -3.2 pA. Since the mEPSCs reversed near 0 mV (data not shown), this corresponds to a single NMDA channel conductance of 46 pS. The average single channel conductance (13 events from 4 cells) was estimated as 45 $\pm$ 2 pS in embryonic reticulospinal neurons. More detailed single channel studies over a range of potentials will be needed to confirm this estimate of the conductance. We were unable to detect single-channel NMDA events in

motoneurons due to the lower input resistance of the cells.

Developmental changes in the properties of mEPSCs

As previously presented, the changes in the kinetics of isolated AMPA/kainate mEPSCs were minimal or absent during the developmental periods studied. Therefore any developmental changes in those events detected in the absence of Mg^{2+} ion without any glutamatergic antagonists present could be attributed to changes in the NMDA component of these mixed events. However, it is not definitively known whether an individual event arose from a synapse containing only AMPA/kainate channels, only NMDA channels, or a mixture of both AMPA/kainate and NMDA channels. To explore the composition of these mEPSCs, all events were manually detected and classified as pure AMPA/kainate, pure NMDA, or mixed AMPA/kainate - NMDA events based upon our knowledge of the appearance of the pharmacologically isolated events. Less than 10% of the events resembled pure AMPA/kainate events. The analysis of functionally silent synapses (using AP-5) presented in the preceeding text revealed that as many as one-half of the events could have been pure NMDA. However, as the variably shaped NMDA events were not automatically detected, only a portion of these events would be included in the averages, resulting in an underestimate of their contribution.

A clear developmental trend that we observed was an increase in the amplitude of the extrapolated NMDA component of the reticulospinal (but not motoneuron) mixed synapses. Mixed synapse NMDA event amplitudes in reticulospinal neurons (Table 6.2) more than doubled (4.9-11.6 pA, $P<0.05$) in the transition from embryonic to larval stages. No such trend was observed in the

motoneurons where the average NMDA component was large (ranging from 9.6-12.3 pA, Table 6.2) at all stages examined. In both reticulospinal cells and motoneurons, the difference was statistically significant when average rise times were compared in the same cells before and after AP-5, and average half-widths were 2-4 times slower for mixed events (not shown). These rise times were nonetheless faster than observed for the isolated NMDA events due to the mixed contribution of NMDA and AMPA/kainate receptors under these conditions. The average frequency of these mixed events increased significantly in larval (4.2 ± 1.4 Hz) compared to embryonic (1.2 ± 0.4 Hz) reticulospinal neurons (Table 6.1), whereas in motoneurons (Table 6.2), the frequency remained at approximately 1 Hz throughout the stages of larval development examined.

In some motoneurons (see Methods) the AMPA/kainate component did not contribute to the peak amplitude, but its presence was inferred from the presence of fast rise times in the mixed events. Furthermore, 2 exponentials were used to fit the averaged events, both being attributed to NMDA receptor activation. The decay of the majority of averaged, mixed events was best fit with 3 exponentials where the fast exponential was attributed to the AMPA/kainate component and the slower 2 exponentials to the NMDA component. The slower 2 exponentials attributed to the NMDA component are labeled τ_{off1} and τ_{off2} in Tables 6.1 and 6.2. The time course of τ_{off1} and τ_{off2} were variable at all stages of development in both reticulospinal and motoneurons, making it difficult to distinguish developmental trends. The NMDA component of all the mixed events (calculated from the means presented in Tables 6.1 and 6.2) was τ_{off1} = 11 ms,

τ_{off2} = 60 ms (34%), and τ_{off1} = 7.4 ms, τ_{off2} = 37 ms (22%) in reticulospinal neurons and motoneurons respectively.

DISCUSSION

We observed that reticulospinal neurons and motoneurons of the curarized zebrafish embryo and larva had spontaneous mEPSCs that were entirely glutamatergic. This is not surprising as glutamate is the main excitatory transmitter of the vertebrate nervous system. However, because we included D-tubocurarine, this would have blocked cholinergic synapses if these occurred, as reported in spinal interneurons (Perrins and Roberts 1995b) and between motoneurons (Perrins and Roberts 1995a) of the *Xenopus* embryo. In preliminary (unpublished) experiments (n = 8) using a high magnesium/low calcium solution instead of D-tubocurarine to suppress muscle contractions, we failed to detect spontaneous cholinergic mEPSCs. This indicates that glutamate is indeed the main if not sole excitatory transmitter in the developing zebrafish. In the absence of TTX, both types of neurons we examined showed bursts of PSCs, suggesting that these may be related to fictive swimming or escape behaviors, although we did not examine this in any detail. The amplitude histograms of the mEPSCs were skewed (non-gaussian) towards larger events, as described for glycinergic mIPSCs in the larval zebrafish hindbrain (Legendre and Korn 1994). Such variability in quantal size may be accounted for by presynaptic factors, such as variation in quantal content or multiquantal release, or by postsynaptic factors including receptor properties and densities (Bekkers and Stevens 1996; Bekkers

et al. 1990; Legendre and Korn 1994; Nusser et al. 1997; Ulrich and Luscher 1993).

The AMPA/kainate component of the mEPSC

In the presence of TTX and at -70 mV, near the normal resting potential, the mEPSCs were entirely due to AMPA/kainate receptor activation and these were well space-clamped in the whole-cell recordings. The AMPA/kainate component of the mEPSCs showed voltage-independent kinetics that were fast, both in their rise times and biexponential decay time constants. These fast kinetics are consistent with those reported for synaptic potentials in the Mauthner neuron of the goldfish (Wolszon et al. 1997) and at central synapses in the mammalian brain (reviewed by Edmonds et al. 1995) where the decay time course of EPSCs is usually monoexponential. However, a second decay phase has been reported for cerebellar granule cells (Barbour et al. 1994; Silver et al. 1992).

The NMDA component of the mEPSC

An NMDA component of the mEPSCs was revealed only in the absence of Mg^{2+} ion or at depolarized potentials, as expected if Mg^{2+} ion blocks NMDA receptors at the resting membrane potential in zebrafish as in other preparations. Recently the NR1 subunit has been cloned in another teleost and shows a high degree (overall 88%) of homology with the mammalian subunit, including essentially identical (>98%) ligand binding sites and pore region (Bottai et al. 1998), the latter being the presumed Mg^{2+} ion binding site. The kinetics of the NMDA component of the mEPSCs were an order of magnitude slower than those of the AMPA/kainate component with respect to both the rise times and biexponential decays. In reticulospinal neurons of the youngest embryos

examined, single channel openings with a conductance of approximately 45 pS were estimated. This is similar to the conductances described for other native NMDA receptors activated at single synapses in the immature mammalian brain (Gibb and Colquhoun 1991; Lester and Jahr 1992; LoTurco et al. 1991; Silver et al. 1992), in cultured spinal neurons (Robert et al. 1998), and in embryonic *Xenopus* spinal neurons (Zhang and Auerbach 1995).

The NMDA component remained essentially biexponential over the stages examined, and the time constants did not vary much with development, remaining relatively fast with the slower decay being between 30 and 60 ms. At several immature (early post-natal) mammalian central synapses, the evoked NMDA responses last several hundred milliseconds, and a decrease in the decay phase has been observed during development (Carmignoto and Vicini 1992; Crair and Malenka 1995; Golshani et al. 1998; Hestrin 1992; Ramoa and McCormick 1994). This has also been observed at the level of single NMDA channels isolated in outside-out patches (Carmignoto and Vicini 1992; Hestrin 1992), indicating a developmental alteration of NMDA channel properties that is likely due to a switch in subunit composition (Flint et al. 1997; Monyer et al. 1994). The mEPSCs in zebrafish embryos and larvae were apparently already fast, suggesting that at these early stages there are no major changes in the kinetic properties of the receptors. Glycinergic synapses in the Mauthner neuron are also thought to be mature by hatching (approximately 52 hpf; Triller et al. 1997). It thus appears that the zebrafish has a remarkably rapid maturation of central synapses, occurring during embryonic development. As we recorded from neurons 1.2 days (28 hpf) and older in the hindbrain, where axogenesis starts

between 20-21 hpf (Mendelson 1985), it may be that the earliest period of functional synaptogenesis is as brief as a few hours.

A developmental trend that was observed in the NMDA component of mixed synapses was a doubling in event amplitudes in reticulospinal neurons but not in motoneurons during the stages examined. A likely explanation is an increase in the number of NMDA receptors at synapses onto reticulospinal neurons. The frequency of mixed glutamatergic mEPSCs also tended to increase in the reticulospinal neurons throughout the stages examined, presumably reflecting synaptogenesis. It thus appears that new synapses are continually added in the hindbrain of the zebrafish embryo and larva and that these vary in their AMPA/kainate and NMDA receptor content with one-half of the synapses lacking the former and thus being functionally silent under resting conditions. Interestingly, the hindbrain appears to mature over a longer period than the spinal cord in the developing zebrafish. Thus swimming, which is mediated by a spinal central pattern generator, begins at 28 hpf and reaches a maximal rate by approximately day 2 (Buss and Drapeau 2001a; Saint-Amant and Drapeau 1998). In contrast, hindbrain Mauthner neurons mediating escape behaviors are responsive to sensory inputs from the auditory and visual systems only a few days after hatching (Eaton and Farley 1973), which is the period when large numbers of afferent synapses are formed onto the Mauthner cell dendrites (Kimmel et al. 1981). Thus, the extended development of the NMDA component of glutamatergic synapses may be related to the protracted development of afferent innervation in the hindbrain.

Functionally Silent Synapses

Approximately one-half of the mEPSCs had an NMDA component but lacked an AMPA/kainate component both in reticulospinal and motor neurons at all stages examined. A smaller fraction (approximately 20%) of these types of responses also was observed for dorsal horn neurons in the neonatal rat spinal cord (Bardoni et al. 1998). These responses thus resemble 'silent' central synapses (Durand et al. 1996; Isaac et al. 1995; Kullmann 1994; Liao et al. 1995; Losi et al. 2002; Wu et al. 1996) at which the evoked NMDA component is thought to precede the AMPA/kainate component, thus being functionally silent due to Mg^{2+} ion block at the resting potential. The activation of NMDA responses, presumably coincident with a depolarizing event, and consequent calcium influx has been proposed as a mechanism of plasticity for the induction of AMPA/kainate receptor expression at synapses in these brain regions, triggering conversion from functionally silent to mature synapses (Wu et al. 1996). It may be that these functionally silent synapses in zebrafish locomotor regions are activated during swimming once the cells have passed spike threshold and the Mg^{2+} ion block is removed from the NMDA channel. The functionally silent synapses could thus contribute to locomotor drive potentials and be especially important in providing a positive feedback pathway.

TABLES AND FIGURES

Table 6.1. Reticulospinal neurons

	1.2-1.5 days embryonic	2.2-2.3 days larval	3.0-3.1 days larval
V_m (mV)	-57 ± 2.0	-63 ± 2.4	-61 ± 3.7
R_i (GΩ)	1.0 ± 0.18*	0.45 ± 0.08	0.19 ± 0.02*
Isolated AMPA/kainate EPSCs			
τ_{off1} (ms)	0.71 ± 0.08	0.56 ± 0.04	0.60 ± 0.04
τ_{off2} (ms)	4.0 ± 0.7	3.5 ± 0.4	3.3 ± 0.6
(% amplitude)	(14 ± 3)	(11 ± 1)	(5 ± 1)
Amplitude (pA)	12.9 ± 0.9	17.4 ± 1.8	17.1 ± 2.2
20-80 % Rise time (ms)	0.22 ± 0.02	0.24 ± 0.02	0.25 ± 0.02
Frequency (Hz)	0.5 ± 0.3	2.1 ± 0.5	2.6 ± 1.4
n	6	15	4
Mixed EPSCs			
τ_{off1} (ms)	12.5 ± 4.3	9.8 ± 3.4	10.6 ± 2.5
τ_{off2} (ms)	59 ± 18	71 ± 22	50 ± 14
(% amplitude)	(32 ± 8)	(28 ± 8)	(42 ± 12)
Extrapolated NMDA			
Amplitude $\tau_{off1\ and\ 2}$ (pA)	4.9 ± 0.9*	8.8 ± 1.7	11.6 ± 1.1*
20-80 % Rise time (ms)	0.45 ± 0.08	0.46 ± 0.05	0.63 ± 0.13
Frequency (Hz)	1.2 ± 0.4*	2.3 ± 0.5	4.2 ± 1.4*
n	7	7	4

EPSCs, excitatory postsynaptic currents; NMDA, *N*-methyl-D-aspartate. $P<0.05$.

Table 6.2. Spinal Motoneurons

	2-3 days hatching	3-4 days larval	4-5 days larval
V_m (mV)	-65 ± 1.8*	-69 ± 2.1	-71 ± 1.2*
R_i (GΩ)	0.41 ± 0.07	0.39 ± 0.10	0.23 ± 0.05
Isolated AMPA/kainate EPSCs			
τ_{off1} (ms)	0.78 ± 0.16	0.54 ± 0.06	0.54 ± 0.03
τ_{off2} (ms)	6.2 ± 0.9	3.3 ± 0.6	3.2 ± 0.2
(% amplitude)	(16 ± 5)	(20 ± 4)	(13 ± 2)
Amplitude (pA)	13.7 ± 2.3	18.3 ± 2.7	16.7 ± 3.3
20-80 % Rise time (ms)	0.22 ± 0.02	0.18 ± 0.01	0.19 ± 0.01
Frequency (Hz)	0.39 ± 0.12	0.49 ± 0.14	1.62 ± 1.11
n	7	7	6
Mixed EPSCs			
τ_{off1} (ms)	8.6 ± 2.2	5.5 ± 1.0	8.2 ± 2.0
τ_{off2} (ms)	44.6 ± 10.2	36.3 ± 8.6	30.1 ± 9.1
(% amplitude)	(21 ± 5.6)	(20 ± 2.7)	(24 ± 4.4)
Extrapolated NMDA			
Amplitude $\tau_{off1\ and\ 2}$ (pA)	12.3 ± 1.9	9.6 ± 1.0	10.6 ± 1.6
20-80 % Rise time (ms)	0.79 ± 0.16	0.41 ± 0.09	0.75 ± 0.18
Frequency (Hz)	0.71 ± 0.36	0.82 ± 0.32	1.02 ± 0.18
n	8	8	7

* $P<0.05$.

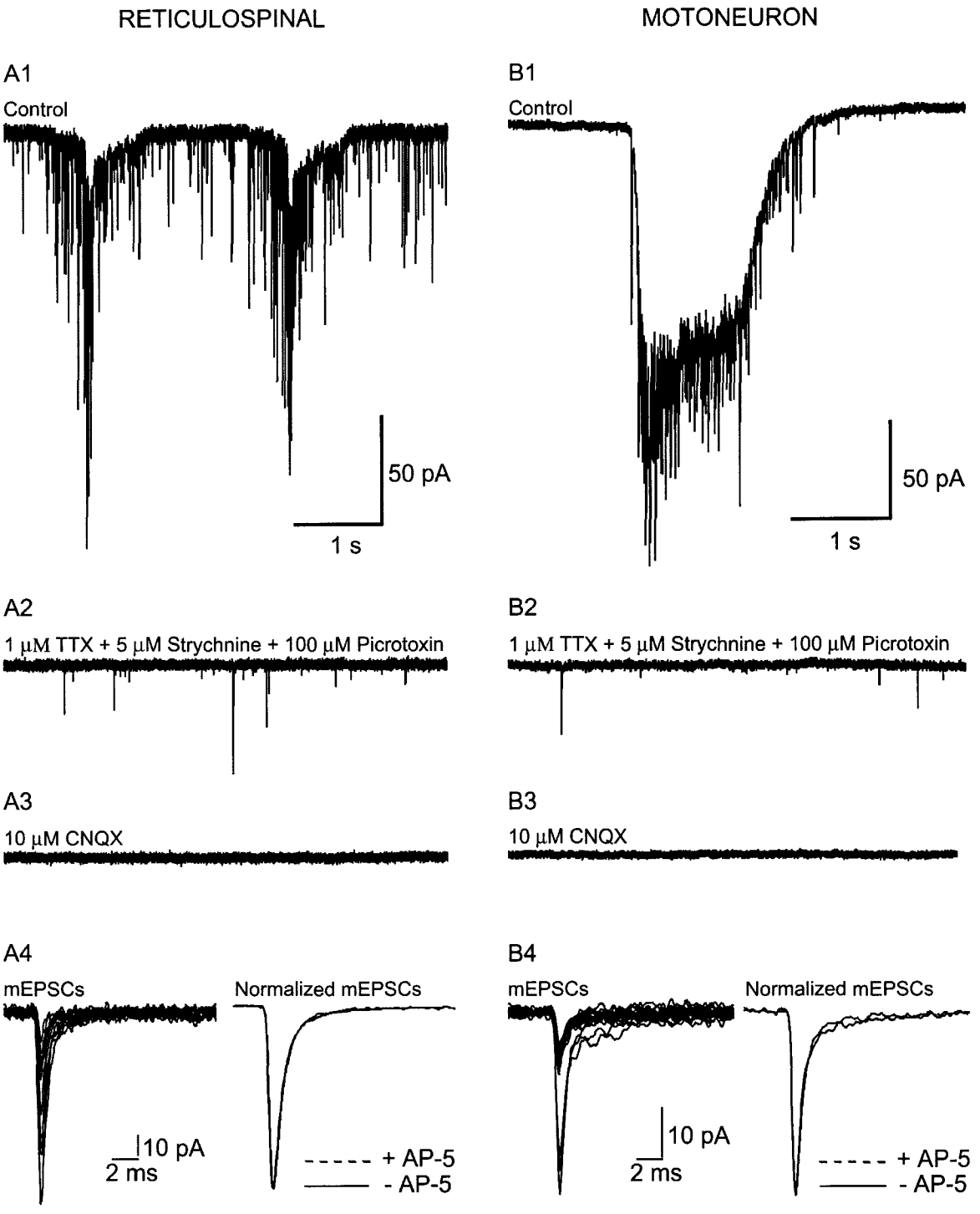

Figure 6.1. Spontaneous synaptic activity. Whole-cell recordings of spontaneously occurring synaptic activity in a reticulospinal neuron (A) and a motoneuron (B). Activity before (A1 and B1) and after (A2 and B2) bath application of 1 μM TTX, 5 μM strychnine, and 100 μM picrotoxin. Holding potential for both neurons was -70 mV. (A3 and B3) No miniature EPSCs were recorded after bath application of 10 μM CNQX. (A4 and B4) Individual (overlapped) mEPSCs recorded in the presence of TTX, strychnine, and picrotoxin. Right traces in A4 and B4 show averaged, normalized mEPSCs overlaid with a similar trace of mEPSCs recorded in the presence of 50 μM AP-5 (dashed line).

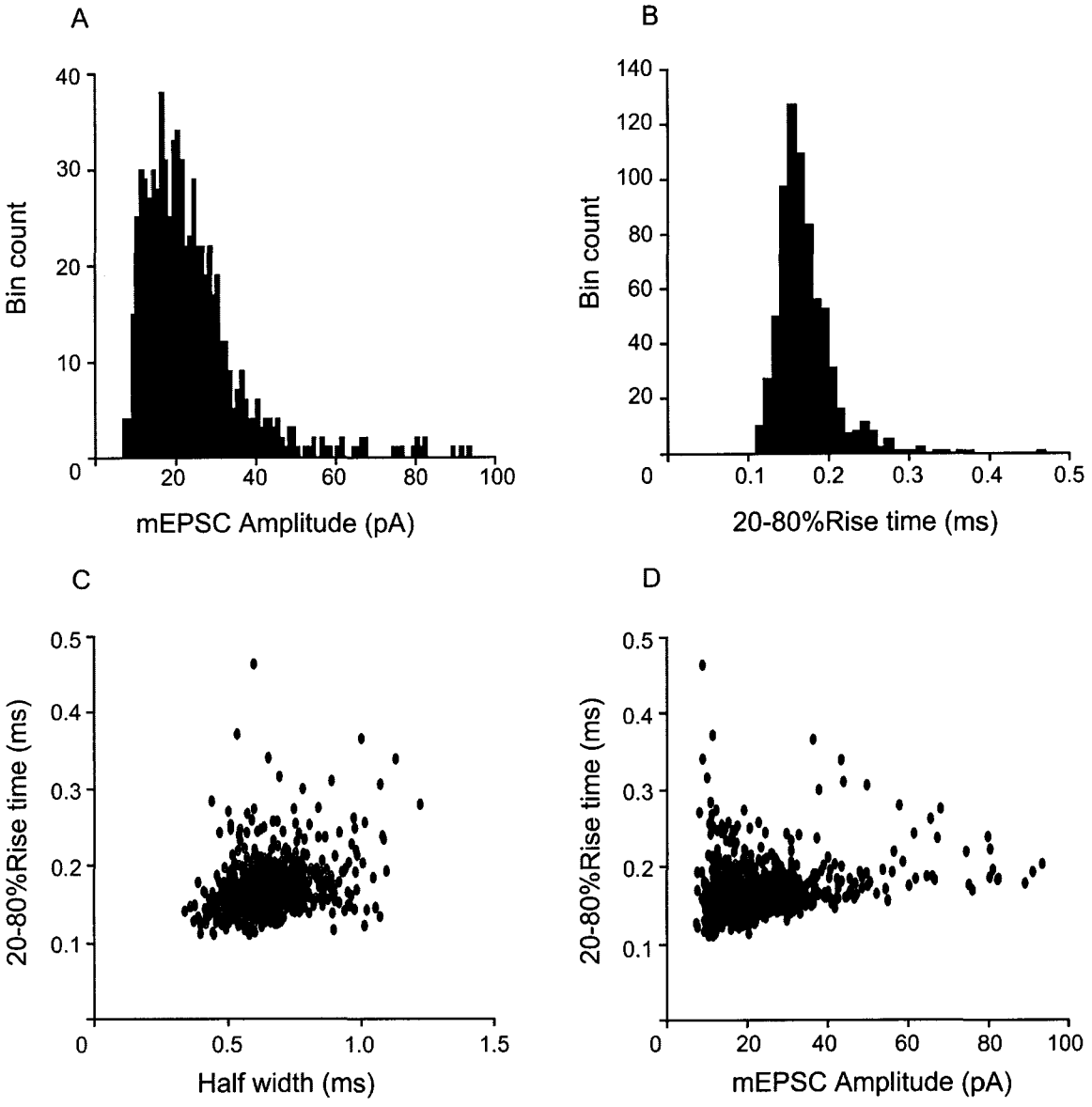

Figure 6.2. Isolated AMPA/kainate mEPSCs. A: Amplitude histogram of mEPSCs from a reticulospinal neuron recorded in the presence of 1 μM TTX, 5 μM strychnine and 100 μM picrotoxin (average: 24.0 ± 0.5 pA; *n* = 710 events; bin width = 1 pA). B: 20-80% rise time distribution of mEPSCs (average: 0.172 ± 0.001 ms; bin width = 10 μs). C: scatter plot of the rise time *vs* half-width of the events. D: scatter plot of rise time *vs* mEPSC amplitude. Note the lack of correlation in C ($R = 0.31$) and in D ($R = 0.16$). Holding potential was -70 mV.

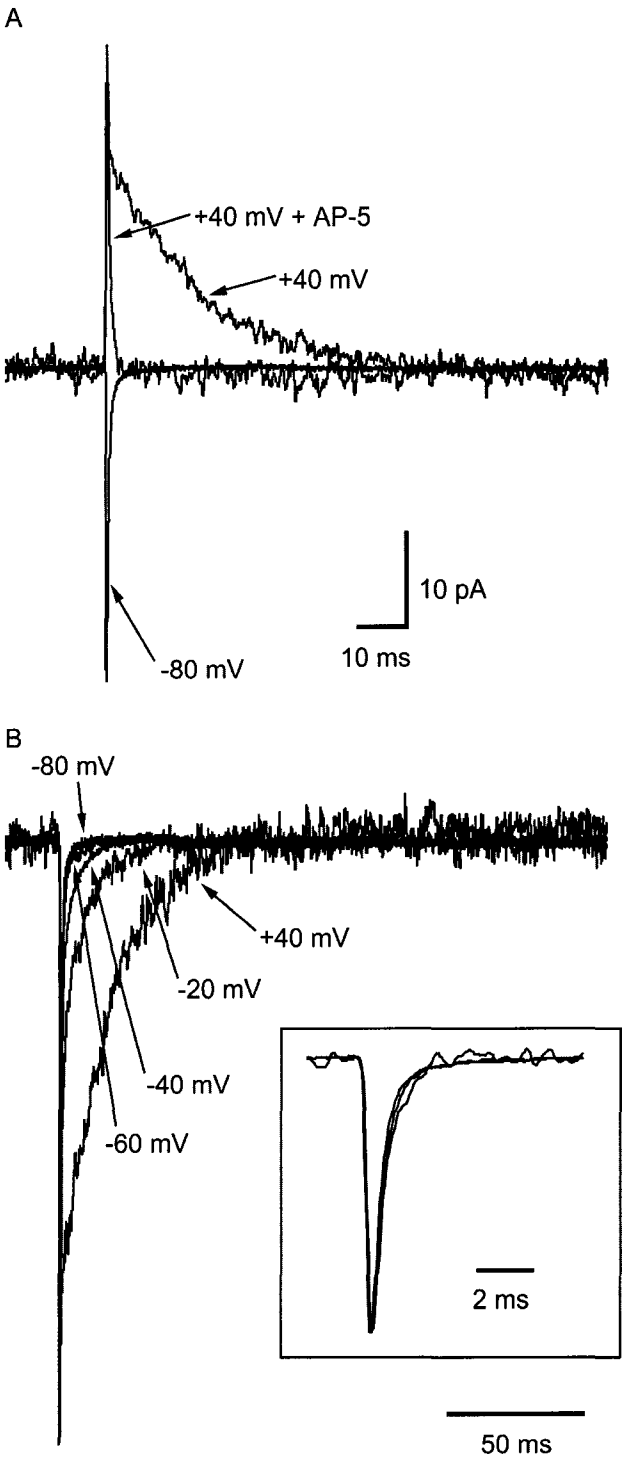

Figure 6.3. NMDA component of the mEPSCs at positive holding potentials. A: recording from a day 3 motoneuron at 2 different holding potentials (-80mV and +40 mV). Note the appearance of a slowly decaying component at +40 mV that is AP-5-sensitive. B: normalized traces at several different holding potentials (-80, -60, -40, -20, and +40 mV). The NMDA component is more apparent at positive holding potentials. Inset: normalized, overlaid AMPA/kainate mEPSCs in the presence of 50 μM AP-5 at -80, -40, and +40 mV. Note that the traces all have similar decay time courses. All traces are averages of ≥25 individual events.

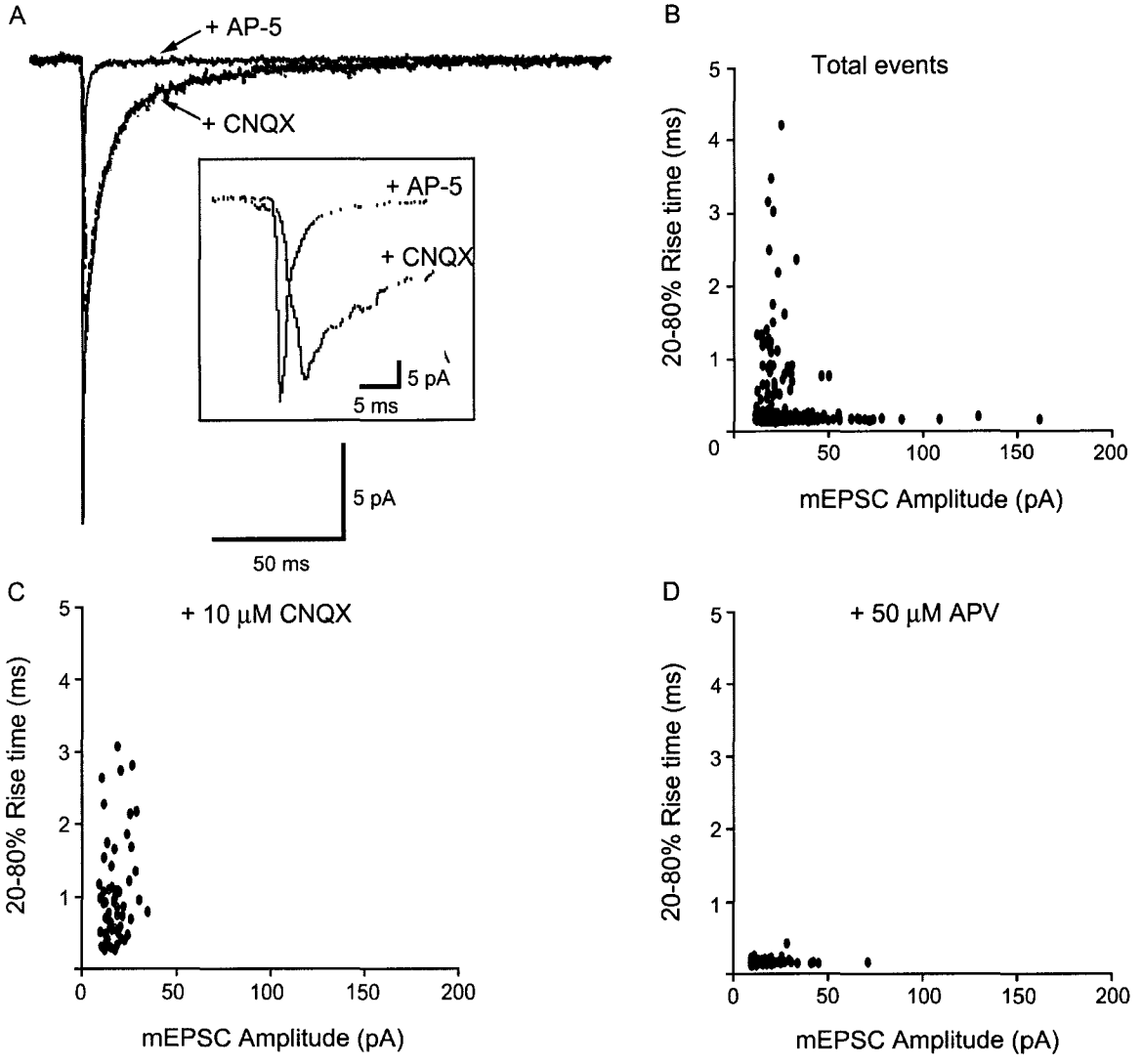

Figure 6.4. Isolation and detection of individual AMPA/kainate and NMDA events in Mg^{2+}-free recording solution. A: Averaged mEPSCs recorded in a day 3 motoneuron in the presence of either 10 μM CNQX or 50 μM AP-5. Inset: peak currents and rising phases on an expanded time scale. B: scatter plots of 20-80% rise time *vs* amplitude and in the presence of 10 μM CNQX (C) or 50 μM AP-5 (D). Note the different populations of slower events in C and faster events in D. The holding potential was -70 mV.

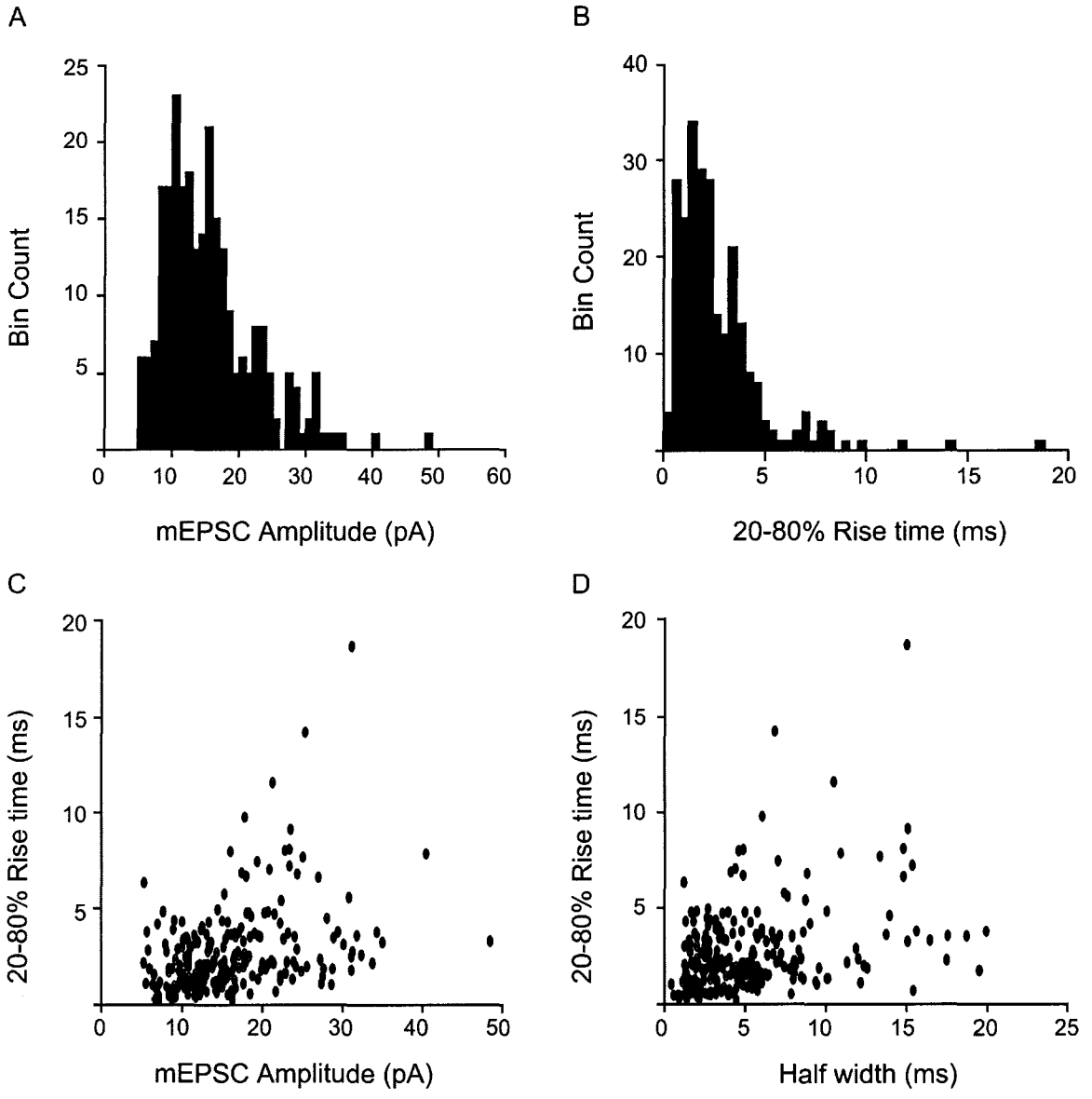

Figure 6.5. Parameters of isolated NMDA mEPSCs taken from 4 separate reticulospinal neurons. A: amplitude distribution (average: 15.8 ± 0.5 pA; *n* = 246; bin width = 1 pA). B: 20-80% rise time distribution of pooled NMDA mEPSCs. Average: 2.5 ± 0.3 ms (bin width = 0.5 ms). C: scatter plot of rise time *vs* amplitude for NMDA mEPSCs (*R* = 0.38). D: plot of rise time *vs* half-width of NMDA mEPSCs (*R* = 0.36). The holding potential was -70 mV.

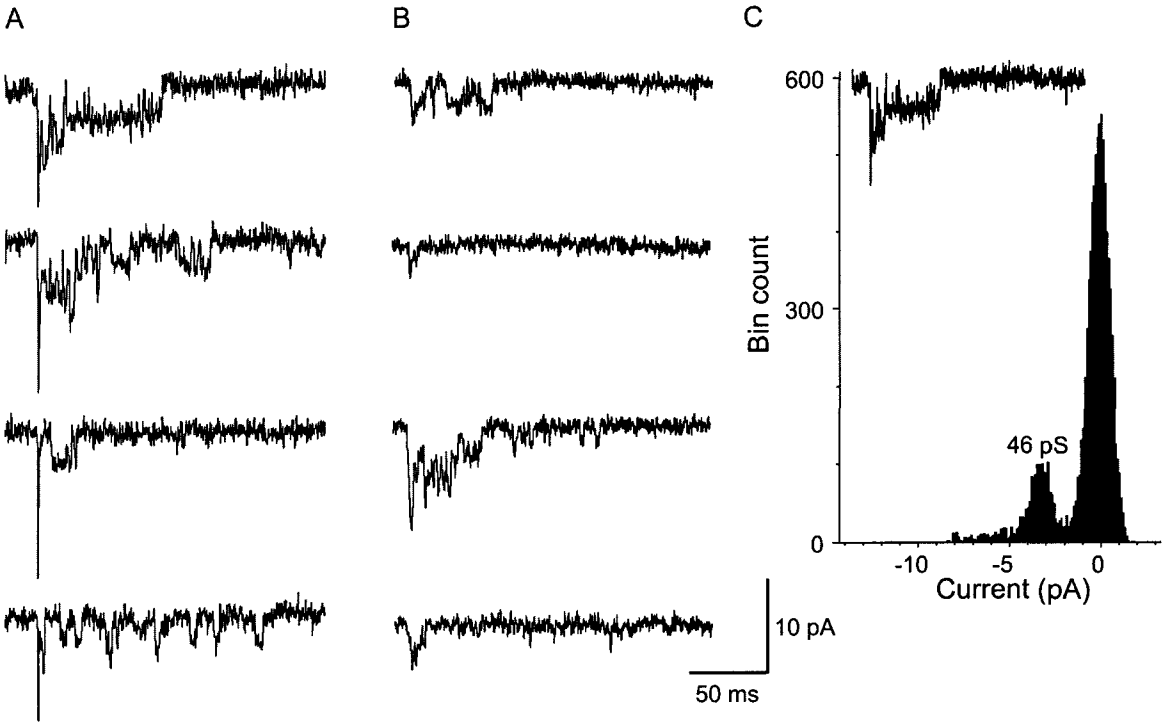

Figure 6.6. Late currents show NMDA single channel events in Mg^{2+}-free recording solution. A: examples of 4 glutamatergic mEPSCs detected in a reticulospinal neuron of a 1.5 day-old embryo held at -70 mV in which the signal to noise ratio is high. B: examples of predominantly NMDA events from the same cell. C: point by point histogram of the first mixed event from A (shown in the inset) revealing a principal peak at -3.2 pA which corresponds to a single-channel conductance of 46 pS.

Chapter Seven : Electrophysiological Characteristics of Motoneurons

LINKING STATEMENT

Although it was clearly established that a rhythmic glutamatergic drive patterns motoneuron output during fictive swimming, intrinsic firing properties of the motoneurons themselves could also play a role in patterning motor output to ER and EW locomotor muscle. This Chapter examines the intrinsic electrophysiological properties of motoneurons by studying the conductances that contribute to bursts of action potentials and the termination of these bursts.

ABSTRACT

The physiological and pharmacological properties of the motoneuron membrane and action potential were investigated in larval zebrafish using whole-cell patch current clamp recording techniques. During larval development (hatching to free-swimming, days 2-4), the resting membrane conductance increased in a population of motoneurons, which tended to reduce the apparent outward rectification of the membrane. Depolarizing current injection evoked a brief (approximately 10-30 ms) burst of action potentials. Action potentials were eliminated in tetrodotoxin (TTX), repolarized by tetraethylammonium (TEA)- and 3,4-diaminopyridine (3,4-AP)-sensitive potassium conductances, and had a cobalt-sensitive, high-threshold calcium component that activated a potassium conductance. In the presence of TTX, TEA, and 3,4-AP, a transient calcium spike of similar duration as the bursts of action potentials was evoked. With large depolarization, repetitive firing of calcium spikes could be observed at a frequency comparable to that of bursts of action potentials normally seen during fictive swimming. The conductances contributing to action potential burst termination are hypothesized to play a role in patterning the motoneuron output in these rapidly swimming fish.

INTRODUCTION

Larval zebrafish swim with rapid undulating body movements (Budick and O'Malley 2000a; Buss and Drapeau 2001a; Fuiman and Webb 1988; Saint-Amant and Drapeau 1998) powered by the contraction of embryonic red and white

myotomal muscle (Buss and Drapeau 2000a). Myotomal muscle is driven by a motoneuron-evoked synaptic drive that alternates between ipsilateral and contralateral myotomes and propagates in a rostral to caudal direction (Buss and Drapeau 2002). The coordinated motor output generated during swimming is maintained in paralyzed preparations (Buss and Drapeau 2001a; Buss and Drapeau 2002), thus allowing an electrophysiological analysis of motoneuron activation. During fictive swimming, motoneurons receive a glutamatergic and glycinergic synaptic drive (Buss and Drapeau 2001a). The glutamatergic drive is highly rhythmic, driving motoneurons to spike threshold and patterning the motor output to myotomal muscle. There has been considerable investigation of the activity of motoneurons during zebrafish motor behaviours (Fetcho and O'Malley 1995; Saint-Amant and Drapeau 2000; Saint-Amant and Drapeau 2001), including synaptic inputs to (Ali et al. 2000a) and from motoneurons (Buss and Drapeau 2000a; Drapeau and Legendre 2001; Drapeau et al. 2001; Legendre et al. 2000; Nguyen et al. 1999) and their growth and development (Eisen 1999; Eisen and Melancon 2001; Lewis and Eisen 2001; Westerfield and Eisen 1988). However, there is a paucity of information on the intrinsic electrophysiological properties of zebrafish motoneurons in general and larval motoneurons in particular.

In this study, the electrophysiological and pharmacological properties of the motoneuron action potential and membrane were investigated in larval zebrafish using whole-cell patch current clamp recording techniques. Fast sodium-dependent action potentials, a high threshold calcium conductance and repolarizing potassium conductances were observed and their features were

related to the motoneuron firing pattern during swimming.

METHODS

Experiments were performed on zebrafish (Tubingen and Longfin lines) larvae raised at 28.5 °C and obtained from a breeding colony maintained according to Westerfield (1995). All procedures were carried out in compliance with the guidelines stipulated by the Canadian Council for Animal Care and McGill University. The experimental methodology has been described (Buss and Drapeau 2001a; Drapeau et al. 1999). Results are taken from 84 morphologically identified (dye-filled) motoneurons (located dorsal or lateral to the central canal) of zebrafish aged 1.9-2.5 (day 2), 3.0-3.5 (day 3), and 4.1-4.4 (day 4) days postfertilization, that encompass the period from hatching to free-swimming.

Experiments were performed at room temperature (approximately 22 °C). The Evan's fish saline recording solution (Buss and Drapeau 2001a; Drapeau et al. 1999) contained (in mM) 134 NaCl, 2.9 KCl, 2.1 $CaCl_2$, 1.2 $MgCl_2$, 10 HEPES, 0-10 glucose, osmolarity adjusted (with glucose) to 290 mOsm and pH 7.8. Larvae were paralyzed by immersion in α-bungarotoxin (10 μM; n=16) for 10-20 minutes, or D-tubocurarine (15 μM; n=68) for the duration of the experiment. Similar observations were made using α-bungarotoxin or D-tubocurarine. Patch clamp electrodes (4-7 MΩ) were pulled from thin-walled Kimax-51 borosilicate glass and were filled with either a potassium gluconate (*n*=70) or cesium gluconate solution (*n*=14). The potassium gluconate solution was composed of (in mM) 116 D-gluconic acid potassium salt, 16 KCl, 2 $MgCl_2$, 10 HEPES, 10

EGTA, 4 Na_2ATP, 0.2% sulforhodamine B, osmolarity 280-290 mOsm, pH adjusted to 7.2. In the cesium gluconate solution, potassium gluconate and KCl were replaced with cesium gluconate and CsCl. Tetrodotoxin (TTX; 1 μM), tetraethylammonium chloride (TEA; 5 mM), 3,4-diaminopyridine (3,4-AP; 1 mM), or cobalt chloride (1 mM) were dissolved in fish saline (constant osmolarity was maintained by replacing glucose with equivalent amounts of TEA, 3,4-AP, or cobalt) and applied by bath perfusion. The actions of TTX, TEA, 3,4-AP, cobalt, and cesium intracellular solution on the action potential and membrane properties were investigated in day 2 (newly hatched) larvae. A liquid junction potential of –10 mV was experimentally determined according to Barry and Lynch (1991) and Neher (1992) and records were corrected for this potential.

Recordings were performed with an Axoclamp-2A patch clamp amplifier (0.01 headstage; 10 kHz low-pass filter) and digitized at 20-40 kHz. All chemicals were purchased from Sigma Chemical Co. (St. Louis, MO). Analyses were performed using pClamp 8 or Axograph 4.4 software (Axon Instruments). Motoneurons were held at –75 mV by current injection and all measurements were made from this potential. Short (2 ms) or long (300 ms) depolarizing current pulses were used to evoke single spikes or bursts of action potentials, respectively. The steady state membrane potential at the end of long current pulses was used to construct VI curves. Input resistances (R_I) were calculated from the slopes of the VI relation for voltages between -105 to -75 mV, -75 to –45 mV, and >–45 mV. The ratio of $R_{I\ (>-45\ mV)}$ to $R_{I\ (-75\ to\ -45\ mV)}$ was used as an index of outward rectification (rectification ratio) of the membrane; a ratio of 1 indicates

a linear relationship. Membrane time constants (τ_{fast} and τ_{slow}) were determined by fitting the voltage response to long current pulses (resulting in hyperpolarizations of 15-25 mV) with a sum of exponential curves. Capacitance was calculated by dividing τ_{fast} by $R_{I\ (-105\ to\ -75\ mV)}$. Rheobase was the smallest current that could initiate an action potential during long (300 ms) current pulses. Spike after-hyperpolarization measurements were performed on the single action potential evoked at rheobase; the steady state potential following the spike was used as baseline. Instantaneous firing frequency was determined by taking the inverse of the time between the 1st and 2nd, 2nd and 3rd, and 3rd and 4th action potentials in a burst. Because of the wide range of motoneuron input resistances, injected current was normalized to rheobase current and firing frequencies are presented for current pulses 1.5 and 2.0 times rheobase current. Spike threshold, amplitude, rise time, and half-width measurements were made on single action potentials evoked during threshold short current pulses. Action potentials initiated on the decay of the short pulse; spike threshold was measured as the most negative potential reached during the decay prior to spike initiation. Rise time was defined as the time between the action potential upstroke and peak, and half-width as the time from peak amplitude to when the action potential had decayed to 50% of its amplitude. Results are presented as mean ± SE throughout the text. The term significant denotes a relationship with $P<0.01$ determined using the Student's *t*-test, paired *t*-test, Mann-Whitney rank sum test, Wilcoxon signed rank test, or Spearman rank order correlation test.

RESULTS

Active and Passive Properties

The resting membrane potential of motoneurons ranged from -63 to -79 mV (mean = -74 ± 0.4 mV) and did not change during the developmental period examined (Table 7.1). Nearly all (93%) motoneurons responded to sustained depolarization by firing a short (approximately 10-30 ms) burst of action potentials followed by a period of silence, erratically occurring action potentials, or delayed clusters of action potentials (Figures 7.1, 7.4, 7.5, 7.6 and 7.8). However, five motoneurons (7%) responded by firing throughout the current injection. Four of these were day 2 motoneurons having a high input resistance (mean = 640 ± 78 MΩ; -75 to –45 mV range), and small to medium sized amplitude action potentials (mean = 53 ± 9.3 mV), and one was a day 4 motoneuron with an average spike amplitude (79 mV) and a low input resistance (84 MΩ). During the burst, instantaneous firing frequencies of up to 800 Hz were observed. Instantaneous firing frequencies accommodated rapidly during the first four spikes and significantly higher (P=<0.001) frequencies were observed when stimulation strength was increased from 1.5 to 2.0 times rheobase (Table 7.2). Instantaneous firing frequencies were significantly higher (P=<0.001) in day 3-4 *vs* day 2 motoneurons (Table 7.2). During the sustained depolarization, when the membrane is more positive than E_K, a hyperpolarization following the action potential was observed in 90% of motoneurons. Measured at rheobase, the after-hyperpolarization could reach up to 13 mV and last up to 40 ms (Table 7.1).

Membrane potentials used for constructing VI relationships were measured at the end of 300 ms current steps, when the initial burst of action

potentials had terminated and a steady state potential had been reached. Three distinct components were observed in the VI relationship (Figure 7.1C), which included an inward rectification at potentials negative to V_m and an outward rectification at potentials near spike threshold (mean spike threshold = –37 ± 0.6 mV). Input resistances were calculated from the slopes of the VI relation over these three voltage ranges, *i.e.*, negative to V_m (-75 to -105 mV), positive to V_m (-75 to –45 mV), and near spike threshold (>-45 mV). From day 2 to day 3-4, there was a significant decrease in the input resistance of the membrane measured during subthreshold steps negative and positive to the resting potential, while there was no significant change in the input resistance at potentials near spike threshold (Table 7.1). Consistent with the decrease in input resistance negative to spike threshold, rheobase current increased significantly from day 2 to day 3-4 (Table 7.1). Interestingly, while there was no significant change in the input resistance of the outwardly rectifying portion of the VI relationship (*i. e.*, V_m >-45 mV), there was a change in the apparent outward rectification (*i. e.*, the VI curve became more linear), as quantified by the rectification ratio ($R_{I\ (>-45\ mV)}/R_{I\ (-75\ to\ -45\ mV)}$), which increased 73% from day 2 to day 3-4 (Table 7.1). Together, these findings indicate that the decrease in outward rectification was due to a conductance increase at membrane potentials negative to spike threshold (*i. e.*, < -45 mV).

In addition to the parallel developmental changes in input resistance and rheobase, there was also a strong negative relationship (rs=-0.96; *P*=<0.001) between input resistance and rheobase (Figure 7.2A). Figure 7.2A also shows

that although mean input resistance ($R_{I\ (-105\ to\ -75\ mV)}$ and $R_{I\ (-75\ to\ -45\ mV)}$) and rheobase values changed significantly from day 2 to day 3-4 (Table 7.1), their values overlap in many motoneurons at all ages. However, a population of motoneurons (n=11) with input resistances less than 125 MΩ, and rheobase values greater than 250 pA (values never observed in day 2 motoneurons), appeared at day 3-4. Motoneurons within this population had larger rectification ratios (means of 0.59 ± 0.06 *vs* 0.27 ± 0.01; P<0.001) and contained the neurons with the most linear VI relationships (Figure 7.1) observed in this study (three motoneurons with rectification ratios ranging from 0.79 to 0.86).

The developmental changes in input resistance and rheobase could be due to an increase in conductance per unit area of membrane (*e.g.*, ion channel insertion) or because of a developmental increase in motoneuron size. However, the values of capacitance (a measure of membrane area and motoneuron size) overlapped considerably at all ages (Figure 7.2B), and mean values did not change significantly from day 2 to day 3-4 (Table 7.1), ruling out motoneuron size as the only changing variable. A decrease in the fast component of the membrane time constant (τ_{fast}), that accounted for approximately 85% of the membrane charging, accompanied the decrease in input resistance (Table 7.1). Conductance and capacitance were strongly correlated (Figure 7.2B; rs=0.75; P<0.001) indicating that the largest neurons had the highest conductance. A closer examination of individual age classes revealed an additional trend in this relationship. The relationship of day 3 and day 4 motoneurons was shifted to the left and was steeper, indicating that there is an increase in specific membrane

conductance during development. Thus, the decrease in outward rectification observed in this study is due to an additional "leak" conductance that is active at the resting membrane potential (although small changes in motoneuron capacitance, obscured by the large overlap in motoneuron capacitances and sizes, cannot be ruled out).

Interestingly, the duration of the action potential burst was approximately the length of a swim cycle (Buss and Drapeau 2001a; Buss and Drapeau 2002). The conductances active during the outwardly rectifying portion of the VI curve were thus likely to be responsible for the termination of the action potential burst and so these conductances were investigated pharmacologically. Because there was no change observed in the action potential bursting from day 2 to 4, a pharmacological investigation of motoneuron membrane and bursting properties was only performed in day 2 larvae, an age where stable, high resolution motoneuron recordings were made with the greatest success.

Pharmacology

Action potentials were initiated during the decay of voltage transients generated following short 2 ms current injections (Figure 7.3) indicating a remote spike initiation site. Mean spike threshold was –37 ± 0.6 mV and ranged from -49 mV to -24 mV and was correlated with input resistance (rs=-0.407; P=<0.001; -75 to –45 mV range) and spike rise time (rs=-0.51; P=<0.001). Spikes were generally close to 0 mV at their peak (mean amplitude = 75 ± 1.4 mV; range 30 mV to 95 mV). These findings are also consistent with an axonal spike initiation site. Spikes elicited by short 2 ms current injections were not followed by a noticeable hyperpolarization (Figure 7.3). However, E_K (approximately -97 mV) is

close to the resting potential and closer examination revealed that the decay time-course of voltage transients following action potentials were faster, in 68% of motoneurons, than the decay of sub-threshold voltage transients. Indeed, as stated above, spikes evoked by rheobasic current pulses displayed a marked after-hyperpolarization.

Action potentials were generated by a voltage-activated sodium conductance as they were abolished by TTX (Figure 7.3A; n=6) and not cobalt (Figure 7.3B; n=5), although cobalt increased spike threshold by 11 $\pm$ 2 mV (p=0.004). Addition of the potassium channel blockers TEA (Figure 7.3C; n=6) or 3,4-AP (Figure 7.3D; n=5) prolonged the duration of the action potential (Table 7.3), revealing that it is terminated by potassium conductances. Rise times increased in TEA and 3,4-AP whereas there was no large change in spike threshold (Table 7.3).

When sodium-dependent action potentials were blocked by TTX, and potassium conductances antagonized with TEA and 3,4-AP, a high-threshold transient potential was observed at membrane potentials between –10 and –25 mV (Figure 7.4). This depolarizing potential was blocked by cobalt and is thus defined as a calcium-dependent action potential. The calcium spike activated slowly and 2 ms current pulses were ineffective whereas 10 ms pulses were.

In addition to a calcium spike, TTX also unmasked a slowly activating outward conductance, which was presumably responsible for late outward rectification (Figure 7.5). In the presence of TEA and 3,4-AP, the outward rectification was reduced and addition of cobalt reduced it further (Figure 7.6).

Sustained trains of high-threshold (>0mV), cobalt-sensitive, calcium-dependent action potentials (at 60-80 Hz) were also observed (3/4 motoneurons) following the initial calcium spike (Figure 7.6B). When applied alone, cobalt reduced the outward rectification, decreased the firing frequency of the action potential burst (33 ± 12% decrease; determined from the first inter-spike interval normalized to 1.5 or 2.0 times rheobase), and blocked the erratically occurring or delayed clusters of action potentials that can follow the bursts (Figure 7.7). Cobalt also reduced the level of membrane noise. Although TEA, 3,4-AP, and cobalt had the greatest effect on the outwardly rectifying portion of the VI relationship, they also had minor effects at more negative potentials. Rheobase current decreased 26 ± 3% in TEA and 3,4-AP, while it increased 35 ± 14% in cobalt.

It was anticipated that TEA and 3,4-AP would facilitate repetitive action potential firing if the outward rectification they reduce contributed to burst termination. Application of TEA or 3,4-AP led to repetitive firing, at 20 to 70 Hz, following the initial prolonged action potential (Figure 7.8). However, these potassium channel blockers do not block all potassium channels (*e.g.*, the calcium dependent potassium conductance discussed below) and, to further reduce potassium conductances, intracellular potassium ion was replaced with the less permeant ion cesium. With a cesium ion based intracellular solution, short 2 ms current pulses initiated a prolonged after discharge (lasting 170-1000 ms), sustained by a plateau potential (5/14 motoneurons), that was not observed in cobalt solutions (Figure 7.9). Even in motoneurons that did not fire an after discharge, the action potential was broadened similarly to action potentials

observed in TEA or 3,4-AP (Figure 7.9B). Motoneurons examined using cesium-ion based intracellular solutions had significantly larger mean half-widths (27 ± 3 ms), rise times (0.61 ± 0.05 ms), and a lower spike threshold (-43 ± 0.8 *vs* –37 ± 0.6 mV) than those recorded with potassium gluconate-based intracellular solutions. In cobalt, the prolonged action potential was attenuated to 57 ± 0.1% of its duration (n=5; P=0.001) and short pulse current threshold increased by 24 ± 2% (P=0.003). The prolonged action potential was completely blocked in TTX (not shown).

DISCUSSION

The action potential recorded from motoneurons of larval zebrafish is initiated distal to the soma, is generated primarily by a TTX sensitive sodium ion conductance, but also features a voltage-dependent calcium ion component, and is terminated by a potassium ion conductance sensitive to TEA and 3,4-AP. Steady state VI curves revealed an inwardly rectifying conductance at voltages negative to resting potential and an outwardly rectifying conductance at voltages near spike threshold. From hatching to the free-swimming stage, average membrane input resistance at potentials negative to spike threshold decreased, and VI relationships became more linear even though the input resistance of the suprathreshold outwardly rectifying segment of the VI curves did not change significantly. The decrease in input resistance was not accounted for simply by increases in motoneuron size, as reflected by less variable membrane capacitance estimates, but rather by an increase in specific membrane

conductance. The population of motoneurons examined had a wide range of input resistances, capacitance values (sizes), and rheobase current thresholds, supporting the presence of graded motoneuron recruitment during swimming at these larval stages (Buss and Drapeau 2002).

Greater than 90% of motoneurons responded to long depolarizing current pulses by firing a brief (approximately 10 to 30 ms) burst of action potentials at all ages. A strong outward rectification, antagonized by voltage-activated potassium channel antagonists (TEA and 3,4-AP), intracellular cesium, and cobalt, contributes strongly to burst termination. The role of potassium conductances in burst termination is most clearly demonstrated in Figure 7.9 where a sustained plateau potential appears when intracellular potassium ions are replaced with impermeant cesium ions. Although not tested directly, cobalt is likely preventing the activation of a calcium-dependent potassium ion (and/or chloride ion) conductance by blocking a voltage activated calcium influx. A high-threshold, cobalt-sensitive, calcium conductance was also observed when sodium and potassium conductances were decreased in TEA, 3,4-AP, and TTX (Figure 7.6) and this calcium spike could fire repetitively during a long current pulse. Furthermore, the sustained after discharges observed using cesium ion-based intracellular solutions were not observed, short pulse current thresholds were increased, and action potential half widths were reduced, in the presence of cobalt. Based on these observations, we hypothesize that the high-threshold calcium spike, activated by sodium dependent action potentials, may provide an electrogenic contribution to action potential bursting.

This is the first study to examine the electrophysiological properties of

motoneurons in a larval fish. With the exception of the lamprey, there have been few physiological investigations of fish locomotor motoneurons. Fish motoneurons generally have low resting membrane potentials: mean = -75 mV in goldfish, (Fetcho 1992a); mean = -75 mV in a Japanese teleost, (Bando 1975); <-80 mV in 25% of stingray motoneurons, (Williams et al. 1984); mean = -75 mV in lamprey (Buchanan 1993) and similar to that observed in larval zebrafish with a mean = -74 mV. Depolarizing after potentials have been observed in goldfish, a Japanese teleost, and stingray motoneurons while an after-hyperpolarization was observed in stingray motoneurons (Bando 1975; Fetcho 1992a; Williams et al. 1984) and lamprey (see below). In larval zebrafish, an after-hyperpolarization was not observed when action potentials where evoked by short pulses from the negative resting membrane potential but was observed when the membrane was held at more depolarized levels. The after-hyperpolarization of larval zebrafish motoneurons could be obscured by the fast membrane time constant, the proximity to E_K, or to calcium chelation by the intracellular solution. However, examination of the VI relationship after the calcium conductance was blocked with cobalt did reveal the presence of a calcium-activated conductance, which was likely mediated by potassium ions.

Interestingly, Buss and Drapeau (2001a) reported a mean spike threshold of –46 ± 0.8 mV; determined by measuring the amplitude at which rhythmic locomotor drive potentials initiated action potentials during fictive swimming. This value is approximately 9 mV closer to the resting potential than the spike threshold determined by using somatic current injections in this study (-37 ± 0.6

mV). The more negative spike threshold observed during fictive swimming could be because excitatory locomotor synapses are located electrically closer to the axonal spike initiation zone than the somatic patch electrode point current source. In addition, there could be a locomotor-related reduction in spike threshold, as reported in the cat (Krawitz et al. 2001).

Fin (Rovainen and Birnberger 1971) and myotomal (Teravainen and Rovainen 1971) motoneurons have been examined in detail in lamprey, where motoneurons to twitch fibers have lower input resistances than those to slow fibers (Teravainen and Rovainen 1971). The VI relation determined at potentials 20 mV positive and negative to the resting membrane potential are linear and input resistances, action potential thresholds, and instantaneous firing frequencies are considerably lower in the lamprey (Buchanan 1993). Similar to larval zebrafish, the action potential is prolonged in TEA or 4-AP, and blocked by TTX (Hess and El Manira 2001; Kemnitz 1997; Matsushima et al. 1993; Wallen et al. 1989). A calcium-activated potassium conductance, transient A-type current, and high-threshold calcium current has also been described in lamprey motoneurons (El Manira and Bussieres 1997; Grillner and Wallen 1985; Grillner et al. 2001; Hess and El Manira 2001; Hill et al. 1992; Matsushima et al. 1993; Wallen et al. 1989).

The duration of the action potential bursts observed during long depolarizing current pulses closely approximates the duration of the active period of a swim cycle (Buss and Drapeau 2001a; Buss and Drapeau 2002). The factors contributing to burst termination may include a high-threshold inactivating calcium spike and voltage- and calcium-dependent potassium conductances. Together

these conductances would help sculpt the period of action potential firing so that it is consistent with the period of rhythmic excitatory drive to the motoneurons. If the same conductances are present in interneurons of the central pattern generator for swimming, they could also underlie the generation of rhythmic locomotor network activity.

TABLES AND FIGURES

Table 7.1. Action potential and membrane properties of day 2 and 3-4 motoneurons

Parameter	Day 2 (*n*=47)	Day 3-4 (*n*=23)
V_m (mV)	-74 ± 0.5	-73 ± 0.6
Spike Threshold (mV)	-38 ± 0.6	-36 ± 1.1
Spike Amplitude (mV)	75 ± 1.9	75 ± 1.6
Spike Rise Time (ms)	0.34 ± 0.02	0.30 ± 0.03
Spike After Hyperpolarization (mV)	6 ± 0.4 (*n*=42)	5 ± 0.6 (*n*=22)
Spike After Hyperpolarization (ms)	11 ± 1.3 (*n*=42)	9.1 ± 1.9 (*n*=22)
Rheobase (pA)	120 ± 8 *	222 ± 25 *
Capacitance (pA)	15.6 ± 0.7	17.4 ± 1.3
τ_{fast} (ms)	3.4 ± 0.2 *	2.6 ± 0.3 *
τ_{slow} (ms)	36 ± 2.6	47 ± 5.8
τ_{slow} (%)	15 ± 1.4	13 ± 1.6
$R_{I\ (-105\ to\ -75\ mV)}$ (MΩ)	255 ± 28 *	180 ± 32 *
$R_{I\ (-75\ to\ -45\ mV)}$ (MΩ)	315 ± 31 *	215 ± 36 *
$R_{I\ (>-45\ mV)}$ (MΩ)	84 ± 11	77 ± 8
Rectification Ratio $R_{I\ (>-45\ mV)}/R_{I\ (-75\ to\ -45\ mV)}$	0.26 ± 0.02 *	0.45 ± 0.04 *

Values shown are means ± SE. * Significant difference of means (P<0.01) determined using the Student's *t*-test or Mann-Whitney rank sum test.

Table 7.2. Instantaneous action potential firing frequency in day 2 and 3-4 motoneurons

Rheobase (R)	Day 2 (Hz)			Day 3-4 (Hz)		
	1st	2nd	3rd	1st	2nd	3rd
1.5 X R	235 ± 10.4 (*n*=46)	182 ± 10.5 (*n*=40)	154 ± 10.3 (*n*=24)	331 ± 16.7 (*n*=46)	289 ± 15.5 (*n*=45)	252 ± 13.3 (*n*=38)
2.0 X R	335 ± 10.3 (*n*=20)	269 ± 11.5 (*n*=20)	222 ± 11.0 (*n*=18)	409 ± 28.4 (*n*=20)	403 ± 21.6 (*n*=18)	354 ± 21.1 (*n*=18)

Table 7.3. Actions of TEA and 3,4-AP on the motoneuron action potential

Parameter	TEA (n=6)	3,4-AP (n=5)
Spike Half Width	14 ± 3 times longer *	13 ± 3.3 times longer *
Spike Rise Time	2.7 ± 0.2 times longer *	2.0 ± 0.1 times longer *
Spike Voltage Threshold	6 ± 2 mV decrease	2 ± 1 mV decrease

Values shown are means ± SE. * Significant difference of means (P<0.01) determined using the Student's t-test or Mann-Whitney rank sum test.

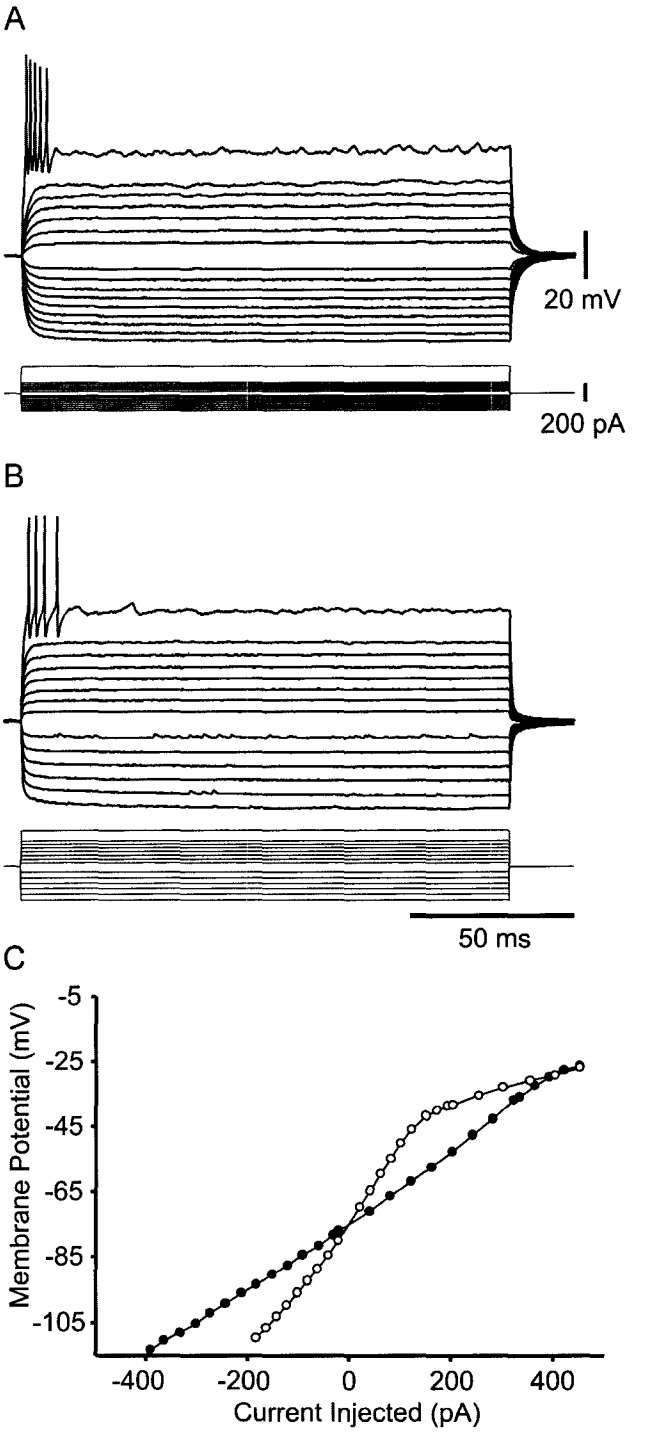

Figure 7.1. Motoneurons of day 2 (A) and day 4 (B) zebrafish respond to long depolarizing current pulses by firing a short burst of action potentials. VI curves (C) of the day 2 (○) and day 4 (•) motoneurons shown in A and B. Both motoneurons have a similar input resistance at membrane potentials >-30 mV whereas large differences are apparent at more negative membrane potentials. Traces shown are from a typical day 2 motoneuron and a day 4 motoneuron with a high rectification ratio.

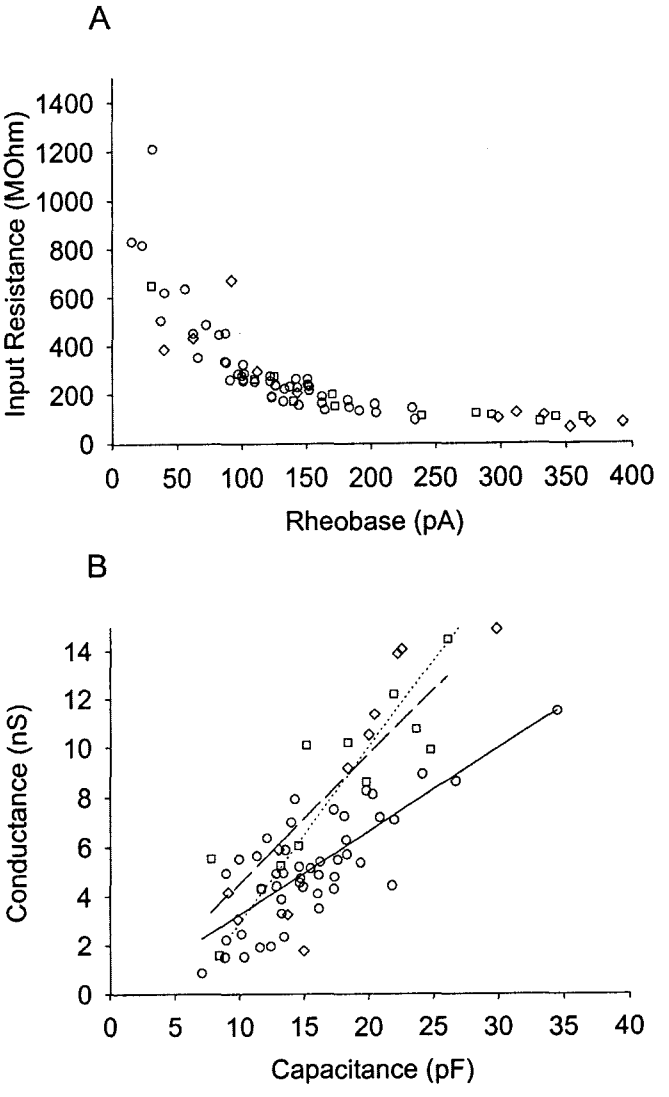

Figure 7.2. There is a negative relationship between input resistance (-75 to –45 mV) and rheobase current (A) and a positive relationship between conductance (-105 to –75 mV) and capacitance (B). ○ (day 2), □ (day 3), and ◇ (day 4). B: linear regressions are fit to day 2 (—; R=0.77), day 3 (----; R=0.88), and day 4 (· · ·; R=0.90) values.

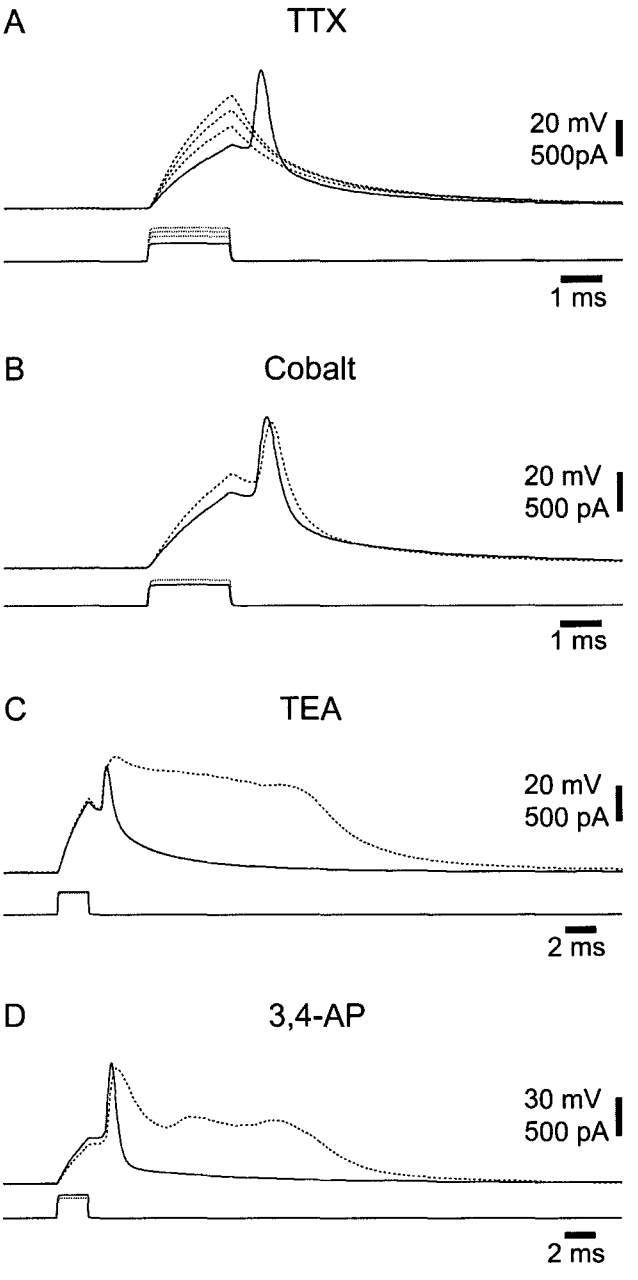

Figure 7.3. Pharmacological properties of the motoneuron action potential. Motoneuron response and stimulus waveform are shown as solid (control traces) and dashed (treated traces) lines. The action potential is eliminated by TTX (1 μm) (A) but not cobalt (1 mM) (B), although spike threshold increased in 1 mM cobalt. TEA (1 mM) (C) and 3,4-AP (1 mM) (D) broaden the action potential. Day 2 motoneurons.

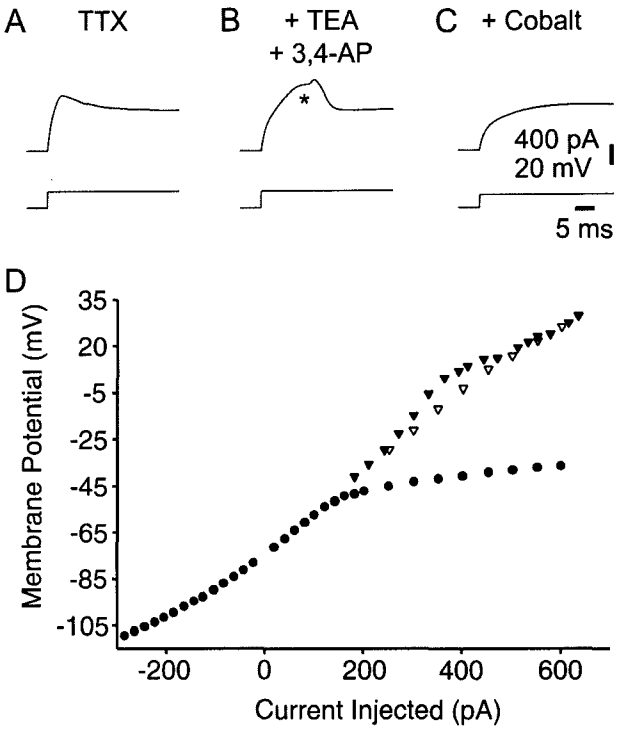

Figure 7.4. A high theshold calcium spike (*) is revealed when sodium and potassiun conductances are antagonized. The first 40 ms of 300 ms long depolarizing current pulses are shown in A-C. The traces in A and B-D are from two different motoneurons also shown in Figures 7.5 and 7.6 respectively. The calcium spike (*) is revealed when the potassium conductances are blocked by TEA and 3,4-AP (A-B), and is blocked by cobalt (C). The peak of the calcium spike was measured and plotted before (▼) and after (▽) it was antagonized with cobalt (D). The steady state outward rectification observed prior to pharmacological treatments (•) is shown in D.

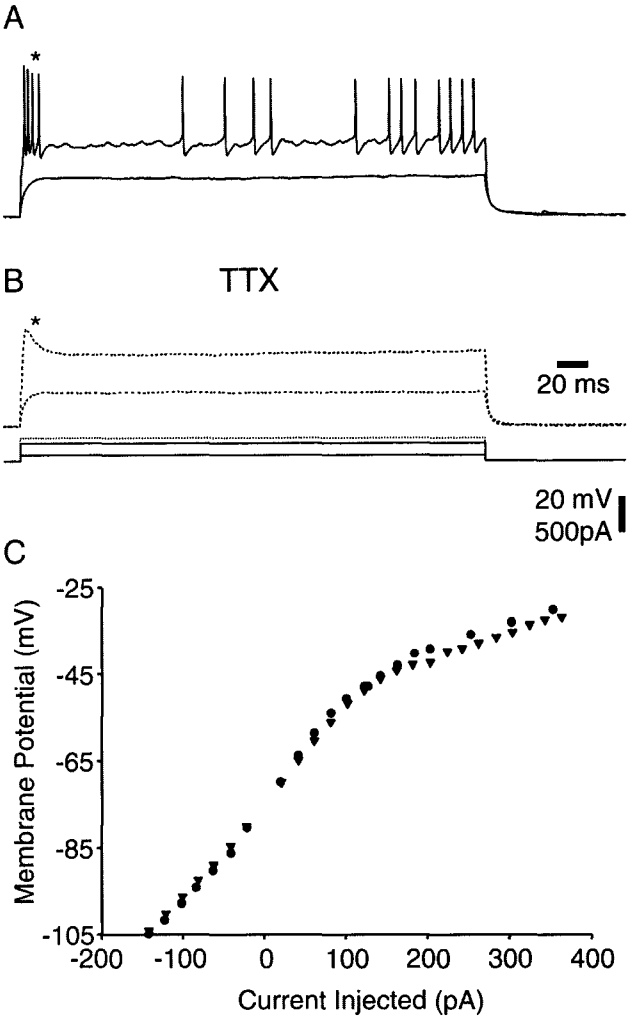

Figure 7.5. TTX blocks action potentials and reveals an outward rectification causing a transient depolarization. Control (A, —; C, •) and TTX (B, ----; C, ▼). At steady state values, TTX has little effect on the VI relationship (C). * indicate a burst of action potentials in A and an apparent transient depolarization of comparable duration in B. Day 2 motoneuron.

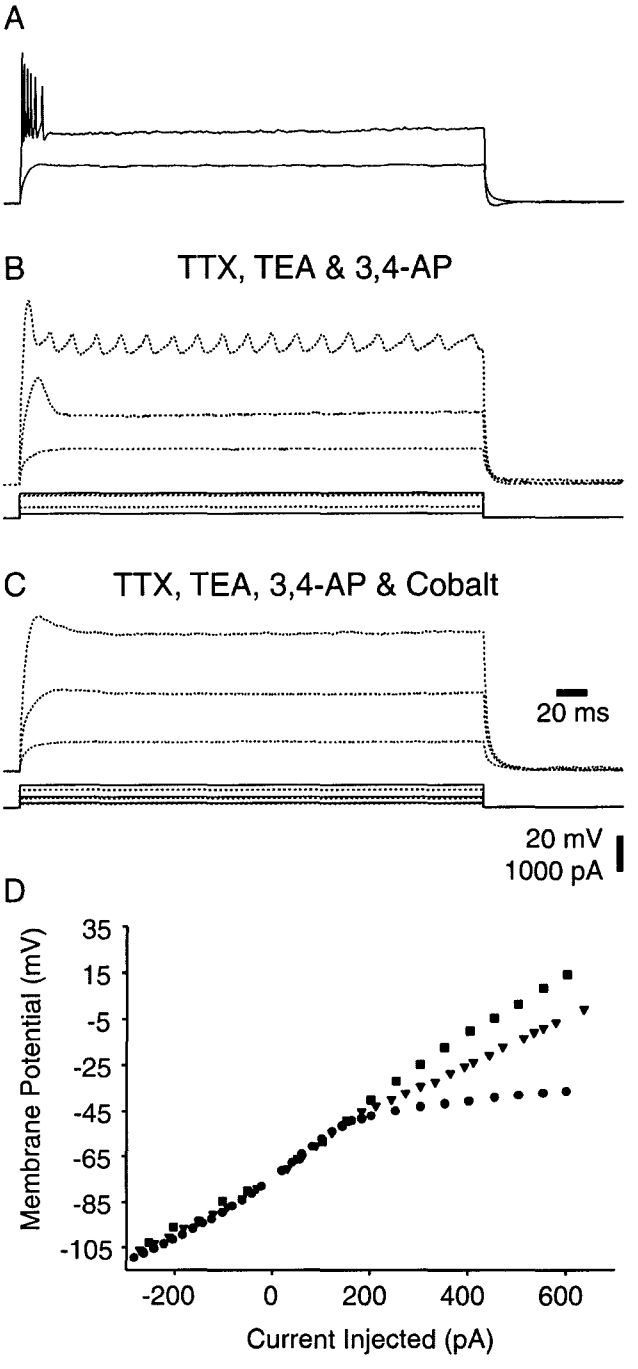

Figure 7.6. A high-threshold, TTX-resistant, cobalt-sensitive oscillation (B) due to a calcium conductance (C) is observed in motoneurons after sodium and potassium conductances are antagonized with TTX, TEA, and 3,4-AP. Control (A, —; D, •); TTX, TEA, and 3,4-AP (B, ----; D, ▼); TTX, TEA, 3,4-AP, and cobalt (C, ----; D, ■). TEA, 3,4-AP, and cobalt reduce the steady state outward rectifiation observed in the VI relationship (D). Day 2 motoneuron.

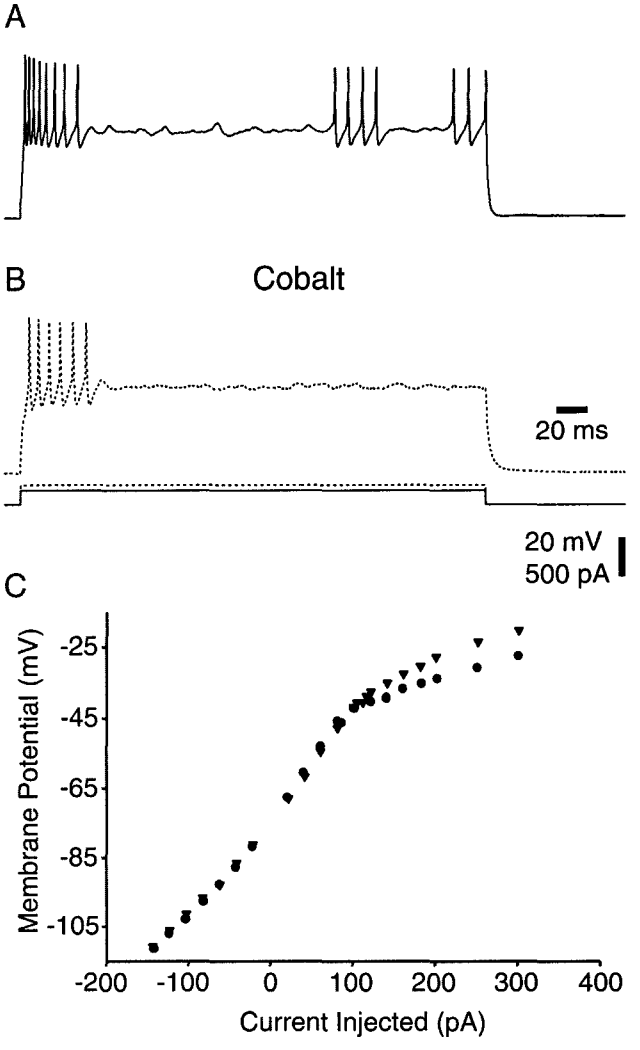

Figure 7.7. Cobalt slows the firing rate in the burst of action potentials and eliminates any delayed firing after the initial action potential burst. Control (A, —; C, •) and cobalt (B, ---; C, ▼). Cobalt reduces the steady state outward rectification observed in the VI relationship (C). Day 2 motoneuron.

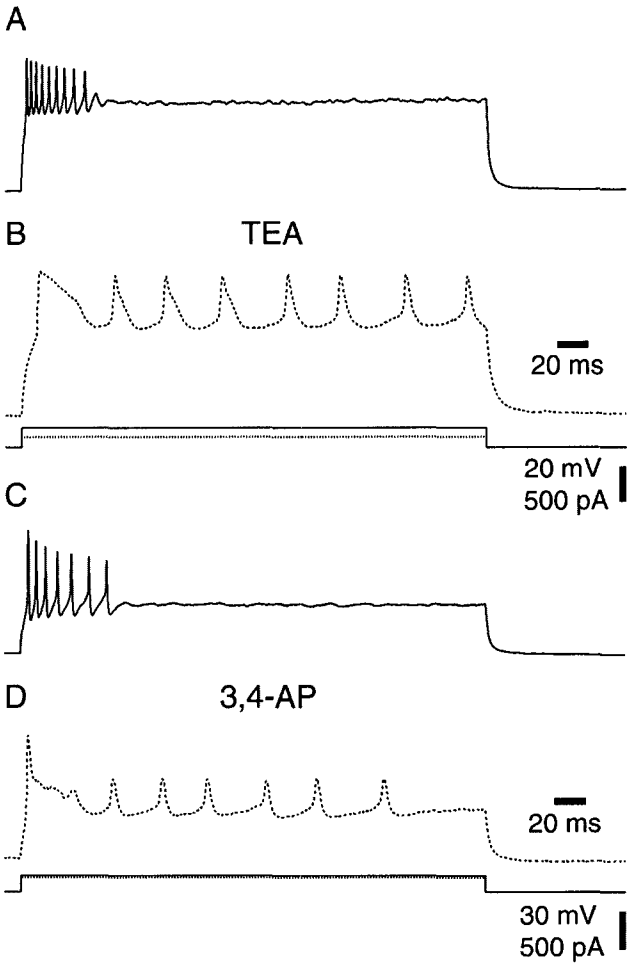

Figure 7.8. Motoneurons fire repetitively after TEA (B) or 3,4-AP (D) is used to block potassium conductances. Control traces — (A-D) and TEA (B) and 3,4-AP (D) traces ---. Day 2 motoneurons.

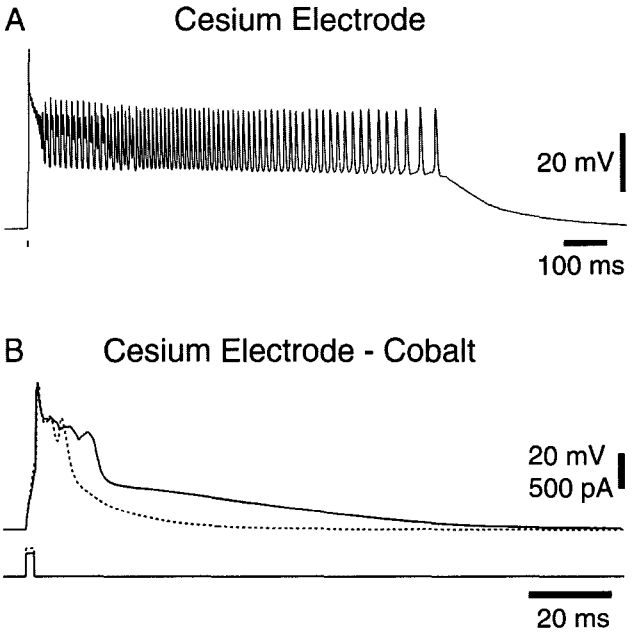

Figure 7.9. A prolonged after discharge, sustained by a plateau potential, is observed in 5/14 day 2 motoneurons when a cesium based intracellular pipette solution is used (A). Prolonged action potentials (—) are observed in motoneurons that do not display after discharges (B). Cobalt shortens the duration of the prolonged action potentials observed with intracellular cesium solutions (B, ----).

Appendix: Calculation of the liquid-liquid junction potential

Liquid-liquid junction potentials (Barry and Lynch 1991; Neher 1992) were determined experimentally by recording the steady state voltage difference between a patch pipette (containing an electrode solution) and a bath solution of extracellular fish saline or the patch pipette electrode solution. A 3 M KCl agar bridge separated the bath solution from a Ag-AgCl electrode immersed in 3 M KCl. Experimentally determined junction potentials were 1 to 3 mV more positive than junction potentials calculated using the generalized Henderson Liquid Junction Potential Equation included in Axon Instruments pClamp 8 software. This difference is likely due to a small junction potential of the salt bridge reference electrode as well as to errors in the estimation of ion activity (derived from ion concentration) in the generalized Henderson Liquid Junction Potential Equation. The error in estimating ion activity is likely to be significant in these electrolyte solutions where [Cl^-] varies from 10-145 mM. All membrane potential values have been corrected for liquid-liquid junctions potential using experimentally determined values.

Liquid-liquid junction potentials

Intracellular [Cl^-]	Experimental	Henderson Equation
10	+12	+15
20	+10	+14
40	+8	+12
80	+6	+9
140	+3	+4

General Discussion

The development of the zebrafish motor unit and its activation during swimming were examined. Larval swimming is powered by two types of axial locomotor muscle that have the properties of tonic (embryonic red) and twitch (embryonic white) vertebrate muscles. These muscles are recruited in the adult pattern very early in larval development. The locomotor muscle is synaptically driven by rhythmically active myotomal motoneurons. Motoneurons receive a highly rhythmic glutamatergic synaptic drive (with AMPA/kainate and NMDA components), which drives motoneurons to spike threshold, as well as a less structured glycinergic synaptic drive. Motoneurons have intrinsic conductances that facilitate the generation of short, high frequency, bursts of action potentials that are sustained, and then actively terminated, for a period as long as the active period of a swimming cycle. The physiological properties of the muscle contractile apparatus, synaptic drive and the excitability of the motoneuron membrane are optimized for producing the rapid undulatory swimming that is required for propelling the small inert larvae through their viscous aquatic environment.

Locomotion has been studied at a detailed cellular level in a variety of vertebrates (mammals, reptiles, birds, amphibians, elasmobranch fishes and lampreys) but never, until now, at early developmental stages in a fish (Grillner et al. 1986; Herman et al. 1976; Stein et al. 1997). The generation of locomotor rhythms is fundamentally similar in all vertebrates, including zebrafish. In all vertebrates examined, a glutamatergic synaptic drive rhythmically excites motoneurons to spike threshold and intrinsic motoneuron properties contribute to

the generation of rhythmic output. The development of the spinal cord, anatomic division of spinal motor and sensory systems, neurotransmitter phenotypes and spinal neuron projection patterns are recognizably similar in all vertebrates. Of course there are differences, as would be expected after nearly half a billion years of evolution. These include the locomotor glycinergic drive, which although necessary for coordinated locomotion in all vertebrates, occurs both on and off cycle in cat and zebrafish motoneurons but is highly phasic in amphibian tadpoles and lamprey, occurring as a rhythmic mid-cycle inhibition. Also very different are the mechanics of locomotion, which range from undulatory swimming to tetrapod locomotion. What is learned from studies on zebrafish locomotion and motor control will further our understanding of mammalian motor systems.

An understanding of the development and function of the zebrafish motor system, which was investigated in this Thesis, is still at a preliminary stage. In particular, the kinetic and pharmacological properties of the conductances responsible for membrane excitability and polarization in both motoneurons and locomotor muscle need to be examined. For example, which potassium channels contribute to burst termination in motoneurons and which chloride channels contribute to the different chloride ion permeability of ER and EW muscle fibers? These questions would be best approached using voltage-clamp techniques combined with pharmacological and ion substitution manipulations. The physiology of ER and EW muscle also requires further study including why contraction thresholds differ and what are the mechanisms of excitation-contraction coupling in the two fiber types. Furthermore, the distribution of motoneuron endplates and whether ion channels (*e. g.* sodium and chloride ion

channels) are uniformly distributed on the membranes of ER and EW fibers should be examined. An obvious next step in understanding how motoneurons are synaptically activated during swimming is to identify and then study the synaptic physiology and intrinsic membrane properties of the premotor interneurons that provide the glutamatergic and glycinergic synaptic drive to motoneurons. It would be very interesting to determine the neural mechanisms underlying the unique recruitment of ER and EW muscle during swimming. To do this motoneurons that innervate ER and EW muscle would need to be identified and then examined during different fictive swimming undulation rates. Whether the intrinsic membrane properties or synaptic activation of motoneurons to ER and EW muscle differ would be worth investigating. Furthermore, this Thesis only examined a limited, though behaviorally significant, developmental time window and it would be interesting to find out what further changes occur in late larval and adult life, as well as during the transition from the embryonic coiling to swimming behaviors.

The ultimate goal of this research should be to elucidate how the nervous system generates the coordinated motor output required for swimming. To solve this problem, it will be necessary to identify the interneurons and descending neurons that contribute to the swimming behavior as well as understand the connectivity and intrinsic membrane properties of these neurons. Future studies will need to unequivocally identify the interneurons and descending neurons active during locomotion and this will not be an easy task. It will not be sufficient to rely only on morphological identification and neurotransmitter phenotype as synaptic connectivity (*e. g.*, location in reflex pathways) will need to be

considered. At present, this will not be an easy task, but the use of molecular markers uniquely expressed by interneuron populations (Briscoe and Ericson 2001) may aid in this investigation (see below).

There is a greater understanding of the neural basis of motor control in other vertebrate model organisms, compared to zebrafish. A continued comparative physiology approach would be useful for gaining a greater understanding of the zebrafish motor unit and learning what fundamental principles of motor control have been conserved during vertebrate evolution. Few studies have addressed the functioning of the zebrafish axial sensory system, reflex pathways, state dependent reflex modulation, presynaptic inhibition, neuromodulation, synaptic plasticity, descending systems or segmental spinal cord organization. The organization of the pectoral fin motoneuronal pool, how rhythmic activity is generated for fin movements, and whether there are differences between axial and fin motoneurons would be worthwhile pursuing. Such a comparison would be particularly interesting because of the homologies between tetrapod limbs and pectoral fins. Clearly there is still much to be learned.

In addition to the more classical approaches, the stage is also set for approaching the study of motor control and locomotion using genetic and molecular techniques. Zebrafish are amenable to forward genetics approaches and many mutants have been identified in genetic screens that are necessary for embryonic development as well as motor control (Driever et al. 1996; Golling et al. 2002; Granato et al. 1996; Haffter et al. 1996). Thus, there is the potential for identifying the genes involved in the development of the locomotor system. However, genetic screens are designed to gain understanding of what individual

genes do and not how genes control the development of motor behaviors. Hundreds of genes may contribute to something as rudimentary as the growth of a motoneuron axon into locomotor muscle and individual genes may have different functions when expressed in different tissues. I think it is unlikely that individual genes could have evolved to control complicated aspects of locomotor behavior such as rostral-caudal phase lags during swimming. The forward genetic approach is indispensable for identifying genes but its immediate value (the long term value of knowing the function of every gene is not disputed) for gaining understanding of how motor behaviors develop remains to be determined. However, a detailed understanding of the function and development of the motor system (as undertaken in this Thesis) will allow for a precise characterization of zebrafish mutant phenotypes affecting the motor unit and locomotor behaviors.

Reverse genetic approaches are becoming increasingly feasible in zebrafish and within the next decade knock-in and knock-out technology may be routine. This would allow the restricted over-expression or under-expression of selected genes, in selected tissues, at selected times of development, thus allowing the effects of genes that cause gross abnormalities or death when mutated to be examined in select tissues. However, this is already possible in mice and any important genes that are discovered in zebrafish will undoubtedly have homologues in mice, where the experiments can performed, although with greater difficulty and expense. So why develop the zebrafish as a model?

There are other advantages for studying zebrafish and these are what attracted investigators prior to its status as a genetic model organism. Embryonic

and larval zebrafish are small, easy to rear, transparent, and have far fewer neurons than rats and cats. They are the vertebrate equivalent of invertebrate motor control model organisms, such as the locust or leech (Burrows 1996; Muller et al. 1981), which have a relatively small number of accessible and identifiable neurons. In addition, larval zebrafish have small, electrically compact, spinal neurons that allow voltage clamp recording techniques to be used during locomotor behaviors *in vivo*. These are important advantages for the cellular neurophysiologist and with decades of dedicated work we would elucidate neuronal connectivity and synaptic and membrane properties in zebrafish without the use of molecular or genetic techniques. However, using the genetic and molecular tools available in the zebrafish will speed the process and lead to a deeper, genetic, molecular and neurophysiological understanding of motor control. In the near future, we will be able to use the promoters of interneuron specific transcription factors to drive fluorescent markers in identified neurons in living animals. This will revolutionize the study of synaptic connectivity between identified neurons and facilitate the deciphering of neuronal connectivity. We will be able to stop the expression of selected ion channels in specific interneurons, or remove selected interneurons from the locomotor network, and understand their function. In addition to understanding locomotion in zebrafish, we should be able to apply much of this knowledge in biomedical research and ultimately increase our understanding of how we control, or lose control, of our own movements.

This thesis takes the first of many steps to fulfil these goals. It characterizes the development of the zebrafish motor unit and compares these

findings with what is already known in other vertebrates. My findings indicate that the motor system of zebrafish is organized similarly to other vertebrates. These similarities are what make this organism such a good model organism for learning about the development of vertebrate motor control and locomotion.

Literature Cited

ALEXANDER R. The orientation of muscle fibres in the myomeres of fishes. *J Mar Biol Ass U K* 49: 263-290, 1969.

ALFORD S and SIGVARDT KA. Excitatory neurotransmission activates voltage-dependent properties in neurons in spinal motor system of lamprey. *J Neurophysiol* 62: 334-341, 1989.

ALFORD S and WILLIAMS TL. Endogenous activation of glycine and NMDA receptors in lamprey spinal cord during fictive locomotion. *J Neurosci* 9: 2792-2800, 1989.

ALI DW, BUSS RR and DRAPEAU P. Properties of miniature glutamatergic EPSCs in neurons of the locomotor regions of the developing zebrafish. *J Neurophysiol* 83: 181-191, 2000a.

ALI DW, DRAPEAU P and LEGENDRE P. Development of spontaneous glycinergic currents in the Mauthner neuron of the zebrafish embryo. *J Neurophysiol* 84: 1726-1736, 2000b.

ALNAES E, JANSEN JKS and RUDJORD T. Spontaneous junctional activity of fast and slow parietal muscle fibres of the hagfish. *Acta Physiol Scand* 60: 240-255, 1964.

ALTRINGHAM JD and JOHNSTON IA. Quantitative histochemical studies of the peripheral innervation of cod (Gadus morhua) fast myotomal muscle fibres. *J Comp Physiol A* 143: 123-127, 1981.

ALTRINGHAM JD and JOHNSTON IA. The mechanical properties of polyneuronally innervated, myotomal muscle fibres isolated from a teleost fish (Myoxocephalus scorpius). *Pflugers Arch* 412: 524-529, 1988.

ALTRINGHAM JD and ELLERBY DJ. Fish swimming: patterns in muscle function. *J Exp Biol* 202: 3397-3403, 1999.

ALVAREZ-LEEFMANS FJ and RUSSELL JM. *Chloride channels and carriers in nerve, muscle, and glial cells*. New York, Plenum Press, 1990, 425 *pp*.

ANDERSEN P, JANSEN JKS and LOYNING Y. Slow and fast muscle fibres in the atlantic hagfish (Myxine glutinosa). *Acta Physiol Scand* 57: 167-179, 1963.

ARMSTRONG PB and HIGGINS DC. Behavioral encephalization in the bullhead embryo and its neuroanatomical correlates. *J Comp Neurol* 143: 371-384, 1971.

AUERBACH AA and BENNETT MV. A rectifying electrotonic synapse in the central nervous system of a vertebrate. *J Gen Physiol* 53: 211-237, 1969a.

AUERBACH AA and BENNETT MV. Chemically mediated transmission at a giant fiber synapse in the central nervous system of a vertebrate. *J Gen Physiol* 53: 183-210, 1969b.

BALEZINA OP and GULYAEV DV. Characteristics of innervation of rapid muscle fibers in the lamprey Lampetra planeri. *J Evol Biochem Physiol* 21: 25-31, 1985.

BANDO T. Synaptic organization in teleost spinal motoneurons. *Jpn J Physiol* 25: 317-331, 1975.

BARBOUR B, KELLER BU, LLANO I and MARTY A. Prolonged presence of glutamate during excitatory synaptic transmission to cerebellar Purkinje cells. *Neuron* 12: 1331-1343, 1994.

BARDONI R, MAGHERINI PC and MACDERMOTT AB. NMDA EPSCs at glutamatergic synapses in the spinal cord dorsal horn of the postnatal rat. *J Neurosci* 18: 6558-6567, 1998.

BARETS A. Contribution a l'étude des systèmes moteurs «lent» et «rapide» du muscle latéral des téléostéens. *Arch Anat Micr Morph Exp* 50: 91-331, 1961.

BARRESI MJ, STICKNEY HL and DEVOTO SH. The zebrafish slow-muscle-omitted gene product is required for Hedgehog signal transduction and the development of slow muscle identity. *Development* 127: 2189-2199, 2000.

BARRESI MJ, D'ANGELO JA, HERNANDEZ LP and DEVOTO SH. Distinct mechanisms regulate slow-muscle development. *Curr Biol* 11: 1432-1438, 2001.

BARRY MA and BENNETT MV. Projections of giant fibers, a class of reticular interneurons, in the brain of the silver hatchetfish. *Brain Behav Evol* 36: 391-400, 1990.

BARRY MJ and O'DONOVAN MJ. The effects of excitatory amino acids and their antagonists on the generation of motor activity in the isolated chick spinal cord. *Brain Res* 433: 271-276, 1987.

BARRY PH and LYNCH JW. Liquid junction potentials and small cell effects in patch-clamp analysis. *J Membr Biol* 121: 101-117, 1991.

BATTY RS. Development of swimming movements and musculature of larval herring (Clupea harengus). *J Exp Biol* 110: 217-229, 1984.

BATUEVA IV. Efficiency of electrical transmission in reticulomotoneuronal synapses of lamprey spinal cord. *Exp Brain Res* 69: 131-139, 1987.

BECKER T, WULLIMANN MF, BECKER CG, BERNHARDT RR and SCHACHNER M. Axonal regrowth after spinal cord transection in adult zebrafish. *J Comp Neurol* 377: 577-595, 1997.

BEKKERS JM and STEVENS CF. Cable properties of cultured hippocampal neurons determined from sucrose-evoked miniature EPSCs. *J Neurophysiol* 75: 1250-1255, 1996.

BEKKERS JM, RICHERSON GB and STEVENS CF. Origin of variability in quantal size in cultured hippocampal neurons and hippocampal slices. *Proc Natl Acad Sci U S A* 87: 5359-5362, 1990.

BEKOFF A. Neuroethological approaches to the study of motor development in chicks: achievements and challenges. *J Neurobiol* 23: 1486-1505, 1992.

BENNETT MV. Physiology of electrotonic junctions. *Ann N Y Acad Sci* 137: 509-539, 1966.

BENNETT MV. Gap junctions as electrical synapses. *J Neurocytol* 26: 349-366, 1997.

BERKOWITZ EC. Functional properties of spinal pathways in the carp, Cyprinus Carpio L. *J Comp Neurol* 106: 269-289, 1956.

BERNHARDT RR, CHITNIS AB, LINDAMER L and KUWADA JY. Identification of spinal neurons in the embryonic and larval zebrafish. *J Comp Neurol* 302: 603-616, 1990.

BERNHARDT RR, PATEL CK, WILSON SW and KUWADA JY. Axonal trajectories and distribution of GABAergic spinal neurons in wildtype and mutant zebrafish lacking floor plate cells. *J Comp Neurol* 326: 263-272, 1992.

BERTRAN G and KOTSIAS BA. Chloride currents in skeletal muscles of *Bufo arenarum*. *J Membr Biol* 149: 249-255, 1996.

BEST AC and BONE Q. The terminal neuromuscular junctions of lower chordates. *Z Zellforsch Mikrosk Anat* 143: 495-504, 1973.

BEVENGUT M and CLARAC F. Motoneuronal commands during swimming behaviour in the shore crab. *Brain Res* 520: 330-333, 1990.

BLACKSHAW SE and WARNER AE. Low resistance junctions between mesoderm cells during development of trunk muscles. *J Physiol (Lond)* 255: 209-230, 1976.

BLAGDEN CS, CURRIE PD, INGHAM PW and HUGHES SM. Notochord induction of zebrafish slow muscle mediated by Sonic hedgehog. *Genes Dev* 11: 2163-2175, 1997.

BLIGHT AR. The muscular control of vertebrate swimming movements. *Biol Rev Camb Philos Soc* 52: 181-218, 1977.

BOLTON TB and VAUGHAN-JONES RD. Continuous direct measurement of intracellular chloride and pH in frog skeletal muscle. *J Physiol (Lond)* 270: 801-833, 1977.

BONE Q. Patterns of muscular innervation in the lower chordates. *Int Rev Neurobiol* 6: 99-147, 1964.

BONE Q. On the function of the two types of myotomal muscle fibre in elasmobranch fish. *J Mar Biol Ass U K* 46: 321-349, 1966.

BONE Q. Locomotor muscle. In: *Fish Physiology*, edited by HOAR WS and RANDALL DJ. New York, Academic Press, 1978, p. 361-424.

BONE Q and ONO D. Systematic implications of innervation patterns in teleost myotomes. *Breviora* 470: 1-23, 1982.

BORDE M, PEREDA AE and MORALES FR. Electrophysiological characteristics of the Mauthner cell of the weakly electric fish Gymnotus carapo. *Brain Res* 567: 145-148, 1991.

BOTTAI D, MALER L and DUNN RJ. Alternative RNA splicing of the NMDA receptor NR1 mRNA in the neurons of the teleost electrosensory system. *J Neurosci* 18: 5191-5202, 1998.

BREDER CM. The locomotion of fishes. *Zoologica* 4: 159-297, 1926.

BRETAG AH. Muscle chloride channels. *Physiol Rev* 67: 618-724, 1987.

BRICAUD O, CHAAR V, DAMBLY-CHAUDIERE C and GHYSEN A. Early efferent innervation of the zebrafish lateral line. *J Comp Neurol* 434: 253-261, 2001.

BRISCOE J and ERICSON J. Specification of neuronal fates in the ventral neural tube. *Curr Opin Neurobiol* 11: 43-49, 2001.

BROADIE KS. Development of electrical properties and synaptic transmission at the embryonic neuromuscular junction. *Int Rev Neurobiol* 43: 45-67, 1999.

BROCK LG, COOMBS JS and ECCLES JC. The recording of potentials from motoneurons with an intracellular electrode. *J Physiol (Lond)* 117: 431-462, 1952.

BRODIN L and GRILLNER S. The role of putative excitatory amino acid neurotransmitters in the initiation of locomotion in the lamprey spinal cord. I. The effects of excitatory amino acid antagonists. *Brain Res* 360: 139-148, 1985.

BRUSTEIN E, CHONG M and DRAPEAU P. Development of the serotonergic system, swimming and its modulation in the zebrafish larva. *Soc Neurosci Abst* 26: 830.812, 2000.

BRUSTEIN E, MCKIM SM and DRAPEAU P. Serotonin shapes the locomotor network pattern in the developing zebrafish by modulating quiescent periods. *Soc Neurosci Abst* 27: 2206, 2001.

BUCHANAN JT. Electrophysiological properties of identified classes of lamprey spinal neurons. *J Neurophysiol* 70: 2313-2325, 1993.

BUDICK SA and O'MALLEY DM. Locomotor repertoire of the larval zebrafish: swimming, turning and prey capture. *J Exp Biol* 203: 2565-2579, 2000a.

BUDICK SA and O'MALLEY DM. Minimal behavioral defects are observed after laser-ablation of the nMLF in larval zebrafish. *Soc Neurosci Abst* 26: 60.69, 2000b.

BURKE RE. The use of state-dependent modulation of spinal reflexes as a tool to investigate the organization of spinal interneurons. *Exp Brain Res* 128: 263-277, 1999.

BURROWS M. *The neurobiology of an insect brain*. New York, Oxford University Press, 1996, 682 *pp*.

BUSS RR and DRAPEAU P. Physiological properties of zebrafish embryonic red and white muscle fibers during early development. *J Neurophysiol* 84: 1545-1557, 2000a.

BUSS RR and DRAPEAU P. Synaptic drive to myotomal motoneurons during fictive swimming in the developing zebrafish. *Soc Neurosci Abstr* 26: 830.811, 2000b.

BUSS RR and DRAPEAU P. Synaptic drive to motoneurons during fictive swimming in the developing zebrafish. *J Neurophysiol* 86: 197-210, 2001a.

BUSS RR and DRAPEAU P. The role of zebrafish embryonic red and white muscle in two fictive motor behaviors: coiling and swimming. *Soc Neurosci Abstr* 27: 830.833, 2001b.

BUSS RR and DRAPEAU P. Activation of embryonic red and white muscle fibers during fictive swimming in the developing zebrafish. *J Neurophysiol* 87: 1244-1241, 2002.

BUSS RR, ALI DW and DRAPEAU P. Properties of synaptic currents and fictive motor behaviors in neurons of the locomotor regions of the developing zebrafish. *Soc Neurosci Abstr* 25: 467.463, 1999.

CANFIELD JG and ROSE GJ. Activation of Mauthner neurons during prey capture. *J Comp Physiol* 172: 611-618, 1993.

CARMIGNOTO G and VICINI S. Activity-dependent decrease in NMDA receptor responses during development of the visual cortex. *Science* 258: 1007-1011, 1992.

CASAGRAND JL, GUZIK AL and EATON RC. Mauthner and reticulospinal responses to the onset of acoustic pressure and acceleration stimuli. *J Neurophysiol* 82: 1422-1437, 1999.

CHUA M and BETZ WJ. Characterization of ion channels on the surface membrane of adult rat skeletal muscle. *Biophys J* 59: 1251-1260, 1991.

CLARAC F, VINAY L, CAZALETS JR, FADY JC and JAMON M. Role of gravity in the development of posture and locomotion in the neonatal rat. *Brain Res Brain Res Rev* 28: 35-43, 1998.

CLEMENTS JD and WESTBROOK GL. Activation kinetics reveal the number of glutamate and glycine binding sites on the N-methyl-D-aspartate receptor. *Neuron* 7: 605-613, 1991.

COHEN AH. Intersegmental coordinating system of the lamprey central pattern generator for locomotion. *J Comp Physiol A* 160: 181-193, 1987.

COHEN AH and WALLEN P. The neuronal correlate of locomotion in fish. "Fictive swimming" induced in an in vitro preparation of the lamprey spinal cord. *Exp Brain Res* 41: 11-18, 1980.

COHEN AH and HARRIS-WARRICK RM. Strychnine eliminates alternating motor output during fictive locomotion in the lamprey. *Brain Res* 293: 164-167, 1984.

CONTE CAMERINO D, DE LUCA A, MAMBRINI M and VRBOVA G. Membrane ionic conductances in normal and denervated skeletal muscle of the rat during development. *Pflugers Arch* 413: 568-570, 1989.

COUGHLIN DJ and ROME LC. The roles of pink and red muscle in powering steady swimming in scup, *Stenotomus chrysops*. *Amer Zool* 36: 666-677, 1996.

COUTELLE O, BLAGDEN CS, HAMPSON R, HALAI C, RIGBY PW and HUGHES SM. Hedgehog signalling is required for maintenance of myf5 and myoD expression and timely terminal differentiation in zebrafish adaxial myogenesis. *Dev Biol* 236: 136-150, 2001.

CRAIR MC and MALENKA RC. A critical period for long-term potentiation at thalamocortical synapses. *Nature* 375: 325-328, 1995.

CURRIE PD and INGHAM PW. Induction of a specific muscle cell type by a hedgehog-like protein in zebrafish. *Nature* 382: 452-455, 1996.

CURTI S, FALCONI A, MORALES FR and BORDE M. Mauthner cell-initiated electromotor behavior is mediated via NMDA and metabotropic glutamatergic receptors on medullary pacemaker neurons in a gymnotid fish. *J Neurosci* 19: 9133-9140, 1999.

DALE N. Excitatory synaptic drive for swimming mediated by amino acid receptors in the lamprey. *J Neurosci* 6: 2662-2675, 1986.

DALE N and ROBERTS A. Excitatory amino acid receptors in Xenopus embryo spinal cord and their role in the activation of swimming. *J Physiol (Lond)* 348: 527-543, 1984.

DALE N and ROBERTS A. Dual-component amino-acid-mediated synaptic potentials: excitatory drive for swimming in Xenopus embryos. *J Physiol (Lond)* 363: 35-59, 1985.

DALE N and GRILLNER S. Dual-component synaptic potentials in the lamprey mediated by excitatory amino acid receptors. *J Neurosci* 6: 2653-2661, 1986.

DALE N and KUENZI FM. Ion channels and the control of swimming in the Xenopus embryo. *Prog Neurobiol* 53: 729-756, 1997.

DAY JW, HUSE WD and BENNETT MV. Time course of miniature postsynaptic potentials at the Mauthner fiber giant synapse of the hatchetfish. *Brain Res* 325: 115-128, 1985.

DE GRAAF F, VAN RAAMSDONK W, VAN ASSELT E and DIEGENBACH PC. Identification of motoneurons in the spinal cord of the zebrafish (Brachydanio rerio), with special reference to motoneurons that innervate intermediate muscle fibers. *Anat Embryol* 182: 93-102, 1990.

DE GRAAF F, VAN RAAMSDONK W, VAN ASSELT E and DIEGENBACH PC. Histochemical profiles of motoneurons innervating muscle fibres with different activity patterns in the zebrafish, Brachydanio rerio. *Histochem J* 23: 273-280, 1991.

DE LUCA A, MAMBRINI M and CONTE CAMERINO D. Changes in membrane ionic conductances and excitability characteristics of rat skeletal muscle during aging. *Pflugers Arch* 415: 642-644, 1990.

DE LUCA A, PIERNO S, COCCHI D and CONTE CAMERINO D. Effects of chronic growth hormone treatment in aged rats on the biophysical and pharmacological properties of skeletal muscle chloride channels. *Br J Pharmacol* 121: 369-374, 1997.

DENNIS MJ. Development of the neuromuscular junction: inductive interactions between cells. *Annu Rev Neurosci* 4: 43-68, 1981.

DEVOTO SH, MELANCON E, EISEN JS and WESTERFIELD M. Identification of separate slow and fast muscle precursor cells in vivo, prior to somite formation. *Development* 122: 3371-3380, 1996.

DIAMOND J. The Mauthner Cell. In: *Fish physiology*, edited by HOAR WS and RANDALL DJ. New York, Academic Press, 1971, p. 265-346.

DIAMOND J and HUXLEY AF. The activation and distribution of GABA and L-glutamate receptors on goldfish Mauthner neurones: an analysis of dendritic remote inhibition. *J Physiol (Lond)* 194: 669-723, 1968.

DIAMOND J, ROPER S and YASARGIL GM. The membrane effects, and sensitivity to strychnine, of neural inhibition of the Mauthner cell, and its inhibition by glycine and GABA. *J Physiol (Lond)* 232: 87-111, 1973.

DIDOMENICO R and EATON RC. Seven principles for command and the neural causation of behavior. *Brain Behav Evol* 31: 125-140, 1988.

DIJKGRAAF S. The functioning and significance of the lateral-line organs. *Biol Rev Camb Philos Soc* 38: 51-105, 1962.

DOLDAN MJ, PREGO B, HOLMQVIST BI and DE MIGUEL E. Distribution of GABA-immunolabeling in the early zebrafish (Danio rerio) brain. *Eur J Morphol* 37: 126-129, 1999.

DOUGLAS JR, NOGA BR, DAI X and JORDAN LM. The effects of intrathecal administration of excitatory amino acid agonists and antagonists on the initiation of locomotion in the adult cat. *J Neurosci* 13: 990-1000, 1993.

DRAPEAU P and LEGENDRE P. Neuromuscular transmission on the rebound. *Receptors Channels* 7: 491-496, 2001.

DRAPEAU P, ALI DW, BUSS RR and SAINT-AMANT L. In vivo recording from identifiable neurons of the locomotor network in the developing zebrafish. *J Neurosci Methods* 88: 1-13, 1999.

DRAPEAU P, BUSS RR, ALI DW, LEGENDRE P and ROTUNDO RL. Limits to the development of fast neuromuscular transmission in zebrafish. *J Neurophysiol* 86: 2951-2956, 2001.

DRIEVER W, SOLNICA-KREZEL L, SCHIER AF, NEUHAUSS SC, MALICKI J, STEMPLE DL, STAINIER DY, ZWARTKRUIS F, ABDELILAH S, RANGINI Z, BELAK J and BOGGS C. A genetic screen for mutations affecting embryogenesis in zebrafish. *Development* 123: 37-46, 1996.

DU SJ and DIENHART M. Gli2 mediation of hedgehog signals in slow muscle induction in zebrafish. *Differentiation* 67: 84-91, 2000.

DU SJ, DEVOTO SH, WESTERFIELD M and MOON RT. Positive and negative regulation of muscle cell identity by members of the hedgehog and TGF-beta gene families. *J Cell Biol* 139: 145-156, 1997.

DULHUNTY AF. The dependence of membrane potential on extracellular chloride concentration in mammalian skeletal muscle fibres. *J Physiol (Lond)* 276: 67-82, 1978.

DURAND GM, KOVALCHUK Y and KONNERTH A. Long-term potentiation and functional synapse induction in developing hippocampus. *Nature* 381: 71-75, 1996.

EATON RC and FARLEY RD. Development of the Mauthner neurons in embryos and larvae of the zebrafish, Brachydanio rerio. *Copeia* 4: 673-682, 1973.

EATON RC and FARLEY RD. Mauthner neuron field potential in newly hatched larvae of the zebra fish. *J Neurophysiol* 38: 502-512, 1975.

EATON RC and KIMMEL CB. Directional sensitivity of the Mauthner cell system to vibrational stimulation in zebrafish larvae. *J Comp Physiol A* 140: 337-342, 1980.

EATON RC and HACKETT JT. The role of the Mauthner cell in fast-starts involving escape in teleost fishes. In: *Neural mechanisms of startle behavior*, edited by EATON RC. New York, Plenum Press, 1984, p. 213-266.

EATON RC and DIDOMENICO R. Role of the teleost escape response during development. *Trans Am Fish Soc* 115: 128-142, 1986.

EATON RC and EMBERLEY DS. How stimulus direction determines the trajectory of the Mauthner-initiated escape response in a teleost fish. *J Exp Biol* 161: 469-487, 1991.

EATON RC, BOMBARDIERI RA and MEYER DL. The Mauthner-initiated startle response in teleost fish. *J Exp Biol* 66: 65-81, 1977a.

EATON RC, LAVENDER WA and WIELAND CM. Identification of Mauthner-initiated response patterns in goldfish: Evidence from simultaneous cinematography and electrophysiology. *J Comp Physiol* 144: 521-531, 1981.

EATON RC, NISSANOV J and WIELAND CM. Differential activation of Mauthner and non-Mauthner startle circuits in the zebrafish: implications for functional substitution. *J Comp Physiol A* 155: 813-820, 1984.

EATON RC, DIDOMENICO R and NISSANOV J. Flexible body dynamics of the goldfish C-start: implications for reticulospinal command mechanisms. *J Neurosci* 8: 2758-2768, 1988.

EATON RC, LEE RK and FOREMAN MB. The Mauthner cell and other identified neurons of the brainstem escape network of fish. *Prog Neurobiol* 63: 467-485, 2001.

EATON RC, FARLEY RD, KIMMEL CB and SCHABTACH E. Functional development in the Mauthner cell system of embryos and larvae of the zebra fish. *J Neurobiol* 8: 151-172, 1977b.

EDGLEY SA. Organisation of inputs to spinal interneurone populations. *J Physiol (Lond)* 533: 51-56, 2001.

EDMONDS B, GIBB AJ and COLQUHOUN D. Mechanisms of activation of glutamate receptors and the time course of excitatory synaptic currents. *Annu Rev Physiol* 57: 495-519, 1995.

EISEN JS. Zebrafish make a big splash. *Cell* 87: 969-977, 1996.

EISEN JS. Patterning motoneurons in the vertebrate nervous system. *Trends Neurosci* 22: 321-326, 1999.

EISEN JS and MELANCON E. Interactions with identified muscle cells break motoneuron equivalence in embryonic zebrafish. *Nat Neurosci* 4: 1065-1070, 2001.

EISEN JS, PIKE SH and DEBU B. The growth cones of identified motoneurons in embryonic zebrafish select appropriate pathways in the absence of specific cellular interactions. *Neuron* 2: 1097-1104, 1989.

EISEN JS, PIKE SH and ROMANCIER B. An identified motoneuron with variable fates in embryonic zebrafish. *J Neurosci* 10: 34-43, 1990.

EL MANIRA A and BUSSIERES N. Calcium channel subtypes in lamprey sensory and motor neurons. *J Neurophysiol* 78: 1334-1340, 1997.

EL-FIKY N and WEISER W. Life styles and patterns of development of gills and muscles in larval cyprinids (Cyprinidae; Teleostei). *J Fish Biol* 33: 135-145, 1988.

EL-FIKY N, HINTERLEITNER S and WEISER W. Differentiation of swimming muscles and gills, development of anaerobic power in the larvae of cyprinid fish (Pisces, Teleostei). *Zoomorphology* 107: 126-132, 1987.

EUGENE D and BARETS A. Electrical activity of trout skeletal muscle fibres. *J Physiol (Lond)* 78: 814-820, 1982.

EVANS DH. Fish. In: *Comparative physiology of osmoregulation in animals*, edited by MALOIY GMO. Orlando, Academic Press, 1979, p. 305-390.

EVANS DH. *The physiology of fishes*. New York, CRC Press, 1998,

FABER DS and KORN H. A neuronal inhibition mediated electrically. *Science* 179: 577-578, 1973.

FABER DS and KORN H. Inputs from the posterior lateral line nerves upon the goldfish Mauthner cells. II. Evidence that the inhibitory components are mediated by interneurons of the recurrent collateral network. *Brain Res* 96: 349-356, 1975.

FABER DS, FETCHO JR and KORN H. Neuronal networks underlying the escape response in goldfish. General implications for motor control. *Ann N Y Acad Sci* 563: 11-33, 1989.

FAHLKE C and RUDEL R. Chloride currents across the membrane of mammalian skeletal muscle fibres. *J Physiol (Lond)* 484: 355-368, 1995.

FALCONI A, BORDE M, HENANDEZ-CRUZ A and MORALES F. Mauthner cell-initiated abrupt increase of the electric organ discharge in the weakly electric fish *Gymnotus carapo*. *J Comp Physiol A* 176: 679-689, 1995.

FARNBACH GC, BROWN MJ and BARCHI RL. A maturational defect in passive membrane properties of dystrophic mouse muscle. *Exp Neurol* 62: 539-554, 1978.

FAURE P and KORN H. A nonrandom dynamic component in the synaptic noise of a central neuron. *Proc Natl Acad Sci U S A* 94: 6506-6511, 1997.

FAURE P, KAPLAN D and KORN H. Synaptic efficacy and the transmission of complex firing patterns between neurons. *J Neurophysiol* 84: 3010-3025, 2000.

FEATHERSTONE D, DREWES CD and COATS JR. Noninvasive detection of electrical events during the startle response in larval medaka. *J Exp Biol* 158: 583-589, 1991.

FELDMAN AG and ORLOVSKY GN. Activity of interneurons mediating reciprocal 1a inhibition during locomotion. *Brain Res* 84: 181-194, 1975.

FELSENFELD AL, WALKER C, WESTERFIELD M, KIMMEL C and STREISINGER G. Mutations affecting skeletal muscle myofibril structure in the zebrafish. *Development* 108: 443-459, 1990.

FETCHO JR. Morphological variability, segmental relationships, and functional role of a class of commissural interneurons in the spinal cord of goldfish. *J Comp Neurol* 299: 283-298, 1990.

FETCHO JR. Excitation of motoneurons by the Mauthner axon in goldfish: complexities in a "simple" reticulospinal pathway. *J Neurophysiol* 67: 1574-1586, 1992a.

FETCHO JR. The spinal motor system in early vertebrates and some of its evolutionary changes. *Brain Behav Evol* 40: 82-97, 1992b.

FETCHO JR and FABER DS. Identification of motoneurons and interneurons in the spinal network for escapes initiated by the mauthner cell in goldfish. *J Neurosci* 8: 4192-4213, 1988.

FETCHO JR and SVOBODA KR. Fictive swimming elicited by electrical stimulation of the midbrain in goldfish. *J Neurophysiol* 70: 765-780, 1993.

FETCHO JR and O'MALLEY DM. Visualization of active neural circuitry in the spinal cord of intact zebrafish. *J Neurophysiol* 73: 399-406, 1995.

FLINT AC, MAISCH US, WEISHAUPT JH, KRIEGSTEIN AR and MONYER H. NR2A subunit expression shortens NMDA receptor synaptic currents in developing neocortex. *J Neurosci* 17: 2469-2476, 1997.

FORSTNER H, HINTERLEITER S, MAHR K and WEISER W. Towards a better definition of «metamorphosis» in Coregonus sp.: Biochemical, histological, and physiological data. *Can J Fish Aquat Sci* 40: 1224-1232, 1983.

FOSKETT JK. ClC and CFTR chloride channel gating. *Annu Rev Physiol* 60: 689-717, 1998.

FUIMAN LA. Burst-swimming performance of larval zebra danios and the effects of diel temperature fluctuations. *Trans Am Fish Soc* 115: 143-148, 1986.

FUIMAN LA and WEBB PW. Ontogeny of routine swimming activity and performance in zebra danios (Teleostei: Cyprinidae). *Anim Behav* 36: 250-261, 1988.

FUKAMI Y, FURUKAWA T and ASADA Y. Excitability changes of the Mauthner cell during collateral inhibition. *J Gen Physiol* 48: 584-600, 1965.

FUKUDA J. Chloride spike: a third type of action potential in tissue-cultured skeletal muscle cells from the chick. *Science* 185: 76-78, 1974.

FUKUDA J. Voltage clamp study on inward chloride currents of spherical muscle cells in culture. *Nature* 257: 408-410, 1975.

FUKUDA J, FISCHBACH GD and SMITH TG, JR. A voltage clamp study of the sodium, calcium and chloride spikes of chick skeletal muscle cells grown in tissue culture. *Dev Biol* 49: 412-424, 1976a.

FUKUDA J, HENKART MP, FISCHBACH GD and SMITH TG, JR. Physiological and structural properties of colchicine-treated chick skeletal muscle cells grown in tissue culture. *Dev Biol* 49: 395-411, 1976b.

FURSHPAN EJ. "Electrical transmission" at an excitatory synapse in a vertebrate brain. *Science* 144: 878-880, 1964.

FURSHPAN EJ and FURUKAWA T. Intracellular and extracellular responses of the several regions of the Mauthner cell of the goldfish. *J Neurophysiol* 25: 732-771, 1962.

FURUKAWA T. Synaptic interaction at the mauthner cell of goldfish. *Prog Brain Res* 21: 44-70, 1966.

FURUKAWA T and FURSHPAN EJ. Two inhibitory mechanisms in the Mauthner neurons of goldfish. *J Neurophysiol* 26: 140-176, 1963.

FURUKAWA T, FUKAMI Y and ASADA Y. A third type of inhibition in the Mauthner cell of goldfish. *J Neurophysiol* 26: 759-774, 1963.

FURUKAWA T, FUKAMI Y and ASADA Y. Effects of strychnine and procaine on collateral inhibition of the Mauthner cell of goldfish. *Jpn J Physiol* 14: 386-399, 1964.

GAHTAN E, SANKRITHI N, CAMPOS JB and O'MALLEY DM. Evidence for a widespread brain stem escape network in larval zebrafish. *J Neurophysiol* 87: 608-614, 2002.

GAINER H. Neuromuscular mechanisms of sound production and pectoral spine locking in the banjo catfish, Bunocephalus species. *Physiol Zool* 40: 296-306, 1967.

GAINER H. Multiple innervation of fish skeletal muscle. In: *Experiments in physiology and biochemistry*, edited by KERKUT GA. New York, Academic Press, 1969, p. 191-208.

GAINER H and KLANCHER JE. Neuromuscular junctions in a fast-contracting fish muscle. *Comp Biochem Physiol* 15: 159-165, 1965.

GAO BX, CHENG G and ZISKIND-CONHAIM L. Development of spontaneous synaptic transmission in the rat spinal cord. *J Neurophysiol* 79: 2277-2287, 1998.

GIBB AJ and COLQUHOUN D. Glutamate activation of a single NMDA receptor-channel produces a cluster of channel openings. *Proc R Soc Lond B Biol Sci* 243: 39-45, 1991.

GIDEIRI YBA. The behaviour and neuro-anatomy of some developing teleost fishes. *J Zool (Lond)* 149: 215-241, 1966.

GIDEIRI YBA. Observations on the behaviour of the developing Zoarces viviparus (Zoarcidae). *Hydrobiologia* 31: 60-64, 1968a.

GIDEIRI YBA. The development of behaviour in *Tilapia nilotica* L. *Behaviour* 34: 17-28, 1968b.

GILAT E, HALL DH and BENNETT MV. The giant fiber and pectoral fin adductor motoneuron system in the hatchetfish. *Brain Res* 365: 96-104, 1986.

GLEASON EL and SPITZER NC. AMPA and NMDA receptors expressed by differentiating Xenopus spinal neurons. *J Neurophysiol* 79: 2986-2998, 1998.

GOLLING G, AMSTERDAM A, SUN Z, ANTONELLI M, MALDONADO E, CHEN W, BURGESS S, HALDI M, ARTZT K, FARRINGTON S, LIN S-Y, NISSEN RM and HOPKINS N. Insertional mutagenesis in zebrafish rapidly identifies genes essential for early vertebrate development. *Nature Genetics* 31: 135-140.

GOLSHANI P, WARREN RA and JONES EG. Progression of change in NMDA, non-NMDA, and metabotropic glutamate receptor function at the developing corticothalamic synapse. *J Neurophysiol* 80: 143-154, 1998.

GRAHAM HT and O'LEARY J. Fast central fibers in fish. Properties of Mauthner and Muller fibers of medullospinal system. *J Neurophysiol* 4: 224-242, 1941.

GRANATO M, VAN EEDEN FJ, SCHACH U, TROWE T, BRAND M, FURUTANI-SEIKI M, HAFFTER P, HAMMERSCHMIDT M, HEISENBERG CP, JIANG YJ, KANE DA, KELSH RN, MULLINS MC, ODENTHAL J and NUSSLEIN-VOLHARD C. Genes controlling and mediating locomotion behavior of the zebrafish embryo and larva. *Development* 123: 399-413, 1996.

GREER-WALKER M and PULL GA. A survey of red and white muscle in marine fish. *J Fish Biol* 7: 295-300, 1975.

GRILLNER S. Locomotion in vertebrates: central mechanisms and reflex interaction. Physiol Rev 55: 247-304, 1975.

GRILLNER S and KASHIN S. On the generation and performance of swimming in fish. In: *Neural Control of Locomotion*, edited by HERMAN RM, GRILLNER S, STEIN PSG and STUART DG. New York, Plenum Press, 1975, p. 181-201.

GRILLNER S and WALLEN P. Does the central pattern generation for locomotion in lamprey depend on glycine inhibition? *Acta Physiol Scand* 110: 103-105, 1980.

GRILLNER S and WALLEN P. The ionic mechanisms underlying N-methyl-D-aspartate receptor-induced, tetrodotoxin-resistant membrane potential oscillations in lamprey neurons active during locomotion. *Neurosci Lett* 60: 289-294, 1985.

GRILLNER S, PERRET C and ZANGGER P. Central generation of locomotion in the spinal dogfish. *Brain Res* 109: 255-269, 1976.

GRILLNER S, GEORGOPOULOS AP and JORDAN LM. Selection and initiation of motor behavior. In: *Neurons, Networks,and Motor Behavior*, edited by STEIN D, STUART DG, SELVERSTON S and GRILLNER S. Cambridge, MIT Press, 1997, p. 1-19.

GRILLNER S, PARKER D and EL MANIRA A. Vertebrate locomotion--a lamprey perspective. *Ann N Y Acad Sci* 860: 1-18, 1998a.

GRILLNER S, STEIN PSG, STUART DG, FORSSBERG H and HERMAN RM. *Neurobiology of vertebrate locomotion*. London, Macmillan, 1986, 735 *pp*.

GRILLNER S, WALLEN P, BRODIN L and LANSNER A. Neuronal network generating locomotor behavior in lamprey: circuitry, transmitters, membrane properties, and simulation. *Annu Rev Neurosci* 14: 169-199, 1991.

GRILLNER S, WALLEN P, HILL R, CANGIANO L and EL MANIRA A. Ion channels of importance for the locomotor pattern generation in the lamprey brainstem-spinal cord. *J Physiol (Lond)* 533: 23-30, 2001.

GRILLNER S, EKEBERG, EL MANIRA A, LANSNER A, PARKER D, TEGNER J and WALLEN P. Intrinsic function of a neuronal network - a vertebrate central pattern generator. *Brain Res Brain Res Rev* 26: 184-197, 1998b.

GRUNWALD DJ, KIMMEL CB, WESTERFIELD M, WALKER C and STREISINGER G. A neural degeneration mutation that spares primary neurons in the zebrafish. *Dev Biol* 126: 115-128, 1988.

GUO S, WILSON SW, COOKE S, CHITNIS AB, DRIEVER W and ROSENTHAL A. Mutations in the zebrafish unmask shared regulatory pathways controlling the development of catecholaminergic neurons. *Dev Biol* 208: 473-487, 1999.

HAFFTER P, GRANATO M, BRAND M, MULLINS MC, HAMMERSCHMIDT M, KANE DA, ODENTHAL J, VAN EEDEN FJ, JIANG YJ, HEISENBERG CP, KELSH RN, FURUTANI-SEIKI M, VOGELSANG E, BEUCHLE D, SCHACH U, FABIAN C and NUSSLEIN-VOLHARD C. The identification of genes with unique and essential functions in the development of the zebrafish, *Danio rerio. Development* 123: 1-36, 1996.

HAGEVIK A and MCCLELLAN AD. Role of excitatory amino acids in brainstem activation of spinal locomotor networks in larval lamprey. *Brain Res* 636: 147-152, 1994.

HAGIWARA S and TAKAHASHI K. Resting and spike potentials of skeletal muscle fibres of salt-water elasmobranch and teleost fish. *J Physiol (Lond)* 190: 499-518, 1967.

HAGIWARA S and TAKAHASHI K. Mechanism of anion permeation through the muscle fibre membrane of an elasmobranch fish, *Taeniura lymma*. *J Physiol (Lond)* 238: 109-127, 1974.

HALE ME, RITTER DA and FETCHO JR. A confocal study of spinal interneurons in living larval zebrafish. *J Comp Neurol* 437: 1-16, 2001.

HALL DH, GILAT E and BENNETT MV. Ultrastructure of the rectifying electrotonic synapses between giant fibres and pectoral fin adductor motor neurons in the hatchetfish. *J Neurocytol* 14: 825-834, 1985.

HAMILL OP, MARTY A, NEHER E, SAKMANN B and SIGWORTH FJ. Improved patch-clamp techniques for high-resolution current recording from cells and cell-free membrane patches. *Pflugers Arch* 391: 85-100, 1981.

HANNEMAN E, TREVARROW B, METCALFE WK, KIMMEL CB and WESTERFIELD M. Segmental pattern of development of the hindbrain and spinal cord of the zebrafish embryo. *Development* 103: 49-58, 1988.

HARRIS GL and BETZ WJ. Evidence for active chloride accumulation in normal and denervated rat lumbrical muscle. *J Gen Physiol* 90: 127-144, 1987.

HARRIS JE. Early embryonic movements. *J Obstet Gynaecol Br Commonw* 59: 818-821, 1962.

HATTA K and KORN H. Physiological properties of the Mauthner system in the adult zebrafish. *J Comp Neurol* 395: 493-509, 1998.

HATTA K and KORN H. Tonic inhibition alternates in paired neurons that set direction of fish escape reaction. *Proc Natl Acad Sci U S A* 96: 12090-12095, 1999.

HATTA K, ANKRI N, FABER DS and KORN H. Slow inhibitory potentials in the teleost Mauthner cell. *Neuroscience* 103: 561-579, 2001.

HEISLER N. Acid-base regulation in fishes. In: *Fish physiology*, edited by HOAR WS and RANDALL DJ. New York, Academic Press, 1984, p. 315-401.

HERMAN RM, GRILLNER S, STEIN PSG and STUART DG. *Neural control of locomotion*. New York, Plenum Press, 1976, 822 *pp*.

HERRICK CJ. *George Ellett Coghill, naturalist and philosopher*. Chicago, The University of Chicago Press, 1949, 280 *pp*.

HESS D and EL MANIRA A. Characterization of a high-voltage-activated IA current with a role in spike timing and locomotor pattern generation. *Proc Natl Acad Sci U S A* 98: 5276-5281, 2001.

HESTRIN S. Developmental regulation of NMDA receptor-mediated synaptic currents at a central synapse. *Nature* 357: 686-689, 1992.

HIDAKA T and TOIDA N. Biophysical and mechanical properties of red and white muscle fibres in fish. *J Physiol (Lond)* 201: 49-59, 1969a.

HIDAKA T and TOIDA N. Neuromuscular transmission and excitation-contraction coupling in fish red muscle. *Jpn J Physiol* 19: 130-142, 1969b.

HIGASHIJIMA S, BHATT DH, MANDEL G and FETCHO JR. Neurotransmitter properties of spinal interneurons in embryonic/larval zebrafish. *Soc Neurosci Abst* 830.4: 2001.

HILL R, MATSUSHIMA T, SCHOTLAND J and GRILLNER S. Apamin blocks the slow AHP in lamprey and delays termination of locomotor bursts. *Neuroreport* 3: 943-945, 1992.

HIRSCH JE, BIGBEE JW and FINE ML. Continuous adult development of multiple innervation in toadfish sonic muscle. *J Neurobiol* 36: 348-356, 1998.

HISAOKA KK and FIRLIT CF. Further studies on the embryonic development of the zebrafish, Brachydanio rerio (Hamilton-Buchanan). *J Morphol* 107: 205-225, 1960.

HOFF K and WASSERSUG RJ. Tadpole locomotion: Axial movement and tail functions in a largely vertebraeless vertebrate. *Amer Zool* 40: 62-76, 2000.

HOLMES WN and DONALDSON EM. The body compartment and the distribution of electrolytes. In: *Fish Physiology*, edited by HOAR WS and RANDALL DJ. New York, Academic Press, 1969, p. 1-89.

HOOKER D. *The prenatal origin of behaviour*. Lawrence, University of Kansas Press, 1952, 143 *pp*.

HORI Y and KANDA K. Developmental alterations in NMDA receptor-mediated currents in neonatal rat spinal motoneurons. *Neurosci Lett* 205: 99-102, 1996.

HUDSON RC. Polyneuronal innervation of the fast muscles of the marine teleost Cottus scorpius L. *J Exp Biol* 50: 47-67, 1969.

HUERTA M and STEFANI E. Potassium and caffeine contractures in fast and slow muscles of the chicken. *J Physiol (Lond)* 318: 181-189, 1981.

HUGHES SM and SALINAS PC. Control of muscle fibre and motoneuron diversification. *Curr Opin Neurobiol* 9: 54-64, 1999.

HUI CS and CHEN W. Origin of delayed outward ionic current in charge movement traces from frog skeletal muscle. *J Physiol (Lond)* 479: 109-125, 1994.

HULTBORN H. State-dependent modulation of sensory feedback. *J Physiol (Lond)* 533: 5-13, 2001.

HUNTER JR. Swimming and feeding behavior of larval anchovy Engraulis mordax. *Fish Bull* 70: 821-838, 1972.

HUSE WD, DAY JW and BENNETT MV. Postsynaptic currents at the Mauthner fiber giant synapse of the hatchetfish. *Brain Res* 325: 129-141, 1985.

HUTTER OF and WARNER AE. Action of some foreign cations and anions on the chloride permeability of frog muscle. *J Physiol (Lond)* 189: 445-460, 1967a.

HUTTER OF and WARNER AE. The effect of pH on the 36-Cl efflux from frog skeletal muscle. *J Physiol (Lond)* 189: 427-443, 1967b.

HUTTER OF and WARNER AE. The pH sensitivity of the chloride conductance of frog skeletal muscle. *J Physiol (Lond)* 189: 403-425, 1967c.

HUTTER OF and WARNER AE. The voltage dependence of the chloride conductance of frog muscle. *J Physiol (Lond)* 227: 275-290, 1972.

IMBODEN M, DEVIGNOT V, KORN H and GOBLET C. Regional distribution of glycine receptor messenger RNA in the central nervous system of zebrafish. *Neuroscience* 103: 811-830, 2001a.

IMBODEN M, DE SAINT JAN D, LEULIER F, KORN H, GOBLET C and BREGESTOVSKI P. Isolation and characterization of an alpha 2-type zebrafish glycine receptor subunit. *Neuroscience* 103: 799-810, 2001b.

ISAAC JT, NICOLL RA and MALENKA RC. Evidence for silent synapses: implications for the expression of LTP. *Neuron* 15: 427-434, 1995.

JANKOWSKA E. Interneuronal relay in spinal pathways from proprioceptors. *Prog Neurobiol* 38: 335-378, 1992.

JANKOWSKA E. Spinal interneuronal systems: identification, multifunctional character and reconfigurations in mammals. *J Physiol (Lond)* 533: 31-40, 2001.

JANKOWSKA E, JUKES MG, LUND S and LUNDBERG A. The effect of DOPA on the spinal cord. 5. Reciprocal organization of pathways transmitting excitatory action to alpha motoneurones of flexors and extensors. *Acta Physiol Scand* 70: 369-388, 1967a.

JANKOWSKA E, JUKES MG, LUND S and LUNDBERG A. The effect of DOPA on the spinal cord. 6. Half-centre organization of interneurones transmitting effects from the flexor reflex afferents. *Acta Physiol Scand* 70: 389-402, 1967b.

JAYNE BC and LAUDER GV. How swimming fish use slow and fast muscle fibers: implications for models of vertebrate muscle recruitment. *J Comp Physiol A* 175: 123-131, 1994.

JAYNE BC and LAUDER GV. New data on axial locomotion in fishes: how speed affects diversity of kinematics and motor patterns. *Amer Zool* 36: 642-655, 1996.

JENTSCH TJ, FRIEDRICH T, SCHRIEVER A and YAMADA H. The CLC chloride channel family. *Pflugers Arch* 437: 783-795, 1999.

JOHNSTON IA. Contractile properties of fish fast muscle fibres. *Mar Biol Lett* 1: 323-328, 1980.

JOHNSTON IA. Structure and function of fish muscles. *Symp Zool Soc Lond* 48: 71-113, 1981.

JOHNSTON IA. On the design of fish myotomal muscles. *Mar Behav Physiol* 9: 83-98, 1983.

JONTES JD, BUCHANAN J and SMITH SJ. Growth cone and dendrite dynamics in zebrafish embryos: early events in synaptogenesis imaged in vivo. *Nat Neurosci* 3: 231-237, 2000.

JORDAN LM. Factors determining motoneuron rhythmicity during fictive locomotion. *Symp Soc Exp Biol* 37: 423-444, 1983.

JORDAN LM. Initiation of locomotion in mammals. *Ann N Y Acad Sci* 860: 83-93, 1998.

KAHN JA. Patterns of synaptic inhibition in motoneurons and interneurons during fictive swimming in the lamprey, as revealed by Cl- injections. *J Comp Physiol A* 147: 189-194, 1982.

KAHN JA and ROBERTS A. The central nervous origin of the swimming motor pattern in embryos of *Xenopus laevis*. *J Exp Biol* 99: 185-196, 1982.

KAHN JA, ROBERTS A and KASHIN SM. The neuromuscular basis of swimming movements in embryos of the amphibian *Xenopus laevis*. *J Exp Biol* 99: 175-184, 1982.

KASHIN SM, FELDMAN AG and ORLOVSKY GN. Locomotion of fish evoked by electrical stimulation of the brain. *Brain Res* 82: 41-47, 1974.

KEMNITZ CP. Dopaminergic modulation of spinal neurons and synaptic potentials in the lamprey spinal cord. *J Neurophysiol* 77: 289-298, 1997.

KIDOKORO Y. Developmental changes of membrane electrical properties in a rat skeletal muscle cell line. *J Physiol (Lond)* 244: 129-143, 1975.

KIMMEL CB. Reticulospinal and vestibulospinal neurons in the young larva of a teleost fish, *Brachydanio rerio*. *Prog Brain Res* 57: 1-23, 1982.

KIMMEL CB, PATTERSON J and KIMMEL RO. The development and behavioral characteristics of the startle response in the zebra fish. *Dev Psychobiol* 7: 47-60, 1974.

KIMMEL CB, EATON RC and POWELL SL. Decreased fast-start performance of zebrafish larvae lacking Mauthner neurons. *J Comp Physiol A* 140: 343-350, 1980.

KIMMEL CB, SESSIONS SK and KIMMEL RJ. Morphogenesis and synaptogenesis of the zebrafish Mauthner neuron. *J Comp Neurol* 198: 101-120, 1981.

KIMMEL CB, POWELL SL and METCALFE WK. Brain neurons which project to the spinal cord in young larvae of the zebrafish. *J Comp Neurol* 205: 112-127, 1982.

KIMMEL CB, METCALFE WK and SCHABTACH E. T reticular interneurons: a class of serially repeating cells in the zebrafish hindbrain. *J Comp Neurol* 233: 365-376, 1985.

KIMMEL CB, HATTA K and METCALFE WK. Early axonal contacts during development of an identified dendrite in the brain of the zebrafish. *Neuron* 4: 535-545, 1990.

KIMMEL CB, BALLARD WW, KIMMEL SR, ULLMANN B and SCHILLING TF. Stages of embryonic development of the zebrafish. *Dev Dyn* 203: 253-310, 1995.

KLEIN MG. Properties of the chloride conductance associated with temperature acclimation in muscle fibres of green sunfish. *J Exp Biol* 114: 581-598, 1985.

KLEIN MG and PROSSER CL. The effects of temperature acclimation on the resting membrane of skeletal muscle fibres from green sunfish. *J Exp Biol* 114: 563-579, 1985.

KLOCKE R, STEINMEYER K, JENTSCH TJ and JOCKUSCH H. Role of innervation, excitability, and myogenic factors in the expression of the muscular chloride channel ClC-1. A study on normal and myotonic muscle. *J Biol Chem* 269: 27635-27639, 1994.

KOHNO K. Symmetrical axo-axonic synapses in the axon cap of the goldfish Mauthner cell. *Brain Res* 23: 255-258, 1970.

KORN H and FABER DS. An electrically mediated inhibition in goldfish medulla. *J Neurophysiol* 38: 452-471, 1975a.

KORN H and FABER DS. Inputs from the posterior lateral line nerves upon the goldfish Mauthner cell. I. Properties and synaptic localization of the excitatory component. *Brain Res* 96: 342-348, 1975b.

KORN H and FABER DS. Vertebrate central nervous system: same neurons mediate both electrical and chemical inhibitions. *Science* 194: 1166-1169, 1976.

KORN H, TRILLER A and FABER DS. Structural correlates of recurrent collateral interneurons producing both electrical and chemical inhibitions of the Mauthner cell. *Proc R Soc Lond B Biol Sci* 202: 533-538, 1978.

KORN H, FABER DS and TRILLER A. Convergence of morphological, physiological, and immunocytochemical techniques for the study of single Mauthner cells. In: *Handbook of chemical neuroanatomy, Volume 8: Analysis of neuronal microcircuits and synaptic interactions*, edited by BJORKLUND A, HOKFELT T, WOUTERLOOD FG and VAN DEN POL AN. Elsevier, 1990, p. 403-480.

KOTRSCHAL K, BRANDSTATTER R, GOMAHR A, JUNGER H, PALZENBERGER M and ZAUNREITER M. Brain and sensory systems. In: *Cyprinid fishes: systematics, biology and exploitation*, edited by WINFIELD IJ and NELSON JS. New York, Chapman and Hall, 1991, p. 284-331.

KRAWITZ S, FEDIRCHUK B, DAI Y, JORDAN LM and MCCREA DA. State-dependent hyperpolarization of voltage threshold enhances motoneurone excitability during fictive locomotion in the cat. *J Physiol (Lond)* 532: 271-281, 2001.

KULLBERG R and OWENS JL. Comparative development of end-plate currents in two muscles of Xenopus laevis. *J Physiol (Lond)* 374: 413-427, 1986.

KULLBERG RW, LENTZ TL and COHEN MW. Development of the myotomal neuromuscular junction in Xenopus laevis: an electrophysiological and fine-structural study. *Dev Biol* 60: 101-129, 1977.

KULLMANN DM. Amplitude fluctuations of dual-component EPSCs in hippocampal pyramidal cells: implications for long-term potentiation. *Neuron* 12: 1111-1120, 1994.

KUWADA JY, BERNHARDT RR and NGUYEN N. Development of spinal neurons and tracts in the zebrafish embryo. *J Comp Neurol* 302: 617-628, 1990a.

KUWADA JY, BERNHARDT RR and CHITNIS AB. Pathfinding by identified growth cones in the spinal cord of zebrafish embryos. *J Neurosci* 10: 1299-1308, 1990b.

LAALE HW. The biology and use of zebrafish, Brachydanio rerio in fisheries research. A literature review. *J Fish Biol* 10: 121-173, 1977.

LEBEDA FJ and ALBUQUERQUE EX. Membrane cable properties of normal and dystrophic chicken muscle fibers. *Exp Neurol* 47: 544-557, 1975.

LEE RK and EATON RC. Identifiable reticulospinal neurons of the adult zebrafish, Brachydanio rerio. *J Comp Neurol* 304: 34-52, 1991.

LEGENDRE P. Pharmacological evidence for two types of postsynaptic glycinergic receptors on the Mauthner cell of 52-h-old zebrafish larvae. *J Neurophysiol* 77: 2400-2415, 1997.

LEGENDRE P. A reluctant gating mode of glycine receptor channels determines the time course of inhibitory miniature synaptic events in zebrafish hindbrain neurons. *J Neurosci* 18: 2856-2870, 1998.

LEGENDRE P. Voltage dependence of the glycine receptor-channel kinetics in the zebrafish hindbrain. *J Neurophysiol* 82: 2120-2129, 1999.

LEGENDRE P and KORN H. Glycinergic inhibitory synaptic currents and related receptor channels in the zebrafish brain. *Eur J Neurosci* 6: 1544-1557, 1994.

LEGENDRE P and KORN H. Voltage dependence of conductance changes evoked by glycine release in the zebrafish brain. *J Neurophysiol* 73: 2404-2412, 1995.

LEGENDRE P, ALI DW and DRAPEAU P. Recovery from open channel block by acetylcholine during neuromuscular transmission in zebrafish. *J Neurosci* 20: 140-148, 2000.

LEHMANN-HORN F and JURKAT-ROTT K. Voltage-gated ion channels and hereditary disease. *Physiol Rev* 79: 1317-1372, 1999.

LEONARD RB. Vertical undulations in the atlantic stingray and comparisons with other models. In: *Neurobiology of Vertebrate Locomotion*, edited by GRILLNER S, STEIN PSG, STUART DG, FORSSBERG H and HERMAN RM. London, Macmillan, 1986, p. 157-171.

LESTER RA and JAHR CE. NMDA channel behavior depends on agonist affinity. *J Neurosci* 12: 635-643, 1992.

LEWIS KE and EISEN JS. Hedgehog signaling is required for primary motoneuron induction in zebrafish. *Development* 128: 3485-3495, 2001.

LEWIS KE, CURRIE PD, ROY S, SCHAUERTE H, HAFFTER P and INGHAM PW. Control of muscle cell-type specification in the zebrafish embryo by Hedgehog signalling. *Dev Biol* 216: 469-480, 1999.

LIAO D, HESSLER NA and MALINOW R. Activation of postsynaptically silent synapses during pairing-induced LTP in CA1 region of hippocampal slice. *Nature* 375: 400-404, 1995.

LIN JW and FABER DS. Synaptic transmission mediated by single club endings on the goldfish Mauthner cell. II. Plasticity of excitatory postsynaptic potentials. *J Neurosci* 8: 1313-1325, 1988a.

LIN JW and FABER DS. Synaptic transmission mediated by single club endings on the goldfish Mauthner cell. I. Characteristics of electrotonic and chemical postsynaptic potentials. *J Neurosci* 8: 1302-1312, 1988b.

LINDSEY CC. Form, function, and locomotory habits in fish. In: *Fish Physiology*, edited by HOAR WS and RANDALL DJ. New York, Academic Press, 1978, p. 1-100.

LIU DW and WESTERFIELD M. Function of identified motoneurones and co-ordination of primary and secondary motor systems during zebra fish swimming. *J Physiol (Lond)* 403: 73-89, 1988.

LIU DW and WESTERFIELD M. The formation of terminal fields in the absence of competitive interactions among primary motoneurons in the zebrafish. *J Neurosci* 10: 3947-3959, 1990.

LIU DW and WESTERFIELD M. Clustering of muscle acetylcholine receptors requires motoneurons in live embryos, but not in cell culture. *J Neurosci* 12: 1859-1866, 1992.

LIU KS and FETCHO JR. Laser ablations reveal functional relationships of segmental hindbrain neurons in zebrafish. *Neuron* 23: 325-335, 1999.

LOO DD, MCLARNON JG and VAUGHAN PC. Some observations on the behaviour of chloride current--voltage relations in *Xenopus* muscle membrane in acid solutions. *Can J Physiol Pharmacol* 59: 7-13, 1981.

LORENT K, LIU KS, FETCHO JR and GRANATO M. The zebrafish *space cadet* gene controls axonal pathfinding of neurons that modulate fast turning movements. *Development* 128: 2131-2142, 2001.

LORKOVIC H and TOMANEK RJ. Potassium and chloride conductances in normal and denervated rat muscles. *Am J Physiol* 232: C109-114, 1977.

LOSI G, PRYBYLOWSKI K, FU Z, LUO JH and VICINI S. Silent synapses in developing cerebellar granule neurons. *J Neurophysiol* 87: 1263-1270, 2002.

LOTURCO JJ, BLANTON MG and KRIEGSTEIN AR. Initial expression and endogenous activation of NMDA channels in early neocortical development. *J Neurosci* 11: 792-799, 1991.

MA PM. Catecholaminergic systems in the zebrafish. I. Number, morphology, and histochemical characteristics of neurons in the locus coeruleus. *J Comp Neurol* 344: 242-255, 1994a.

MA PM. Catecholaminergic systems in the zebrafish. II. Projection pathways and pattern of termination of the locus coeruleus. *J Comp Neurol* 344: 256-269, 1994b.

MA PM. Catecholaminergic systems in the zebrafish. III. Organization and projection pattern of medullary dopaminergic and noradrenergic neurons. *J Comp Neurol* 381: 411-427, 1997.

MACDONALD JA. Fast decay of fish synaptic currents. *Experientia* 39: 230-231, 1983.

MACDONALD JA and MONTGOMERY JC. Rate-compensated synaptic events in antarctic fish: Consequences of homeoviscous cold-adaptation. *Experientia* 42: 806-808, 1986.

MADDEN DR. The structure and function of glutamate receptor ion channels. *Nat Rev Neurosci* 3: 91-101, 2002.

MARTIN SC, HEINRICH G and SANDELL JH. Sequence and expression of glutamic acid decarboxylase isoforms in the developing zebrafish. *J Comp Neurol* 396: 253-266, 1998.

MATSUOKA M and IWAI T. Development of the myotomal musculature in the red sea bream Pagrus major. *Bull Japan Soc Sci Fish* 50: 29-36, 1984.

MATSUSHIMA T, TEGNER J, HILL RH and GRILLNER S. GABAB receptor activation causes a depression of low- and high-voltage- activated Ca2+ currents, postinhibitory rebound, and postspike afterhyperpolarization in lamprey neurons. *J Neurophysiol* 70: 2606-2619, 1993.

MAYER ML and WESTBROOK GL. The physiology of excitatory amino acids in the vertebrate central nervous system. *Prog Neurobiol* 28: 197-276, 1987.

MCCREA DA. Spinal circuitry of sensorimotor control of locomotion. *J Physiol (Lond)* 533: 41-50., 2001.

MCCREA DA, PRATT CA and JORDAN LM. Renshaw cell activity and recurrent effects on motoneurons during fictive locomotion. *J Neurophysiol* 44: 475-488, 1980.

MCDONALD DG and MILLIGAN CL. Chemical properties of the blood. In: *Fish Physiology*, edited by HOAR WS, RANDALL DJ and FARRELL AP. New York, Academic Press, 1992, p. 55-133.

MELANCON E, LIU DW, WESTERFIELD M and EISEN JS. Pathfinding by identified zebrafish motoneurons in the absence of muscle pioneers. *J Neurosci* 17: 7796-7804, 1997.

MENDELSON B. Soma position is correlated with time of development in three types of identified reticulospinal neurons. *Dev Biol* 112: 489-493, 1985.

MENDELSON B. Development of reticulospinal neurons of the zebrafish. II. Early axonal outgrowth and cell body position. *J Comp Neurol* 251: 172-184, 1986a.

MENDELSON B. Development of reticulospinal neurons of the zebrafish. I. Time of origin. *J Comp Neurol* 251: 160-171, 1986b.

METCALFE WK. Organization and development of the zebrafish posterior lateral line. In: *The mechanosensory lateral line. Neurobiology and evolution*, edited by COOMBS S, GORNER P and MUNZ H. New York, Springer-Verlag, 1989, p. 147-159.

METCALFE WK, KIMMEL CB and SCHABTACH E. Anatomy of the posterior lateral line system in young larvae of the zebrafish. *J Comp Neurol* 233: 377-389, 1985.

METCALFE WK, MENDELSON B and KIMMEL CB. Segmental homologies among reticulospinal neurons in the hindbrain of the zebrafish larva. *J Comp Neurol* 251: 147-159, 1986.

METCALFE WK, MYERS PZ, TREVARROW B, BASS MB and KIMMEL CB. Primary neurons that express the L2/HNK-1 carbohydrate during early development in the zebrafish. *Development* 110: 491-504, 1990.

MODEL PG, SPIRA ME and BENNETT MV. Synaptic inputs to the cell bodies of the giant fibers of the hatchetfish. *Brain Res* 45: 288-295, 1972.

MONYER H, BURNASHEV N, LAURIE DJ, SAKMANN B and SEEBURG PH. Developmental and regional expression in the rat brain and functional properties of four NMDA receptors. *Neuron* 12: 529-540, 1994.

MOORE LE, HILL RH and GRILLNER S. Voltage clamp analysis of lamprey neurons--role of N-methyl-D-aspartate receptors in fictive locomotion. *Brain Res* 419: 397-402, 1987.

MOS W and VAN DER STELT A. Efficiency in relation to the design of the segmented body musculature in *Brachydanio rerio*. *Neth J Zool* 32: 123-143, 1982.

MOS W, ROBERTS BL and WILLIAMSON R. Activity patterns of motoneurons in the spinal dogfish in relation to changing fictive locomotion. *Philos Trans R Soc Lond B Biol Sci* 330: 329-339, 1990a.

MOS W, ROBERTS BL and WILLIAMSON R. Interneuronal activity patterns during fictive locomotion of spinal dogfish. *Philos Trans R Soc Lond B Biol Sci* 330: 341-349, 1990b.

MULLER KJ, NICHOLLS JG and STENT GS. *Neurobiology of the leech*. Cold Spring Harbor, Cold Spring Harbor Laboratory, 1981, 320 *pp*.

MULLER UK, STAMHUIS EJ and VIDELER JJ. Hydrodynamics of unsteady fish swimming and the effects of body size: comparing the flow fields of fish larvae and adults. *J Exp Biol* 203: 193-206, 2000.

MYERS PZ. Spinal motoneurons of the larval zebrafish. *J Comp Neurol* 236: 555-561, 1985.

MYERS PZ, EISEN JS and WESTERFIELD M. Development and axonal outgrowth of identified motoneurons in the zebrafish. *J Neurosci* 6: 2278-2289, 1986.

MYERS PZ, SIPPLE BA, HASAKA T and QUTUB H. Automated analysis of spontaneous motor activity in the embryonic zebrafish, *Danio rerio*. *J Comput Assist Microsc* 9: 169-181, 1997.

NAG AC and NURSALL JR. Histogenesis of white and red muscle fibres of trunk muscles of a fish Salmo gairdneri. *Cytobios* 6: 227-246, 1972.

NAKAJIMA Y. Fine structure of the synaptic endings on the Mauthner cell of the goldfish. *J Comp Neurol* 156: 379-402, 1974.

NEHER E. Correction for liquid junction potentials in patch clamp experiments. *Methods Enzymol* 207: 123-131, 1992.

NGUYEN PV, ANIKSZTEJN L, CATARSI S and DRAPEAU P. Maturation of neuromuscular transmission during early development in zebrafish. *J Neurophysiol* 81: 2852-2861, 1999.

NICOLAYSEN K. Spread of the junction potential in the T-system in hagfish slow muscle fibres. *Acta Physiol Scand* 96: 50-57, 1976a.

NICOLAYSEN K. The spread of the action potential through the T-system in hagfish twitch muscle fibres. *Acta Physiol Scand* 96: 29-49, 1976b.

NICOLL RA and MALENKA RC. Contrasting properties of two forms of long-term potentiation in the hippocampus. *Nature* 377: 115-118, 1995.

NISSANOV J and EATON RC. Reticulospinal control of rapid escape turning maneuvers in fishes. *Amer Zool* 29: 103-121, 1989.

NOGA BR, SHEFCHYK SJ, JAMAL J and JORDAN LM. The role of Renshaw cells in locomotion: antagonism of their excitation from motor axon collaterals with intravenous mecamylamine. *Exp Brain Res* 66: 99-105, 1987.

NORRIS W, NEYT C, INGHAM PW and CURRIE PD. Slow muscle induction by Hedgehog signalling in vitro. *J Cell Sci* 113: 2695-2703, 2000.

NUSSER Z, CULL-CANDY S and FARRANT M. Differences in synaptic GABA(A) receptor number underlie variation in GABA mini amplitude. *Neuron* 19: 697-709, 1997.

O'CONNELL CP. Development of organ systems in the northern anchovy, Engraulis mordax, and other teleosts. *Amer Zool* 2: 429-446, 1981.

OGATA T. Structure of motor endplates in the different fiber types of vertebrate skeletal muscles. *Arch Histol Cytol* 51: 385-424, 1988.

O'MALLEY DM, KAO YH and FETCHO JR. Imaging the functional organization of zebrafish hindbrain segments during escape behaviors. *Neuron* 17: 1145-1155, 1996.

ONO F, HIGASHIJIMA S, SHCHERBATKO A, FETCHO JR and BREHM P. Paralytic zebrafish lacking acetylcholine receptors fail to localize rapsyn clusters to the synapse. *J Neurosci* 21: 5439-5448, 2001.

ONO RD. Dual motor innervation in the axial musculature of fishes. *J Fish Biol* 22: 395-408, 1983.

ORSAL D, PERRET C and CABELGUEN JM. Evidence of rhythmic inhibitory synaptic influences in hindlimb motoneurons during fictive locomotion in the thalamic cat. *Exp Brain Res* 64: 217-224, 1986.

OZAKI S, YAMADA T, IIZUKA M, NISHIMARU H and KUDO N. Development of locomotor activity induced by NMDA receptor activation in the lumbar spinal cord of the rat fetus studied in vitro. *Brain Res Dev Brain Res* 97: 118-125, 1996.

PALADE PT and BARCHI RL. Characteristics of the chloride conductance in muscle fibers of the rat diaphragm. *J Gen Physiol* 69: 325-342, 1977.

PAPPAS GD and BENNETT MV. Specialized junctions involved in electrical transmission between neurons. *Ann N Y Acad Sci* 137: 495-508, 1966.

PARSONS R. *Handbook of electrochemical constants*. London, Butterworths Scientific Publications, 1959, p. 20-27.

PEREDA AE, BELL TD and FABER DS. Retrograde synaptic communication via gap junctions coupling auditory afferents to the Mauthner cell. *J Neurosci* 15: 5943-5955, 1995.

PERRET C and CABELGUEN JM. Main characteristics of the hindlimb locomotor cycle in the decorticate cat with special reference to bifunctional muscles. *Brain Res* 187: 333-352, 1980.

PERRINS R and ROBERTS A. Cholinergic and electrical motoneuron-to-motoneuron synapses contribute to on-cycle excitation during swimming in Xenopus embryos. *J Neurophysiol* 73: 1005-1012, 1995a.

PERRINS R and ROBERTS A. Cholinergic contribution to excitation in a spinal locomotor central pattern generator in Xenopus embryos. *J Neurophysiol* 73: 1013-1019, 1995b.

PIERNO S, DE LUCA A, BECK CL, GEORGE AL, JR. and CONTE CAMERINO D. Aging-associated down-regulation of ClC-1 expression in skeletal muscle: phenotypic-independent relation to the decrease of chloride conductance. *FEBS Lett* 449: 12-16, 1999.

PLAUT I. Effects of fin size on swimming performance, swimming behaviour and routine activity of zebrafish Danio rerio. *J Exp Biol* 203: 813-820, 2000.

PLAUT II and GORDON M. Swimming Metabolism of Wild-Type and Cloned Zebrafish Brachydanio Rerio. *J Exp Biol* 194: 209-223, 1994.

POON MLT. Induction of swimming in lamprey by L-DOPA and amino acids. *J Comp Physiol* 136: 337-344, 1980.

POZNANSKY MJ and STEELE JA. Membrane electrical properties of developing fast-twitch and slow-tonic muscle fibres of the chick. *J Physiol (Lond)* 347: 633-640, 1984.

PRATT CA and JORDAN LM. Ia inhibitory interneurons and Renshaw cells as contributors to the spinal mechanisms of fictive locomotion. *J Neurophysiol* 57: 56-71, 1987.

PROCTOR C, MOSSE PRL and HUDSON RCL. A histochemical and ultrastructural study of the development of the propulsive musculature of the brown trout, Salmo trutta L., in relation to its swimming behavior. *J Fish Biol* 16: 309-329, 1980.

PRUGH JI, KIMMEL CB and METCALFE WK. Noninvasive recording of the Mauthner neurone action potential in larval zebrafish. *J Exp Biol* 101: 83-92, 1982.

PUSCH M and JENTSCH TJ. Molecular physiology of voltage-gated chloride channels. *Physiol Rev* 74: 813-827, 1994.

RAIBLE DW and KRUSE GJ. Organization of the lateral line system in embryonic zebrafish. *J Comp Neurol* 421: 189-198, 2000.

RALL W. Time constants and electrotonic length of membrane cylinders and neurons. *Biophys J* 9: 1483-1508, 1969.

RAMOA AS and MCCORMICK DA. Enhanced activation of NMDA receptor responses at the immature retinogeniculate synapse. *J Neurosci* 14: 2098-2105, 1994.

RATHMAYER W. Inhibition through neurons of the common inhibitory type (CI-Neurons) in crab muscles. In: *Frontiers in crustacean neurobiology*, edited by WIESE K, KRENZ W-D, TAUTZ J, REICHERT H and MULLONEY B. Boston, Birkhauser Verlag, 1990, p. 271-278.

RESCAN PY, COLLET B, RALLIERE C, CAUTY C, DELALANDE JM, GOLDSPINK G and FAUCONNEAU B. Red and white muscle development in the trout (Oncorhynchus mykiss) as shown by in situ hybridisation of fast and slow myosin heavy chain transcripts. *J Exp Biol* 204: 2097-2101, 2001.

RETZLAFF E. A mechanism for excitation and inhibition of the Mauthner's cells in teleost: a histological and neurophysiological study. *J Comp Neurol* 107: 209-225, 1957.

RIBERA AB and NUSSLEIN-VOLHARD C. Zebrafish touch-insensitive mutants reveal an essential role for the developmental regulation of sodium current. *J Neurosci* 18: 9181-9191, 1998.

RICHARDS C and POLLACK ED. Development of spontaneous motility in the guppy embryo (*Lebistes reticulatus*) and the effect of spinal transection. *J Exp Zool (Lond)* 244: 223-229, 1987.

RITCHIE AK and FAMBROUGH DM. Electrophysiological properties of the membrane and acetylcholine receptor in developing rat and chick myotubes. *J Gen Physiol* 66: 327-355, 1975.

RITTER DA, BHATT DH and FETCHO JR. In vivo imaging of zebrafish reveals differences in the spinal networks for escape and swimming movements. *J Neurosci* 21: 8956-8965, 2001.

ROBERT A, BLACK JA and WAXMAN SG. Endogenous NMDA-receptor activation regulates glutamate release in cultured spinal neurons. *J Neurophysiol* 80: 196-208, 1998.

ROBERTS A. Early functional organization of spinal neurons in developing lower vertebrates. *Brain Res Bull* 53: 585-593, 2000.

ROBERTS A, SOFFE SR and DALE N. Spinal interneurons and swimming in frog embryos. In: *Neurobiology of Vertebrate Locomotion*, edited by GRILLNER S, STEIN PSG, STUART DG and FORSSBERG H. London, Macmillan, 1986, p. 279-306.

ROBERTS A, SOFFE SR, WOLF ES, YOSHIDA M and ZHAO FY. Central circuits controlling locomotion in young frog tadpoles. *Ann N Y Acad Sci* 860: 19-34, 1998.

ROBERTS BL. The organization of the nervous system of fishes in relation to locomotion. *Symp Zool Soc Lond* 48: 115-136, 1981.

ROBERTS BL. Neural mechanisms underlying escape behaviour in fishes. *Rev Fish Biol Fisher* 2: 243-266, 1992.

ROHRBOUGH J and SPITZER NC. Ca(2+)-permeable AMPA receptors and spontaneous presynaptic transmitter release at developing excitatory spinal synapses. *J Neurosci* 19: 8528-8541, 1999.

ROVAINEN CM. Neurobiology of lampreys. *Physiol Rev* 59: 1007-1077, 1979.

ROVAINEN CM and BIRNBERGER KL. Identification and properties of motoneurons to fin muscle of the sea lamprey. *J Neurophysiol* 34: 974-982, 1971.

ROY S, WOLFF C and INGHAM PW. The u-boot mutation identifies a Hedgehog-regulated myogenic switch for fiber-type diversification in the zebrafish embryo. *Genes Dev* 15: 1563-1576, 2001.

RUDEL R and LEHMANN-HORN F. Membrane changes in cells from myotonia patients. *Physiol Rev* 65: 310-356, 1985.

RUSSELL DF and WALLEN P. On the control of myotomal motoneurones during "fictive swimming" in the lamprey spinal cord in vitro. *Acta Physiol Scand* 117: 161-170, 1983.

RUSSELL IJ. Central and peripheral inhibition of lateral line input during the startle response in goldfish. *Brain Res* 80: 517-522, 1974.

SAINT-AMANT L and DRAPEAU P. Time course of the development of motor behaviors in the zebrafish embryo. *J Neurobiol* 37: 622-632, 1998.

SAINT-AMANT L and DRAPEAU P. Motoneuron activity patterns related to the earliest behavior of the zebrafish embryo. *J Neurosci* 20: 3964-3972, 2000.

SAINT-AMANT L and DRAPEAU P. Synchronization of an embryonic network of identified spinal interneurons solely by electrical coupling. *Neuron* 31: 1035-1046, 2001.

SCHEETZ AJ and CONSTANTINE-PATON M. Modulation of NMDA receptor function: implications for vertebrate neural development. *Faseb J* 8: 745-752, 1994.

SCHNEIDER H, VOLLENWEIDER D and DOECKS FN. Control of pectoral fin activity in zebrafish. *Soc Neurosci Abst* 27: 2205, 2001.

SCHOMBURG ED, PETERSEN N, BARAJON I and HULTBORN H. Flexor reflex afferents reset the step cycle during fictive locomotion in the cat. *Exp Brain Res* 122: 339-350, 1998.

SCHUETZE SM and ROLE LW. Developmental regulation of nicotinic acetylcholine receptors. *Annu Rev Neurosci* 10: 403-457, 1987.

SCOTT JW, ZOTTOLI SJ, BEATTY NP and KORN H. Origin and function of spiral fibers projecting to the goldfish Mauthner cell. *J Comp Neurol* 339: 76-90, 1994.

SEYFARTH EA and ZOTTOLI SJ. Ludwig Mauthner (1840-1894): neuroanatomist and noted ophthalmologist in Fin-de-Siecle Vienna. *Brain Behav Evol* 37: 252-259, 1991.

SHAPOVALOV AI. Interneuronal synapses with electrical, dual and chemical mode of transmission in vertebrates. *Neuroscience* 5: 1113-1124, 1980.

SHEFCHYK SJ and JORDAN LM. Excitatory and inhibitory postsynaptic potentials in alpha-motoneurons produced during fictive locomotion by stimulation of the mesencephalic locomotor region. *J Neurophysiol* 53: 1345-1355, 1985a.

SHEFCHYK SJ and JORDAN LM. Motoneuron input-resistance changes during fictive locomotion produced by stimulation of the mesencephalic locomotor region. *J Neurophysiol* 54: 1101-1108, 1985b.

SHENK WD and DAVIDSON M. A study of the terminal innervation of a fast-acting fish muscle. *Biol Bull* 130: 135-140, 1966.

SHERRINGTON CS. *The integrative action of the nervous system.* Cambridge, Cambridge University Press, 1947, 433 *pp.*

SILLAR KT and ROBERTS A. Segregation of NMDA and non-NMDA receptors at separate synaptic contacts: evidence from spontaneous EPSPs in Xenopus embryo spinal neurons. *Brain Res* 545: 24-32, 1991.

SILVER RA, TRAYNELIS SF and CULL-CANDY SG. Rapid-time-course miniature and evoked excitatory currents at cerebellar synapses in situ. *Nature* 355: 163-166, 1992.

SKOGLUND CR. Neuromuscular mechanisms of sound production in Opsanus tau. *Biol Bull* 117: 438, 1959.

SOFFE SR and PERRINS R. Neuronal firing properties and swimming motor patterns in young tadpoles of four amphibians: *Xenopus*, *Rana*, *Bufo* and *Triturus*. *J Comp Physiol A* 181: 71-81, 1997.

SOFFE SR, CLARKE JDW and ROBERTS A. Swimming and other centrally generated motor patterns in newt embryos. *J Comp Physiol A* 152: 535-544, 1983.

SPALDING BC, TABER P, SWIFT JG and HOROWICZ P. Zinc inhibition of chloride efflux from skeletal muscle of *Rana pipiens* and its modification by external pH and chloride activity. *J Membr Biol* 116: 195-214, 1990.

SPRUCE AE and MOODY WJ. Developmental sequence of expression of voltage-dependent currents in embryonic *Xenopus laevis* myocytes. *Dev Biol* 154: 11-22, 1992.

STANFIELD PR. Electrical properties of white and red muscle fibres of the elasmobranch fish *Scyliorhinus canicula*. *J Physiol (Lond)* 222: 161-186, 1972.

STEFANELLI A. The Mauthnerian apparatus in the ichthyopsida; its nature and function and correlated problems of neurohistogenesis. *Q Rev Biol* 26: 17-34, 1951.

STEFANI E and STEINBACH AB. Resting potential and electrical properties of frog slow muscle fibres. Effect of different external solutions. *J Physiol (Lond)* 203: 383-401, 1969.

STEHOUWER DJ and FAREL PB. Central and peripheral controls of swimming in anuran larvae. *Brain Res* 195: 323-335, 1980.

STEIN PSG, GRILLNER S, SELVERSTON AI and STUART DG. *Neurons, networks, and motor behavior.* Cambridge, Massachusetts Institute of Technology Press, 1997, 305 *pp*.

STEINMEYER K, ORTLAND C and JENTSCH TJ. Primary structure and functional expression of a developmentally regulated skeletal muscle chloride channel. *Nature* 354: 301-304, 1991.

STICKNEY HL, BARRESI MJ and DEVOTO SH. Somite development in zebrafish. *Dev Dyn* 219: 287-303, 2000.

STOIBER W and SANGER AM. An electron microscopic investigation into the possible source of new muscle fibres in teleost fish. *Anat Embryol (Berl)* 194: 569-579, 1996.

STOIBER W, HASLETT JR, GOLDSCHMID A and SANGER AM. Patterns of superficial fibre formation in the European pearlfish (Rutilus frisii meidingeri) provide a general template for slow muscle development in teleost fish. *Anat Embryol (Berl)* 197: 485-496, 1998.

STOKES MD. Larval locomotion of the lancelet Branchiostoma floridae. *J Exp Biol* 200: 1661-1680, 1997.

SUWA H, SAINT-AMANT L, TRILLER A, DRAPEAU P and LEGENDRE P. High-affinity zinc potentiation of inhibitory postsynaptic glycinergic currents in the zebrafish hindbrain. *J Neurophysiol* 85: 912-925, 2001.

SVOBODA KR and FETCHO JR. Interactions between the neural networks for escape and swimming in goldfish. *J Neurosci* 16: 843-852, 1996.

SVOBODA KR, LINARES AE and RIBERA AB. Activity regulates programmed cell death of zebrafish Rohon-Beard neurons. *Development* 128: 3511-3520, 2001.

TAKAHASHI M, NARUSHIMA M, MURAYAMA Y and ODA Y. Functional development of the recurrent inhibitory network of the Mauthner cell in zebrafish larvae. *Neurosc Res Suppl* 24: S131, 2000.

TAKEUCHI A. Neuromuscular transmission of fish skeletal muscles investigated with intracellular microelectrode. *J Cell Comp Physiol* 54: 211-220, 1959.

TASAKI I, HAGIWARA S and WATANABE A. Action potentials recorded from inside a Mauthner cell of the catfish. *Jpn J Physiol* 4: 79-90, 1954.

TERAVAINEN H. Anatomical and physiological studies on muscles of lamprey. *J Neurophysiol* 34: 954-973, 1971.

TERAVAINEN H and ROVAINEN CM. Fast and slow motoneurons to body muscle of the sea lamprey. *J Neurophysiol* 34: 990-998, 1971.

TREVARROW B, MARKS DL and KIMMEL CB. Organization of hindbrain segments in the zebrafish embryo. *Neuron* 4: 669-679, 1990.

TRILLER A and KORN H. Morphologically distinct classes of inhibitory synapses arise from the same neurons: ultrastructural identification from crossed vestibular interneurons intracellularly stained with HRP. *J Comp Neurol* 203: 131-155, 1981.

TRILLER A, ROSTAING P, KORN H and LEGENDRE P. Morphofunctional evidence for mature synaptic contacts on the Mauthner cell of 52-hour-old zebrafish larvae. *Neuroscience* 80: 133-145, 1997.

UEMATSU K and IKEDA T. The midbrain locomotor region and induced swimming in the carp *Cyprinus carpio*. *Nippon Suisan Gakk* 59: 783-788, 1993.

UEMATSU K and TODO T. Identification of the midbrain locomotor nuclei and their descending pathways in the teleost carp, Cyprinus carpio. *Brain Res* 773: 1-7, 1997.

UEMATSU K, IKEDA T, OHTA K and MUROMOTO C. Fictive swimming induced by electrical and tactile stimulations in carp. *Fisheries Sci* 60: 533-535, 1994.

ULRICH D and LUSCHER HR. Miniature excitatory synaptic currents corrected for dendritic cable properties reveal quantal size and variance. *J Neurophysiol* 69: 1769-1773, 1993.

VAN ASSELT E, DE GRAAF F and VAN RAAMSDONK W. Ultrastructural characteristics of zebrafish spinal motoneurons innervating glycolytic white, and oxidative red and intermediate muscle fibers. *Acta Histochem* 95: 31-44, 1993.

VAN ASSELT E, DE GRAAF F, SMIT-ONEL MJ and VAN RAAMSDONK W. Spinal neurons in the zebrafish labeled with fluoro-gold and wheat-germ agglutinin. *Neuroscience* 43: 611-622, 1991.

VAN RAAMSDONK W, POOL CW and TE KRONNIE G. Differentiation of muscle fiber types in the teleost Brachydanio rerio. *Anat Embryol (Berl)* 153: 137-155, 1978.

VAN RAAMSDONK W, TEKRONNIE G, POOL CW and VAN DE LAARSE W. An immune histochemical and enzymic characterization of the muscle fibres in myotomal muscle of the teleost Brachydanio rerio, Hamilton-Buchanan. *Acta Histochem* 67: 200-216, 1980.

VAN RAAMSDONK W, BOSCH TJ, SMIT-ONEL MJ and MASLAM S. Organisation of the zebrafish spinal cord: distribution of motoneuron dendrites and 5-HT containing cells. *Eur J Morphol* 34: 65-77, 1996.

VAN RAAMSDONK W, POOL CW, MIJZEN P, MOS W and VAN DER STELT A. On the relation between movements and the shape of somites in early embryos of the teleost Brachydanio rerio. *Bijdr Dierk* 46: 261-274, 1977.

VAN RAAMSDONK W, MOS W, TEKRONNIE G, POOL CW and MIJZEN P. Differentiation of the musculature of the teleost Brachydanio rerio. II. Effects of immobilization on the shape and structure of somites. *Acta Morphol Neerl Scand* 17: 259-273, 1979.

VAN RAAMSDONK W, VAN'T VEER L, VEEKEN K, HEYTING C and POOL CW. Differentiation of muscle fiber types in the teleost Brachydanio rerio, the zebrafish. Posthatching development. *Anat Embryol* 164: 51-62, 1982a.

VAN RAAMSDONK W, VAN'T VEER L, VEEKEN K, TEKRONNIE T and DE JAGER S. Fiber type differentiation in fish. *Mol Physiol* 2: 31-47, 1982b.

VAN RAAMSDONK W, MOS W, SMIT-ONEL MJ, VAN DER LAARSE WJ and FEHRES R. The development of the spinal motor column in relation to the myotomal muscle fibers in the zebrafish (Brachydanio rerio). I. Posthatching development. *Anat Embryol* 167: 125-139, 1983.

VAN RAAMSDONK W, SMIT-ONEL M, SCHOLTEN G, HEMRIKA W and ROBBE B. Metabolic specialization of spinal neurons and the myotomal muscle in post-hatching stages of the zebrafish, Brachydanio rerio. A histochemical study. *Z Mikrosk Anat Forsch* 101: 318-330, 1987.

VAN RAAMSDONK W, VAN DER STELT A, DIEGENBACH PC, VAN DE BERG W, DE BRUYN H, VAN DIJK J and MIJZEN P. Differentiation of the musculature of the teleost Brachydanio rerio. I. Myotome shape and movements in the embryo. *Z Anat Entwickl-Gesch* 145: 321-342, 1974.

VASCOTTO SG, BECKHAM Y and KELLY GM. The zebrafish's swim to fame as an experimental model in biology. *Biochem Cell Biol* 75: 479-485, 1997.

VAUGHAN P and NOK FC. Effects of SITS on chloride permeation in Xenopus skeletal muscle. *Can J Physiol Pharmacol* 56: 1051-1054, 1978.

VAUGHAN P and TROTTER M. The influence of voltage conditioning on chloride currents in amphibian muscle membrane: the sigmoid conductance-voltage relation extended into the outward current region. *Can J Physiol Pharmacol* 60: 604-609, 1982.

VEGGETTI A, MASCARELLO F, SCAPOLO PA, ROWLERSON A and CARNEVALI C. Muscle growth and myosin isoform transitions during development of a small teleost fish, Poecilia reticulata (Peters) (Atheriniformes, Poeciliidae): a histochemical, immunohistochemical, ultrastructural and morphometric study. *Anat Embryol (Berl)* 187: 353-361, 1993.

VIEIRA VLA and JOHNSTON IA. Influence of temperature on muscle-fibre development in larvae of the herring *Clupea harengus*. *Mar Biol* 112: 333-341, 1992.

WALLEN P and WILLIAMS TL. Fictive locomotion in the lamprey spinal cord *in vitro* compared with swimming in the intact and spinal animal. *J Physiol (Lond)* 347: 225-239, 1984.

WALLEN P, BUCHANAN JT, GRILLNER S, HILL RH, CHRISTENSON J and HOKFELT T. Effects of 5-hydroxytryptamine on the afterhyperpolarization, spike frequency regulation, and oscillatory membrane properties in lamprey spinal cord neurons. *J Neurophysiol* 61: 759-768, 1989.

WARDLE CS, VIDELER JJ and ALTRINGHAM JD. Tuning in to fish swimming waves: body form, swimming mode and muscle function. *J Exp Biol* 198: 1629-1636, 1995.

WARNER AE. Kinetic properties of the chloride conductance of frog muscle. *J Physiol (Lond)* 227: 291-312, 1972.

WASSERSUG RJ. Locomotion in amphibian larvae (or "why aren't tadpoles built like fishes?"). *Amer Zool* 29: 65-84, 1989.

WATERMAN RE. Development of the lateral musculature in the teleost, Brachydanio rerio: a fine structural study. *Am J Anat* 125: 457-493, 1969.

WEBB PW and WEIHS D. Functional locomotor morphology of early life history stages of fishes. *Trans Am Fish Soc* 115: 115-127, 1986.

WEIHS D. Energetic significance of changes in swimming modes during growth of larval anchovy, Engraulis mordax. *Fish Bull* 77: 597-604, 1980.

WEINBERG ES, ALLENDE ML, KELLY CS, ABDELHAMID A, MURAKAMI T, ANDERMANN P, DOERRE OG, GRUNWALD DJ and RIGGLEMAN B. Developmental regulation of zebrafish MyoD in wild-type, no tail and spadetail embryos. *Development* 122: 271-280, 1996.

WEIS JS. Analysis of the development of the nervous system of the zebrafish, *Brachydanio rerio*. I. The normal morphology and development of the spinal cord and ganglia of the zebrafish. *J Embryol Exp Morphol* 19: 109-119, 1968.

WESTERFIELD M. *The zebrafish book. A guide for the laboratory use of zebrafish (Brachydanio rerio)*. Eugene, University of Oregon Press, 1995, 385 *pp*.

WESTERFIELD M and EISEN JS. Neuromuscular specificity: pathfinding by identified motor growth cones in a vertebrate embryo. *Trends Neurosci* 11: 18-22, 1988.

WESTERFIELD M, MCMURRAY JV and EISEN JS. Identified motoneurons and their innervation of axial muscles in the zebrafish. *J Neurosci* 6: 2267-2277, 1986.

WESTNEAT MW, HALE ME, MCHENRY MJ and LONG JH. Mechanics of the fast-start: muscle function and the role of intramuscular pressure in the escape behavior of amia calva and polypterus palmas. *J Exp Biol* 201: 3041-3055, 1998.

WHITING HP. Functional development of the nervous system. In: *Biochemistry of the developing nervous system*, edited by WAELSCH H. New York, Academic Press, 1955, p. 85-103.

WHITING HP, BANNISTER LH, BARWICK RE and BONE Q. Early locomotor behaviour and the structure of the nervous system in embryos and larvae of the Australian lungfish, *Neoceratodus forsteri. J Zool (Lond)* 226: 175-198, 1992.

WIENS TJ. Common and specific inhibition in leg muscles of decapods: sharpened distinctions. *J Neurobiol* 20: 458-469, 1989.

WIEST FC. The specialized locomotory apparatus of the freshwater hatchetfish family Gasteropelecidae. *J Zool (Lond)* 236: 571-592, 1995.

WILLIAMS BJ, DROGE MH and LEONARD RB. Intracellular recording from pectoral fin motoneurons of the stingray Dasyatis sabina, an elasmobranch fish. *J Neurophysiol* 51: 666-679, 1984.

WILLIAMS JA, BARRIOS A, GATCHALIAN C, RUBIN L, WILSON SW and HOLDER N. Programmed cell death in zebrafish rohon beard neurons is influenced by TrkC1/NT-3 signaling. *Dev Biol* 226: 220-230, 2000.

WILSON DM. Functions of giant Mauthner's neurons in the lungfish. *Science* 129: 841-842, 1959.

WOLSZON LR, PEREDA AE and FABER DS. A fast synaptic potential mediated by NMDA and non-NMDA receptors. *J Neurophysiol* 78: 2693-2706, 1997.

WU G, MALINOW R and CLINE HT. Maturation of a central glutamatergic synapse. *Science* 274: 972-976, 1996.

WULLIMANN MF, RUPP B and REICHERT H. *Neuroanatomy of the zebrafish brain: a topological atlas*. Boston, Birkhauser, 1996, 144 *pp*.

YASARGIL GM nd DIAMOND J. Startle-response in teleost fish: an elementary circuit for neural discrimination. *Nature* 220: 241-243, 1968.

YOSHIDA M, MATSUURA K and UEMATSU K. Developmental changes in the swimming behavior and underlying motoneuron activity in the larval angelfish, *Pterophyllum scalare*. *Zoolog Sci* 13: 229-234, 1996.

ZHANG Y and AUERBACH A. Kinetic properties of NMDA receptors in embryonic Xenopus spinal neurons. *J Neurophysiol* 74: 153-161, 1995.

ZOTTOLI SJ. Correlation of the startle reflex and Mauthner cell auditory responses in unrestrained goldfish. *J Exp Biol* 66: 243-254, 1977.

ZOTTOLI SJ. Comparative morphology of the Mauthner cell in fish and amphibians. In: *Neurobiology of the Mauthner cell*, edited by FABER DS and KORN H. New York, Raven Press, 1978, p. 13-45.

ZOTTOLI SJ. Electrophysiological and morphological characterization of the winter flounder Mauthner cell. *J Comp Physiol* 143: 541-553, 1981.

ZOTTOLI SJ and FABER DS. Properties and distribution of anterior VIIIth nerve excitatory inputs to the goldfish Mauthner cell. *Brain Res* 174: 319-323, 1979.

ZOTTOLI SJ and FABER DS. An identifiable class of statoacoustic interneurons with bilateral projections in the goldfish medulla. *Neuroscience* 5: 1287-1302, 1980.

ZOTTOLI SJ and FABER DS. The Mauthner cell: what has it taught us? *The Neuroscientist* 6: 26-38, 2000.